Title

Sensing the Electrical Activity of Cells Through Molecular Wires by Photoinduced-Electron Transfer

Author

Boggess, Steven Cody

Publication Date

2020

Peer reviewed|Thesis/dissertation

Sensing the Electrical Activity of Cells Through Molecular Wires by Photoinduced-Electron Transfer

By

Steven C. Boggess

A dissertation submitted in partial satisfaction of the
requirements for the degree of
Doctor of Philosophy
in
Chemistry
in the
Graduate Division
of the
University of California, Berkeley

Committee in charge:

Professor Evan W. Miller, Chair
Professor Christopher J. Chang
Professor Kevin E. Healy

Fall 2019

Sensing the Electrical Activity of Cells Through Molecular Wires by Photoinduced-Electron Transfer

By Steven C. Boggess

Abstract

Sensing the Electrical Activity of Cells Through Molecular Wires by Photoinduced-Electron Transfer

By

Steven C. Boggess

Doctor of Philosophy in Chemistry

University of California, Berkeley

Professor Evan W. Miller, Chair

Fluorescent voltage sensitive dyes (VSDs) provide an attractive, complementary method to traditional electrophysiology techniques and are important tools for studying rapid changes of membrane potential in excitable cells. The VoltageFluor family of VSDs reports this rapid activity with high sensitivity using photoinduced-electron transfer (PeT) as the voltage sensitive trigger. This mechanism provides sub-millisecond response kinetics and our laboratory has shown it can be tuned by exchanging the identity of the electron donor and fluorophore. However, the identity and architecture of the molecular wire remained unexplored. The work presented herein addresses this gap in knowledge, exploring different strategies for tuning PeT through modifications to the molecular wire. Chapter 1 represents an initial attempt, replacing the link between the molecular wire and the fluorophore with an amide. This insulates the fluorophore to slow PeT and results in less sensitive, but brighter, indicators. However, membrane staining was poor with these new indicators and *in vitro* measurements did not predict brightness in cells. Chapter 2 builds upon the insight of Chapter 1, exchanging the phenylene-vinylene molecular wire for a fluorene monomer. This fluorene-based wire provided indicators with bright membrane stains, maintained voltage sensitivity, and was shown to be less phototoxic. Low voltage sensitivity limited the utility of the indicators. Chapter 3 addresses this limitation by adding conjugation to the scaffold with a vinyl spacer to make indicators with up to a 3.5-fold improvement in sensitivity over fluorene-based indicators. Finally, Chapter 4 describes a collaborative effort to assess the effect of aniline conformation on the voltage sensing properties of VoltageFluor indicators. We found the sensitivity and fluorescence lifetime of these conformationally restricted aniline could be tuned over an order of magnitude. These results show the importance of electronic interaction of the aniline with the molecular wire for a PeT-based voltage sensor.

For my grandparents, Georgia and Manfred Wegner

Table of Contents

Acknowledgements

To my advisor Evan, you have been nothing short of a fantastic mentor for the past five years and are the primary source for much of my personal and scientific growth. You truly care about your students, and that makes a huge difference when navigating the challenges of graduate school. While my time in the lab has come to an end, I know you will continue to be a mentor throughout my career.

To everyone I worked with in the Miller lab over the last five years, thank you. I was lucky to have such wonderful people as colleagues and I learned something from each of you. Vince, Parker, Rishi, and Alisha deserve credit for paving the way as Evan's first students. You made the transition into the lab much easier and were one of the major reasons I joined in the first place. I'm also thankful for the people I joined the lab with: Julia, Gloria, Jenna and Pei. Graduate school presents its fair share of challenges, but I was lucky to have four friends to help me through it. I could always count on Julia and Pei for help with tissue culture and microscopy, while Gloria and Jenna are two talented synthetic chemists who shared their knowledge when I needed it. All four of you are awesome people and scientists and I'm incredibly sad that I won't be able to walk over and bother you at your desks whenever I want anymore, but I know I will continue to see you around the Bay as you continue with the next step in your careers. I am thankful for the two undergraduates, Shivaani and Amy, that I had the opportunity to work with. You both worked incredibly hard to become great scientists and I believe that you will both find success as you work toward your own graduate degrees. To the rest of the Miller lab, I'll miss the coffee runs, Friday Snack Shack lunches, and all the fun times in lab. You all kept me going even when things weren't going well, thank you all so much!

To all my friends in Berkeley, you all kept me sane for the last five years. Thank you for helping me climb literal and metaphorical mountains, teaching me to ski, and for inviting me to play soccer with you (go Soctopus!). You all helped me to forget about lab and take a break when I needed it the most. I look forward to spending more time with you all and to continue exploring the Bay. To my friends from college and back home in Colorado, each of you had role in keeping me grounded and motivating me to keep working hard. Thank you all for your love and support!

To Kristin, I couldn't ask for a better partner. You've supported me when I was down, challenged me when I needed a push, and reminded me to have fun by being your goofball self. I can't wait for more of our adventures together!

To my parents Mike and Michel, you deserve recognition for your enduring support. While it is hard for me to put into words, it means a lot to have two people that push me to be a better person and chase my aspirations. I don't think I would've made it to this point without you. To my siblings Hannah and Daniel, I love you both and always look forward to seeing you when we are at home. To my grandparents Manny and Georgia, to whom I dedicate this thesis to, you are two of the hardest working people I know and inspire me to do my best work. I love you all very much and can't thank you enough for your support.

Chapter 1:

Amide-linked Molecular Wires for Brighter Voltage Sensing Indicators

Abstract

This chapter presents the design, synthesis, and characterization of amide-linked VoltageFluor indicators. This new scaffold replaces the vinyl linkage between the molecular wire and chromophore in the VoltageFluor scaffold in order to tune the voltage sensitive properties. Previously, the molecular wire architecture had not been explored as an avenue for tuning the properties of VoltageFluors. Although *in vitro* quantum yields of these amide VoltageFluors (AVFs) are greater than previous VoltageFluors (0.18 vs 0.06), AVFs suffer from poor membrane localization and are much dimmer in cells. As expected, the voltage sensitivity of these AVFs was lower (8-16% F/F_o) than VF2.1.Cl (26% F/F_o). However, the findings of this research suggest that modifications to the molecular wire and its electronic coupling to the fluorophore could help tune future voltage-sensing scaffolds.

1.1 Motivation and design strategy

Significant strides in understanding excitable cells like neurons and cardiomyocytes have been made over the last few decades, largely in part to the development and optimization of tools such as patch-clamp electrophysiology. This series of techniques utilizes a glass micropipette equipped with an electrode to make direct contact with a cell, allowing the users to manipulate and record the voltage across the cell membrane. This voltage, known as the cell membrane potential (V_{mem}), changes rapidly in neurons and cardiomyocytes to facilitate the function of these cells. These changes, or action potentials, cause the release of neurotransmitters into synapses between neurons in the brain which allow these specialized cells to form vast networks that give rise to behavior and cognitive function. In the heart, sheets of cardiomyocytes coordinate contraction with action potential waves through gap junctions. These contractions pump blood carrying oxygen and nutrients throughout the body. The importance of V_{mem} and these electrical waveforms drives the need to continue to improve methods that can be used to study cellular processes.

While a powerful tool to directly study electrical activity, it is difficult to investigate the neuronal circuitry of more than a few neurons simultaneously with electrophysiology, preventing analysis of the properties that arise from larger networks.[1] Furthermore, it is difficult to study cardiac syncytia with these techniques due to space-clamp concerns, limiting studies to single myocytes or the use of multi-electrode arrays (MEA) which measure the surrounding field potential. Tracking membrane voltage changes with fluorescent sensors has the potential to fill a void in understanding of the brain by providing means to study interactions between neuronal cells with high resolution. Previous approaches to voltage-sensitive dyes (VSD) suffer from either poor signal-noise or slow kinetics, which hampers their use in more complex cell preparations.[2,3] The recent development of the VoltageFluor (VF) series of VSDs has made a vast improvement on functional imaging, with field-leading voltage sensitivities up to 63% per 100 mV and physiologically relevant response kinetics.[4–6] VF dyes operate under a photoinduced electron transfer (PeT) process, in which a fluorophore PeT acceptor is linked to a PeT donor through a phenylene vinylene molecular wire (**Scheme 1-1**). At a resting membrane potential, fluorescence is quenched by PeT as the electric field accelerates electron transfer through the membrane to the fluorophore on the extracellular leaflet. When the membrane depolarizes, fluorescence becomes brighter as the rate of PeT is reduced.

Although the first generations of VF dyes have good voltage sensitivities and signal to noise, our understanding of the PeT-based mechanism of voltage sensing remains incomplete, making the rational design of VF dyes with improved properties difficult. Previous reports demonstrated that the aniline donor could be further substituted to tune the voltage sensitivity of the indicator, however these dyes were also dim in comparison to the original VF2.1.Cl.[5] One explanation could be that PeT, the voltage sensitive mechanism, quenches these fluorophores so effectively in these indicators such that, even though they exhibit large percent changes in fluorescence, the resulting signals are difficult to record. It is desirable to build voltage indicators that are not only highly sensitive to changes in V_{mem}, but also emit a large number of photons in order to detect what is a signal apart from noise.[7] To that end, the architecture of the molecular wire (**Scheme 1-1**), which helps facilitate PeT in the low dielectric environment of the membrane, is an attractive component of these molecules to explore further. It was hypothesized that modifying the capability of the

molecular wire to facilitate PeT could help tune the balance of sensitivity and brightness of VoltageFluor indicators.

1.2 Synthesis and characterization of sarcosine amide-linked VoltageFluors

We sought to explore the effect of breaking the conjugation between the phenylene-vinylene molecular wire and the pendant ring of the chromophore in the VF2.1.Cl by replacing the vinyl group with an amide (**Scheme 1-1**). In theory, this would insulate the fluorophore from PeT—making less sensitive but overall brighter indicators. The synthesis of these indicators began by coupling electron rich-styrenes[5,6] to 4-bromonitrobenzene via a Pd-catalyzed cross coupling to produce wires **1**, **2**, and **3** (**Scheme 1-2**). These were then reduced to the aniline (**4**, **5**, and **6**) with tin (II) chloride. This route was used in lieu of direct coupling with 4-bromoaniline as this cross-coupling reaction produced the internal coupling isomer and was low yielding. Coupling aniline wires to the 4-carboxy-2',7'-dichlorofluorescein with HATU yielded carboxy-amide VoltageFluors **7-9**, which were isolated by column chromatography. However, others in our laboratory have shown that VoltageFluor indicators with 2-carboxy substituents do not localize properly to the cell membrane, but addition of an N-methylsarcosine recovers proper membrane localization.[8] HATU coupling with Boc-protected N-methylsarcosine and subsequent deprotection with zinc chloride produced sarcosine Amide-VoltageFluors [sarcAVFs, **13-15** (**Scheme 1-2)**].

These indicators exhibit absorption and emission profiles that are similar to vinyl-linked VoltageFluors, with a maximum absorption around 515 nm that is slightly blue-shifted compared to VF2.1.Cl (**Table 1-1**, **Figure 1-1**). A second absorption max, attributed to the conjugated molecular wire, was also blue shifted in respect to VF2.1.Cl, which is expected due to the decrease in conjugation from replacement with an amide. These sarcAVFs had a maximum emission between 531 and 537 nm, which is approximately equivalent to VF2.1.Cl. Somewhat satisfyingly, the measured relative quantum yield of fluorescence (Φ_{FL}) of sarcAVFs was higher (sarcAVF2.1.Cl, 4.7X; sarcAVF2.1.(diOMe)Cl, 3.5X) or the same (AVF2.1.(OMe)Cl) to VF2.1.Cl (**Table 1-1**), suggesting the decoupling of the molecular wire and fluorophore through an amide linkage produced dyes that would be brighter than the original phenylene-vinylene scaffold.

However, studies in HEK293T cells quickly showed that *in vitro* quantum yield measurements are not a satisfactory predictor of brightness in cells for membrane-localized VoltageFluor dyes. In order to observe any signal from the membrane of cells staining with these sarcAVFs, incubation with 5 μM of the indicator was required, 25 times what is required for VF2.1.Cl (**Figure 1-2**). Furthermore, the localization of these indicators is not restricted to the plasma membrane. This is apparent with wide-field microscopy, particularly when compared to the excellent membrane localization of VF2.1.Cl. Still, we were interested in the effect of the amide linkage on voltage sensitivity (**Figure 1-3**). Despite a poor membrane stain, tandem whole-cell voltage clamp and fluorescence microscopy experiments showed sarcAVF2.1.Cl is voltage sensitive [8.6% per 100 mV (**Table 1-1**, **Figure 1-3**)] to changes in V_{mem} in HEK293T cells, although the resulting fluorescence trace is noisy due to the high amount of background and low overall signal. Indicators sarcAVF2.1.(OMe)Cl and sarcAVF2.1.(diOMe)Cl had signals too dim to make voltage sensitivity measurements.

1.3 Synthesis and characterization of sulfonated amide VoltageFluors (AVFs)

The performance of sarcAVFs was disappointing, however one reason for their poor membrane localization and signal in cells could be that the N-methyl sarcosine substituent is not sufficient for 1) solubilization of the indicator or 2) preventing internalization of the indicator. In the VF2.1.Cl scaffold, a sulfonic acid substituent plays this role, as it exists primarily as the ionized sulfonate at a physiological pH (**Scheme 1-1**).[5,6] We pursued the synthesis of amide-linked VoltageFluors with a sulfonic acid in place of the N-methylsarcosine to produce AVFs (**Scheme 1-3**). First, synthesis of a new 4-carboxy-2-sulfonic acid dichlorofluorescein began with aromatic substitution of *p*-xylene with chlorosulfonic acid to produce **16**. Stirring with ammonium hydroxide produce sulfonamide **17**, which was then oxidized using $KMnO_4$ to produce 4-carboxysaccharin, **18**. Condensation with 4-chlororesorcinol in methane sulfonic acid at high temperature gave the desired fluorescein derivative **19**. Using an analogous coupling that produced carboxyAVFs, heating with HATU and aniline wires **6**, **7**, or **8** provided three new AVF indicators [**20**, **21**, **22** (**Scheme 1-3**)].

These sulfonated AVFs have similar spectroscopic properties to sarcAVFs *in vitro*, including high quantum yields in comparison to VF2.1.Cl (**Table 1-1**, **Figure 1-4**). Membrane localization is improved over sarcAVFs; clear staining at the membrane is observed (**Figure 1-5**). Still, higher concentrations of AVFs are required, as incubation of HEK293T cells with 1 μM AVF2.1.Cl produces signal that is comparable to loading VF2.1.Cl at 0.2 μM. Electron-rich AVFs are still very dim in cells, even when loading at higher concentrations (**Figure 1-5b,c**).

Gratifyingly, the increased signal of these AVF indicators produce fluorescence responses in voltage-clamped HEK293T cells that are easily recorded (**Figure 1-6**). AVF2.1.Cl (**20**) proved to be the most sensitive of all AVF indicators tested (16.3% per 100 mV), and also produces traces with the best signal-to-noise due to its brighter staining. AVF2.1.(OMe)Cl is surprisingly less sensitive, even with the addition of a methoxy substituent on the aniline donor that has been shown previously to boost sensitivity to V_{mem} changes.[5,8] Due to a poor membrane stain, the voltage sensitivity of AVF2.1.(diOMe)Cl could not be recorded.

1.4 Conclusion and outlook

Poor signal from the membrane hampers the ability to record membrane potential changes in cells using any of the synthesized amide-linked VoltageFluor indicators. The results from this study suggest that simply exchanging the vinyl link between the chromophore and the molecular wire (**Scheme 1-1**) for an amide linkage perturbed other factors that are necessary for a membrane voltage probe. Namely, these probes must localize to the outer leaflet of the cell membrane and remain there in order to record fluctuations in the potential. In the amide-linked scaffolds, the addition of heteroatoms reduces the lipophilicity of the molecular wire which allows VoltageFluors to passively intercalate into the lipid bilayer. As previously mentioned, *in vitro* quantum yields are not adequate to predict relative brightness in cells for membrane localized indicators. This is likely due to confounding factors unrelated to the photophysical properties of the indicator, such as solubility and membrane affinity. While amide-linked VoltageFluors had higher quantum yields on average than previous VoltageFluors, decreased affinity for the membrane would result in a dimmer signal in cells.

While amide-linked VoltageFluors did not perform well as voltage indicators, findings with AVF2.1.Cl suggest that modifications to the molecular wire can tune voltage sensitivity, potentially in a predictable manner. All components other than the linkage between the chromophore and molecular wire being the same, AVF2.1.Cl exhibited voltage sensitivity that was nearly half that of VF2.1.Cl (**Table 1-1**). This reduction in sensitivity was predicted due to the reduction in conjugation with the amide, thus insulating the wire and PeT. Lessons from this family of compounds suggest that other molecular wires that are more insulating but do not contain heteroatoms, such as oligofluorenes and polyalkynes, might present attractive targets for voltage-sensitive scaffolds.

1.5 Materials and methods

1.5.1 General method for chemical synthesis and characterization

Palladium acetate was purchased from Strem Chemicals. Deuterated solvents were purchased from Cambridge Isotope Laboratories. All other reagents, including anhydrous solvents, were purchased from Sigma-Aldrich and used without further purification. References to previously synthesized compounds are provided along with characterization data. Thin layer chromatography (TLC) (Silicycle, F254, 250 μm) and preparative thin layer chromatography (PTLC) (Silicycle, F254, 1000 μm) were performed on glass backed plates pre-coated with silica gel and were visualized by fluorescence quenching under UV light. Flash column chromatography was performed on Silicycle Silica Flash F60 (230–400 Mesh) using a forced flow of air at 0.5–1.0 bar. NMR spectra were measured on Bruker AV-300 MHz, AVB-400 MHz, AVQ-400 MHz, and Bruker AV-600 MHz. Chemical shifts are expressed in parts per million (ppm) and are referenced to $CDCl_3$ (7.26 ppm, 77.0 ppm), d_6-DMSO (2.50 ppm, 40 ppm), or d_4-MeOD (3.35 ppm). Coupling constants are reported as Hertz (Hz). Splitting patterns are indicated as follows: s, singlet; d, doublet; t, triplet; q, quartet; dd, doublet of doublet; m, multiplet. High performance liquid chromatography (HPLC) and low resolution ESI Mass Spectrometry were performed on an Agilent Infinity 1200 analytical instrument coupled to an Advion CMS-L ESI mass spectrometer. The column used for the analytical HPLC was Phenomenex Luna 5 μm C18(2) (4.6 mm I.D. × 125 mm) with a flow rate of 1.0 mL/min. The mobile phases were MQ-H2O with 0.05% trifluoroacetic acid (eluent A) and HPLC grade acetonitrile with 0.05% trifluoroacetic acid (eluent B). Signals were monitored at 254, 350 and 480 nm over 10 min with a gradient of 10-100% eluent B unless otherwise noted. Semi-preparative high-performance liquid chromatography (HPLC) was performed on the same system with a semi-preparative Phenomenex Luna C18(2) column.

1.5.2 Spectroscopic studies

Stock solutions of amide-linked VoltageFluors were prepared in DMSO (1 mM) and diluted with PBS (10 mM KH2PO4, 30 mM Na2HPO4·7H2O, 1.55 M NaCl, pH 7.2) solution containing 0.10 % (w/w) SDS (1:200 to 1:1000 dilution). UV-Vis absorbance and fluorescence spectra were recorded using a Shimadzu 2501 Spectrophotometer (Shimadzu) and a Quantamaster Master 4 L-format scanning spectrofluorometer (Photon Technologies International). The fluorometer is equipped with an LPS-220B 75-W xenon lamp and power supply, A-1010B lamp housing with integrated igniter, switchable 814 photon-counting/analog photomultiplier detection unit, and MD5020 motor driver. Samples were measured in 1-cm path length quartz cuvettes (Starna Cells).

Relative quantum yields (Φ_{Fl}) were calculated by comparison to fluorescein (Φ_{Fl} = 0.93 in 0.1 M NaOH). Briefly, peak absorbance values were matched for amide-linked VoltageFluors (in PBS + 0.1% SDS) and fluorescein (in 0.1 M NaOH). Fluorescence spectra were taken of absorbance-matched samples (excitation: 450 nm) from 460-700 nm. Integration of the emission spectra were compared and used to calculate the relative quantum yield by the equation: $\frac{A_{fluorescein}}{A_x} x \frac{I_x}{I_{fluorescein}} x 0.93$ where *A* is the absorbance value at the excitation wavelength (450 nm) and *I* is the integration of the emission spectra.

1.5.3 Cell Culture, dye loading, and imaging

Human embryonic kidney (HEK) 293T cells were acquired from the UC Berkeley Cell Culture Facility. Cells were passaged and plated onto 12 mm glass coverslips coated with Poly-D-Lysine (PDL; 1 mg/mL; Sigma-Aldrich) to a confluency of ~15% and 50% for electrophysiology and imaging, respectively. HEK293T cells were plated and maintained in Dulbecco's modified eagle medium (DMEM) supplemented with 4.5 g/L D-glucose, 10% fetal bovine serum (FBS), and 1% Glutamax.

Amide-linked VoltageFluors were diluted to the indicated concentrations from DMSO stock dilutions in Hanks buffered salt solution (HBSS). Cells were incubated in these solutions for 20 minutes at 37 °C before changing to fresh (no-dye) HBSS solution for imaging.

Microscopic images were acquired with a W-Plan-Apo 20x/1.0 water objective (Zeiss) and OrcaFlash4.0 sCMOS camera (Hamamatsu). For fluorescence images, the excitation light was delivered from a LED (100 ms exposure time) at 475/34 (bandpass) nm and emission was collected with an emission filter (bandpass; 540/50 nm) after passing through a dichroic mirror (510 nm LP). The fluorescence response to membrane potential changes was captured from an Evolve 128 EMCCD camera (Photometrics) at a sampling rate of 0.5 kHz.

1.5.4 Electrophysiology

Pipettes were pulled from borosilicate glass (Sutter Instruments, BF150-86-10), with a resistance of 5–6 MΩ, and were filled with an internal solution; 125 mM potassium gluconate, 1 mM EGTA, 10 mM HEPES, 5 mM NaCl, 10 mM KCl, 2 mM ATP disodium salt, 0.3 mM GTP trisodium salt (pH 7.25, 285 mOsm). Recordings were obtained with an Axopatch 200B amplifier (Molecular Devices) at room temperature. The signals were digitized with a Digidata 1440A, sampled at 50 kHz and recorded with pCLAMP 10 software (Molecular Devices) on a PC. Fast capacitance was compensated in the on-cell configuration. For all electrophysiology experiments, recordings were only pursued if series resistance in voltage clamp was less than 30 MΩ. For whole-cell, voltage clamp recordings in HEK293T cells, cells were held at -60 mV and hyper- and de-polarizing steps applied from -100 to +100 mV in 20 mV increments

1.5.5 Synthetic methods

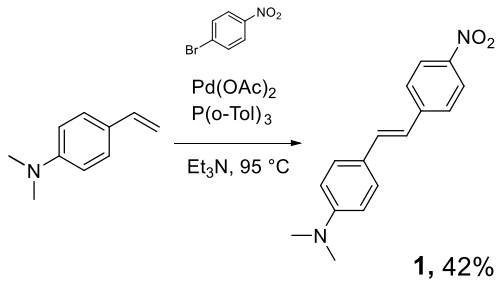

Synthesis of (E)-N,N-dimethyl-4-(4-nitrostyryl)aniline, 1

N,N-dimethyl-4-vinylaniline (0.58 g, 3.9 mmol), 4-bromo-nitrobenzene (0.95 g, 4.7 mmol), palladium(II) acetate (8.3 mg, 0.04 mmol), P(*o*-tol)$_3$ (24 mg, 0.08 mmol) were added to a flame dried Schlenk flask, which was evacuated and backfilled with N_2 (3X). This was stirred in anhydrous triethylamine (2 mL) at 95 °C for 18 hours. This was diluted in dichloromethane and filtered over celite. Filtrate was washed with NH_4Cl and brine, then dried with $MgSO_4$ and concentrated onto silica. **1** was purified by flash chromatography (5% ethyl acetate in hexanes), yielding a red solid (0.45 g, 42%)

^{1}H NMR (300 MHz, Chloroform-d) δ 8.18 (d, J = 8.7 Hz, 2H), 7.56 (d, J = 8.7 Hz, 2H), 7.45 (d, J = 8.7 Hz, 3H), 7.19 (s, 1H), 6.93 (d, J = 16.2 Hz, 1H), 6.72 (d, J = 8.6 Hz, 2H), 3.02 (s, 6H).

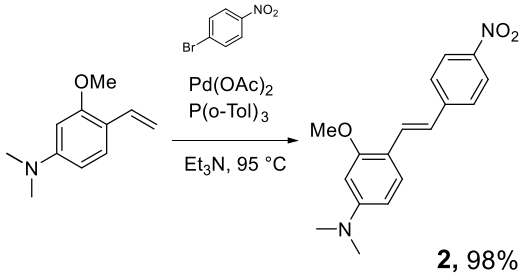

Synthesis of (E)-3-methoxy-N,N-dimethyl-4-(4-nitrostyryl)aniline, 2

3-methoxy-N,N-dimethyl-4-vinylaniline (0.27 g, 1.5 mmol), 4-bromo-nitrobenzene (0.47 g, 2.3 mmol), palladium(II) acetate (3.4 mg, 0.02 mmol), P(*o*-tol)$_3$ (9 mg, 0.03 mmol) were added to a flame dried Schlenk flask, which was evacuated and backfilled with N_2 (3X). This was stirred in anhydrous triethylamine (2 mL) at 95 °C for 18 hours. This was diluted in dichloromethane and filtered over celite. Filtrate was washed with NH_4Cl and brine, then dried with $MgSO_4$ and concentrated onto silica. **2** was purified by flash chromatography (5-10% ethyl acetate in hexanes), yielding a red solid (0.45 g, 98%)

^{1}H NMR (400 MHz, Chloroform-d) δ 8.17 (d, J = 8.4 Hz, 2H), 7.64 – 7.55 (m, 3H), 7.49 (d, J = 8.7 Hz, 1H), 6.99 (d, J = 16.2 Hz, 1H), 6.36 (d, J = 8.7 Hz, 1H), 6.21 (s, 1H), 3.92 (s, 3H), 3.04 (d, J = 1.4 Hz, 6H).

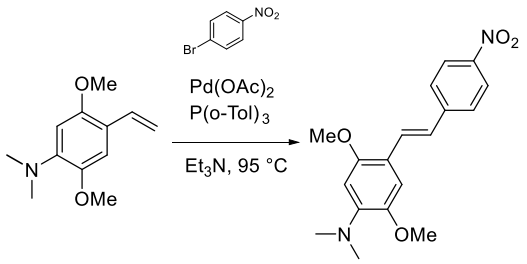

3, 23%

Synthesis of (E)-2,5-dimethoxy-N,N-dimethyl-4-(4-nitrostyryl)aniline, 3

2,5-dimethoxy-N,N-dimethyl-4-vinylaniline (0.31 g, 1.5 mmol), 4-bromo-nitrobenzene (0.37 g, 1.8 mmol), palladium(II) acetate (3.4 mg, 0.02 mmol), P(*o*-tol)$_3$ (9 mg, 0.03 mmol) were added to a flame dried Schlenk flask, which was evacuated and backfilled with N_2 (3X). This was stirred in anhydrous triethylamine (2 mL) at 95 °C for 18 hours. This was diluted in dichloromethane and filtered over celite. Filtrate was washed with NH_4Cl and brine, then dried with $MgSO_4$ and concentrated onto silica. **3** was purified by flash chromatography (5-10% ethyl acetate in hexanes), yielding a red solid (0.11 g, 23%)

^{1}H NMR (400 MHz, Chloroform-*d*) δ 8.21 – 8.16 (m, 2H), 7.65 – 7.60 (m, 3H), 7.07 (s, 1H), 7.02 (d, *J* = 16.3 Hz, 1H), 6.51 (s, 1H), 3.92 (s, 3H), 3.90 (s, 3H), 2.88 (s, 6H).

^{13}C NMR (101 MHz, CDCl3) δ 152.44, 146.23, 146.03, 145.06, 144.45, 128.06, 126.35, 124.07, 123.72, 117.53, 109.36, 102.39, 56.29, 55.97, 42.91.

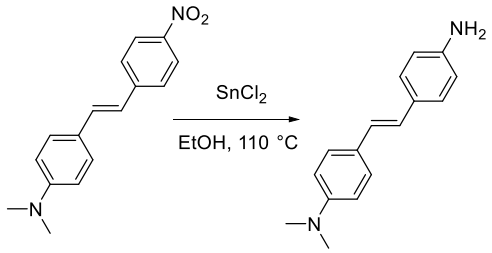

1 **4**, 44%

Synthesis of (E)-4-(4-aminostyryl)-N,N-dimethylaniline, 4

1 (0.4 g, 1.5 mmol), and tin(II) chloride (1.7 g, 7.5 mmol) were suspended in ethanol, then refluxed for 2.5 hours. This was then cooled and quenched with aqueous sodium bicarbonate solution. This was filtered over basic alumina, then washed with dichloromethane. **4** was then purified by a silica plug (30% ethyl acetate in hexanes), yielding a yellow solid (0.16 g, 44%).

^{1}H NMR (600 MHz, Chloroform-*d*) δ 7.37 (d, *J* = 8.4 Hz, 2H), 7.31 – 7.29 (m, 2H), 6.85 (d, *J* = 5.9 Hz, 2H), 6.71 (d, *J* = 8.4 Hz, 2H), 6.68 – 6.65 (m, 2H), 3.68 (s, 2H), 2.97 (s, 6H).

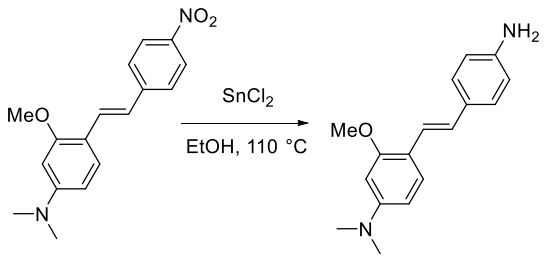

2 **5**, 33%

Synthesis of (E)-4-(4-aminostyryl)-3-methoxy-N,N-dimethylaniline, 5

2 (0.2 g, 0.67 mmol), and tin(II) chloride (0.76 g, 3.4 mmol) were suspended in ethanol, then refluxed for 5 hours. This was then cooled and quenched with aqueous sodium bicarbonate solution. This was filtered over basic alumina, then washed with dichloromethane. **5** was then purified by a silica plug (30% ethyl acetate in hexanes), yielding a yellow solid (60 mg, 33%).

^{1}H NMR (400 MHz, Chloroform-*d*) δ 7.47 (d, *J* = 8.5 Hz, 1H), 7.34 (d, *J* = 8.1 Hz, 2H), 7.27 – 7.20 (m, 1H), 6.89 (d, *J* = 16.4 Hz, 1H), 6.67 (d, *J* = 8.1 Hz, 2H), 6.37 (dd, *J* = 8.7, 2.4 Hz, 1H), 6.26 (d, *J* = 2.4 Hz, 1H), 3.90 (s, 3H), 3.67 (s, 2H), 3.00 (s, 6H).

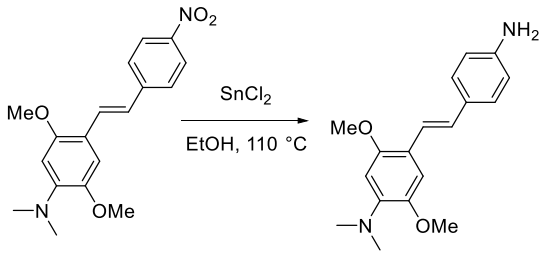

3 **6**, 15%

Synthesis of (E)-4-(4-aminostyryl)-2,5-dimethoxy-N,N-dimethylaniline, 6

3 (0.11 g, 0.33 mmol), and tin(II) chloride (0.43 g, 1.9 mmol) were suspended in ethanol, then refluxed for 12 hours. This was cooled, then quenched with aqueous sodium bicarbonate solution. This was filtered over basic alumina, then washed with dichloromethane. **6** was then purified by a silica plug (30% ethyl acetate in hexanes + 1% triethylamine), yielding a yellow solid (15 mg, 15%).

^{1}H NMR (400 MHz, Chloroform-*d*) δ 7.38 (d, *J* = 8.2 Hz, 2H), 7.30 (s, 1H), 7.09 (s, 1H), 6.93 (d, *J* = 16.4 Hz, 1H), 6.71 (d, *J* = 8.1 Hz, 2H), 6.57 (s, 1H), 3.95 (s, 3H), 3.89 (s, 3H), 2.86 (s, 6H), 2.85 (s, 2H).

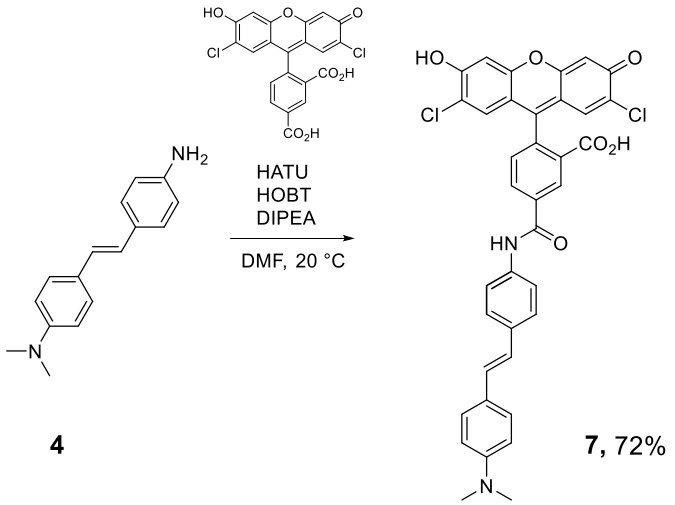

4 **7**, 72%

Synthesis of (E)-2-(2,7-dichloro-6-hydroxy-3-oxo-3H-xanthen-9-yl)-5-((4-(4-(dimethylamino)styryl)phenyl)carbamoyl)benzoic acid, 7

4 (40 mg, 0.17 mmol) and 4-(2,7-dichloro-6-hydroxy-3-oxo-3H-xanthen-9-yl)isophthalic acid (fluorescein, 50 mg, 0.11 mmol) was added to a vial. HATU (96 mg, 0.25 mmol) and HOBT (38 mg, 0.28 mmol) was added as a solution in DMF (0.45 M, 0.5M, 0.5 mL) at 0 °C. Diisopropylethylamine (0.1 mL, 0.56 mmol) was added, and the reaction was allowed to for 18 hours at 20 °C. This was extracted in 2:1 dichloromethane:isopropanol, then washed with 0.1 M HCl and brine. This was dried with $MgSO_4$ and concentrated onto silica. **7** was purified by flash chromatography (5-7% MeOH in dichloromethane +1% trifluoroacetic acid), yielding an orange solid (59 mg, 72%).

^{1}H NMR (400 MHz, DMSO-d_6) δ 10.62 (s, 1H), 8.59 (s, 1H), 8.36 (dd, J = 8.1, 1.6 Hz, 1H), 7.81 (d, J = 8.1 Hz, 2H), 7.56 (d, J = 8.4 Hz, 2H), 7.52 (d, J = 8.0 Hz, 1H), 7.45 (d, J = 8.4 Hz, 2H), 7.11 (d, J = 16.4 Hz, 1H), 7.01 (d, J = 10.1 Hz, 1H), 6.96 (s, 2H), 6.79 – 6.75 (m, 3H), 2.95 (s, 6H).

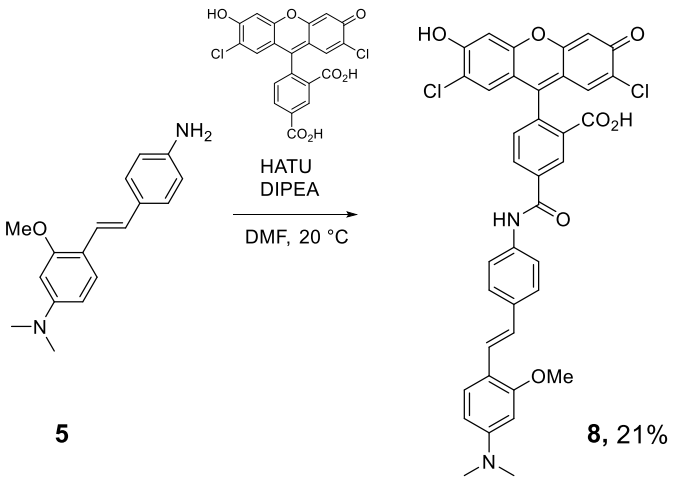

5 **8**, 21%

Synthesis of (E)-2-(2,7-dichloro-6-hydroxy-3-oxo-3H-xanthen-9-yl)-5-((4-(4-(dimethylamino)-2-methoxystyryl)phenyl)carbamoyl)benzoic acid, 8

4-(2,7-dichloro-6-hydroxy-3-oxo-3H-xanthen-9-yl)isophthalic acid (fluorescein, 50 mg, 0.11 mmol) and HATU (47 mg, 0.12 mmol) were added to a vial and stirred in anhydrous DMF (1 mL). Diisopropylethylamine (0.1 mL, 0.56 mmol) was added, and the reaction was stirred for 30 minutes before the addition of **5** (30 mg, 0.11 mmol). Finally, this was stirred at 20 °C for 18 hours. This was extracted in 2:1 dichloromethane:isopropanol, then washed with 0.1 M HCl and brine. This was dried with $MgSO_4$ and concentrated onto silica. **8** was purified by flash chromatography (5% MeOH in dichloromethane +1% trifluoroacetic acid), yielding an orange solid (16 mg, 21%).

Analytical HPLC retention time 15.01 min; MS (ESI+) m/z for $C_{38}H_{29}Cl_2N_2O_7$ $[M+H]^+$ 695.1; found 695.3.

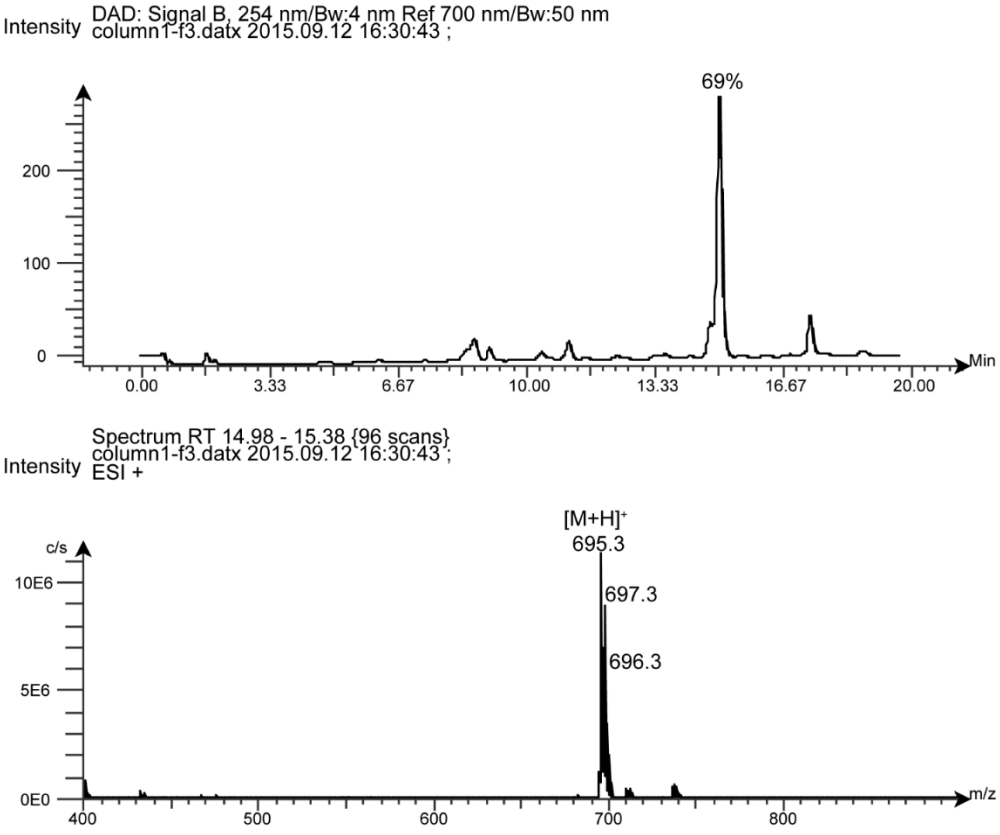

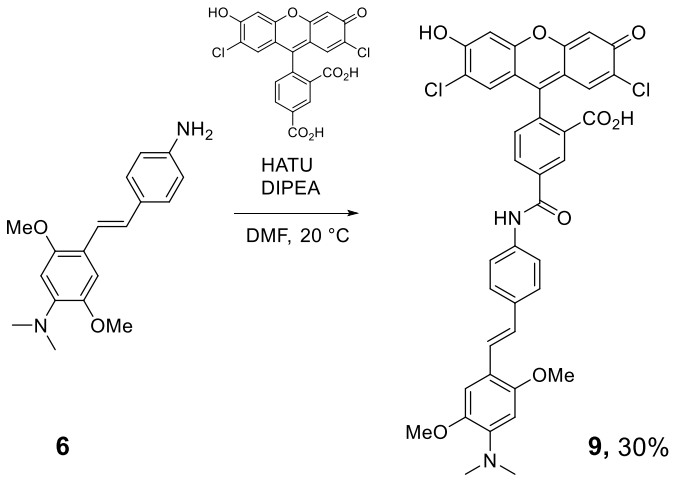

6 **9,** 30%

Synthesis of (E)-2-(2,7-dichloro-6-hydroxy-3-oxo-3H-xanthen-9-yl)-5-((4-(4-(dimethylamino)-2,5-dimethoxystyryl)phenyl)carbamoyl)benzoic acid, 9

4-(2,7-dichloro-6-hydroxy-3-oxo-3H-xanthen-9-yl)isophthalic acid (fluorescein, 50 mg, 0.11 mmol) and HATU (47 mg, 0.12 mmol) were added to a vial and stirred in anhydrous DMF (1 mL). Diisopropylethylamine (0.1 mL, 0.56 mmol) was added, and the reaction was stirred for 30 minutes before the addition of **6** (34 mg, 0.11 mmol). Finally, this was stirred at 20 °C for 18 hours. This was extracted in 2:1 dichloromethane:isopropanol, then washed with 0.1 M HCl and brine. This was dried with $MgSO_4$ and concentrated onto silica. **9** was purified by flash chromatography (5% MeOH in dichloromethane +1% trifluoroacetic acid), yielding an orange solid (24 mg, 30%).

Analytical HPLC retention time 5.13 min; MS (ESI+) m/z for $C_{39}H31Cl_2N_2O_8$ $[M+H]^+$ 625.1; found 725.4.

^{1}H NMR (600 MHz, DMSO-d_6) δ 11.14 (s, 2H), 10.63 (s, 1H), 8.58 (s, 1H), 8.34 (d, J = 8.1 Hz, 1H), 7.84 (d, J = 8.2 Hz, 2H), 7.58 (d, J = 8.3 Hz, 2H), 7.50 (d, J = 8.0 Hz, 1H), 7.32 (s, 1H), 6.91 (s, 2H), 6.75 (s, 2H), 3.93 (s, 2H), 3.86 (s, 3H).

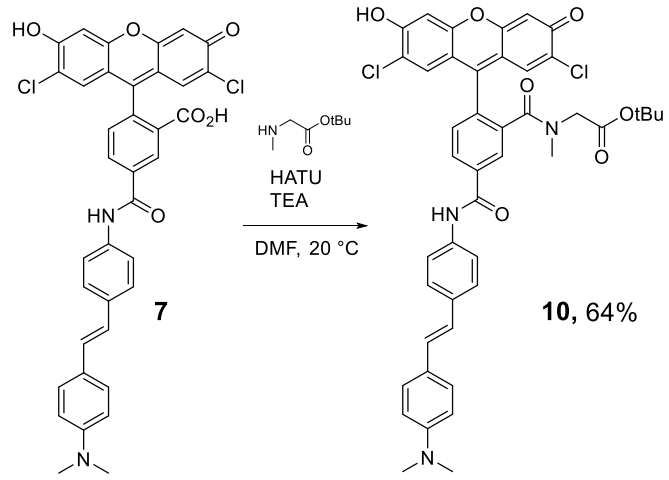

7 **10,** 64%

Synthesis of tBuSarcAVF2.1.Cl, 10

7 (25 mg, 38 µmol) and HATU (16 mg, 0.04 mmol) were added to a dram vial, then stirred in anhydrous DMF (0.2 mL) and triethylamine (0.03 mL) for 30 minutes. Sarcosine *tert*-butyl ester (7 mg, 38 µmol) was then added, and reaction was stirred for 18 hours at 20 °C. **10** was purified by preparative TLC (7% MeOH in DCM) to yield an orange solid (19 mg, 64%).

Analytical HPLC retention time 15.25 min; MS (ESI+) m/z for $C_{44}H_{40}Cl_2N_3O_7$ $[M+H]^+$ 792.2; found 792.6.

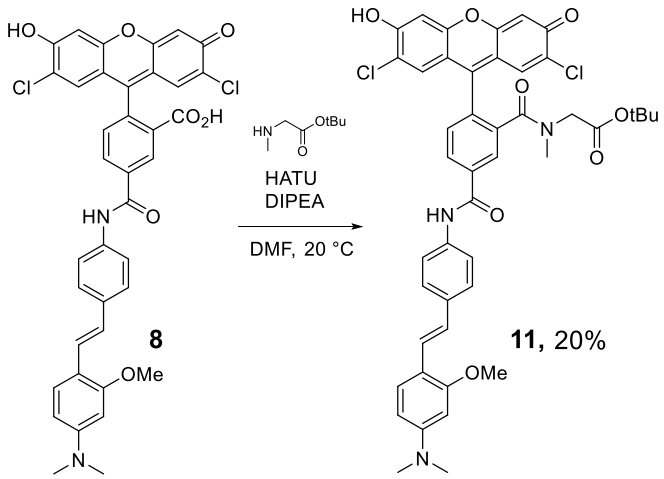

Synthesis of tBuSarcAVF2.1.(OMe)Cl, 11

8 (15 mg, 22 µmol) and HATU (10 mg, 0.03 mmol) were added to a dram vial, then stirred in anhydrous DMF (0.5 mL) and triethylamine (0.02 mL) for 30 minutes. Sarcosine *tert*-butyl ester (4 mg, 26 µmol) was then added, and reaction was stirred for 18 hours at 20 °C. **11** was purified by preparative TLC (7% MeOH in DCM) to yield an orange solid (3.6 mg, 20%).

Analytical HPLC retention time 15.67 min; MS (ESI+) m/z for $C_{45}H_{42}Cl_2N_3O_8$ $[M+H]^+$ 822.2; found 822.4.

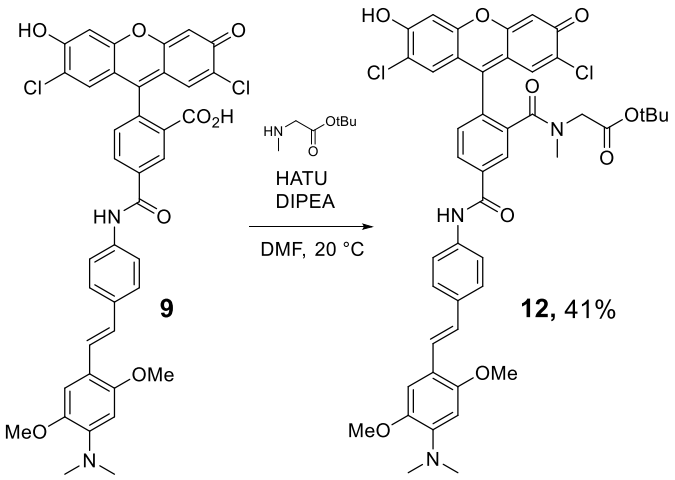

Synthesis of tBuSarcAVF2.1.(diOMe)Cl, 12

9 (6 mg, 8.3 µmol) and HATU (3.5 mg, 9 µmol) were added to a dram vial, then stirred in anhydrous DMF (0.5 mL) and triethylamine (0.1 mL) for 30 minutes. Sarcosine *tert*-butyl ester (1.5 mg, 8.3 µmol) was then added, and reaction was stirred for 18 hours at 20 °C. **11** was purified by preparative TLC (7% MeOH in DCM) to yield an orange solid (2.9 mg, 41%).

Analytical HPLC retention time 15.67 min; MS (ESI+) m/z for $C_{46}H_{44}Cl_2N_3O_9$ $[M+H]^+$ 852.2; found 852.5.

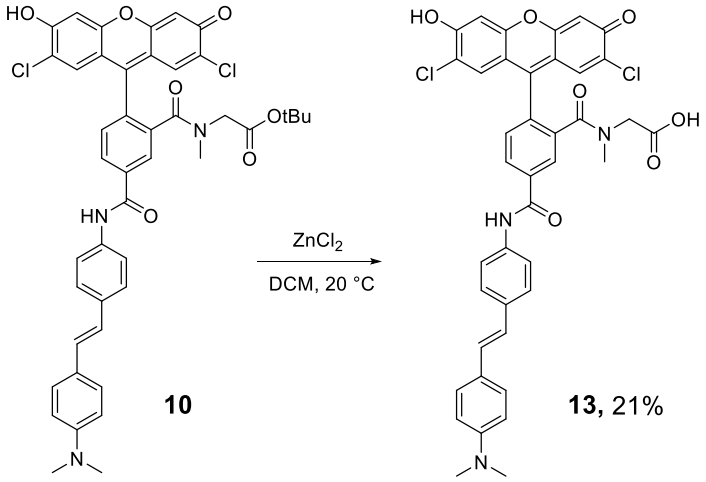

Synthesis of sarcAVF2.1.Cl, 13

A vial was charged with **10** (19 mg, 0.02 mmol) and $ZnCl_2$ (27 mg, 0.12 mmol). This was suspended in anhydrous dichloromethane (10 mL) and stirred at 20 °C for 12 hours. The reaction was concentrated *in vacuo*, then extracted with 2:1 dichloromethane:isopropanol, washing with water (3X) and brine. **13** was then purified by semi-preparative HPLC (40-70% MeCN in water +0.05% FA) to yield a red solid (3.8 mg, 21%)

Analytical HPLC retention time 9.93 min; MS (ESI+) m/z for $C_{40}H_{32}Cl_2N_3O_7$ $[M+H]^+$ 736.2; found 736.4.

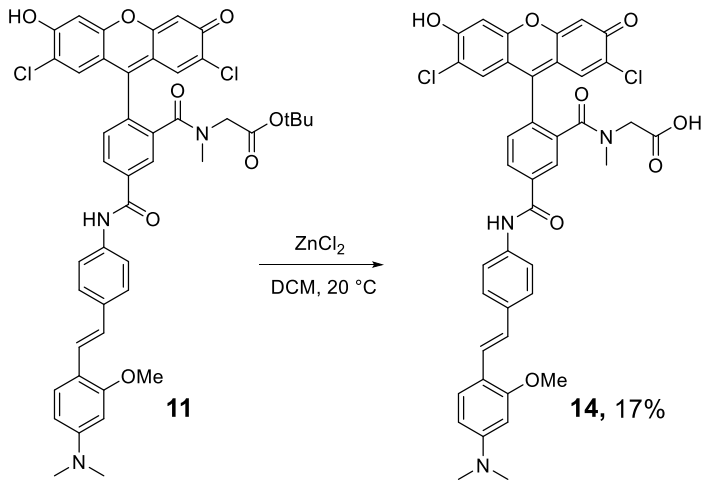

Synthesis of sarcAVF2.1.(OMe)Cl, 14

A vial was charged with **11** (3.6 mg, 4.4 µmol) and $ZnCl_2$ (4.9 mg, 0.02 mmol). This was suspended in anhydrous dichloromethane (10 mL) and stirred at 20 °C for 12 hours. The reaction was concentrated *in vacuo*, then extracted with 2:1 dichloromethane:isopropanol, washing with water (3X) and brine. **13** was then purified by semi-preparative HPLC (30-80% MeCN in water +0.05% FA) to yield a red solid (0.6 mg, 17%)

Analytical HPLC retention time 12.00 min; MS (ESI+) m/z for $C_{41}H_{34}Cl_2N_3O_8$ $[M+H]^+$ 766.2; found 766.2.

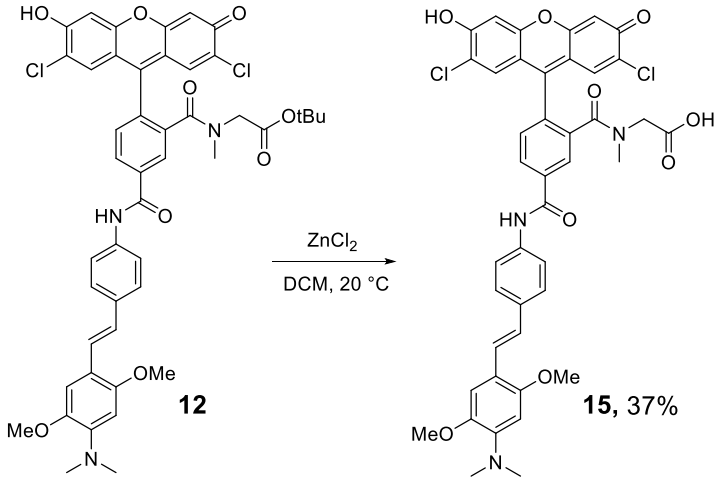

Synthesis of sarcAVF2.1.(diOMe)Cl, 15

A vial was charged with **12** (2.9 mg, 3.4 µmol) and $ZnCl_2$ (3.8 mg, 0.02 mmol). This was suspended in anhydrous dichloromethane (10 mL) and stirred at 20 °C for 12 hours. The reaction was concentrated *in vacuo*, then extracted with 2:1 dichloromethane:isopropanol, washing with water (3X) and brine. **13** was then purified by semi-preparative HPLC (30-80% MeCN in water +0.05% FA) to yield a red solid (1 mg, 37%)

Analytical HPLC retention time 5.49 min; MS (ESI+) m/z for $C_{42}H_{36}Cl_2N_3O_9$ $[M+H]^+$ 796.2; found 796.4.

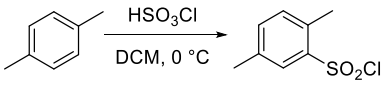

16, 93%

Synthesis of 2,5-dimethylbenzenesulfonyl chloride, 16

p-xylene (1.1 g, 10.6 mmol) was added to stirring anhydrous dichloromethane (10 mL) at 0 °C under a stream of N_2. HSO_3Cl (3 mL) was added dropwise before allowing the reaction to warm to room temperature and stir for 1 hour. This was then poured into ice water, extracted into dichloromethane, and washed with brine. Drying with $MgSO_4$ and concentration *in vacuo* produced **16** as a yellow oil (2 g, 93%)

^{1}H NMR (300 MHz, Chloroform-d) δ 7.87 (d, J = 1.8 Hz, 1H), 7.40 (dd, J = 8.1, 1.8 Hz, 1H), 7.29 (d, J = 7.7 Hz, 1H), 2.73 (s, 3H), 2.41 (s, 3H).

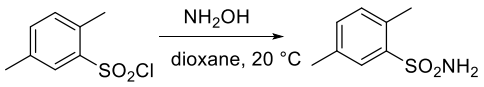

16 **17**, 81%

Synthesis of 2,5-dimethylbenzenesulfonamide, 17

16 (2 g, 9.9 mmol) was suspended in anhydrous dioxane (20 mL) and stirred at 0 °C. Ammonium hydroxide (20%w/v, 6.5 mL, 50 mmol) was added dropwise. This was stirred for 16 hours, allowing to warm to room temperature. **17** was extracted with ethyl acetate and washed with brine (2X), dried with $MgSO_4$, then concentrated to dryness *in vacuo* to yield a white solid (1.5 g, 81%).

^{1}H NMR (400 MHz, Chloroform-d) δ 8.58 (s, 2H), 7.95 (s, 1H), 7.74 (d, J = 10.3 Hz, 1H), 6.94 (s, 1H), 2.79 (s, 6H).

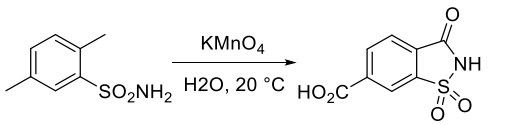

17 **18**, 82%

Synthesis of 6-carboxysaccharin, 18

17 (1 g, 5.3 mmol) was suspended in 0.5 M KOH (18 mL) at heated at 40 °C until dissolved. $KMnO_4$ (2.6 g, 16 mmol) was added and the reaction was stirred at 40 °C for 4.5 hours. MeOH (15 mL) was then used to dilute the reaction, then stirred for 1 hour at room temperature. This was basified to pH 8, then filtered over celite. The filtrate was concentrated to give an off-white powder (0.98 g, 82%).

^{1}H NMR (400 MHz, Methanol-d4) δ 7.93 (s, 1H), 7.37 (d, J = 7.8 Hz, 1H), 7.18 (d, J = 7.7 Hz, 1H).

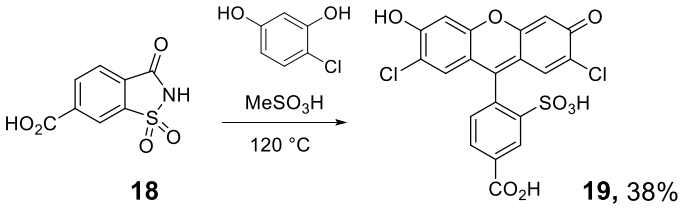

18 **19**, 38%

Synthesis of 4-(2,7-dichloro-6-hydroxy-3-oxo-3H-xanthen-9-yl)-3-sulfobenzoic acid, 19

6-carboxysaccharin **18** (0.5 g, 2.2 mmol) and 4-chlororesorcinol (0.64 g, 4.4 mmol) were combined in methanesulfonic acid (10 mL). This was stirred at 120 °C for 22 hours, then cooled and precipitated with diethyl ether (20 mL). An orange solid was collected by filtration, **19** (0.4 g, 38%).

^{1}H NMR (300 MHz, DMSO-d6) δ 8.08 – 8.03 (m, 1H), 7.78 (s, 1H), 7.38 (d, J = 8.0 Hz, 1H), 6.91 (s, 1H), 6.86 (s, 1H), 6.74 (s, 1H), 6.72 (s, 1H).

Analytical HPLC retention time 3.15 min; MS (ESI+) m/z for $C_{36}H_{27}Cl_2N_2O_7S$ $[M+H]^+$ 481.1; found 480.9

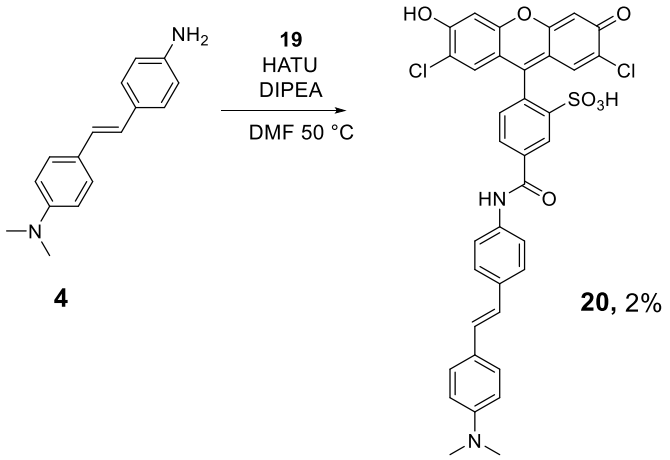

4 **20**, 2%

Synthesis of AVF2.1.Cl, 20

19 (50 mg, 0.1 mmol) and HATU (47 mg, 0.12 mmol) were combined in a vial, then dissolved in anhydrous DMF (0.5 mL) and diisopropylethylamine (0.05 mL). This was stirred for 30 minutes before addition of **4** (30 mg, 0.12 mmol). The reaction was then stirred at 50 °C for 4 hours. Reaction was cooled to room temperature and precipitated with diethyl ether (5 mL). The red precipitate was purified further by semi-preparative HPLC (30-80% MeCN in water + 0.05% trifluoroacetic acid) to yield **20** as a red solid (1.8 mg, 2%).

Analytical HPLC retention time 5.55 min; MS (ESI+) m/z for $C_{36}H_{27}Cl_2N_2O_7S$ $[M+H]^+$ 701.1; found 701.4.

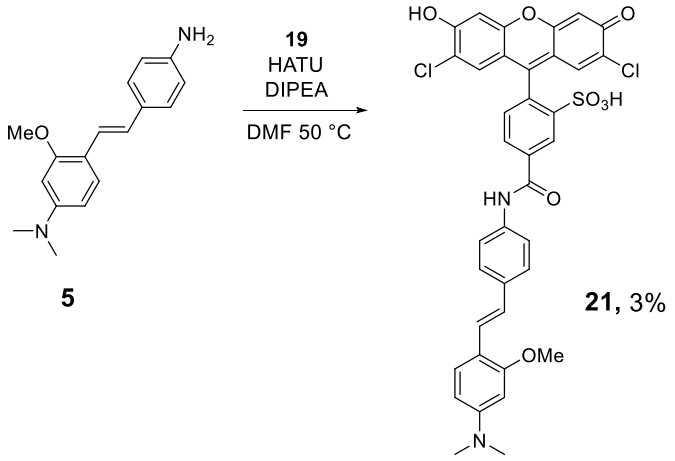

5 **21**, 3%

Synthesis of AVF2.1.(OMe)Cl, 21

19 (35 mg, 73 µmol) and HATU (68 mg, 0.18 mmol) were combined in a vial, then dissolved in anhydrous DMF (1 mL) and diisopropylethylamine (0.07 mL). This was stirred for 30 minutes before addition of **5** (30 mg, 0.12 mmol). The reaction was then stirred at 50 °C for 4 hours. Reaction was cooled to room temperature and precipitated with diethyl ether (5 mL). The red precipitate was purified further by semi-preparative HPLC (30-80% MeCN in water + 0.05% trifluoroacetic acid) to yield **21** as a red solid (1.5 mg, 3%).

Analytical HPLC retention time 6.43 min; MS (ESI+) m/z for $C_{37}H_{29}Cl_2N_2O_8S$ $[M+H]^+$ 731.1; found 731.3.

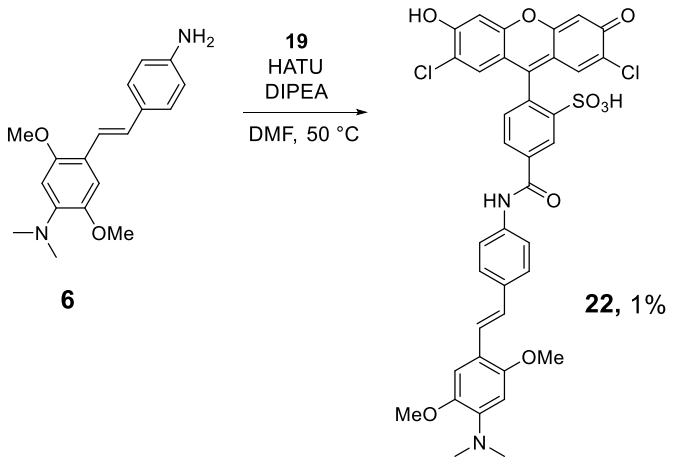

Synthesis of AVF2.1.(diOMe)Cl, 22

19 (50 mg, 0.10 mmol) and HATU (98 mg, 0.26 mmol) were combined in a vial, then dissolved in anhydrous DMF (1 mL) and diisopropylethylamine (0.09 mL). This was stirred for 30 minutes before addition of **6** (37 mg, 0.12 mmol). The reaction was then stirred at 50 °C for 4 hours. Reaction was cooled to room temperature and precipitated with diethyl ether (5 mL). The red precipitate was purified further by semi-preparative HPLC (10-50% MeCN in water + 0.05% trifluoroacetic acid) to yield **22** as a red solid (2 mg, 1%).

Analytical HPLC retention time 6.43 min; MS (ESI+) m/z for $C_{38}H_{31}Cl_2N_2O_9S$ $[M+H]^+$ 761.1; found 761.3.

1.6 Figures and schemes

Scheme 1-1. *Amide linkage modification to VoltageFluor scaffold*

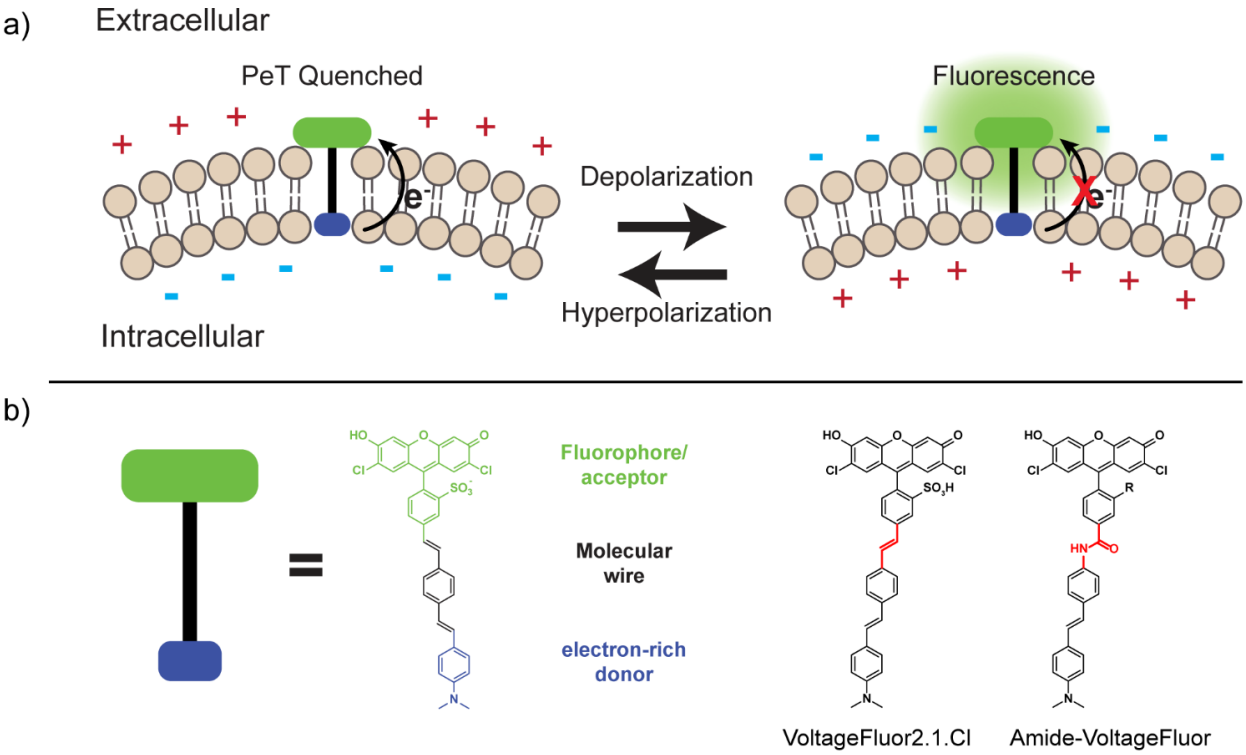

Scheme 1-1: Amide linkage modification to VoltageFluor scaffold

Scheme 1-2. *Synthesis of sarcosine-Amide VoltageFluor Dyes (sarcAVFs)*

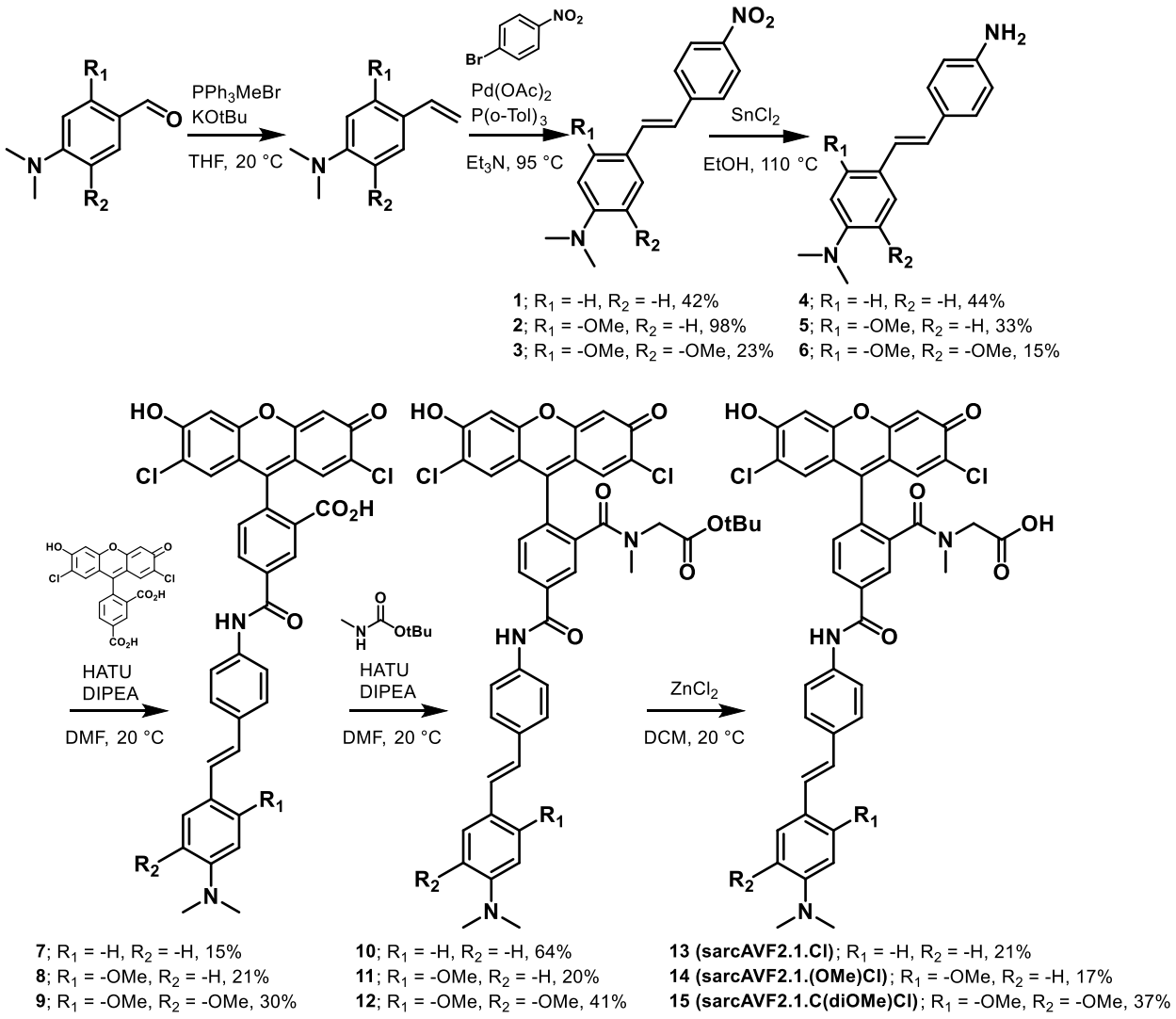

1; R_1 = -H, R_2 = -H, 42%
2; R_1 = -OMe, R_2 = -H, 98%
3; R_1 = -OMe, R_2 = -OMe, 23%
4; R_1 = -H, R_2 = -H, 44%
5; R_1 = -OMe, R_2 = -H, 33%
6; R_1 = -OMe, R_2 = -OMe, 15%

7; R_1 = -H, R_2 = -H, 15%
8; R_1 = -OMe, R_2 = -H, 21%
9; R_1 = -OMe, R_2 = -OMe, 30%
10; R_1 = -H, R_2 = -H, 64%
11; R_1 = -OMe, R_2 = -H, 20%
12; R_1 = -OMe, R_2 = -OMe, 41%
13 (sarcAVF2.1.Cl); R_1 = -H, R_2 = -H, 21%
14 (sarcAVF2.1.(OMe)Cl); R_1 = -OMe, R_2 = -H, 17%
15 (sarcAVF2.1.C(diOMe)Cl); R_1 = -OMe, R_2 = -OMe, 37%

Scheme 1-2: Synthesis of sarcosine-Amide VoltageFluor Dyes (sarcAVFs)

Scheme 1-3. *Synthesis of sulfonated Amide VoltageFluor Dyes (AVFs)*

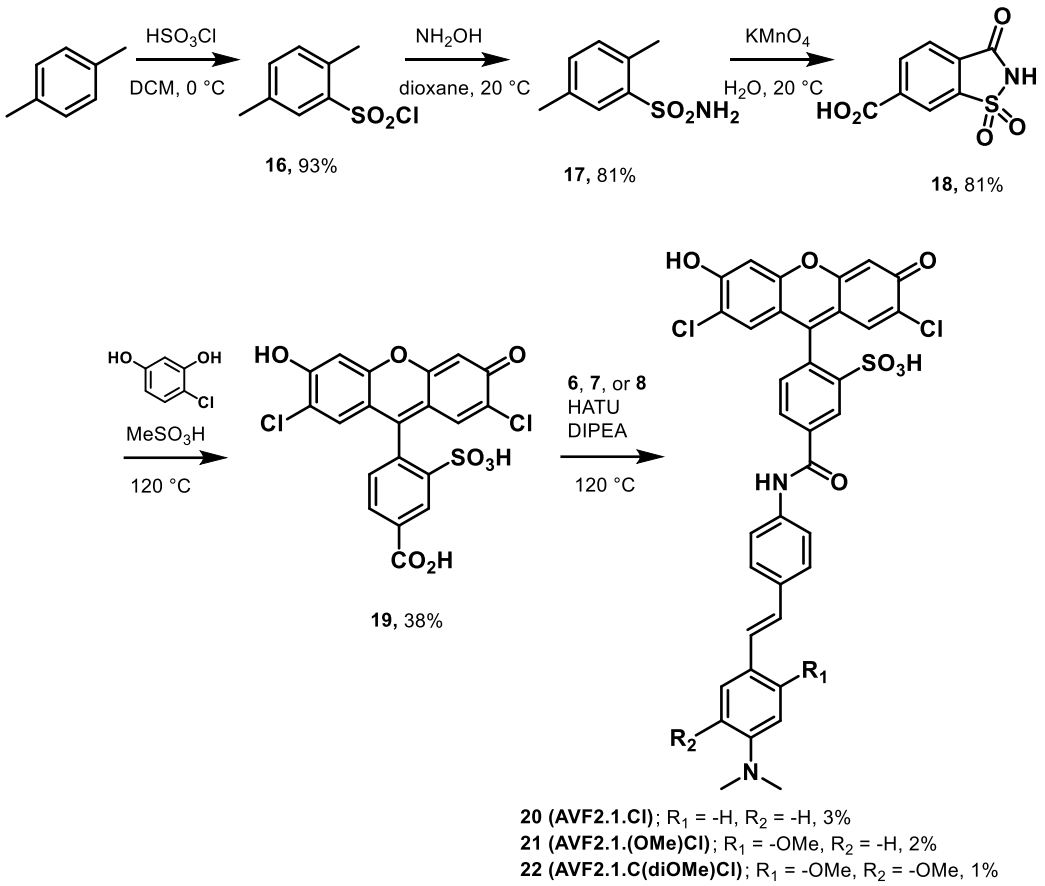

Scheme 1-3: Synthesis of sulfonated Amide VoltageFluor Dyes (AVFs)

Table 1-1. *Spectroscopic and voltage-sensing properties of amide-linked VoltageFluors*

Entry[a]	R_1	R_2	Absorbance [nm][a]	Emission [nm][a]	QY[a]	% $\Delta F/F$[b]	Loading [μM]
sarcAVF2.1.Cl (**13**)	-H	-H	515	533	0.28	8.6 ± 0.7	5.0
sarcAVF2.1.(OMe)Cl (**14**)	-OMe	-H	515	537	0.06	-	5.0
sarcAVF2.1.(diOMe)Cl (**15**)	-OMe	-OMe	517	531	0.21	-	5.0
AVF2.1.Cl (**20**)	-H	-H	511	530	0.19	16.3 ± 0.2	1.0
AVF2.1.(OMe)Cl (**21**)	-OMe	-H	512	530	0.08	9.3 ± 0.4	5.0
AVF2.1.(diOMe)Cl (**22**)	-OMe	-OMe	512	531	0.19	-	5.0
VF2.1.Cl[c]	-H	-H	522	535	0.06	27 ± 1	0.2

[a] Measured in PBS + 0.1% SDS (pH = 7.2). [b] per 100 mV. Recorded in HEK 293T cells at 0.5 kHz optical sampling rate. Error is ± SEM. [c] Literature reported values[6]

Figure 1-1. *Absorption and emission profiles of sarcosine amide-VoltageFluors (sarcAVFs)*

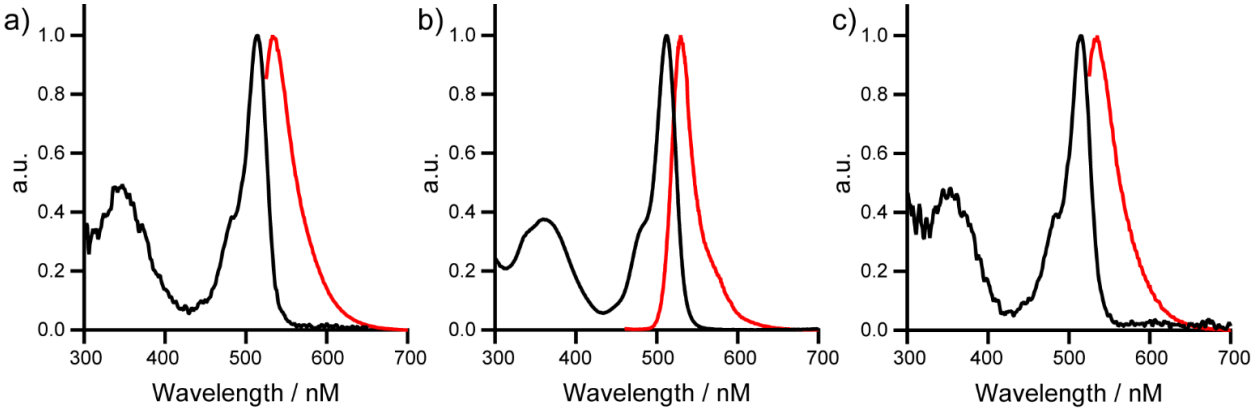

Figure 1-1: Absorption and emission profiles of sarcosine amide-VoltageFluors **13 [**sarcAVF2.1.Cl (a)], **14** [sarcAVF2.1.(OMe)Cl (b)], and **15** [sarcAVF2.1.(diOMe)Cl (c)]. Spectra were acquired at an indicator concentration of 1 µM in phosphate buffered saline (PBS) solution + 0.1% SDS.

Figure 1-2. *Membrane localization of sarcAVFs in HEK293T cells*

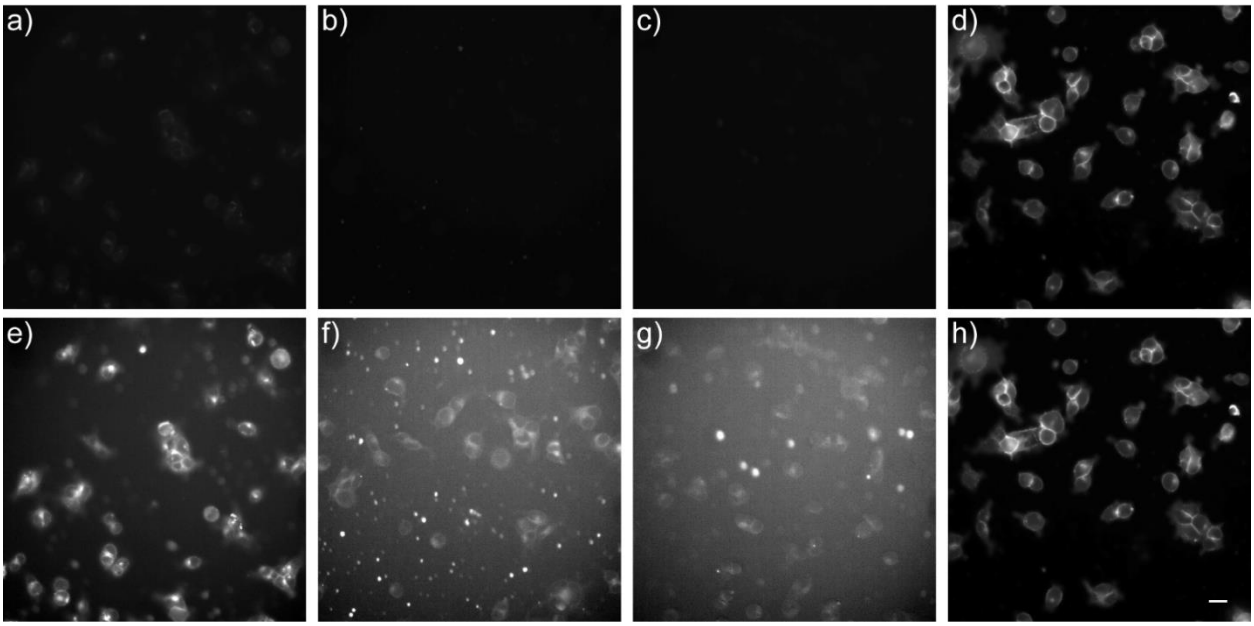

Figure 1-2: Membrane localization of sarcAVFs in HEK293T cells compared to VF2.1.Cl. Top row: epifluorescence micrographs of (a) sarcAVF2.1.Cl, (b) sarcAVF2.1.(OMe)Cl, and (c) sarcAVF2.1.(diOMe)Cl normalized to pixel intensity histogram of (d) VF2.1.Cl. Bottom row: the same micrographs with pixel intensity histograms adjusted to show membrane localization of each indicator. SarcAVFs were incubated in HEK293T cells in HBSS at a concentration 25 times greater (5 µM) than VF2.1.Cl (0.2 µM). Staining of sarcAVF2.1.Cl (a, e) appears more diffuse than VF2.1.Cl (d, h), suggesting this indicator is not restricted to the outer leaflet of the cell membrane. More electron rich indicators sarcAVF2.1.(OMe)Cl and sarcAVF2.1.(diOMe)Cl localize similarly, but are much dimmer and puncta are visible (f, g). Scale bar is 20 µm.

Figure 1-3. *Voltage sensitivity of sarcAVF2.1.Cl in HEK239T cells*

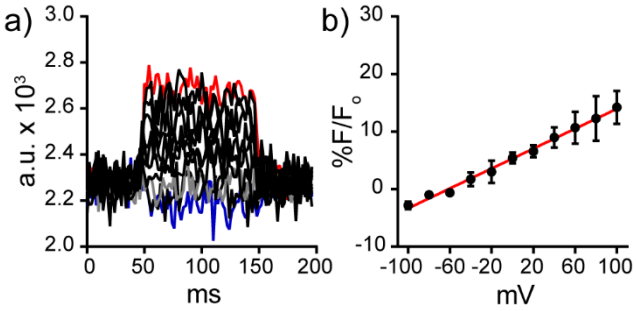

Figure 1-3: Voltage sensitivity of sarcAVF2.1.Cl in HEK239T cells under whole-cell voltage clamp. (a) The membrane potential of HEK293T cells stained with 5 µM sarcAVF2.1.Cl was manipulated between +100 mV (red trace) and -100 mV (blue) from a holding potential of -60 mV (grey) in 20 mV increments. Simultaneously recording the fluorescence of the membrane stain produced voltage steps that are concatenated to show the relative F/F_o. (b) Plot of $\%F/F_o$ versus the voltage-clamped mV step shows a linear response of 8.6%, averaged over two cell recordings. Error bars are ± SEM.

Figure 1-4. *Absorption and emission profiles of amide-VoltageFluors (AVFs)*

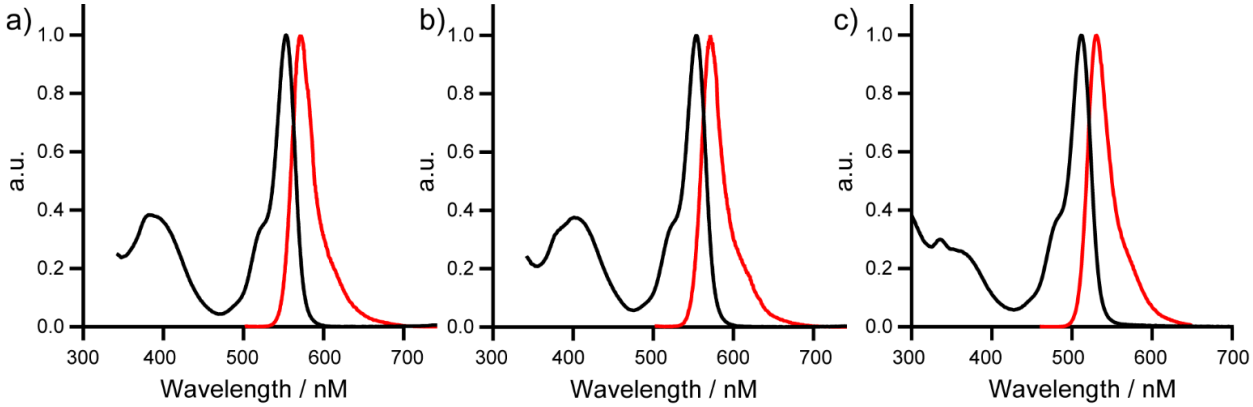

Figure 1-4: Absorption and emission profiles of amide-VoltageFluors **20** [AVF2.1.Cl (a)], **21** [AVF2.1.(OMe)Cl (b)], and **22** [AVF2.1.(diOMe)Cl (c)]. Spectra were acquired at an indicator concentration of 1 µM in phosphate buffered saline (PBS) solution + 0.1% SDS.

Figure 1-5. *Membrane localization of AVFs in HEK293T cells*

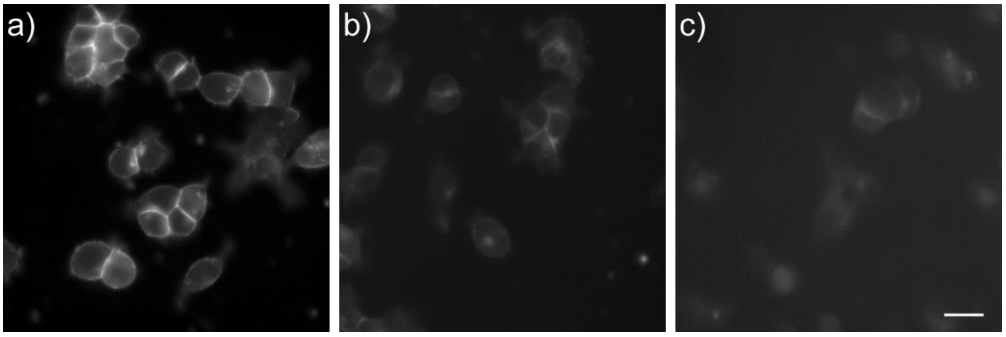

Figure 1-5: Membrane localization of AVFs in HEK293T cells. Epifluorescence micrographs of (a) AVF2.1.Cl (1 µM), (b) AVF2.1.(OMe)Cl (5 µM), and (c) AVF2.1.(diOMe)Cl (5 µM) show localized membrane signal. Similar to the sarcAVF scaffold, the more electron rich AVF indicators exhibit poorer membrane signal. Scale bar is 20 µm.

Figure 1-6. *Voltage sensitivity of AVF sensors in HEK239T cells*

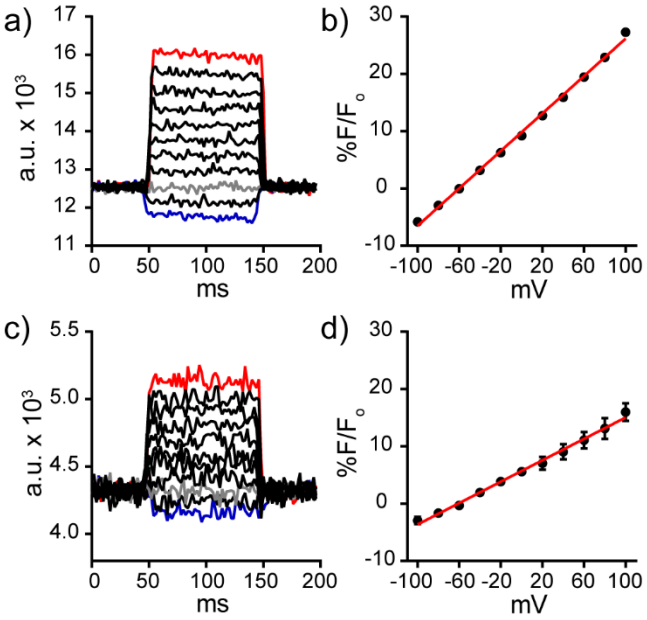

Figure 1-6: Voltage sensitivity of AVF2.1.Cl and AVF2.1(OMe)Cl in HEK239T cells under whole-cell voltage clamp. (a) The membrane potential of HEK293T cells stained with 1 µM AVF2.1.Cl was manipulated between +100 mV (red trace) and -100 mV (blue) from a holding potential of -60 mV (grey) in 20 mV increments. (b) Plot of $\%F/F_o$ versus the voltage-clamped mV step shows a linear response of 16.3%, averaged over 3 cell recordings. (c) Representative concatenated voltage trace of a HEK293T cell stained with 5 µM AVF2.1(OMe).Cl, manipulated with the same voltage-clamp protocol as (a). (d) Plot of $\%F/F_o$ versus the voltage-clamped mV step shows a linear response of 9.4%, averaged over 3 cell recordings. Error bars are ± SEM.

1.7 References

(1) Peterka, D. S.; Takahashi, H.; Yuste, R. Imaging Voltage in Neurons. *Neuron* **2011**, *69* (1), 9–21.

(2) Miller, E. W. Small Molecule Fluorescent Voltage Indicators for Studying Membrane Potential. *Curr. Opin. Chem. Biol.* **2016**, *33*, 74–80.

(3) Kulkarni, R. U.; Miller, E. W. Voltage Imaging : Pitfalls and Potential. *ACS Biochem.* **2017,** *56* (39), 5171-5177.

(4) Kulkarni, R. U.; Yin, H.; Pourmandi, N.; James, F.; Adil, M. M.; Schaffer, D. V.; Wang, Y.; Miller, E. W. A Rationally Designed, General Strategy for Membrane Orientation of Photoinduced Electron Transfer-Based Voltage-Sensitive Dyes. *ACS Chem. Biol.* **2017**, *12* (2), 407–413.

(5) Woodford, C. R.; Frady, E. P.; Smith, R. S.; Morey, B.; Canzi, G.; Palida, S. F.; Araneda, R. C.; Kristan, W. B.; Kubiak, C. P.; Miller, E. W.; et al. Improved PeT Molecules for Optically Sensing Voltage in Neurons. *J. Am. Chem. Soc.* **2015**, *137* (5), 1817–1824.

(6) Miller, E. W.; Lin, J. Y.; Frady, E. P.; Steinbach, P. A.; Kristan, W. B.; Tsien, R. Y. Optically Monitoring Voltage in Neurons by Photo- Induced Electron Transfer through Molecular Wires. *Proc. Natl. Acad. Sci. U. S. A.* **2011**, *109* (6), 2114–2119.

(7) Sjulson, L.; Miesenböck, G. Optical Recording of Action Potentials and Other Discrete Physiological Events: A Perspective from Signal Detection Theory. *Physiology (Bethesda).* **2007**, *22*, 47–55.

(8) Deal, P. E.; Kulkarni, R. U.; Al-Abdullatif, S. H.; Miller, E. W. Isomerically Pure Tetramethylrhodamine Voltage Reporters. *J. Am. Chem. Soc.* **2016**, *138* (29), 9085–9088.

Chapter 2:

Fluorene-Based Molecular Scaffolds for Fluorescent Voltage Indicators

Abstract

The ability to non-invasively monitor membrane potential dynamics in excitable cells like neurons and cardiomyocytes promises to revolutionize our understanding of the physiology and pathology of the brain and heart. Here, we report the design, synthesis, and application of a new class of fluorescent voltage indicators that make use of a fluorene-based molecular wire as a voltage-sensing domain to provide fast and sensitive measurements of membrane potential in both mammalian neurons and human-derived cardiomyocytes. We show that the best of the new probes, fluorene VoltageFluor 2 (fVF 2), readily reports on action potentials in mammalian neurons, detects perturbations to the cardiac action potential waveform in human induced pluripotent stem cell-derived cardiomyocytes, shows a substantial decrease in phototoxicity compared to existing molecular wire-based indicators, and can monitor cardiac action potentials for extended periods of time. Together, our results demonstrate the generalizability of a molecular wire approach to voltage sensing and highlight the utility of fVF 2 for interrogating membrane potential dynamics.

Portions of this work were published in *ACS Chemical Biology*:

Boggess, S. C.; Gandhi, S. S.; Siemons, B. A.; Huebsch, N.; Healy, K. E.; Miller, E. W. "New Molecular Scaffolds for Fluorescent Voltage Indicators" *ACS Chemical Biology* **2019**, *14*, 390-396.

Portions of this work were performed in collaboration with the following persons:

Synthesis of fVF 0 was assisted by Shivaani Gandhi

iPSC culture and cardiomyocyte differentiation were advised by Brian Siemons

2.1 Design of fluorene-based molecular wires for PeT-based voltage sensing

Optical methods for measuring biochemical and biophysical events in living cells provide a powerful approach for monitoring cellular physiology in a non-invasive and high-throughput manner. The success of such light-based ventures depends critically on the ability to design and construct molecules that change their optical properties, for example, color, fluorescence intensity, or lifetime, in response to changes in the cellular environment.[1] Fluorescence microscopy is one of the most commonly used modalities because it is operationally simple, the instrumentation is widely available, and an ever-growing library of small molecule fluorescent indicators exists to probe the dynamics of a host of cellular analytes, properties, and structures.[2–5] Of particular interest is the plasma membrane. Changes in the electrochemical potential across the lipid bilayer profoundly shape cellular physiology. Excitable cells employ a consortium of ion channels both to maintain tight control over their membrane potential (V_{mem}) and to initiate and propagate rapid changes in V_{mem}. Rapid changes in V_{mem} such as an action potential (AP) drive the unique physiology of excitable cells like neurons and cardiomyocytes. In neurons, APs evoke the release of the neurotransmitter into the synaptic cleft, and in heart tissue, waves of APs coordinate contraction and maintain regular rhythm. Disruption of the frequency, timing, and/or shape of APs is linked to serious human diseases ranging from epilepsy to long QT syndrome. Because of the importance of V_{mem} to both health and disease, robust methods for optically monitoring the membrane potential remain a critical complement to more traditional approaches. The gold standard for measuring V_{mem} and APs in live cells is electrophysiology: direct determination of V_{mem} through the physical interaction between the cell of interest and an electrode. Electrophysiology is highly invasive, low-throughput, and difficult to interpret in samples like cardiac tissue or cardiomyocyte monolayers, where electrical coupling between cells confounds single-cell measurement. Optical recording of the membrane potential using voltage-sensitive fluorescent indicators provides an attractive alternative to probing V_{mem} and AP dynamics in multiple cells, in monolayers, or three-dimensional tissue.[6]

Recently, we initiated a program to develop a new class of voltage-sensitive fluorescent indicators that utilize photoinduced electron transfer (PeT) as a rapid trigger to sense changes in V_{mem}.[7,8] These small molecule voltage-sensitive fluorophores, or VoltageFluors (VF dyes), combine a xanthene-based dye as a fluorescent reporter and a conjugated molecular wire that localizes the indicator to the cell membrane and facilitates PeT from an electron-rich aniline donor to the fluorophore within the low-dielectric environment of the lipid bilayer. Phenylene-vinylene (PV)-based conjugated molecular wires (**Scheme 2-1**, VF2.1.Cl)[9,10] are attractive because of their exceptionally low electron transfer attenuation values in donor−bridge−acceptor (DBA) systems ($\beta = 0.04$ Å^{-1}).[11,12] Within a PV wire framework, voltage sensitivity can be improved by altering the redox potentials of the fluorophore electron acceptor and the aniline electron donor.[13] Additionally, fluorophores such as rhodamine[9] and silicon-rhodamine[10] can be substituted for fluorescein, after some adjustment to the identity of the aniline donor. To date, we have not explored alterations to the identity of the molecular wire component of PeT-based voltage indicators. Now, we present a new class of PeT-based voltage-sensitive fluorescent indicators that use a 9,9-dimethyl-9H-fluorene monomer in place of the canonical 1,4-divinylbenzene moiety (**Scheme 2-1**). In other DBA scaffolds, 2,7-oligofluorene bridges effectively facilitate electron transfer across large distances and demonstrate low β values (0.09 Å^{-1}) comparable to values for

PV wires (0.04 $Å^{-1}$).[14] Because β values depend both on the identity of the wire and on the donor/acceptor pair,[15,16] we wanted to explore fluorene molecular wires as a platform for optical voltage sensing, demonstrating the generalizability of a PeT-based approach to voltage sensing. We now report the design, synthesis, characterization, and application of a new series of fluorene-based VoltageFluors, or fVF dyes.

2.2 Synthesis and characterization of fluorene VoltageFluors

The synthesis of fluorene-based voltage indicators starts with Suzuki−Mirayura cross-coupling of bromo-iodo-fluorene **1**[17] with either boronic ester **8**[18] or phenylboronic acid, providing monomeric fluorenes **2** and **3** as bright yellow solids (**Scheme 2-1**). Attachment to a sulfonated dichlorofluorescein was achieved by Pd-catalyzed cross-coupling of a pinacol boronic ester with the terminal aryl bromide to provide **4** and **5**. Suzuki−Mirayura cross-coupling yielded voltage indicator **6** (fVF 1) and indicator **7** (fVF 0), which lacks an aniline donor (**Scheme 2-1**). For the wires with electron-rich donors [**12** and **13** (**Scheme 2-2**)], transformation of the nitro group to an aniline was performed with tin(II) chloride to yield wires **14** and **15**. This was followed by reductive amination of formaldehyde with $NaCNBH_3$ to provide alkylated wires **16** and **17**. These were prepared via a method similar to that depicted in **Scheme 2-1** to yield electron-rich voltage indicators **20** (fVF 2) and **21** (fVF 3).

New fVF dyes have a λ_{max} centered around 520 nm and a second major absorption band around 340 nm arising from the fluorene molecular wire (**Figure 2-1**, **Figure 2-2**, and **Table 2-1**). Each fVF dye has a maximum emission around 535 nm, indicating little ground state interaction between the fluorene-based molecular wire and xanthene chromophore. fVF 1−3 have fluorescence quantum yields (Φ_{fl}, 0.05−0.19) that are lower than that of control indicator fVF 0 [0.77 (**Table 2-1)**].

To measure the voltage sensitivity of these indicators, we used whole cell voltage-clamp electrophysiology in tandem with epifluorescence microscopy. By applying voltage steps ranging from 100 to −100 mV in 20 mV increments to HEK293T cells stained with fluorene voltage indicators, we observe that indicators fVF 1−3 possess moderate sensitivity to changes in V_{mem}. Similar to PV-based molecular wire voltage indicators, fVF 1−3 become brighter in response to depolarizing (more positive) membrane potentials. The two most sensitive compounds, fVF 2 and 3, have sensitivities of 11 and 13% ΔF/F per 100 mV, respectively; however, fVF 2 has an overall signal that was much brighter in cells, resulting in a better signal-to-noise ratio (SNR) **(Figure 2-1**, **Figure 2-3**, and **Table 2-1**). fVF 1 is also very bright in cells but has a low SNR due to a low sensitivity (5% ΔF/F). Somewhat surprisingly, the electron-deficient compound fVF 0 [**7** (**Scheme 2-1**)] exhibits a small amount of voltage sensitivity, −0.3% ΔF/F per 100 mV, becoming less fluorescent in response to depolarizing potentials (**Figure 2-4**, **Table 2-1**), a behavior that is the opposite of that of every molecular wire indicator synthesized in our laboratory. We chose to characterize fVF 2 in subsequent experiments due to its brightness and superior SNR.

fVF 2 readily detects fast changes in membrane potential in mammalian neurons. In cultured rat hippocampal neurons, fVF 2 gives clear membrane staining (**Figure 2-1e**) and faithfully records evoked action potentials with an average ΔF/F of 5.1% and SNR of 21:1 [n = 54 spikes (**Figure 2-1f**, **Figure 2-5**, **Table 2-2**)]. fVF 2 clearly resolves spontaneous activity in cultured rat hippocampal neurons (**Figure 2-6**). Despite the lower nominal voltage sensitivity of fVF 2 relative

to a first-generation VoltageFluor dye [VF2.1.Cl, 27% ΔF/F per 100 mV in HEK cells,[7] 10% ΔF/F and a SNR of 43:1 in evoked action potentials; n = 54 spikes (**Figure 2-5**)], the improved brightness of fVF 2 relative to VF2.1.Cl [1.2 times brighter in neurons (**Table 2-2**)] makes it useful for recording action potentials in neurons. When we evaluate fVF 2 against an electrochromic VSD with a similar voltage sensitivity, di-4-ANEPPS, we observe evoked spikes with a ΔF/F of −1% and a SNR of 15:1. However, a 5-fold higher concentration was needed to make these recordings (**Figure 2-5** and **Table 2-2**). In addition to reporting on neuronal activity, we detect no changes to neuronal membrane properties or action potential kinetics when comparing the electrophysiological parameters of neurons in the absence or presence of fVF2 (**Figure 2-7** and **Table 2-3**).

2.3 Optical measurement of cisapride cardiotoxicity using fVF 2

We sought to use fVF 2 for optical measurements of cardiac AP waveforms to provide a holistic assessment of drug cardiotoxicity in vitro, a major goal of the Comprehensive in vitro Proarrhythmic Assay (CiPA) initiative.[19–21] We cultured hiPSC-CM monolayers and tested the ability of fVF 2 to report cardiac AP waveforms in spontaneously beating monolayers.[21–25] fVF 2 clearly stains the sarcolemma of hiPSC-CMs and faithfully reports ventricular-like AP waveforms, showing a large increase in fluorescence just before contraction of the monolayer (**Figure 2-8a−e**). Using methods previously described,[26] we calculate the action potential duration (APD) for each AP waveform in the fluorescence trace at 70, 50, and 10% of the maximum depolarization (APD30, APD50, and APD90, respectively).[26–28] To correct for APD variation arising from the difference in beat rate from spontaneously beating monolayers, we used Fridericia's formula to provide a beat-rate corrected APD (cAPD).[28,29] From our optical measurements, we calculated cAPD90 values from 500 to 700 ms in spontaneously beating monolayers after 14 days in culture, consistent with previous reports for hiPSC-CMs.[27,30]

To demonstrate the utility of fVF 2 for parsing the pharmacological effects of drug treatment on cardiomyocytes, we treated hiPSC cardiomyocytes with cisapride. Cisapride, formally a useful gastroprokinetic agent, was withdrawn from the U.S. market in 2000 due to its connection to torsades de pointes (TdP) induced by acquired long QT syndrome caused by blockage of $K_v11.1$.[31] Cisapride is also one of 12 training and calibration compounds used in the CiPA initiative.[20,32] The observation of cardiomyocyte monolayers treated acutely with cisapride results in several phenotypic alterations to cardiac AP, which can be readily detected by fVF 2. At a concentration of 300 nM, we saw three different manifestations of the effect of prolonged cAPD caused by I_{Kr} blockade:[33,34] an extended phase 3 (**Figure 2-8g**), a tachycardia-like train of drastically shortened APs (**Figure 2-8h**), and the appearance of early after depolarizations (EADs) (**Figure 2-8i**). $K_v11.1$/hERG channel blockade results in action potential prolongation (**Figure 2-8g**), which has been connected to a higher risk of TdP and higher arrhythmogenic potential. The rapid, subthreshold spiking activity may be analogous to tachycardia,[35] which was accompanied by a loss of monolayer automaticity (**Figure 2-8h**). The appearance of EADs (**Figure 2-8i**) corresponds to the observed cAPD prolongation and significantly increases the risk of arrhythmia and TdP.

2.4 Phototoxicity of PeT voltage dyes in cardiomyocyte monolayers

Monitoring the effect of potentially cardiotoxic drug relies on the ability to make stable, long-term recordings from cardiomyocytes. When using voltage-sensitive fluorescent indicators, this

often requires careful titration of illumination intensity and indicator concentration to minimize phototoxicity.[35–37] Therefore, we were pleased that fVF 2 displays lower phototoxicity in hiPSC-CMs relative to VF2.1.Cl, which itself requires a light power an order of magnitude lower than that of di-4-ANEPPS, thereby avoiding phototoxic effects.[37] Others note phototoxic effects of di-4-ANEPPS can begin within seconds of illumination.[38] We stained hiPSC-CM monolayers with either fVF 2 or VF2.1.Cl and continuously illuminated them for 10 min and optically recorded membrane potential dynamics every minute. Despite the initial photobleach of fVF 2 (**Figure 2-9a and Figure 2-3i**), the shapes of recorded action potentials (**Figure 2-9c**), SNR (**Figure 2-9e**), and action potential duration (**Figure 2-9f,g**) remain relatively constant (**Figure 2-9cd and Figure 2-10**). In sharp contrast, however, VF2.1.Cl had a dramatic, detrimental impact on cardiomyocyte function. Although VF2.1.Cl initially has a high SNR compared to that of fVF 2 (**Figure 2-9b,e**), the SNR drops quickly after the first minute of illumination (**Figure 2-9b,e**), and both action potential shape (**Figure 2-9d**) and duration (**Figure 2-9f,g**) undergo substantial and significant changes, as early as 2 min into illumination (**Figure 2-9b,d,f,g**). Even after 4 min, only subthreshold activity was recorded with VF2.1.Cl and required an automated analysis script to detect these events (**Figure 2-10h**). After 5 min, monolayers imaged with VF2.1.Cl cease to contract (**Figure 2-9d and Figure 2-10**). However, monolayers imaged with fVF 2 continue to beat even after continuous illumination for 10 min (**Figure 2-9c and Figure 2-10**). Increasing the illumination intensity from 9 to 29 mW/mm2 when making recordings with fVF 2 did not alter cAPD (**Figure 2-10**). Toxicity requires both dye and illumination, as regions of the coverslip not exposed to illumination light beat properly, in the case of fVF 2 (**Figure 2-11**). For VF2.1.Cl, we observe a small increase in cAPD values, which was not statistically significant (**Figure 2-11**). Together, these results suggest that fVF 2 has a phototoxicity that is lower than that of VF2.1.Cl and can be used to measure activity in cardiomyocyte monolayers for prolonged periods of time. Previous reports note slight differences in the structure of transmembrane probes can explain differences in phototoxicity.[38] Experiments are underway to probe the precise molecular mechanisms underlying the faster photobleaching but reduced phototoxicity of fVF 2 compared to that of VF2.1.Cl.

2.5 Determining IC_{50} of cisapride from optical voltage measurements

To assess the ability of fVF 2 to measure changes to cardiac electrophysiology in response to chronic drug treatment, we calculated IC_{50} values for cisapride using in-well dose escalation with optical recording of cAPD. Measurements were taken after incubation with increasing cisapride concentrations in each well from 0.1 to 300 nM. Our optical measurements show an increase in cAPD90 (IC_{50} = 10.6 nM; 14 days in culture) to 300 nM cisapride (**Figure 2-12e,f**), which is in the range of IC_{50} values previously measured for cisapride in other in vitro studies (**Table 2-4**).[32] We also observe an increase in cAPD50 to 100 nM but a decrease at higher concentrations of cisapride. Similarly, the measured cAPD30 seems to vary little from that of the dimethyl sulfoxide vehicle control; however, a decrease is detected at higher concentrations of cisapride (**Figure 2-12e,f**). Together, these results demonstrate the ability to fVF 2 to enable the rapid assembly of dose−response data in hiSPCs using an all-optical approach.

2.6 Conclusions and outlook

In summary, we present the design, synthesis, and application of a new class of molecular wire-based fluorescent indicators. We show, for the first time, that fluorene-based molecular wires provide a platform for PeT-based voltage sensing. In general, these fluorene-based indicators have lower nominal voltage sensitivities (ΔF/F per 100 mV of 5−13% in HEK cells, compared to approximately 27% for VF2.1.Cl) to changes in membrane potential but are brighter than their phenylene-vinylene counterparts. fVF 2 exhibits adequate sensitivity and excellent brightness in cells for reporting AP waveforms in neurons and cardiomyocytes with high SNRs. More importantly, fVF 2 displays a substantially reduced phototoxicity in cardiomyocytes relative to that of VF2.1.Cl, allowing for prolonged, continuous measurement of cardiomyocyte activity. Fluorene-based molecular wires may provide an attractive, general solution to the phototoxicity often associated with voltage-sensitive fluorescent indicators.

2.7 Materials and methods

2.7.1 General method for chemical synthesis and characterization

Chemical reagents and solvents (dry) were purchased from commercial suppliers and used without further purification. References to previously synthesized compounds are provided along with characterization data. Thin layer chromatography (TLC) (Silicycle, F254, 250 μm) and preparative thin layer chromatography (PTLC) (Silicycle, F254, 1000 μm) was performed on glass backed plates pre-coated with silica gel and were visualized by fluorescence quenching under UV light. Flash column chromatography was performed on Silicycle Silica Flash F60 (230–400 Mesh) using a forced flow of air at 0.5–1.0 bar. NMR spectra were measured on Bruker AVB-400 MHz, 100 MHz, AVQ-400 MHz, 100 MHz, Bruker AV-600 MHz, 150 MHz. NMR spectra measured on Bruker AVII-900 MHz, 225 MHz, equipped with a TCI cryoprobe accessory, were performed by Dr. Jeffrey Pelton (QB3). Chemical shifts are expressed in parts per million (ppm) and are referenced to $CDCl_3$ (7.26 ppm, 77.0 ppm) or DMSO (2.50 ppm, 40 ppm). Coupling constants are reported as Hertz (Hz). Splitting patterns are indicated as follows: s, singlet; d, doublet; t, triplet; q, quartet; dd, doublet of doublet; m, multiplet. High-resolution mass spectra (HR-ESI-MS) were measured by the QB3/Chemistry mass spectrometry service at University of California, Berkeley. High performance liquid chromatography (HPLC) and low resolution ESI Mass Spectrometry were performed on an Agilent Infinity 1200 analytical instrument coupled to an Advion CMS-L ESI mass spectrometer. The column used for the analytical HPLC was Phenomenex Luna 5 μm C18(2) (4.6 mm I.D. × 75 mm) with a flow rate of 1.0 mL/min. The mobile phases were MQ-H2O with 0.05% trifluoroacetic acid (eluent A) and HPLC grade acetonitrile with 0.05% trifluoroacetic acid (eluent B). Signals were monitored at 254, 350 and 480 nm over 10 min with a gradient of 10-100% eluent B unless otherwise noted. Ultra-high performance liquid chromatography (UHPLC) for purification of final compounds was performed using a Waters Acquity Autopurificaiton system equipped with a Waters XBridge BEH 5 μm C18 column (19 mm I.D. x 250 mm) with a flow rate of 30.0 mL/min, made available by the Catalysis Facility of Lawrence Berkeley National Laboratory (Berkeley, CA). The mobile phases were MQ-H2O with 0.05% trifluoroacetic acid (eluent A) and HPLC grade acetonitrile with 0.05% trifluoroacetic acid (eluent B). Signals were monitored at 254 and 350 nm over 20 min with a gradient of 10-100% eluent B, unless otherwise noted.

2.7.2 Spectroscopic studies

Stock solutions of fluorene VoltageFluors were prepared in DMSO (500 µM) and diluted with PBS (10 mM KH2PO4, 30 mM Na2HPO4·7H2O, 1.55 M NaCl, pH 7.2) solution containing 0.10 % (w/w) SDS (1:1000 dilution). UV-Vis absorbance and fluorescence spectra were recorded using a Shimadzu 2501 Spectrophotometer (Shimadzu) and a Quantamaster Master 4 L-format scanning spectrofluorometer (Photon Technologies International). The fluorometer is equipped with an LPS-220B 75-W xenon lamp and power supply, A-1010B lamp housing with integrated igniter, switchable 814 photon-counting/analog photomultiplier detection unit, and MD5020 motor driver. Samples were measured in 1-cm path length quartz cuvettes (Starna Cells).

Relative quantum yields (Φ_{Fl}) were calculated by comparison to fluorescein (Φ_{Fl} = 0.93 in 0.1 M NaOH) and rhodamine 6G (Φ_{Fl} = 0.95 in ethanol) as references.[39] Briefly, stock solutions of standards were prepared in DMSO (0.25-1.25 mM) and diluted with appropriate solvent (1:1000 dilution). Absorption and emission (excitation = 485 nm) were taken at 5 concentrations. The absorption value at the excitation wavelength (485 nM) was plotted against the integration of the area of fluorescence curve (495-675 nm). For fluorescein, the integration of the area of the fluorescence curve was also taken with an excitation at 450 nm. The area from 460-675 nm and 495-675 nm was used to extrapolate the area of the fluorescence curve with an excitation at 485 nm. This ensured the full fluorescence area of fluorescein excited at 485 nm was used for Φ_{Fl} calculations. The slope of the linear best fit of the data was used to calculate the relative Φ_{Fl} by the equation $\Phi_{Fl(X)} = \Phi_{Fl(R)}(S_R/S_X)(\eta_X/\eta_R)^2$, where S_R and S_X are the slopes of the reference compound and unknown, respectively, and η is the refractive index of the solution. This method was validated by cross-referencing the reported Φ_{Fl} values of fluorescein and rhodamine 6G to the calculated Φ_{Fl} using the one standard as a reference for the other and vice versa. Calculated Φ_{Fl} within 10% of the reported value for both standards ensured that Φ_{Fl} calculated for fluorene VoltageFluors was reliable within 10% error.

2.7.3 Cell culture

All animal procedures were approved by the UC Berkeley Animal Care and Use Committees and conformed to the NIH Guide for the Care and Use and Laboratory Animals and the Public Health Policy.

Human embryonic kidney (HEK) 293T cells

Cells were acquired from the UC Berkeley Cell Culture Facility. Cells were passaged and plated onto 12 mm glass coverslips coated with Poly-D-Lysine (PDL; 1 mg/mL; Sigma-Aldrich) to a confluency of ~15% and 50% for electrophysiology and imaging, respectively. HEK293T cells were plated and maintained in Dulbecco's modified eagle medium (DMEM) supplemented with 4.5 g/L D-glucose, 10% fetal bovine serum (FBS), and 1% Glutamax.

Rat hippocampal neurons.

Hippocampi were dissected from embryonic day 18 Sprague Dawley rats (Charles River Laboratory) in cold sterile HBSS (zero Ca^{2+}, zero Mg^{2+}). All dissection products were supplied by Invitrogen, unless otherwise stated. Hippocampal tissue was treated with trypsin (2.5%) for 15 min at 37 °C. The tissue was triturated using fire polished Pasteur pipettes, in minimum essential media

(MEM) supplemented with 5% fetal bovine serum (FBS; Thermo Scientific), 2% B-27, 2% 1M D-glucose (Fisher Scientific) and 1% Glutamax. The dissociated cells were plated onto 12 mm diameter coverslips (Fisher Scientific) pre-treated with PDL (as above) at a density of 30-40,000 cells per coverslip in MEM supplemented media (as above). Neurons were maintained at 37 °C in a humidified incubator with 5 % CO2. At 1 day in vitro (DIV) half of the MEM supplemented media was removed and replaced with Neurobasal media containing 2% B-27 supplement and 1% glutamax. Electrophysiological experiments which were performed on 12-15 DIV neurons. Unless stated otherwise, for loading of HEK cells and hippocampal neurons, fluorene VoltageFluors were diluted in DMSO to 500 μM, and then diluted 1:1000 in HBSS. Imaging experiments were performed in HBSS.

Differentiation of hiPSC into cardiomyocytes and culture.

hiPSCs were cultured on Matrigel (1:100 dilution; Corning)-coated 6 well-plates in E8 medium. When the cell confluency reached 80–90%, which is referred as day 0, the medium was switched to RPMI 1640 medium (Life Technologies) containing B27 minus insulin supplement (Life Technologies) and 10 μM CHIR99021 GSK3 inhibitor (Peprotech). At day 1, the medium was changed to RPMI 1640 medium containing B27 minus insulin supplement only. At day 2, medium was replaced to RPMI 1640 medium containing B27 supplement without insulin, and 5 μM IWP4 (Peprotech) for 2 days without medium change. On day 4, medium was replaced to RPMI 1640 medium containing B27 minus insulin supplement for 2 days without medium change. On day 6 and 7, medium was replaced to a serum-free medium - RPMI 1640 containing B27 with insulin supplement. After day 7, the medium was changed every other day. Confluent contracting sheets of beating cells appear between days 7 to 15 and are ready for dissociation after this time.

Confluent sheets were dissociated with 0.25% trypsin-EDTA (8-30 minutes, depending on density and quality of tissue) and plated onto Matrigel (1:100)-coated Ibidi ® 24 well μ-plates (cat no. 82406**)** in RPMI 1640 medium containing B27 supplement (containing insulin). Medium was changed every 3 days until imaging. For loading hiPSC cardiomyocytes, fluorene VoltageFluors were diluted in DMSO to 1 mM, and then diluted 1:1000 in RPMI 1640 with B27 supplement minus Phenol Red. Imaging experiments were performed in RPMI 1640 with B27 supplement minus Phenol Red.

2.7.4 Imaging parameters

For HEK293T cells and rat hippocampal neurons, Epifluorescence imaging was performed on an AxioExaminer Z-1 (Zeiss) equipped with a Spectra-X Light engine LED light (Lumencor), controlled with Slidebook (v6, Intelligent Imaging Innovations). Images were acquired with either a W-Plan-Apo 20x/1.0 water objective (20x; Zeiss) or a W-Plan-Apo 63x/1.0 water objective (63x; Zeiss). Images were focused onto either an OrcaFlash4.0 sCMOS camera (sCMOS; Hamamatsu) or an eVolve 128 EMCCD camera (EMCCD; Photometrix).

Inverted epifluorescence imaging of hiPSC cardiomyocytes was performed on an AxioObserver Z-1 (Zeiss), equipped with a Spectra-X Light engine LED light (Lumencor), controlled with μManager (V1.4, open-source, Open Imaging).[40,41] Images were acquired using a Plan-Apochromat 20/0.8 air objective (20x, Zeiss). Images were focused onto an OrcaFlash4.0 sCMOS camera (sCMOS; Hamamatsu).

More detailed imaging information for each experimental application is expanded below.

Membrane staining and photostability in HEK293T cells

HEK293T cells were incubated with a HBSS solution (Gibco) containing fluorene VoltageFluors (500 nM) at 37°C for 20 min prior to transfer to fresh HBSS (no dye) for imaging. Microscopic images were acquired with a W-Plan-Apo 20x/1.0 water objective (Zeiss) and OrcaFlash4.0 sCMOS camera (Hamamatsu). For fluorescence images, the excitation light was delivered from a LED (20.9 mW/mm^2; 100 ms exposure time) at 475/34 (bandpass) nm and emission was collected with an emission filter (bandpass; 540/50 nm) after passing through a dichroic mirror (510 nm LP).

For photostability experiments HEK cells were incubated separately with fVF 2 (500 nM) and VF2.1.Cl (500 nM) in HBSS at 37°C for 20 min. Data were acquired with a W-Plan-Apo 63x/1.0 objective (Zeiss) and Evolve 128 EMCCD camera (Photometrics). Images (pixel size 0.38 μm × 0.38 μm) were taken every 1 second for 2.5 minutes with constant illumination of LED (46.8 mW/mm^2; 50 ms exposure time). The obtained fluorescence curves (background subtracted) were normalized with the fluorescence intensity at t = 0 and averaged (five different cells of each dye).

Voltage sensitivity in HEK293T cells

Functional imaging of the fluorene VoltageFluors was performed using a 20x water immersion objective paired with image capture from the EMCCD camera at a sampling rate of 0.5 kHz. Fluorene VoltageFluors were excited using the 475 nm LED with an intensity of 20.9 mW/mm^2. For initial voltage characterization emission was collection with the emission filter and dichroic listed above.

Evoked and spontaneous activity in rat hippocampal neurons

Extracellular field stimulation was delivered by a Grass Stimulator connected to a recording chamber containing two platinum electrodes (Warner), with triggering provided through a Digidata 1332A digitizer and pCLAMP 10 software (Molecular Devices). Action potentials were triggered by 1 ms 80 V field potentials delivered at 5 Hz. To prevent recurrent activity the HBSS bath solution was supplemented with synaptic blockers 10 μM 2,3-Dioxo-6-nitro-1,2,3,4-tetrahydrobenzo[f]quinoxaline-7-sulfonamide (NBQX; Santa Cruz Biotechnology) and 25 μM DL-2-Amino-5-phosphonopentanoic acid (APV; Sigma-Aldrich). Functional imaging was performed using the sCMOS camera and a 20x water objective. fVF 2 and VF2.1.Cl (500 nM in HBSS) were excited with a 475/34 (bandpass) nm LED with an intensity of 6.9 mW/mm^2 and emission was collected with an emission filter (bandpass; 540/50 nm) after passing through a dichroic mirror (510 nm LP). Di-4-ANNEPS (2.5 μM in HBSS, incubated for 10 minutes at 25 °C) was excited with an LED (bandpass; 475/34 nm; 6.9 mW/mm^2) and emission was collected with an emission filter (bandpass; 650/60 nm) after passing through a dichroic mirror (594 nM LP). **(Figure 2-5).**

Spontaneous activity from neurons (**Figure 2-6**) was obtained using the sCMOS camera with a 20x objective. fVF 2 was excited using the 475 nm LED with an intensity of 6.9 mW/mm^2 and emission was collected with the filter and dichroic listed above. Images were binned 4x4 to allow sampling rates of 0.5 kHz.

Voltage recordings of hiPSC cardiomyocytes and assessment of phototoxicity

Functional recordings of fVF 2 (1µM) were performed using a 20x air objective paired with a sCMOS camera at a sampling rate of 0.2 kHz (used 4x4 binning and restricted to a 512x125 pixel frame for high-speed acquisition over long periods). fVF 2 was excited at 475/34 (bandpass) nm with an intensity of 9.0 mW/mm^2 and emission was collected with an emission filter (bandpass; 540/50 nm) after passing through a dichroic mirror (510 nm LP). Typical recordings were made for ten seconds.

Phototoxicity of VoltageFluor dyes was assessed in cardiomyocyte monolayers incubated with 1 µM of fVF 2 or VF2.1.Cl. These were exposed to constant illumination from the excitation LED (475/34; bandpass) for up to ten minutes, while typical ten second fluorescence recordings were made at the beginning of each minute. For monolayers incubated with VF2.1.Cl, recordings were halted when a loss of automaticity (spontaneous beating) was observed. (**Figure 2-9, Figure 2-10**). The phototoxicity of fVF 2 was further assessed in relation to increasing power of the excitation source. Ten second recordings were taken after illumination of the region for one minute, using different regions of the monolayer for each recording. Excitation intensity was raised from 9.0 to 28.9 mW/mm^2. (**Figure 2-10**).

2.7.5 Image analysis

Analysis of voltage sensitivity in HEK293T cells was performed using ImageJ (FIJI). Briefly, a region of interest (ROI) encompassing the cell body was selected and average fluorescence intensity was calculated for each frame. For background subtraction, a ROI encompassing a region without cells was selected and the average pixel intensity was calculated for each frame. A linear fit to the background trace was calculated and applied to the background, and this was used to subtract background signal from the fluorescence intensity trace. F/F_o values were calculated by dividing the background subtracted trace by the median value of fluorescence when the cell is held at -60 mV. $\Delta F/F$ values were calculated by plotting the change in fluorescence (ΔF) vs the applied voltage step and finding the slope of a linear best-fit. For analysis of voltage responses in neurons, regions of interest encompassing cell bodies were drawn in ImageJ and the mean fluorescence intensity for each frame extracted. $\Delta F/F$ values were calculated by first subtracting a mean background value from all raw fluorescence frames, bypassing the noise amplification which arises from subtracting background for each frame, to give a background subtracted trace. A baseline fluorescence value is calculated either from the first several (10-20) frames of the experiment for evoked activity, or from the median for spontaneous activity, and was subtracted from each timepoint of the background subtracted trace to yield a ΔF trace. The ΔF was then divided by baseline fluorescence value to give $\Delta F/F$ traces. No averaging has been applied to any voltage traces.

Analysis of action potential (AP) data from hiPSC cardiomyocytes was performed using in-house MATLAB scripts based on previously developed software by the Efimov lab (Washington University, St. Louis, MO).[26] Scripts are available upon request. Briefly, raw OME-tiffs recorded in µManager was read directly into MATLAB for batch-processing of large datasets (>30 Gb per experiment). The mean pixel intensity of the entire image (512x125 pixels) was calculated for each frame and a mean fluorescence trace was extracted for the entire stack. Photobleach correction was performed by subtracting an asymmetric least-squares fit of the data from the mean trace.[42] No

subtraction of background was possible due to staining of the entire monolayer. Individual AP events were identified through threshold detection based on a Schmidtt trigger. Action potential duration (APD) values were calculated for each AP by finding the activation time (time of the maximum derivative of the AP upstroke) and the time the signal returns to 70, 50, and 10% of the maximum depolarization (APD30, APD50, APD90, respectively). APD values were corrected for variation due to spontaneous beat rate by Fridericia's formula (Eq. 2-1). CL is the cycle length, calculated as the time period from the beginning of one beat to the beginning of the succeeding beat.

Equation 2-1:

$$\mathrm{APDc} = \frac{APD}{\sqrt[3]{CL}} \qquad [2\text{-}1]$$

2.7.6 Electrophysiology

For electrophysiological experiments in HEK293T cells and rat hippocampal neurons, pipettes were pulled from borosilicate glass (Sutter Instruments, BF150-86-10), with a resistance of 5–6 MΩ, and were filled with an internal solution; 125 mM potassium gluconate, 1 mM EGTA, 10 mM HEPES, 5 mM NaCl, 10 mM KCl, 2 mM ATP disodium salt, 0.3 mM GTP trisodium salt (pH 7.25, 285 mOsm). Recordings were obtained with an Axopatch 200B amplifier (Molecular Devices) at room temperature. The signals were digitized with a Digidata 1440A, sampled at 50 kHz and recorded with pCLAMP 10 software (Molecular Devices) on a PC. Fast capacitance was compensated in the on-cell configuration. For all electrophysiology experiments, recordings were only pursued if series resistance in voltage clamp was less than 30 MΩ. For whole-cell, voltage clamp recordings in HEK293T cells, cells were held at -60 mV and hyper- and de- polarizing steps applied from -100 to +100 mV in 20 mV increments. For whole-cell, current clamp recordings in rat hippocampal neurons,

2.7.7 Drug-response experiments

For evaluation of cardiac action potentials in response to cisapride, cardiomyocytes were incubated with 1 µM fVF 2 in RPMI plus B27 supplement media (minus Phenol Red) for 20 minutes at 37 °C. For each well containing cardiomyocytes, baseline activity was recorded in three areas of interest (475/34 nm bandpass, emission filter and dichroic listed above; 51.4 mW/mm^2). Cisapride stocks were made in DMSO (0.1-300 µM) and added as a 1:1000 dilution in a 0.1 mL addition of RPMI B27 supplement media (minus Phenol Red). An addition of 0.1% DMSO in a 0.1 mL addition of media was used as a vehicle control. Cardiomyocytes were incubated at 37 °C for 15 minutes with added drug/vehicle and imaged in three different areas of interest per well. The concentration of cisapride was raised through subsequent addition of media containing drug, and the vehicle was matched to add the same percentage of DMSO. This process was repeated for each concentration of cisapride (0.1-300 nM). Dose response curves and IC_{50} values were calculated in GraphPad using APD data extracted from tiff stacks using the above MATLAB scripts.

2.7.8 Synthesis

Preparation of fluorene (FL) molecular wires

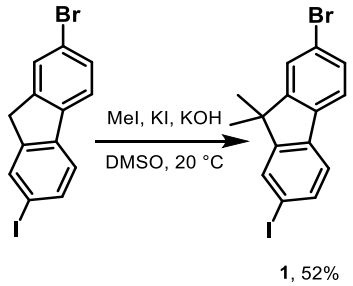

Synthesis of 2-bromo-7-iodo-9,9-dimethyl-9H-fluorene, 1

2-bromo-7-iodo-9H-fluorene (5.0 g, 13.5 mmol) was stirred in DMSO with potassium hydroxide (7.6 g, 134 mmol) and potassium iodide (156 mg, 1.35 mmol) at room temperature. Methyl iodide (4.2 mL, 67.4 mmol) was added dropwise after 10 minutes. The reaction was stirred for 24 hours before pouring into 50 ml of water. An off-white precipitate was collected by filtration. Recrystallization in methanol gave **1** as long, yellow crystals (2.81 g, 52%). NMR spectra matched published values.[17]

^{1}H NMR (400 MHz, Chloroform-d) δ 7.75 (d, J = 1.6 Hz, 1H), 7.66 (dd, J = 8.0, 1.6 Hz, 1H), 7.55 (d, J = 5.8 Hz, 1H), 7.54 (s, 1H), 7.46 (dd, J = 8.1, 1.7 Hz, 1H), 7.43 (d, J = 8.0 Hz, 1H), 1.46 (s, 6H).

^{13}C NMR (101 MHz, CDCl3) δ 136.24, 132.14, 130.33, 126.16, 121.80, 121.52, 47.28, 26.88.

HRMS (EI+) calculated for $C_{15}H_{12}BrI$ 397.9167; Found 397.9170.

Estimated Purity by HPLC: >98%

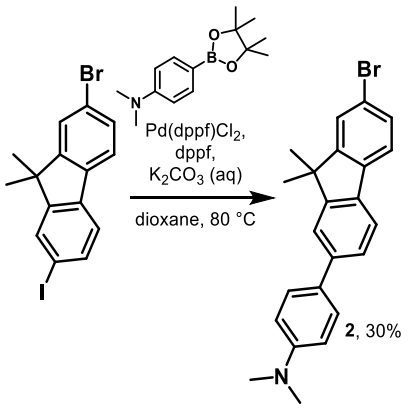

Synthesis of 4-(7-bromo-9,9-dimethyl-9H-fluoren-2-yl)-N,N-dimethylaniline, 2

Compound **8** (800 mg, 3.2 mmol) was combined with compound **1** (1.42 g, 3.6 mmol), 1,1′-ferrocenediyl-bis(diphenylphosphine) (180 mg, 0.32 mmol), and $Pd(dppf)Cl_2$ (27.8 mg, 38 µmol)

in a flame-dried Schlenk flask. This was evacuated/backfilled with N_2 (3x). Anhydrous dioxane (4 mL) and degassed K_2CO_3 (5 M, 1.6 mL) was added, the flask was sealed, and stirred at 80º C. After 18 h, the reaction was cooled and diluted with DCM. This was washed with sat. ammonium chloride (2X) and brine (1X). The organic fraction was collected, dried with $MgSO_4$, and concentrated onto silica *in vacuo*. This was purified by flash chromatography (hexanes to 10% EtOAc in hexanes), affording **2** as a light yellow solid (389 mg, 30%).

^{1}H NMR (600 MHz, Chloroform-*d*) δ 7.70 (d, *J* = 7.9 Hz, 1H), 7.61 – 7.54 (m, 5H), 7.54 (dd, *J* = 7.9, 1.7 Hz, 1H), 7.46 (dd, *J* = 8.0, 1.8 Hz, 1H), 6.86 – 6.81 (m, 2H), 3.02 (s, 6H), 1.52 (s, 6H).

^{13}C NMR (151 MHz, $CDCl_3$) δ 155.80, 153.80, 149.99, 140.96, 138.16, 136.08, 130.02, 129.37, 127.73, 126.04, 125.43, 121.13, 120.55, 120.45, 120.23, 112.77, 47.10, 40.56, 27.10.

HRMS (ESI) m/z: $[M+H]^+$ calculated for $C_{23}H_{23}BrN$ 392.1008; Found 392.1009.

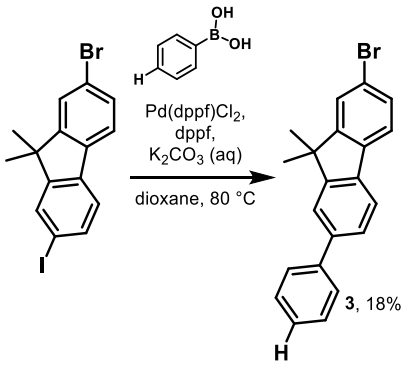

Synthesis of 2-bromo-9,9-dimethyl-7-phenyl-9H-fluorene, 3

Phenylboronic acid (500 mg, 4.1 mmol) was combined with compound **1** (2.88 g, 8.2 mmol) and $Pd(dppf)Cl_2$ (150 mg, 0.21 mmol) in a flame-dried Schlenk flask. This was evacuated/backfilled with N_2 (3x). Anhydrous dioxane (3 mL) and degassed K_2CO_3 (2 M, 300 µL) was added, the flask was sealed, and stirred at 80º C. After 18 h, the reaction was cooled and diluted with DCM. This was washed with sat. ammonium chloride (2X) and brine (1X). The organic fraction was collected, dried with $MgSO_4$, and concentrated onto silica *in vacuo*. This was purified by flash chromatography (hexanes to 10% toluene in hexanes), affording **3** as a white solid (260 mg, 18%).[43]

^{1}H NMR (600 MHz, Chloroform-*d*) δ 7.75 (dd, *J* = 7.9, 0.6 Hz, 1H), 7.69 – 7.64 (m, 2H), 7.64 (dd, *J* = 1.6, 0.7 Hz, 1H), 7.63 – 7.58 (m, 2H), 7.59 (s, 0H), 7.58 (d, *J* = 1.3 Hz, 1H), 7.51 – 7.45 (m, 3H), 7.38 (s, 1H), 1.54 (s, 6H).

^{13}C NMR (151 MHz, $CDCl_3$) δ 155.91, 153.88, 141.41, 140.89, 137.88, 137.36, 130.16, 128.80, 127.28, 127.20, 126.40, 126.16, 121.44, 121.41, 121.06, 120.34, 47.21, 27.09.

HRMS (EI+) calculated for $C_{21}H_{17}Br$ 348.0514; Found 348.0520.

Estimated Purity by HPLC: 92%

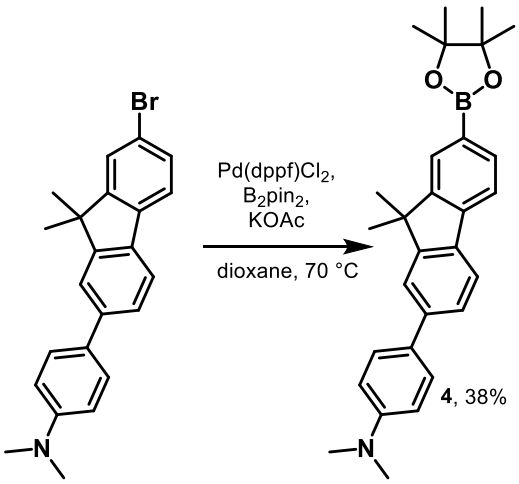

Synthesis of 4-(9,9-dimethyl-7-(4,4,5,5-tetramethyl-1,3,2-dioxaborolan-2-yl)-9H-fluoren-2-yl)-N,N-dimethylaniline, 4

Compound **2** (150 mg, 0.38 mmol) was combined with Pd(dppf)Cl_2 (5.6 mg, 7.6 µmol), bis(pinacolato)diboron (146 mg, 0.573 mmol), and potassium acetate (113 mg, 1.14 mmol) in a flame dried Schlenk flask. The flask was evacuated/backfilled with nitrogen (3x). Anhydrous dioxane (2 mL) was added and the flask, was sealed, and stirred at 70º C. After 18 h, the reaction was cooled, then extracted with DCM. This was washed twice with sat. ammonium chloride (2x) and brine (1x). Organics were collected, dried with $MgSO_4$, and concentrated onto silica. This was purified by flash chromatography (10-20% EtOAc in hexanes), affording **4** as a yellow solid (64 mg, 38%).

^{1}H NMR (600 MHz, Chloroform-*d*) δ 7.89 (t, *J* = 0.9 Hz, 1H), 7.82 (dd, *J* = 7.5, 1.0 Hz, 1H), 7.77 (d, *J* = 7.9 Hz, 1H), 7.73 (dd, 1H), 7.61 (d, *J* = 1.6 Hz, 1H), 7.59 – 7.56 (m, 2H), 7.55 (dd, *J* = 7.9, 1.7 Hz, 1H), 6.85 – 6.82 (m, 2H), 3.01 (s, 6H), 1.55 (s, 6H), 1.39 (s, 12H).

^{13}C NMR (151 MHz, $CDCl_3$) δ 155.03, 153.05, 150.11, 142.33, 141.19, 137.12, 134.07, 129.75, 128.82, 127.95, 125.43, 120.79, 120.67, 119.33, 112.95, 83.85, 83.64, 47.03, 40.76, 27.35, 25.18, 25.07.

HRMS (ESI) m/z: $[M+H]^+$ calculated for $C_{29}H_{35}BNO_2$ 440.2755; found: 440.2753.

Estimated Purity by HPLC: >99%

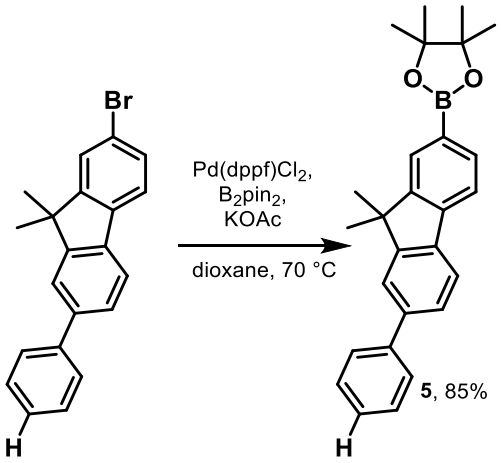

Synthesis of 2-(9,9-dimethyl-7-phenyl-9H-fluoren-2-yl)-4,4,5,5-tetramethyl-1,3,2-dioxaborolane, 5

Compound **13** (350 mg, 0.89 mmol) was combined with $Pd(dppf)Cl_2$ (32.6 mg, 45 µmol), bis(pinacolato)diboron (341 mg, 1.3 mmol), and potassium acetate (263 mg, 2.7 mmol) in a flame dried Schlenk flask. The flask was evacuated/backfilled with nitrogen (3x). Anhydrous dioxane (3 mL) was added and the flask was sealed and stirred at 70º C. After 18 h, the reaction was cooled, then extracted with DCM. The crude reaction was washed twice with sat. ammonium chloride (2x) and brine (1x). Organics were collected, dried with $MgSO_4$, and concentrated onto silica. This was purified by flash chromatography (hexanes to 10% EtOAc in hexanes), affording **5** as a white solid (334 mg, 85%).[43]

^{1}H NMR (600 MHz, Chloroform-d) δ 7.92 (s, 1H), 7.85 (d, J = 7.5 Hz, 1H), 7.82 (dd, J = 7.8, 1.5 Hz, 1H), 7.77 (dd, J = 7.6, 1.4 Hz, 1H), 7.68 (d, J = 9.3 Hz, 2H), 7.67 (d, J = 4.3 Hz, 1H), 7.60 (dd, J = 7.8, 1.6 Hz, 1H), 7.48 (td, J = 7.8, 1.6 Hz, 2H), 7.40 – 7.35 (m, 1H), 1.57 (d, J = 1.6 Hz, 6H), 1.40 (d, J = 1.6 Hz, 12H).

^{13}C NMR (151 MHz, CDCl3) δ 154.91, 152.99, 141.82, 141.56, 140.91, 138.19, 133.95, 128.74, 127.21, 127.17, 126.18, 121.44, 120.69, 119.39, 83.73, 46.94, 27.14, 24.90, 24.85.

HRMS (EI+) calculated for $C_{27}H_{29}BO_2$ 396.2261; Found 396.2267.

Estimated Purity by HPLC: >99%

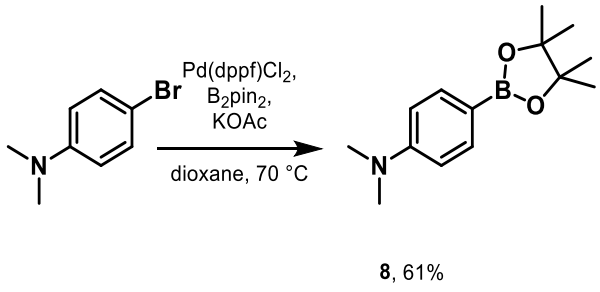

Synthesis of N,N-dimethyl-4-(4,4,5,5-tetramethyl-1,3,2-dioxaborolan-2-yl)aniline, 8

4-bromo-N,N-dimethylaniline (500 mg, 2.5 mmol), Pd(dppf)Cl_2 (36.6 mg, 50 µmol), bis(pinacolato)diboron (952 mg, 3.75 mmol), and potassium acetate (736 mg, 7.5 mmol) were combined in a flame-dried Schlenk flask. The flask was evacuated/backfilled with nitrogen (3x). Anhydrous dioxane (4 mL) was added and the flask, was sealed, and stirred at 80º C. After 18 h, the reaction was cooled, then extracted with DCM. This was washed with sat. ammonium chloride (2x) and brine (1x). Organics were collected, dried with $MgSO_4$, and concentrated onto silica. This was purified by flash chromatography (hexanes to 10% EtOAc in hexanes), affording **8** as a grey powder (294 mg, 60.9%). Reported NMR spectra matched published spectra.[18]

^{1}H NMR (400 MHz, Chloroform-*d*) δ 7.71 (d, *J* = 8.7 Hz, 2H), 6.70 (d, *J* = 8.7 Hz, 2H), 3.00 (s, 6H), 1.34 (s, 12H).

^{13}C NMR (101 MHz, $CDCl_3$) δ 152.57, 136.17, 111.27, 83.17, 40.14, 24.88.

HRMS (ESI) m/z: $[M+H]^+$ calculated for $C_{15}H_{13}BrI$ 248.1816; Found 248.1813.

Estimated Purity by HPLC: >99%

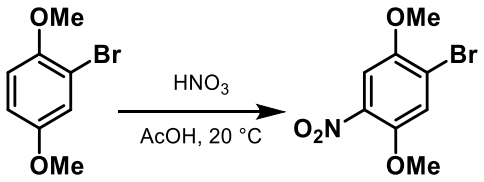

9,100%

Synthesis of 1-bromo-2,5-dimethoxy-4-nitrobenzene, 9

1-bromo-2,5-dimethoxybenzene (2.0 mmol, 5.0 g) was added to stirring glacial acetic acid (10 mL) at room temperature. Concentrated nitric acid (2 mL) was then added dropwise to the reaction, immediately causing the colorless solution to become yellow. This was stirred for 15 minutes before putting on ice and precipitating by addition of water. **9** was collected as a yellow precipitate by filtration (6.0 g, 100%). Reported NMR spectra matched published spectra.[44]

^{1}H NMR (400 MHz, Chloroform-d) δ 7.46 (s, 1H), 7.33 (s, 1H), 3.93 (s, 3H), 3.91 (s, 3H).

^{13}C NMR (101 MHz, CDCl3) δ 149.62, 147.60, 119.28, 118.58, 108.68, 57.35, 57.04.

HRMS (EI+) calculated for $C_8H_8BrNO_4$ 260.9637; Found 260.9640.

Estimated Purity by HPLC: >99%

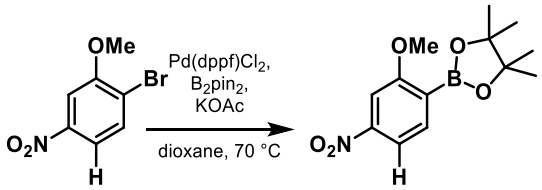

10, 44%

Synthesis of 2-(2-methoxy-4-nitrophenyl)-4,4,5,5 -tetramethyl-1,3,2-dioxaborolane, 10

1-bromo-2-methoxy-4-nitrobenzene (2.0 g, 8.6 mmol), Pd(dppf)Cl_2 (126 mg, 172 µmol), bis(pinacolato)diboron (3.3 g, 12.9 mmol), and potassium acetate (2.5 g, 25.9 mmol) were combined in a flame-dried Schlenk flask. The flask was evacuated/backfilled with nitrogen (3x). Anhydrous dioxane (8 mL) was added and the flask, was sealed, and stirred at 70º C. After 18 h, the reaction was cooled, then extracted with DCM. This was washed twice with sat. ammonium chloride and once with brine. Organics were collected, dried with $MgSO_4$, and concentrated onto silica. This was purified by flash chromatography (5% EtOAc in hexanes to 20% EtOAc in hexanes), affording **10** as a yellow solid (1.02 g, 44%).[45]

^{1}H NMR (400 MHz, DMSO-d6) δ 7.80 (dd, J = 8.1, 1.9 Hz, 1H), 7.76 (d, J = 8.1 Hz, 1H), 7.70 (d, J = 1.9 Hz, 1H), 3.88 (s, 3H), 1.30 (s, 12H).

^{13}C NMR (101 MHz, DMSO) δ 164.52, 151.03, 137.36, 115.14, 105.48, 84.33, 83.29, 56.49, 25.29.

HRMS EI+ calculated for $C_{13}H_{18}BNO_2$ 279.1278; found 279.1277.

Estimated Purity by HPLC: >99%

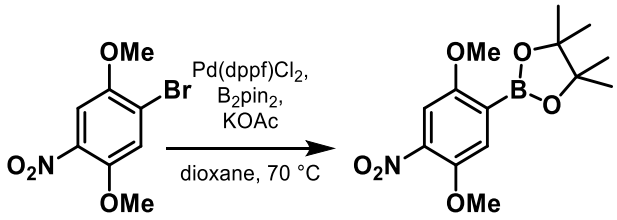

11, 62%

Synthesis of 2-(2,5-dimethoxy-4-nitrophenyl)-4,4,5,5-tetramethyl-1,3,2-dioxaborolane, 11

Compound **9** (5.0 g, 19 mmol), Pd(dppf)Cl_2 (279 mg, 0.38 mmol), bis(pinacolato)diboron (7.3 g, 7.3 mmol), and potassium acetate (5.6 g, 57 mmol) were combined in a flame-dried Schlenk flask. The flask was evacuated and then backfilled with nitrogen (3X). Anhydrous dioxane (10 mL) was added and the flask, was sealed, and stirred at 70º C. After 18 h, the reaction was cooled, then extracted with DCM. This was washed twice with sat. ammonium chloride and once with brine. Organics were collected, dried with $MgSO_4$, and concentrated onto silica. This was purified by

flash chromatography (20% EtOAc in hexanes to 30% EtOAc in hexanes), affording **11** as a yellow solid (3.68 g, 62%).

^{1}H NMR (400 MHz, Chloroform-d) δ 7.37 (s, 1H), 7.32 (s, 1H), 3.95 (s, 3H), 3.83 (s, 3H), 1.37 (s, 12H).

^{13}C NMR (101 MHz, CDCl3) δ 157.31, 146.58, 141.09, 121.91, 107.43, 84.33, 57.19, 56.69, 25.05, 24.83.

HRMS (EI+) calculated for $C_{14}H_{20}BNO_6$ 309.1384; Found 309.1388.

Estimated Purity by HPLC: >99%

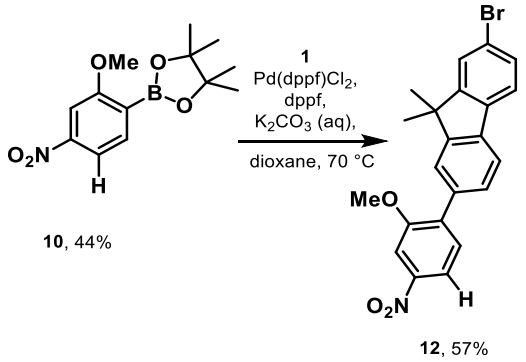

Synthesis of 2-bromo-7-(2-methoxy-4-nitrophenyl)-9,9-dimethyl-9H-fluorene, 12

Compound **10** (500 mg, 1.79 mmol) was combined with compound **1** (1.26 g, 3.58 mmol), and Pd(dppf)Cl_2 (65.5 mg, 90 µmol) in a flame-dried Schlenk flask. This was evacuated/backfilled with N_2 (3x). Anhydrous dioxane (3 mL) and degassed 2 M K_2CO_3 (1 mL) was added and was subjected to three freeze-pump-thaw cycles. The flask was sealed and stirred at 80 ºC. After 18 h, the reaction was cooled and diluted with DCM. This was washed with sat. ammonium chloride (2X) and brine (1X). The organic fraction was collected, dried with $MgSO_4$, and concentrated onto silica *in vacuo*. This was purified by flash chromatography (10-40% DCM in hexanes), affording **12** as a light-yellow powder (431 mg, 57%).

^{1}H NMR (600 MHz, DMSO-d_6) δ 7.94 – 7.91 (m, 1H), 7.91 (d, *J* = 4.4 Hz, 1H), 7.88 (d, *J* = 2.2 Hz, 1H), 7.83 (d, *J* = 5.8 Hz, 1H), 7.82 (s, 1H), 7.71 (d, *J* = 1.6 Hz, 1H), 7.64 (d, *J* = 8.3 Hz, 1H), 7.55 – 7.54 (m, 1H), 7.53 (s, 1H), 3.92 (s, 3H), 1.47 (s, 6H).

^{13}C NMR (151 MHz, DMSO) δ 157.04, 156.61, 153.50, 147.99, 137.90, 137.77, 137.28, 135.96, 131.68, 130.53, 129.06, 126.62, 124.20, 122.77, 121.28, 120.56, 116.30, 106.89, 56.74, 47.46, 26.90.

HRMS (EI+) calculated for $C_{22}H_{18}BrNO_3$ 423.0470; Found 423.0475.

Estimated Purity by HPLC: 89%

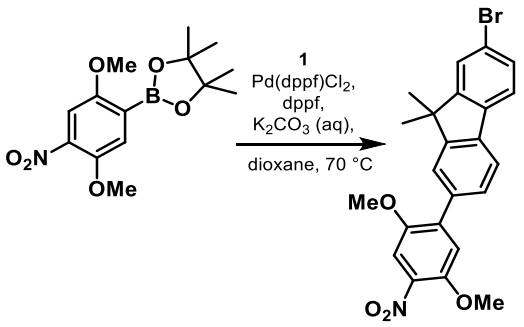

13, 68%

Synthesis of 2-bromo-7-(2,5-dimethoxy-4-nitrophenyl)-9,9-dimethyl-9H-fluorene, 13

Compound **11** (1.50 g, 4.85 mmol) was combined with compound **1** (2.13 g, 5.33 mmol), 1,1′-ferrocenediyl-bis(diphenylphosphine) (269 mg, 0.485 mmol), and $Pd(dppf)Cl_2$ (177 mg, 0.243 mmol) in a flame-dried Schlenk flask. This was evacuated/backfilled with N_2 (3x). Anhydrous dioxane (6 mL) and degassed 5 M K_2CO_3 (1.9 mL) was added and was subjected to three freeze-pump-thaw cycles. The flask was sealed and stirred at 80º C. After 18 h, the reaction was cooled and diluted with DCM. This was washed with sat. ammonium chloride (2X) and brine (1X). The organic fraction was collected, dried with $MgSO_4$, and concentrated onto silica *in vacuo*. This was purified by flash chromatography (1-10% EtOAc in hexanes), affording **13** as a light-yellow powder (1.5 g, 68%).

^{1}H NMR (600 MHz, Chloroform-d) δ 7.76 (d, J = 7.8 Hz, 1H), 7.62 (d, J = 8.0 Hz, 1H), 7.59 (d, J = 1.3 Hz, 1H), 7.58 (s, 1H), 7.57 (d, J = 1.2 Hz, 1H), 7.52 – 7.47 (m, 2H), 7.12 (s, 1H), 3.99 (s, 3H), 3.85 (s, 3H), 1.53 (s, 6H).

^{13}C NMR (151 MHz, CDCl3) δ 155.94, 153.20, 149.84, 147.76, 138.41, 137.85, 137.66, 137.55, 135.71, 130.25, 128.51, 126.21, 123.67, 121.59, 121.51, 119.85, 116.67, 108.79, 57.24, 56.43, 47.23, 26.98.

HRMS (EI+) calculated for $C_{23}H_{20}BrNO_4$ 453.0576; Found 453.0582.

Estimated Purity by HPLC: >99%

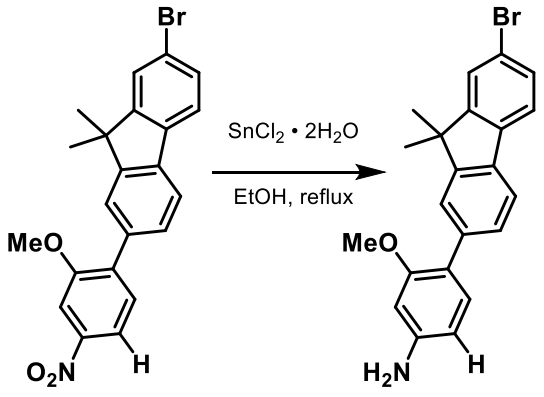

14, 93%

Synthesis of 4-(7-bromo-9,9-dimethyl-9H-fluoren-2-yl)-3-methoxyaniline, 14

Compound **12** (500 mg, 1.18 mmol) and tin(II) chloride dihydrate (1.3 g, 5.89 mmol) was suspended in 5 ml ethanol, then set to stir at reflux for 90 minutes. The reaction was allowed to cool and was then then precipitated using sat. $NaHCO_3$ solution. This was stirred for 30 min before filtering and the filtrate was collected and concentrated to dryness. This was resuspended in EtOAc, then washed once with saturated $NaHCO_3$ and twice with Brine. The organics were collected, dried with $MgSO_4$, and concentrated to give **14** as a fine yellow powder. (436 mg, 93%). This was used without further purification.

^{1}H NMR (600 MHz, DMSO-d_6) δ 7.76 (d, J = 1.9 Hz, 1H), 7.73 (s, 1H), 7.73 (d, J = 15.2 Hz, 1H), 7.52 (d, J = 1.5 Hz, 1H), 7.49 (dd, J = 8.0, 1.8 Hz, 1H), 7.38 (dd, J = 7.9, 1.6 Hz, 1H), 7.02 (d, J = 8.2 Hz, 1H), 6.32 (d, J = 2.0 Hz, 1H), 6.25 (dd, J = 8.1, 2.1 Hz, 1H), 5.33 (s, 2H), 3.68 (s, 3H), 1.43 (s, 6H).

^{13}C NMR (151 MHz, DMSO) δ 157.46, 156.35, 153.13, 139.27, 138.45, 135.10, 131.27, 130.31, 128.45, 126.44, 123.42, 122.10, 120.29, 120.05, 106.99, 98.12, 55.50, 47.20, 27.09.

HRMS (ESI) m/z: $[M+H]^+$ calculated for $C_{22}H_{21}BrNO$ 394.0801; Found 394.0805.

Estimated Purity by HPLC: >95%

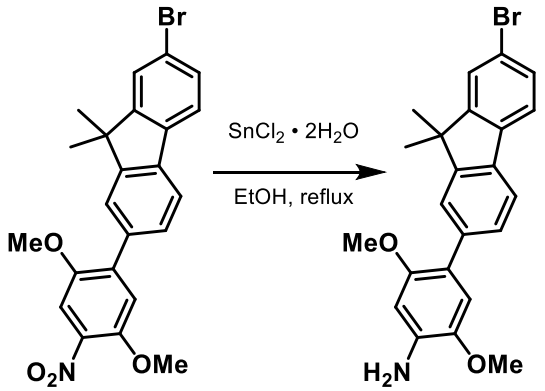

15, 77%

Synthesis of 4-(7-bromo-9,9-dimethyl-9H-fluoren-2-yl)-2,5-dimethoxyaniline, 15

Compound **13** (400 mg, 0.734 mmol) and tin(II) chloride dihydrate (828 mg, 3.67 mmol) was suspended in 2 ml ethanol, then set to stir at reflux for 30 minutes. The reaction was allowed to cool and was then then precipitated using sat. $NaHCO_3$ solution. This was stirred for 30 min before filtering and the filtrate was collected and concentrated to dryness. This was resuspended in EtOAc, then washed once with saturated $NaHCO_3$ and twice with brine. The organics were collected, dried with $MgSO_4$, and concentrated to give **15** as a fine yellow powder. (241 mg, 77%). This was used without further purification.

^{1}H NMR (600 MHz, Chloroform-d) δ 7.69 (d, J = 7.8 Hz, 1H), 7.57 (t, J = 8.4 Hz, 2H), 7.56 (d, J = 8.9 Hz, 1H), 7.50 (dd, J = 7.9, 1.5 Hz, 1H), 7.45 (dd, J = 8.0, 1.8 Hz, 1H), 6.86 (s, 1H), 6.46 (s, 1H), 3.98 – 3.89 (m, 2H), 3.87 (s, 3H), 3.75 (s, 3H), 1.51 (s, 6H)

^{13}C NMR (151 MHz, CDCl3) δ 155.90, 152.93, 151.15, 141.57, 138.49, 138.27, 136.49, 136.17, 129.98, 128.39, 126.04, 123.62, 121.17, 120.58, 120.20, 119.52, 113.77, 100.35, 56.37, 56.34, 47.08, 27.05.

HRMS (ESI) m/z: $[M+H]^+$ calculated for $C_{23}H_{23}BrNO_2$ 424.0907; Found: 424.0886.

Estimated Purity by HPLC: >99%

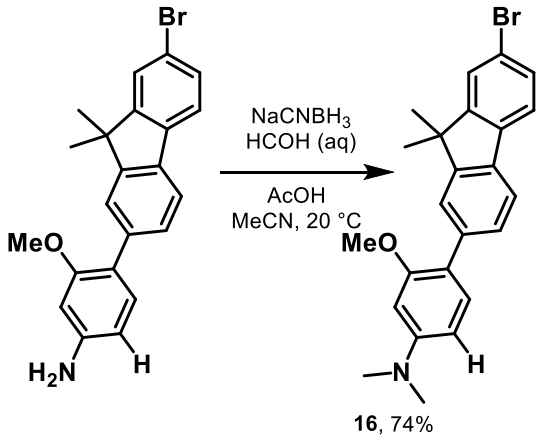

Synthesis of 4-(7-bromo-9,9-dimethyl-9H-fluoren-2-yl)-3-methoxy-N,N-dimethylaniline, 16

Compound **14** (360 mg, 0.913 mmol) was dissolved in 2 ml acetonitrile, then 37% formaldehyde solution (4.57 mmol, 330 µL) was added. This was set to stir at 0º C, then NaCNBH3 (172 mg, 2.74 mmol) was added slowly. Still at 0º C, glacial AcOH was used to adjust the solution to a pH between 5 and 6. The reaction was allowed to warm to room temperature and stir overnight. The reaction was poured over ice and then extracted into DCM. This was washed with 2 M KOH and brine, extracting into DCM three times. This was then dried with MgSO4 and concentrated to give **16** as a yellow powder (318 mg, 74%). This was used without further purification.

^{1}H NMR (600 MHz, DMSO-d6) δ 7.78 – 7.71 (m, 3H), 7.55 (d, J = 1.6 Hz, 1H), 7.49 (dd, J = 8.0, 1.9 Hz, 1H), 7.41 (dd, J = 7.9, 1.6 Hz, 1H), 7.17 (d, J = 9.1 Hz, 1H), 6.38 (d, J = 1.2 Hz, 1H), 6.38 (d, J = 3.5 Hz, 1H), 3.77 (s, 3H), 2.94 (s, 6H), 1.44 (s, 6H).

^{13}C NMR (151 MHz, DMSO) δ 157.46, 156.36, 153.18, 151.75, 138.92, 138.40, 135.33, 131.13, 130.33, 128.50, 126.45, 123.49, 122.15, 120.37, 120.13, 118.45, 105.42, 96.91, 55.75, 47.22, 40.61, 27.09.

HRMS (ESI) m/z: $[M+H]^+$ calculated for $C_{24}H_{25}BrNO$ 422.1114; Found 422.1121.

Estimated Purity by HPLC: 87%

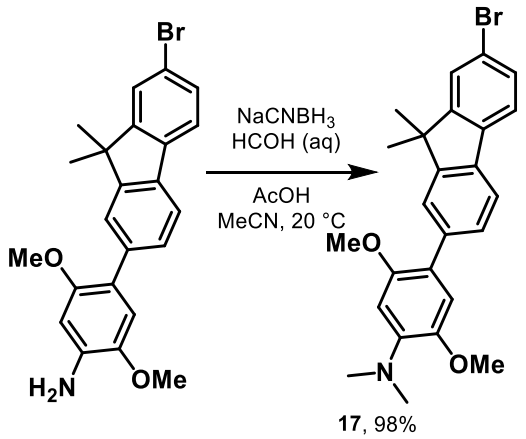

Synthesis of 4-(7-bromo-9,9-dimethyl-9H-fluoren-2-yl)-2,5-dimethoxy-N,N-dimethylaniline, 17

Compound **15** (125 mg, 0.297 mmol) was suspended in 3 ml glacial acetic acid, then paraformaldehyde (45.3 mg, 1.51 mmol) was added while stirring. After stirring for 15 minutes at room temperature, $NaCNBH_3$ (47.4 mg, 0.755 mmol) was added portion-wise and the reaction was stirred overnight. The reaction was neutralized with 2M KOH, then extracted into EtOAc. This was washed with 2 M KOH and brine before collecting drying with $MgSO_4$ and concentrating to give **17** as a yellow solid (67 mg, 98%). This was used without further purification.

^{1}H NMR (600 MHz, Chloroform-d) δ 7.71 (d, J = 7.8 Hz, 1H), 7.59 (s, 1H), 7.58 (d, J = 6.0 Hz, 1H), 7.56 (d, J = 1.8 Hz, 1H), 7.52 (dd, J = 7.8, 1.6 Hz, 1H), 7.46 (dd, J = 8.0, 1.8 Hz, 1H), 6.90 (s, 1H), 6.66 (s, 1H), 3.90 (s, 3H), 3.79 (s, 3H), 2.87 (s, 6H), 1.51 (s, 6H).

^{13}C NMR (151 MHz, CDCl3) δ 155.90, 152.98, 150.67, 146.60, 142.55, 138.17, 138.11, 136.53, 130.01, 128.36, 126.06, 123.65, 121.23, 120.71, 119.58, 114.18, 103.94, 56.68, 56.01, 47.09, 43.19, 27.03.

HRMS (ESI) m/z: $[M+H]^+$ calculated for $C_{25}H_{27}BrNO_2$ 452.1220; found 452.1216

Estimated Purity by HPLC: >99%

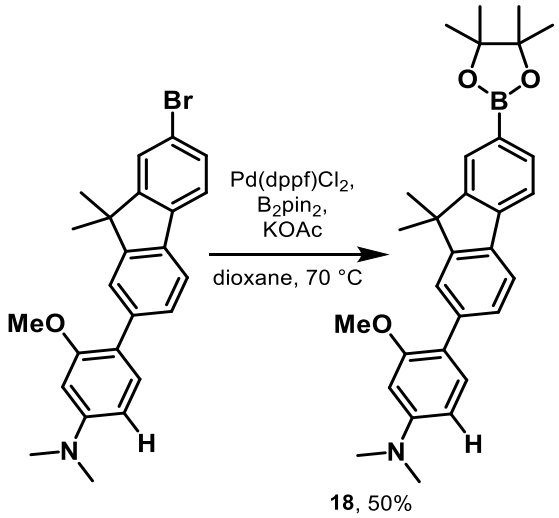

Synthesis of 4-(9,9-dimethyl-7-(4,4,5,5-tetramethyl-1,3,2-dioxaborolan-2-yl)-9H-fluoren-2-yl)-3-methoxy-N,N-dimethylaniline, 18

Compound **16** (230 mg, 0.55 mmol) was combined with Pd(dppf)Cl_2 (20 mg, 27 µmol), bis(pinacolato)diboron (166 mg, 0.65 mmol), and potassium acetate (160 mg, 1.64 mmol) in a flame dried Schlenk flask. The flask was evacuated/backfilled with nitrogen (3x). Anhydrous dioxane (2.5 mL) was added and the flask, was sealed, and stirred at 70º C. After 18 h, the reaction was cooled, then extracted with DCM. This was washed twice with sat. ammonium chloride (2x) and brine (1x). Organics were collected, dried with $MgSO_4$, and concentrated onto silica. This was purified by flash chromatography (5-20% EtOAc in hexanes), affording **18** as a yellow solid (128 mg, 50%).

^{1}H NMR (600 MHz, Chloroform-d) δ 7.89 (s, 1H), 7.82 (dd, J = 7.5, 1.1 Hz, 1H), 7.75 (d, J = 7.9 Hz, 1H), 7.73 (d, J = 7.6 Hz, 1H), 7.59 (s, 1H), 7.53 (dd, J = 7.9, 1.5 Hz, 1H), 7.30 (d, J = 8.4 Hz, 1H), 6.45 (dd, J = 8.5, 2.4 Hz, 1H), 6.38 (s, 1H), 3.85 (s, 3H), 3.03 (s, 6H), 1.39 (s, 12H), 1.27 (s, 6H).

^{13}C NMR (151 MHz, CDCl3) δ 157.37, 153.96, 152.96, 151.36, 142.42, 138.54, 136.77, 133.83, 131.27, 128.61, 128.15, 123.54, 119.81, 119.14, 105.18, 96.58, 83.64, 83.46, 55.50, 46.79, 40.66, 27.13, 25.00, 24.90.

HRMS (ESI) m/z: $[M+H]^+$ calculated for $C_{30}H_{37}BNO_3$ 470.2861; Found 470.2864

Estimated Purity by HPLC: >99%

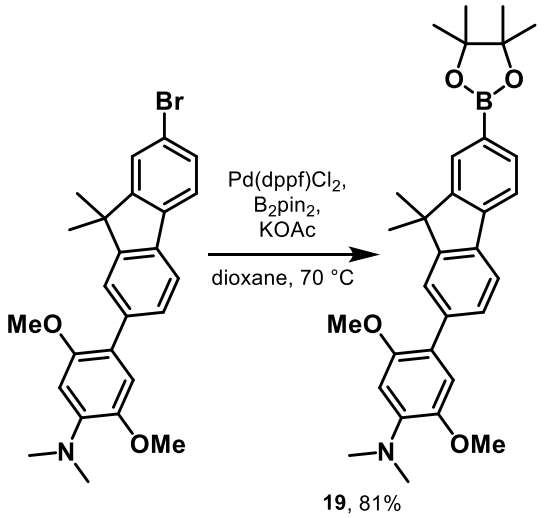

19, 81%

Synthesis of 4-(9,9-dimethyl-7-(4,4,5,5-tetramethyl-1,3,2-dioxaborolan-2-yl)-9H-fluoren-2-yl)-2,5-dimethoxy-N,N-dimethylaniline, 19

Compound **17** (65 mg, 0.143 mmol) was combined with $Pd(dppf)Cl_2$ (5.2 mg, 7.2 µmol), bis(pinacolato)diboron (55 mg, 0.215 mmol), and potassium acetate (42 mg, 0.429 mmol) in a flame dried Schlenk flask. The flask was evacuated/backfilled with nitrogen (3x). Anhydrous dioxane (2 mL) was added and the flask, was sealed, and stirred at 70º C. After 18 h, the reaction was cooled, then extracted with DCM. This was washed twice with sat. ammonium chloride (2x) and brine (1x). Organics were collected, dried with $MgSO_4$, and concentrated onto silica. This was purified by flash chromatography (20-30% EtOAc in hexanes), affording **19** as a yellow solid (58 mg, 81%).

^{1}H NMR (600 MHz, Chloroform-d) δ 7.89 (d, J = 1.1 Hz, 1H), 7.83 (dd, J = 7.5, 1.0 Hz, 1H), 7.77 (d, J = 7.8 Hz, 1H), 7.74 (d, J = 7.5 Hz, 1H), 7.62 (d, J = 1.6 Hz, 1H), 7.52 (dd, J = 7.8, 1.6 Hz, 1H), 6.92 (s, 1H), 6.67 (s, 1H), 3.91 (s, 3H), 3.79 (s, 3H), 2.87 (s, 6H), 1.39 (s, 12H), 1.27 (s, 6H).

^{13}C NMR (151 MHz, CDCl3) δ 154.04, 152.98, 150.68, 146.61, 142.44, 142.17, 138.16, 137.40, 133.86, 128.66, 128.15, 123.94, 123.67, 119.97, 119.25, 114.18, 104.00, 83.69, 56.71, 55.99, 46.85, 43.22, 27.11, 24.99, 24.89.

HRMS (ESI) $[M+H]^+$ calculated for $C_{31}H_{39}BNO_4$+ 500.2967; found 500.2971

Estimated Purity by HPLC: 90%

Synthesis of FL-based voltage indicators:

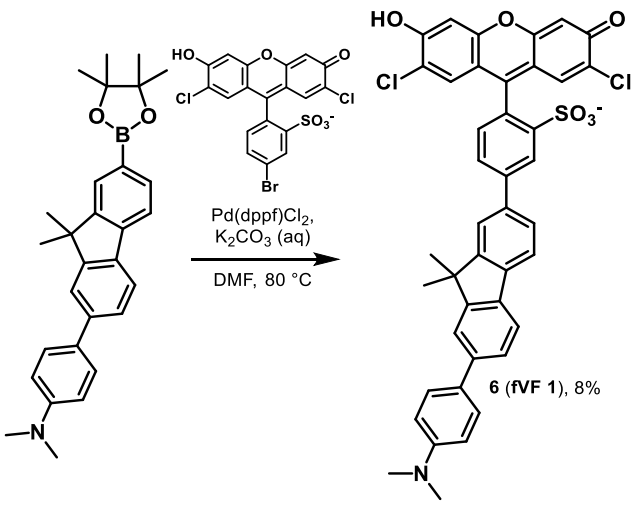

Synthesis of 6 (fVF 1)

Compound **4** (63.9 mg, 0.145 mmol) was combined with 5-bromo-(2',7'-dichloro-sulfofluorescien) (50 mg, 0.097 mmol) and $Pd(dppf)Cl_2$ (3.6 mg, 4.85 µmol) in a flame-dried screw-cap vial with a PTFE/silicon septum. This was evacuated/backfilled with N_2 (3x). Anhydrous DMF (500 µL) and degassed K_2CO_3 (5M, 50 µL) was added, and was subjected to three freeze-pump-thaw cycles. The flask was sealed and stirred at 80º C. After 18 h, the reaction was cooled and concentrated to dryness *in vacuo*. This was taken up in a minimal amount of DCM/MeOH, and then precipitated into diethyl ether. The precipitate was collected by vacuum filtration to obtain a reddish brown solid. A small sample was purified by preparative-HPLC (Water/MeCN + 0.05% TFA) to afford pure **6** as a reddish dust (5.8 mg, **8.0%** yield).

^{1}H NMR (900 MHz, DMSO-d6) δ 8.31 (d, J = 2.0 Hz, 1H), 8.00 (d, J = 1.7 Hz, 1H), 7.98 (d, J = 7.7 Hz, 1H), 7.95 (dd, J = 7.7, 2.0 Hz, 1H), 7.90 (d, J = 7.8 Hz, 1H), 7.81 (d, J = 1.7 Hz, 1H), 7.80 (dd, J = 7.8, 1.7 Hz, 1H), 7.63 (d, J = 8.2 Hz, 2H), 7.61 (dd, J = 7.7, 1.7 Hz, 1H), 7.38 (d, J = 7.6 Hz, 1H), 7.25 – 7.07 (m, 2H), 7.02 (s, 2H), 6.84 (d, J = 8.1 Hz, 2H), 2.97 (s, 6H), 1.59 (s, 6H).

^{13}C NMR (226 MHz, DMSO) δ 157.99, 157.86, 157.72, 157.59, 154.57, 154.52, 151.88, 149.80, 147.47, 141.48, 139.91, 138.60, 137.68, 135.95, 130.36, 129.79, 128.89, 128.02, 127.64, 127.27, 126.01, 125.40, 124.67, 121.22, 120.75, 120.62, 119.90, 119.25, 117.93, 116.60, 115.28, 112.68, 79.11, 78.97, 78.82, 46.78, 29.00, 26.93.

HRMS (ESI) m/z: $[M-H]^-$ calculated for $C_{42}H_{30}Cl_2NO_6$ 746.1176; Found 746.1172

Analytical HPLC retention time: 5.42 min (10-90% MeCN in water for 7.5 min, 90-100% MeCN in water for 2.5 min, 0.05% trifluoroacetic acid as an additive).

Estimated Purity by HPLC: >99%

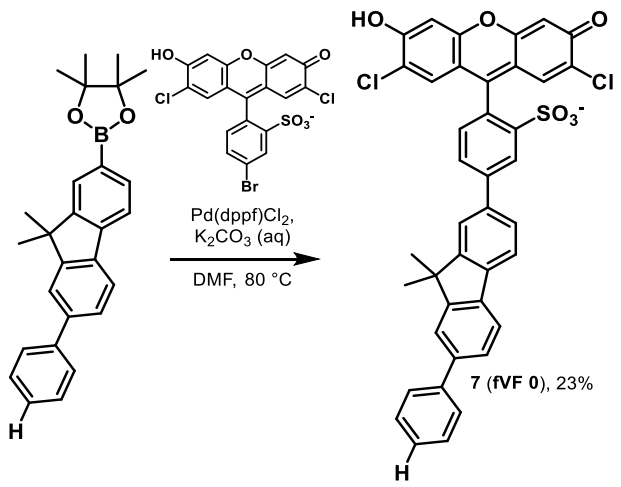

Synthesis of 7 (fVF 0)

Compound **5** (46.1 mg, 0.116 mmol) was combined with 5-bromo-(2',7'-dichloro-sulfofluorescien) (50 mg, 0.097 mmol) and $Pd(dppf)Cl_2$ (3.6 mg, 4.85 µmol) in a flame-dried screw-cap vial with a PTFE/silicon septum. This was evacuated/backfilled with N_2 (3x). Anhydrous DMF (500 µL) and degassed K_2CO_3 (5M, 50 µL) was added, and was subjected to three freeze-pump-thaw cycles. The flask was sealed and stirred at 80º C. After 18 h, the reaction was cooled and concentrated to dryness *in vacuo*. This was taken up in a minimal amount of DCM/MeOH, and then precipitated into diethyl ether. The precipitate was collected by vacuum filtration to obtain a red solid. A small sample was purified by preparative-HPLC (Water/MeCN + 0.05% TFA) to afford pure **7** as a brown dust (15.9 mg, **23%** yield).

^{1}H NMR (900 MHz, DMSO-d6) δ 8.31 (d, J = 2.0 Hz, 1H), 8.02 (dd, J = 4.7, 3.0 Hz, 2H), 7.97 (d, J = 7.8 Hz, 1H), 7.95 (dd, J = 7.7, 2.0 Hz, 1H), 7.90 (d, J = 1.7 Hz, 1H), 7.81 (dd, J = 7.7, 1.7 Hz, 1H), 7.78 – 7.75 (m, 2H), 7.68 (dd, J = 7.7, 1.7 Hz, 1H), 7.49 (t, J = 7.6 Hz, 2H), 7.38 (t, J = 7.9 Hz, 2H), 7.02 (s, 2H), 6.77 (s, 2H), 1.60 (s, 6H).

^{13}C NMR (226 MHz, DMSO) δ 158.11, 157.96, 157.81, 157.66, 154.55, 154.48, 151.67, 147.28, 141.28, 140.31, 139.50, 138.12, 137.97, 137.25, 130.22, 129.62, 128.75, 127.57, 127.17, 126.67, 125.93, 125.74, 125.31, 121.16, 121.07, 120.81, 120.72, 117.01, 115.71, 103.24, 103.15, 48.42, 46.74, 39.77, 39.67, 26.67.

HRMS (ESI) m/z: $[M+H]^+$ calculated for $C_{40}H_{27}Cl_2O_6S$: 705.0900; Found 705.090

Analytical HPLC retention time: 9.26 min (30-80% MeCN in water for 7.5 min, 80-100% MeCN in water for 2.5 min, 0.05% trifluoroacetic acid as an additive).

Estimated Purity by HPLC: >99%

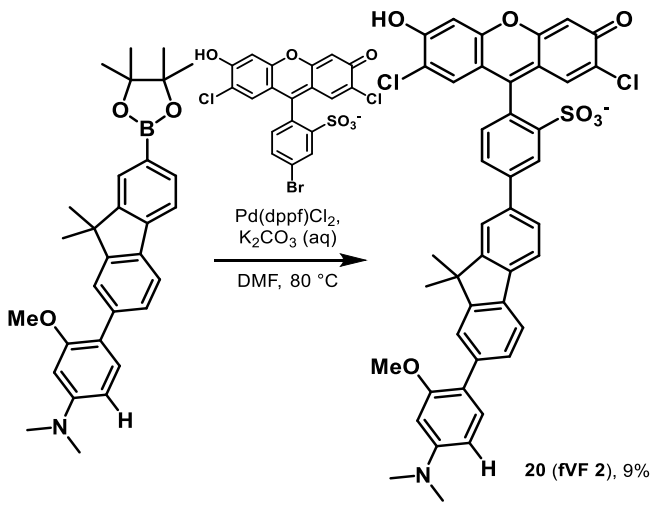

Synthesis of 20 (fVF 2)

Compound **18** (54.6 mg, 0.116 mmol) was combined with 5-bromo-(2',7'-dichloro-sulfofluorescien) (50 mg, 0.097 mmol) and $Pd(dppf)Cl_2$ (3.6 mg, 4.85 µmol) in a flame-dried screw-cap vial with a PTFE/silicon septum. This was evacuated/backfilled with N_2 (3x). Anhydrous DMF (500 µL) and degassed K_2CO_3 (5M, 50 µL) was added, and was subjected to three freeze-pump-thaw cycles. The flask was sealed and stirred at 80º C. After 18 h, the reaction was cooled and concentrated to dryness *in vacuo*. This was taken up in a minimal amount of DCM/MeOH, and then precipitated into diethyl ether. The precipitate was collected by vacuum filtration to obtain a reddish brown solid. A small sample was purified by preparative-HPLC (Water/MeCN + 0.05% TFA) to afford pure **20** as an orange dust (6.8 mg, **9.0%** yield).

**For NMR and analytical HPLC characterization, precipitate from ether was used. Material purified by HPLC was used for spectroscopic experiments and testing in cells.

^{1}H NMR (900 MHz, DMSO-d6) δ 8.31 (s, 1H), 7.98 (s, 1H), 7.95 (d, J = 7.9 Hz, 1H), 7.86 (dd, J = 37.1, 7.7 Hz, 2H), 7.78 (d, J = 7.6 Hz, 1H), 7.62 (s, 1H), 7.46 (d, J = 7.6 Hz, 1H), 7.23 (dd, J = 19.5, 7.9 Hz, 2H), 6.79 (s, 2H), 6.41 (s, 2H), 6.17 (d, J = 6.8 Hz, 2H), 3.81 (s, 3H), 2.97 (s, 6H), 1.56 (s, 6H)

^{13}C NMR (226 MHz, DMSO) δ 173.31, 173.27, 157.04, 156.43, 154.46, 153.43, 152.09, 151.28, 147.28, 140.66, 138.57, 138.19, 137.88, 135.57, 130.73, 130.67, 129.39, 128.61, 128.02, 126.86, 126.61, 126.55, 125.89, 125.56, 123.12, 121.15, 120.51, 119.69, 118.13, 108.99, 108.95, 105.00, 102.68, 102.64, 96.47, 64.90, 55.33, 46.64, 40.20, 26.98, 15.16.

HRMS (ESI) m/z: $[M+H]^+$ calculated for $C_{43}H_{34}Cl_2NO_7S$ 778.1428; Found 778.1436

Analytical HPLC retention time: 5.45 min (10-90% MeCN in water for 7.5 min, 90-100% MeCN in water for 2.5 min, 0.05% trifluoroacetic acid as an additive).

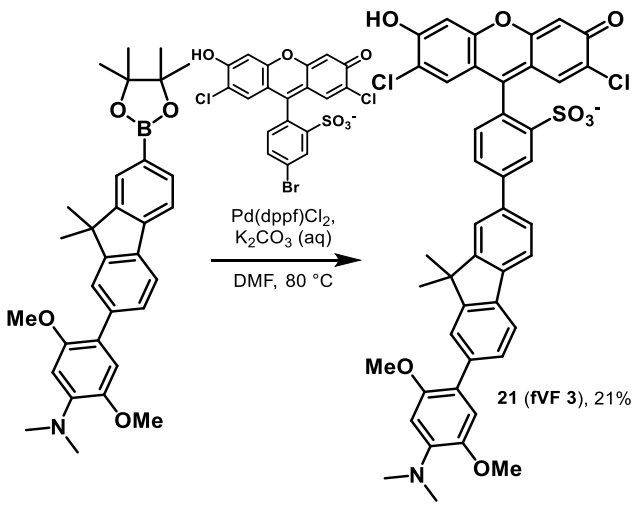

Synthesis of 21 (fVF 3)

Compound **19** (20.0 mg, 0.040 mmol) was combined with 5-bromo-(2',7'-dichloro-sulfofluorescien) (17.2 mg, 0.033 mmol) and $Pd(dppf)Cl_2$ (1.2 mg, 1.7 µmol) in a flame-dried screw-cap vial with a PTFE/silicon septum. This was evacuated/backfilled with N_2 (3x). Anhydrous DMF (500 µL) and degassed K_2CO_3 (5M, 16 µL) was added, and was subjected to three freeze-pump-thaw cycles. The flask was sealed and stirred at 60º C. After 18 h, the reaction was cooled and concentrated to dryness *in vacuo*. This was taken up in a minimal amount of DCM/MeOH, and then precipitated into diethyl ether. The precipitate was collected by vacuum filtration to obtain a dark red solid. This was further purified by preparative-HPLC (Water/MeCN + 0.05% TFA) to afford pure **21** as an orange dust (5.6 mg, **21%** yield).

^{1}H NMR (900 MHz, DMSO-d6) δ 8.31 (s, 1H), 8.02 (s, 1H), 8.01 (d, J = 7.1 Hz, 1H), 7.96 (d, J = 7.7 Hz, 1H), 7.92 (d, J = 7.8 Hz, 1H), 7.70 (s, 1H), 7.81 (d, J = 7.6 Hz, 1H), 7.52 (d, J = 7.6 Hz, 1H), 7.38 (d, J = 7.6 Hz, 1H), 7.25 (t, J = 7.4 Hz, 1H), 7.17 (d, J = 7.5 Hz, 1H), 7.14 (t, J = 7.3 Hz, 1H), 7.02 (s, 2H), 6.79 (s, 1H), 3.89 (s, 3H), 3.79 (s, 3H), 2.94 (s, 6H), 1.58 (s, 6H).

^{13}C NMR (226 MHz, DMSO) δ 154.60, 153.53, 151.83, 150.47, 149.66, 147.49, 145.47, 141.42, 138.46, 137.93, 137.32, 130.35, 129.77, 129.47, 128.87, 128.29, 128.18, 128.00, 127.68, 127.24, 126.37, 126.18, 126.03, 125.42, 125.29, 123.62, 123.56, 121.31, 121.27, 120.80, 119.91, 115.86, 115.84, 115.13, 108.40, 103.35, 103.31, 56.40, 46.74, 45.66, 26.89, 21.02.

HRMS (ESI) m/z: $[M-H]^-$ calculated for $C_{44}H_{34}Cl_2NO_8S$ 806.1388; Found 806.1382.

Analytical HPLC retention time: 4.99 min (10-90% MeCN in water for 7.5 min, 90-100% MeCN in water for 2.5 min, 0.05% trifluoroacetic acid as an additive). Estimated Purity by HPLC: >99%

2.8 Figures and schemes

Scheme 2-1. *Synthesis of Fluorene VoltageFluor Dyes (fVF dyes)*

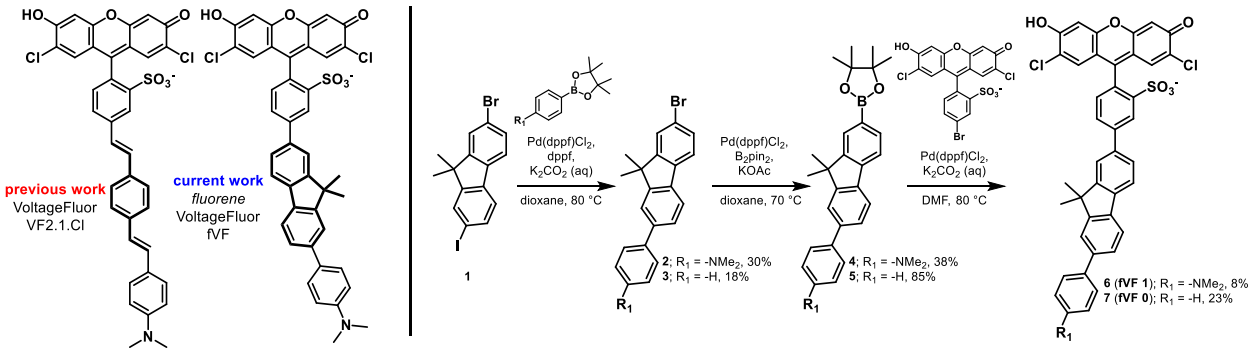

Scheme 2-2. *Synthesis of electron rich Fluorene VoltageFluor Dyes*

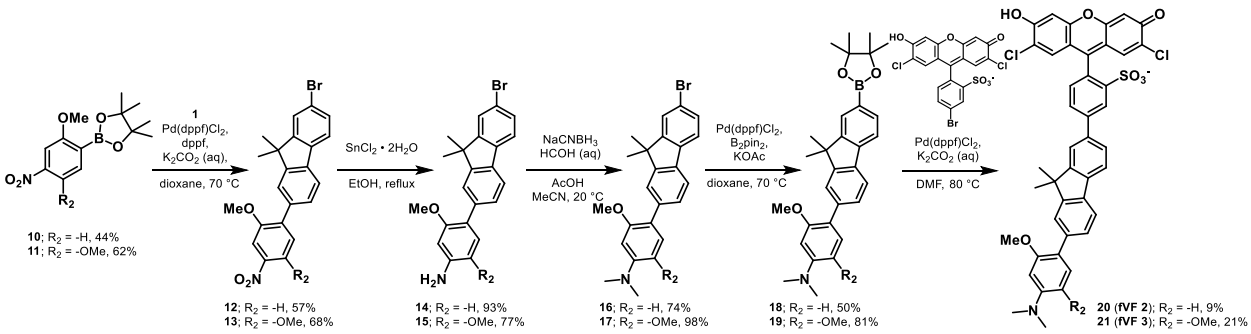

Scheme 2-3. *Synthesis of fluorene VoltageFluor dyes (fVF dyes)*

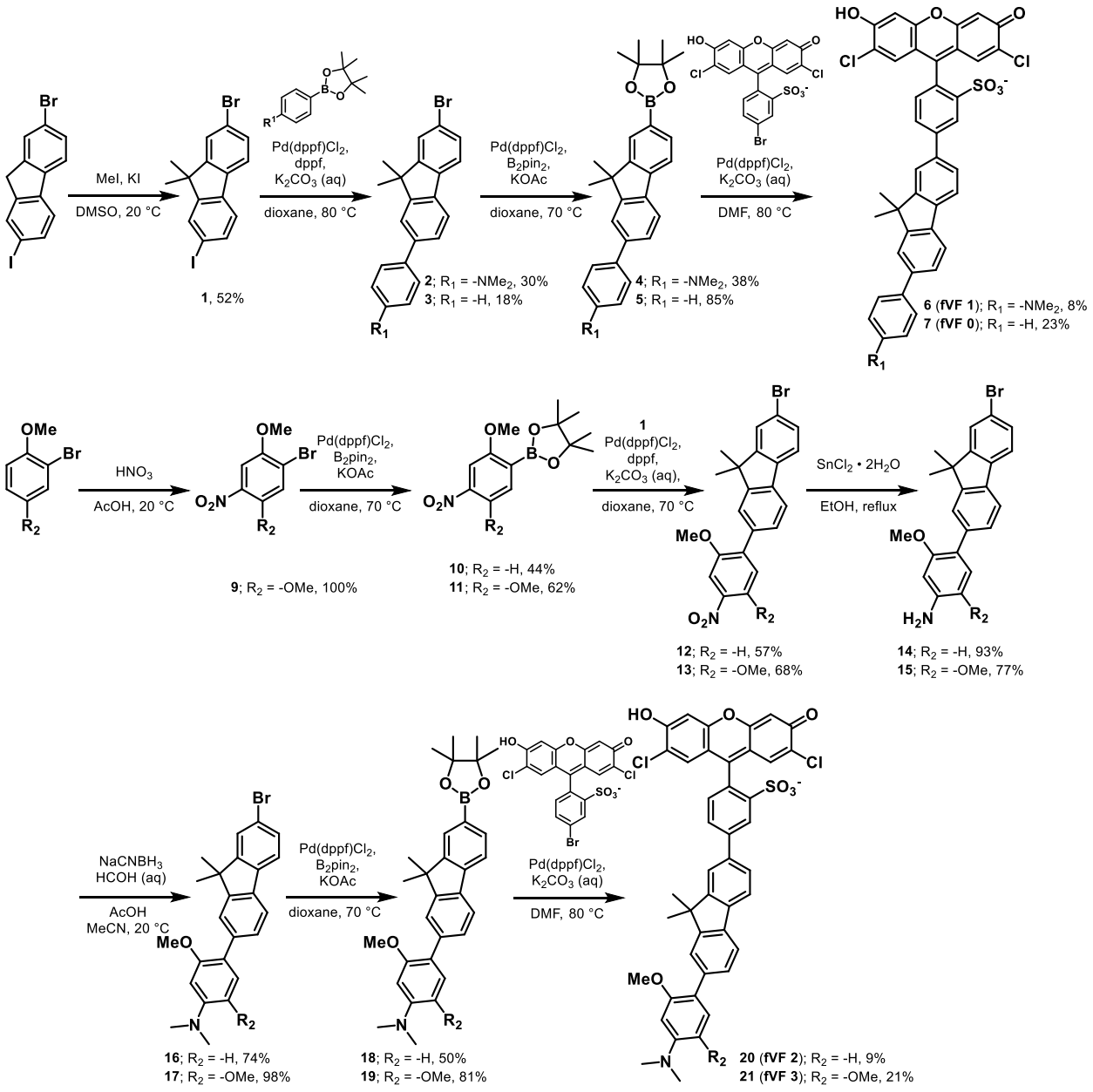

Table 2-1. *Properties of Fluorene VoltageFluor Dyes (fVF dyes)*

Entry[a]	R_1	R_2	Absorbance [nm][a]	Emission [nm][a]	QY[a]	% ΔF/F[b]	SNR [b]
fVF 0 (**7**)	-H	-H	519	535	0.77	-0.3 ± 0.03	1.9:1
fVF 1 (**6**)	$-N(Me)_2$	-H	519	534	0.05	4.7 ± 0.5	22:1
fVF 2 (**20**)	$-N(Me)_2$	-H	520	535	0.07	10.5 ± 0.8	39:1
fVF 3 (**21**)	$-N(Me)_2$	-OMe	520	535	0.19	12.2 ± 1.6	13:1

[a] Measured in PBS + 0.1% SDS (pH = 7.2). [b] per 100 mV. Recorded in HEK293T cells at 0.5 kHz optical sampling rate.

Table 2-2. *Voltage Dye characteristics in neurons*

Dye	SNR	%ΔF/F	Rel. Brightness
fVF 2[a]	21:1	5.2%	1.2
VF2.1.Cl[a]	43:1	10.7%	1
di-4-ANNEPS[b]	15:1	-1.0%	3.7

[a] Dye loaded at 0.5 μM, excited at 475 nm and emission collected with a 540 nm bandpass filter.
[b] Loaded at 2.5 μM, excited at 475 nm and emission collected with a 650 nm bandpass filter

Table 2-3. *Action potential kinetics in neurons incubated with fVF 2*[a]

fVF 2	Half-width (ms)	τ_{rise} (ms)	τ_{decay} (ms)	Amplitude (mV)
(-)	1.7 ± 0.1	0.71 ± 0.03	1.6 ± 0.6	101 ± 7
(+)	1.5 ± 0.3	0.61 ± 0.17	1.5 ± 0.3	101 ± 10

[a] Loaded with 500 nM fVF 2 in HBSS for 20 minutes. Average values presented for each metric with standard deviation. n = 4 cells without (-) fVF 2, n = 5 cells with (+) fVF 2.

Table 2-4. *Measurements of cisapride cardiotoxicity*

Model	Measurement	APD30 IC_{50}	APD50 IC_{50}	APD90 IC_{50}	hERG IC_{50}	CaV1.2 IC_{50}	NaV1.5 IC_{50}	+20% APD90
iPSC Monolayer[a]	optical	6.5 nM	6.4 nM	10.6 nM	-	-	-	-
HEK293[b]	patch-clamp	-	-	-	10 nM	> 130 nM	> 130 nM	-
HEK293[c]	patch-clamp	-	-	-	20 nM	11.8 µM	337 µM	-
iPSC monolayer[d]	optical	-	-	-	-	-	-	10 nM
Guinea Pig cardiomyocytes[e]	patch-clamp	-	-	-	15 nM	-	-	-

[a] From this work. Monolayers were tested after 14 days in culture. [b][32] [c][46] [d][27] [e][47]

Figure 2-1. *Characterization of Fluorene VoltageFluor 2 (fVF 2).*

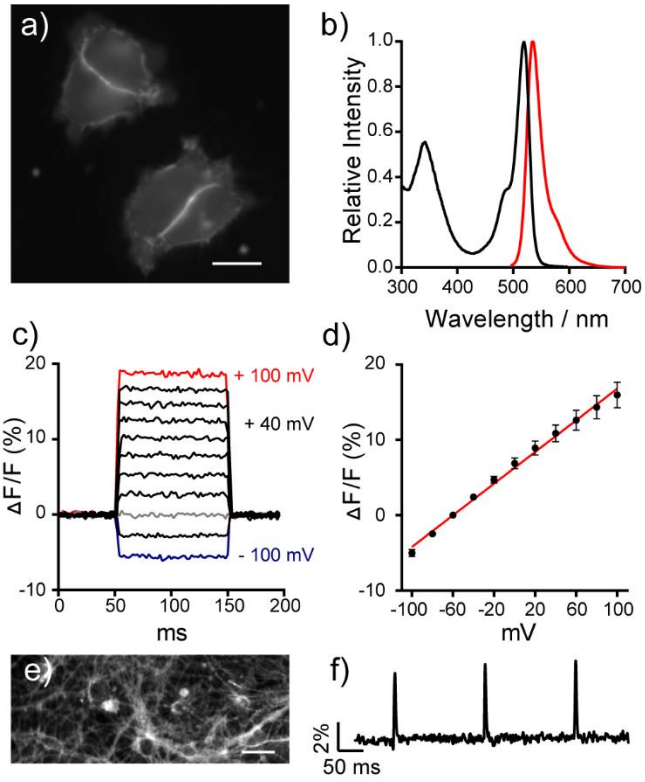

Figure 2-1. Characterization of fluorene VoltageFluor 2 (fVF 2). (a) Live cell fluorescence microscopy image of fVF 2 in HEK cells. The scale bar is 10 µm. (b) Normalized absorption and emission spectra of fVF 2. Spectra were acquired in phosphate-buffered saline (pH 7.2) and 0.1% sodium dodecyl sulfate. For an emission scan, excitation was provided at 485 nm. (c) Voltage sensitivity of fVF 2 in patch-clamped HEK cells. (d) Plot of $\Delta F/F$ vs membrane potential (in millivolts) for fVF 2. The red line is the line of best fit. Error bars are standard errors of the mean for eight independent determinations. (e) Live cell, widefield fluorescence images of rat hippocampal neurons stained with 500 nM fVF 2. The scale bar is 20 µm. (f) Representative $\Delta F/F$ plot of evoked neuronal activity of a single cell recorded optically with fVF 2.

Figure 2-2. *Normalized absorption and emission profiles of Fluorene VoltageFluor (fVF) dyes.*

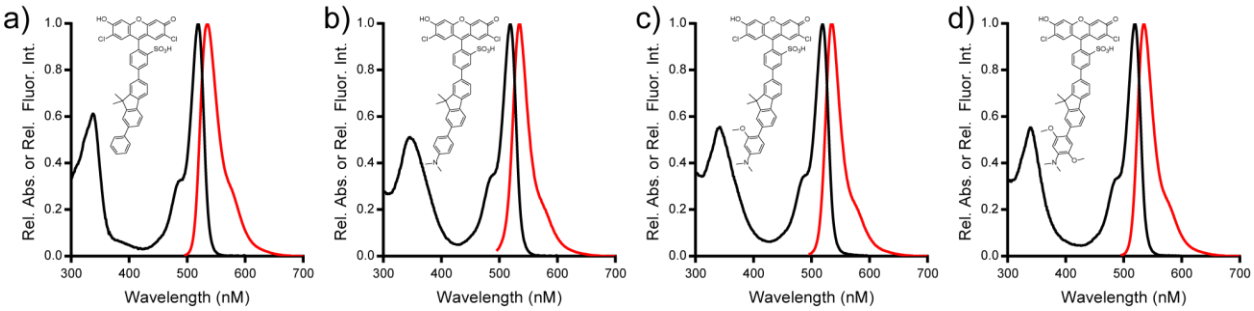

Figure 2-2. Normalized absorption and emission profiles of 7 (fVF 0) (a), 6 (fVF 1) (b), 20 (fVF 2) (c), and 21 (fVF 3) (d). All spectra were acquired at a dye concentration of 1 μM in PBS (pH 7.2) with 0.1% SDS.

Figure 2-3. *Staining and photostability of Fluorene VoltageFluors.*

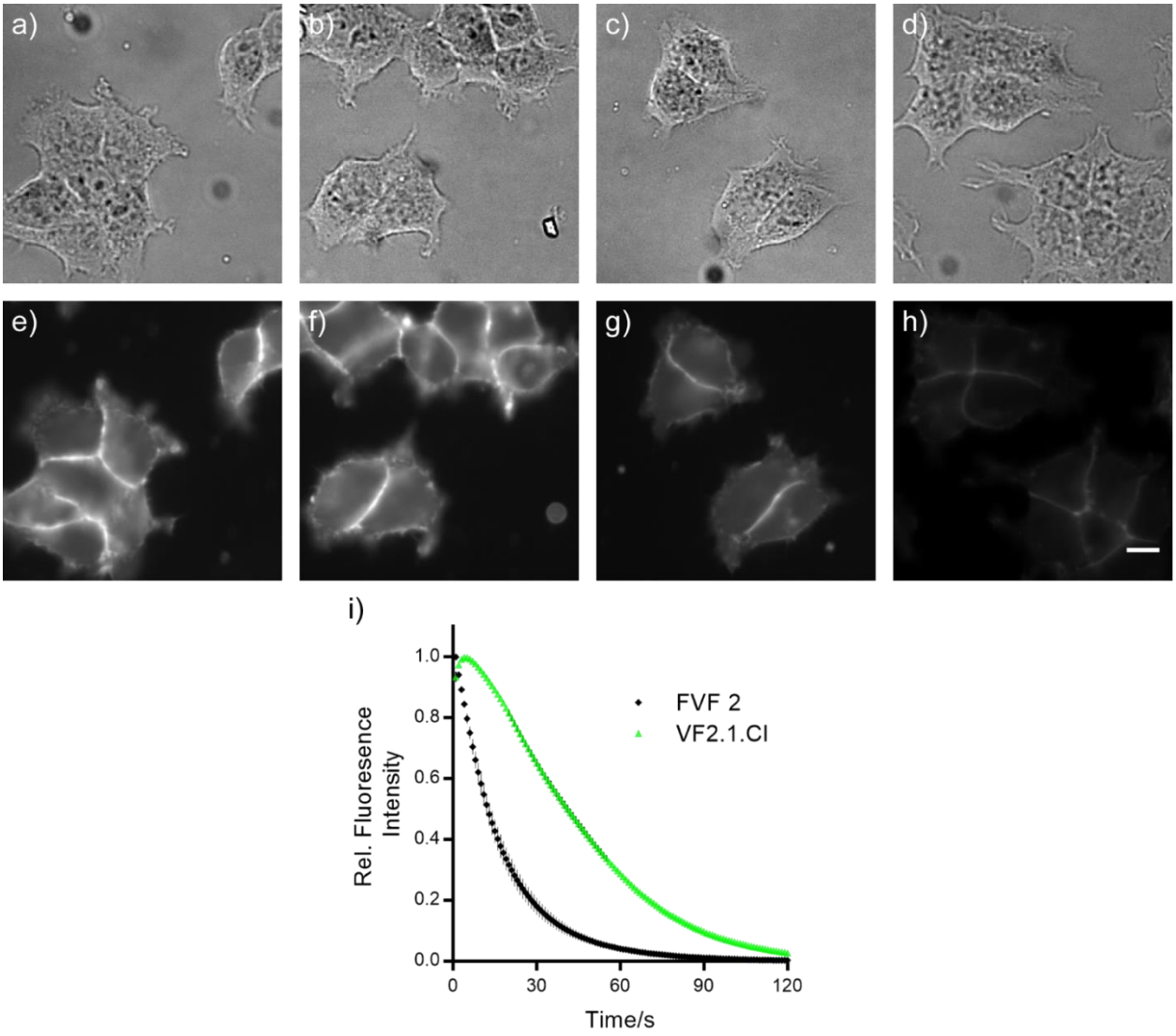

Figure 2-3. Staining and photostability of fluorene-wire voltage indicators. Widefield microscopy DIC and fluorescence images of **7** (a, e), **6** (b, f), **fVF 2** (**20,** c, g), and **21** (d, h), loaded at 500 nM in HEK292T cells for 20 minutes. 10 μm scale bar. Image acquisition and analysis parameters were identical to permit comparison of cellular localization and brightness. (i) Relative photostability of **fVF 2** (black) and VF2.1.Cl (green). Error bars are ± SEM for 5 cells. **fVF 2** exhibits a shorter decay half-life (11.6 ± 0.3 sec) and time constant for the fluorescence decay (τ_{Fl} = 16.7 ± 0.39 sec) than VF2.1.Cl (31.53 ± 0.5 sec, τ_{Fl} = 45.5 ± 0.8 sec).

Figure 2-4. *Voltage sensitivity of fluorene VoltageFluors.*

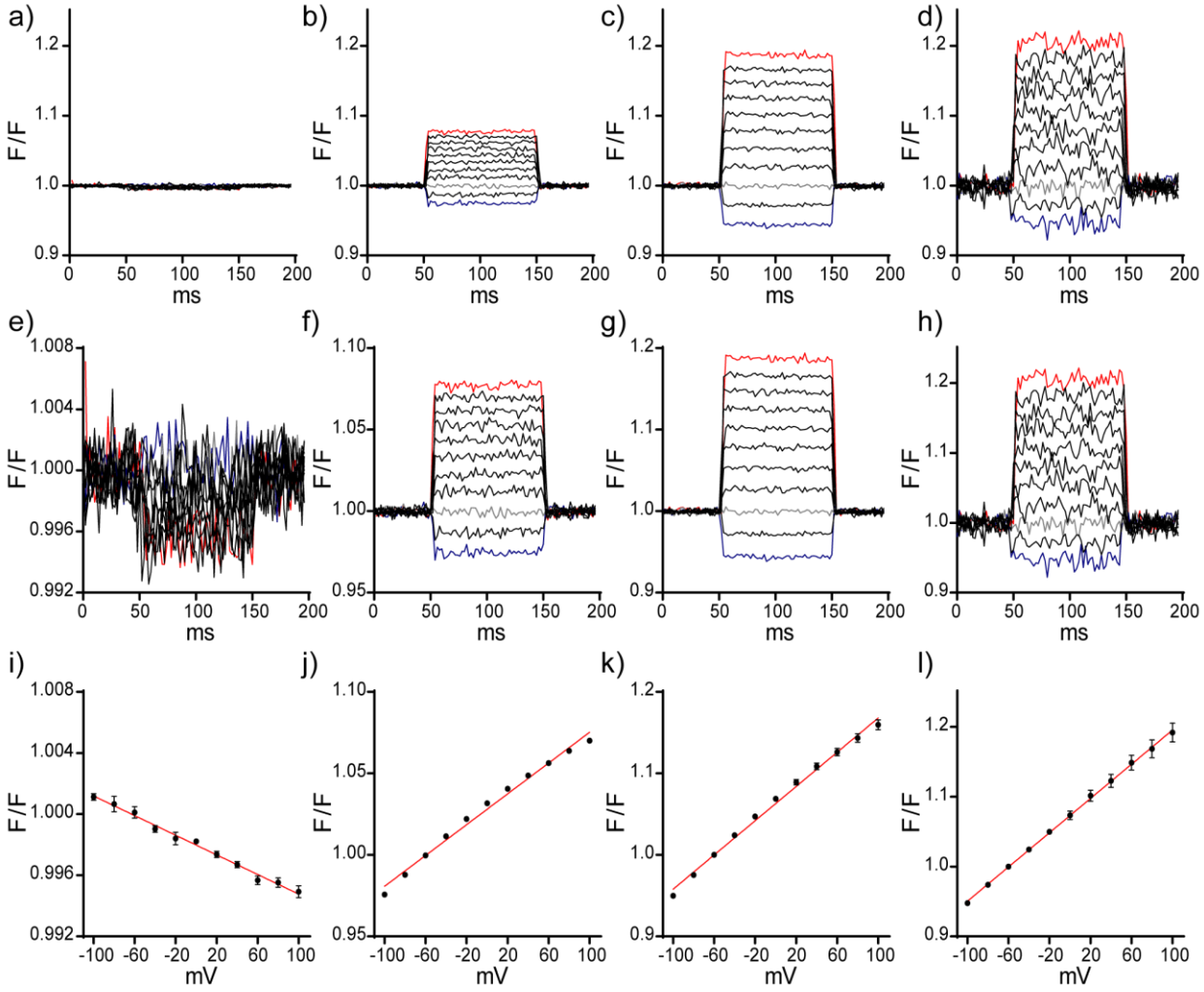

Figure 2-4. Voltage sensitivity of fluorene VoltageFluors in HEK293T cells. **fVF 0** (a, e); **fVF 1** (b, f); **fVF 2** (c, g); **fVF 3** (d, h). (upper row) Plot of fractional change in fluorescence vs time for 100 ms voltage steps ranging from -100 to +100 mV in 20 mV increments form a -60 mV holding potential. (lower row) Linear plot of fractional change in fluorescence vs membrane potential (mV), summarizing data from multiple cells (g, n = 4; f, n = 7; g, n = 8; h, n = 6). Error bars are SEM.

Figure 2-5. *Imaging evoked activity in neurons with voltage indicators*

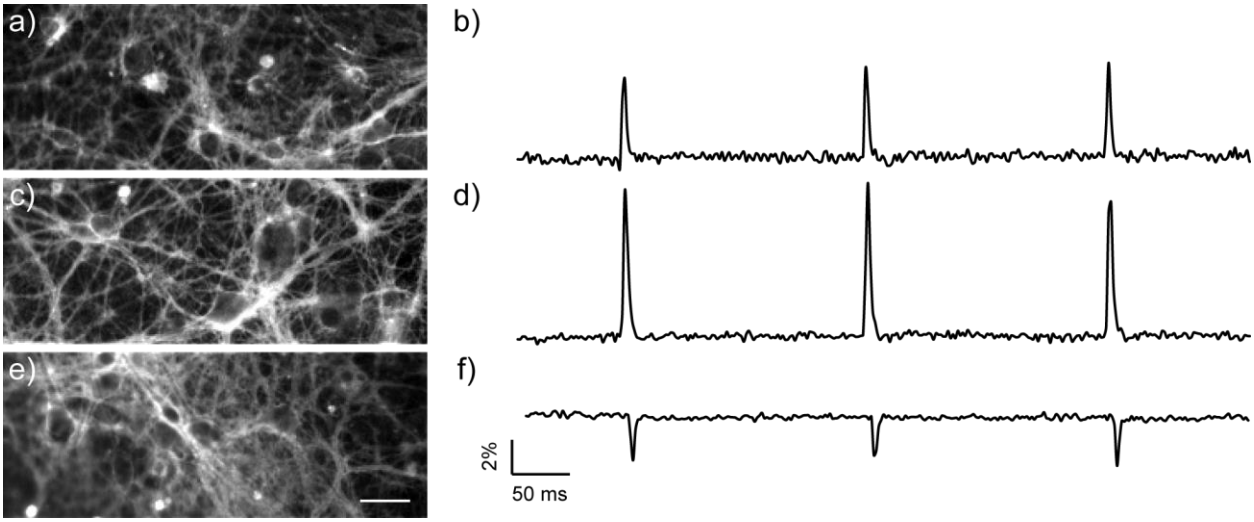

Figure 2-5. Live-cell wide-field fluorescence images of 10-14 DIV rat hippocampal neurons stained with (a) fVF 2 (c) VF2.1.Cl and (e) di-4-ANEPPS at concentrations of 500 nM, 500 nM, and 2.5 µM, respectively. Scale bar is 20 µm. (d-f) Representative Δ*F/F* plots of evoked neuronal activity recorded optically with either (b) FVF 2, (d) VF2.1.Cl, or (f) di-4-ANEPPS.

Figure 2-6. *Optical recordings of spontaneous activity in neurons with Fluorene VoltageFluor 2 (fVF 2).*

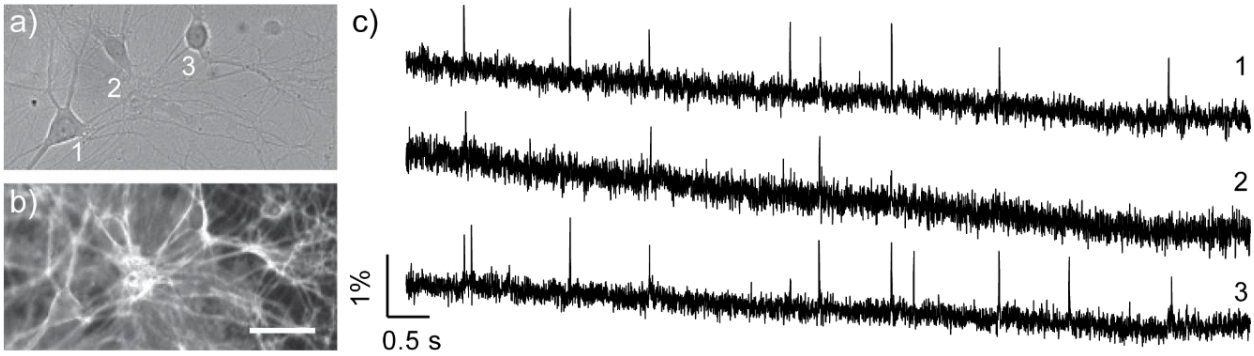

Figure 2-6. Optically recorded spontaneous activity in 14-19 DIV rat hippocampal neurons stained with 500 nM fVF 2. (DIC, a) Neurons 1 through 3 gave optical ΔF/F traces (c) recorded in the fluorescence channel (b). Scale bar is 50 µm. Optical traces (c) are plots of raw fluorescence values from single recordings and are neither filtered nor corrected for photo-bleach.

Figure 2-7. *Action potential kinetics in neurons incubated with VoltageFluor dyes.*

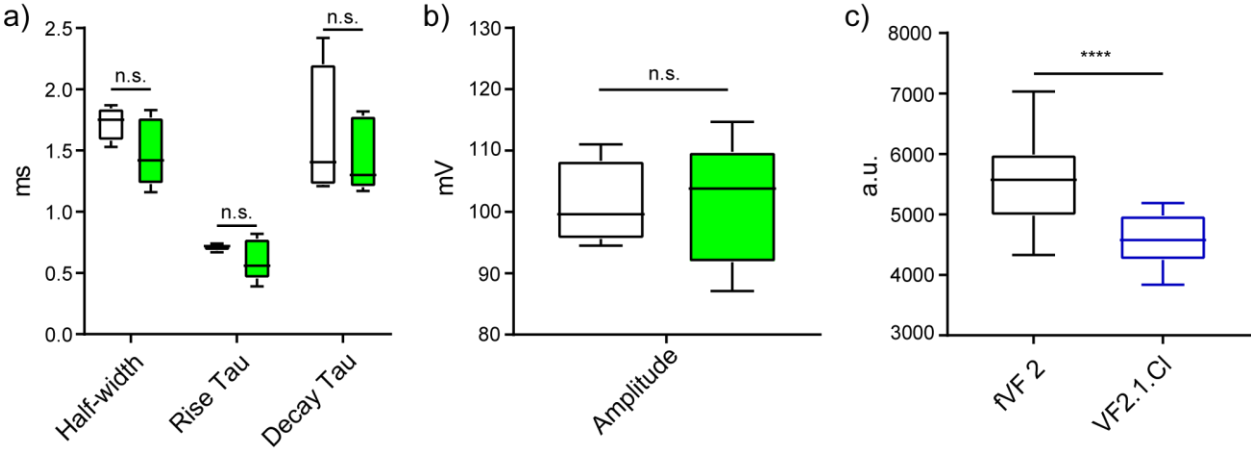

Figure 2-7. Comparison of action potential kinetics recorded in rat hippocampal neurons 10-14 DIV using whole-cell current clamp. (a) Measurement of action potential half-width rise time constant, decay time constant, and (b) action potential amplitude in cells without incubation with fVF 2 (no fill, n = 4 cells) were not statistically significant (t-test, $p > 0.05$) from measurements made in cells incubated with 500 nM fVF 2 (green, n = 5 cells). (c) Comparison of brightness in neurons loaded with 500 nM of dye for 20 minutes. fVF2 (n = 19 cells) is approximately 1.2 times brighter than VF2.1.Cl (n = 14 cells), and statistically significant (students t-test, $p < 0.0001$ = ****)

Figure 2-8. *Fluorene VoltageFluor 2 (fVF 2) reports action potential kinetics in hiPSC-CMs.*

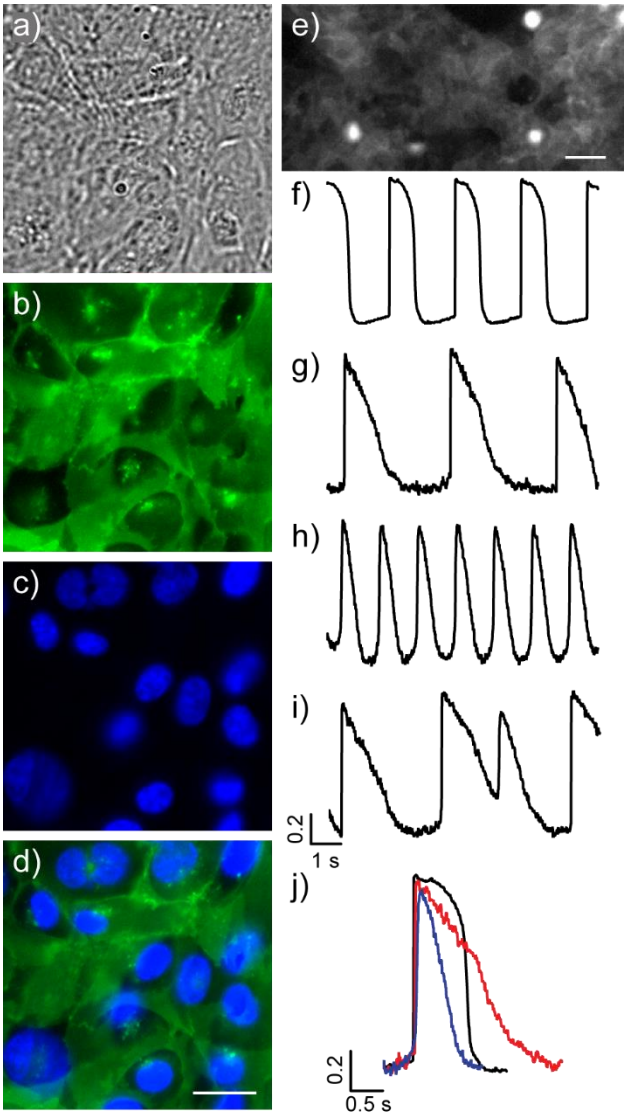

Figure 2-8. Fluorene VoltageFluor 2 (fVF 2) reliably reports on cardiac action potential (cAP) dynamics in human induced pluripotent stem cell-derived cardiomyocytes (hiPSC-CMs). (a) Bright field. (b) Membrane localization of fVF 2 (1 µM) in hiPSC-CM monolayers. (c) Hoechst 33342 nuclear stain. (d) Merge of membrane and nuclear stains. The scale bar is 20 µm. (e) Representative image used to acquire functional AP data. The scale bar is 10 µm. (f–i) Representative fluorescence traces acquired using 1 µM fVF 2. (f) Baseline measurement of a spontaneously contracting monolayer. Treatment with cisapride (300 nM) results in (g) prolonged APs, (h) shorter and more frequent APs, and (i) early after depolarizations (EADs). (j) Overlay of single APs from panels f–h to highlight observed waveform changes from cisapride treatment. The baseline trace in black shows a normal ventricular-like shape; the red trace depicts an extended AP after treatment (from panel g), and the blue trace depicts a shortened AP from a tachycardia-like phenotype (from panel h).

Figure 2-9. *Decreased phototoxicity of Fluorene VoltageFluor 2 (fVF 2) in cardiomyocytes*

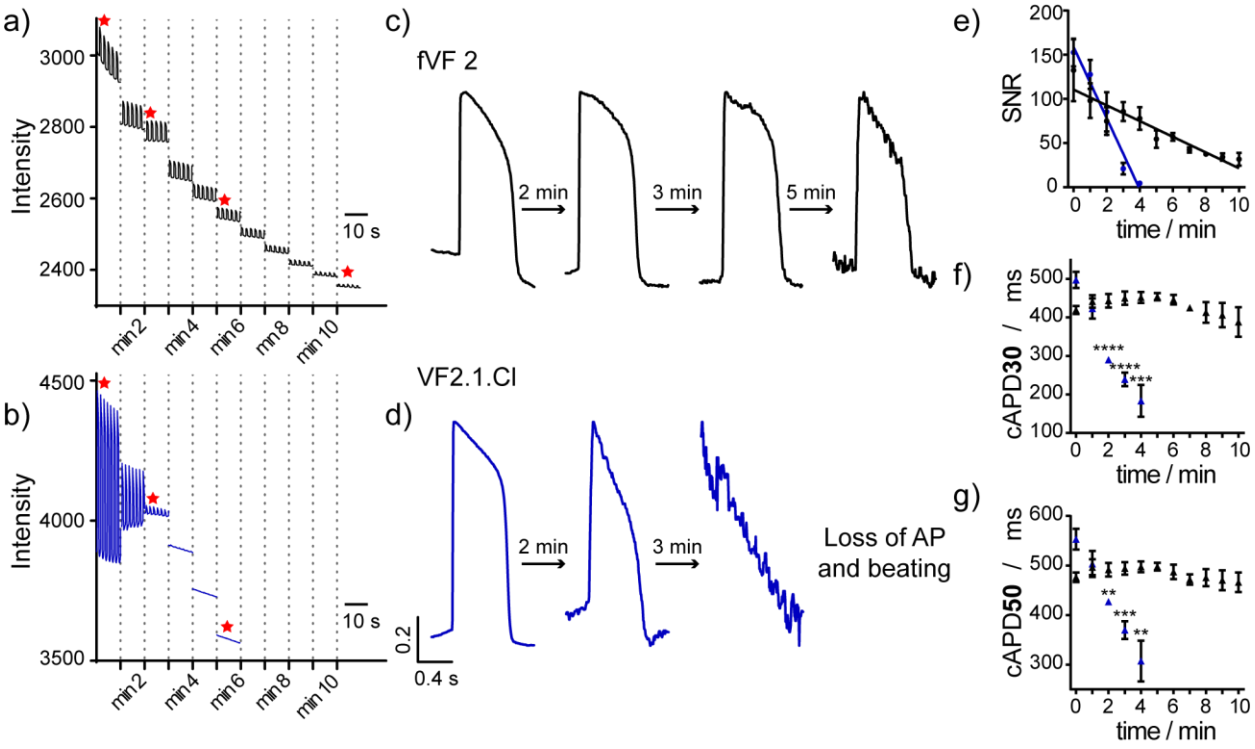

Figure 2-9. fVF 2 displays low phototoxicity in cardiomyocyte monolayers. Fluorescence intensity vs time for (a) fVF 2 and (b) VF2.1.Cl in monolayers of hiSPC-CMs. The raw fluorescence intensity from an entire field of view over an entire 10 s recording session is plotted vs the total illumination time (in minutes). Individual action potential (AP) traces for (c) fVF 2 and (d) VF2.1.Cl are indicated by red stars in panels a and b. Plot of the mean (e) signal-to-noise ratio (SNR), (f) cAPD30, and (g) cAPD50 as a function of total illumination time for fVF 2 (black) and VF2.1.Cl (blue). For panels e−g, mean values are determined from n = 3 independent trials, and error bars are ± standard error of the mean. Statistical tests were two-tailed, unpaired t tests for each cAPD at the indicated time vs time zero. **p < 0.005. ***p < 0.001. **** p < 0.0001.

Figure 2-10. *Phototoxicity of fVF 2 and VF2.1.Cl in cardiomyocytes.*

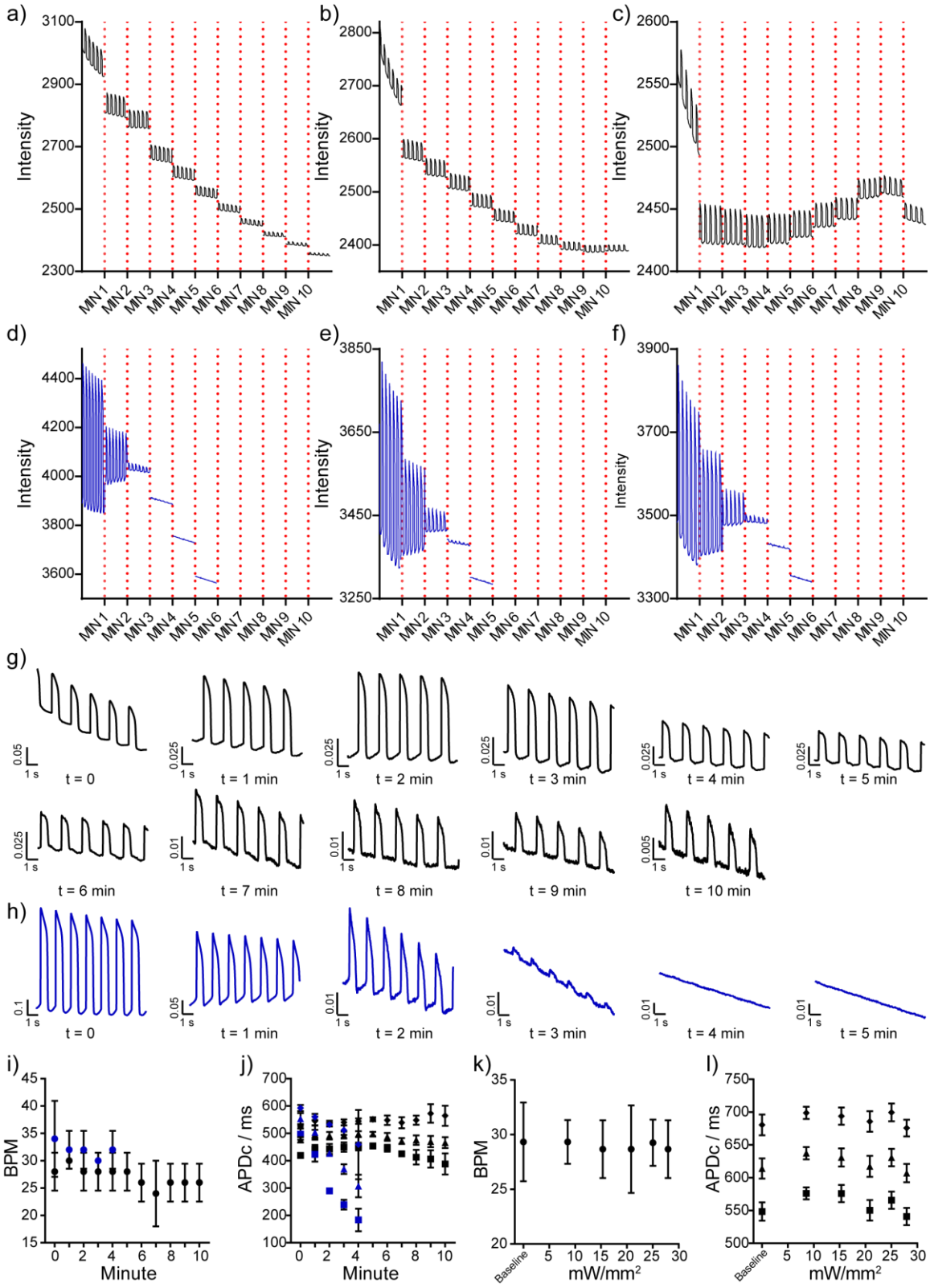

Figure 2-10. Phototoxicity of **fVF 2** and VF2.1.Cl in hiPSC cardiomyocyte monolayers. (a-c) **fVF 2** (black traces) shows a quick initial photobleach, but activity is still recorded after ten minutes of illumination (g). (d-f) VF2.1.Cl (blue traces) has better SNR initially but exhibits phototoxicity after just two minutes of illumination (h). Plots of BPM and cAPD vs time (i-j) and illumination intensity (k-l) show **fVF 2** has negligible phototoxicity with prolonged illumination and increased intensity. Quantification is found is SI Table 2

Figure 2-11. *Light is required for phototoxicity of VoltageFluors in cardiomyocytes.*

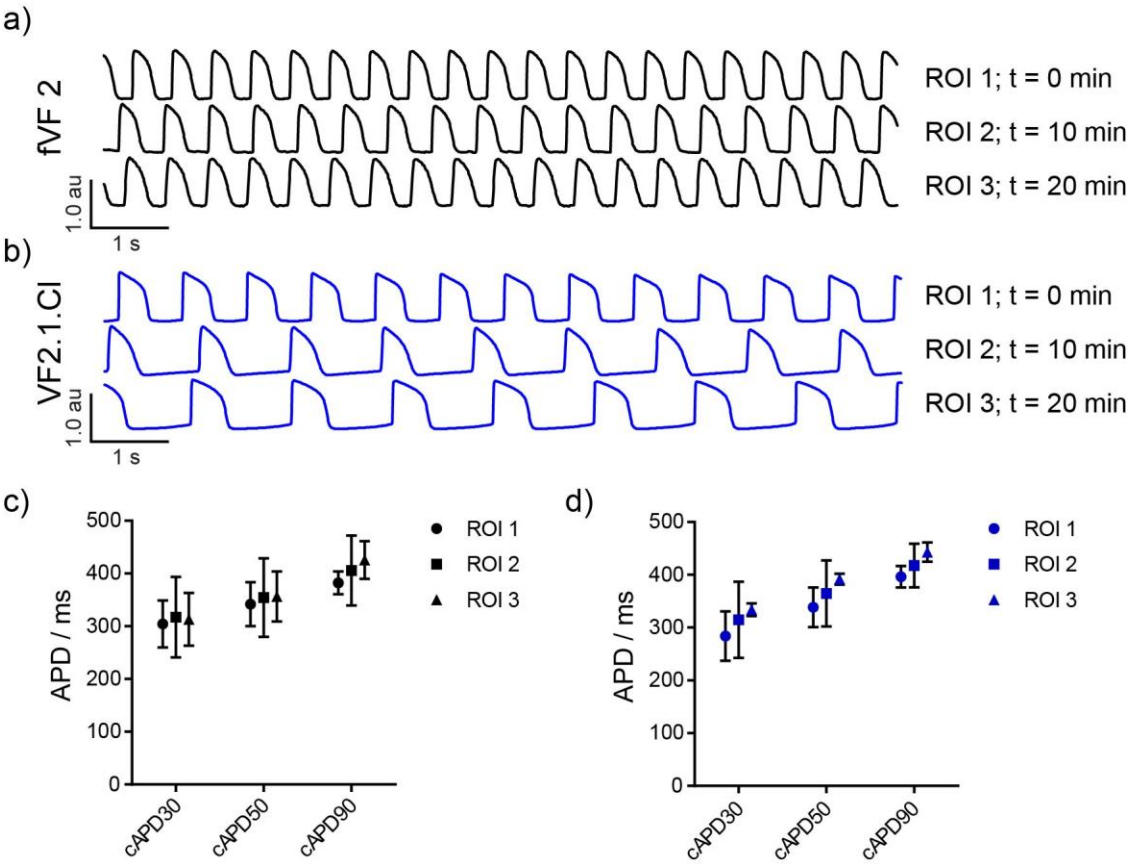

Figure 2-11. Phototoxicity of **fVF 2** and VF2.1.Cl in cardiomyocyte monolayers requires presence of both light and dye. Optical recordings taken with 1 µM **a) fVF 2** and **b)** VF2.1.Cl for 10 seconds, and the LED was left on to continue to illuminate the region of interest (ROI) for 10 minutes, as in **Fig. 3** in the main text. Subsequent 10 second recordings were taken in different regions within the same coverslip and are indicated as ROI 1, 2, or 3. Each new region had not been exposed to illumination light previously. Illumination was continued for a total of 10 minutes after recording from ROI 2, such that recording from ROI 3 occurred greater than 20 minutes after the initial recording in ROI 1. Plots depict the average cAPD30, cAPD50, and cAPD90 measured from **fVF 2** (**c**) or VF2.1.Cl (d) recordings. No significant difference exists for any of the measured cAPD values for **fVF 2** or VF2.1.Cl ($p > 0.05$, Student's t-test). Recordings from 3 separate coverslips were averaged for each region of interest (ROI), error bars are standard deviation of the mean, n = 3 coverslips.

Figure 2-12. *Fluorene VoltageFluor 2 (fVF 2) reveals changes to cardiac action potentials (APs) upon treatment with cisapride.*

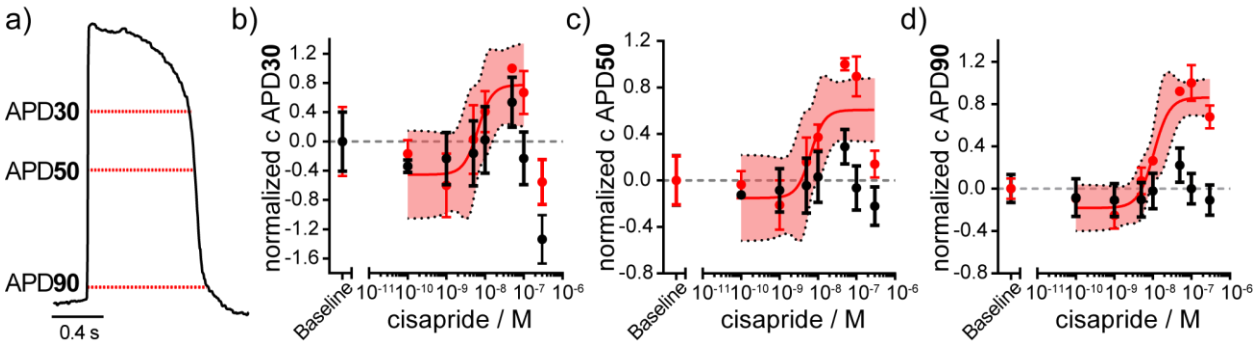

Figure 2-12. Fluorene VoltageFluor 2 (fVF 2) reveals changes to cardiac action potentials (APs) upon treatment with cisapride. (a) Action potential duration (APD) values calculated from the maximum derivative of the depolarization to the repolarization at 70, 50, and 10% of the maximum depolarization value are corrected for beat rate and reported as cAPD30, cAPD50, and cAPD90, respectively. Treatment of monolayers cultured for 14 days with doses of cisapride from 0.1 to 300 nM (red) results in (b) little change in cAPD30, (c) a moderate increase in cAPD50, and (d) a clear increase in cAPD90. Black points indicate data for dimethyl sulfoxide-treated control samples. Plots indicate mean values ± the standard error of the mean for n = 4 independent experiments.

2.9 References

(1) Tsien, R. Y. Building and Breeding Molecules to Spy on Cells and Tumors. *FEBS Lett.* **2005**, *579*, 927–932.

(2) Yun, S. W.; Kang, N. Y.; Park, S. J.; Ha, H. H.; Kim, Y. K.; Lee, J. S.; Chang, Y. T. Diversity Oriented Fluorescence Library Approach (DOFLA) for Live Cell Imaging Probe Development. *Acc. Chem. Res.* **2014**, *47* (4), 1277–1286.

(3) Lavis, L. D. Teaching Old Dyes New Tricks: Biological Probes Built from Fluoresceins and Rhodamines. *Annu. Rev. Biochem.* **2017**, *86* (1), 825–843.

(4) Klymchenko, A. S. Solvatochromic and Fluorogenic Dyes as Environment-Sensitive Probes: Design and Biological Applications. *Acc. Chem. Res.* **2017**, *50* (2), 366–375.

(5) Dal Molin, M.; Verolet, Q.; Colom, A.; Letrun, R.; Derivery, E.; Gonzalez-Gaitan, M.; Vauthey, E.; Roux, A.; Sakai, N.; Matile, S. Fluorescent Flippers for Mechanosensitive Membrane Probes. *J. Am. Chem. Soc.* **2015**, *137* (2), 568–571.

(6) Peterka, D. S.; Takahashi, H.; Yuste, R. Imaging Voltage in Neurons. *Neuron* **2011**, *69* (1), 9–21.

(7) Miller, E. W.; Lin, J. Y.; Frady, E. P.; Steinbach, P. A.; Kristan, W. B.; Tsien, R. Y. Optically Monitoring Voltage in Neurons by Photo- Induced Electron Transfer through Molecular Wires. *Proc. Natl. Acad. Sci. U. S. A.* **2011**, *109* (6), 2114–2119.

(8) Miller, E. W. Small Molecule Fluorescent Voltage Indicators for Studying Membrane Potential. *Curr. Opin. Chem. Biol.* **2016**, *33*, 74–80.

(9) Deal, P. E.; Kulkarni, R. U.; Al-Abdullatif, S. H.; Miller, E. W. Isomerically Pure Tetramethylrhodamine Voltage Reporters. *J. Am. Chem. Soc.* **2016**, *138* (29), 9085–9088.

(10) Huang, Y.-L.; Walker, A. S.; Miller, E. W. A Photostable Silicon Rhodamine Platform for Optical Voltage Sensing. *J. Am. Chem. Soc.* **2015**, *137*, 10767–10776.

(11) Davis, W. B.; Svec, W. A.; Ratner, M. a; Wasielewski, M. R. Molecular-Wire Behaviour in p-Phenylenevinylene Oligomers. *Nature* **1998**, *396*, 60–63.

(12) Pourtois, G.; Beljonne, D.; Cornil, J.; Ratner, M. a.; Brédas, J. L. Photoinduced Electron-Transfer Processes along Molecular Wires Based on Phenylenevinylene Oligomers: A Quantum-Chemical Insight. *J. Am. Chem. Soc.* **2002**, *124* (16), 4436–4447.

(13) Woodford, C. R.; Frady, E. P.; Smith, R. S.; Morey, B.; Canzi, G.; Palida, S. F.; Araneda, R. C.; Kristan, W. B.; Kubiak, C. P.; Miller, E. W.; et al. Improved PeT Molecules for Optically Sensing Voltage in Neurons. *J. Am. Chem. Soc.* **2015**, *137* (5), 1817–1824.

(14) Goldsmith, R. H.; Sinks, L. E.; Kelley, R. F.; Betzen, L. J.; Liu, W.; Weiss, E. a; Ratner, M. A.; Wasielewski, M. R. Wire-like Charge Transport at near Constant Bridge Energy through Fluorene Oligomers. *Proc. Natl. Acad. Sci. U. S. A.* **2005**, *102* (10), 3540–3545.

(15) Eng, M. P.; Albinsson, B. Non-Exponential Distance Dependence of Bridge-Mediated

Electronic Coupling. *Angew. Chemie - Int. Ed.* **2006**, *45* (34), 5626–5629.

(16) Albinsson, B.; Mårtensson, J. Long-Range Electron and Excitation Energy Transfer in Donor-Bridge-Acceptor Systems. *J. Photochem. Photobiol. C Photochem. Rev.* **2008**, *9* (3), 138–155.

(17) Nacci, C.; Viertel, A.; Hecht, S.; Grill, L. Covalent Assembly and Characterization of Nonsymmetrical Single-Molecule Nodes. *Angew. Chemie - Int. Ed.* **2016**, *55* (44), 13724–13728.

(18) Kleeberg, C.; Dang, L.; Lin, Z.; Marder, T. B. A Facile Route to Aryl Boronates: Room-Temperature, Copper-Catalyzed Borylation of Aryl Halides with Alkoxy Diboron Reagents. *Angew. Chemie - Int. Ed.* **2009**, *48* (29), 5350–5354.

(19) Sager, P. T.; Gintant, G.; Turner, J. R.; Pettit, S.; Stockbridge, N. Rechanneling the Cardiac Proarrhythmia Safety Paradigm: A Meeting Report from the Cardiac Safety Research Consortium. *Am. Heart J.* **2014**, *167* (3), 292–300.

(20) Colatsky, T.; Fermini, B.; Gintant, G.; Pierson, J. B.; Sager, P.; Sekino, Y.; Strauss, D. G.; Stockbridge, N. The Comprehensive in Vitro Proarrhythmia Assay (CiPA) Initiative — Update on Progress. *J. Pharmacol. Toxicol. Methods* **2016**, *81*.

(21) Mathur, A.; Loskill, P.; Shao, K.; Huebsch, N.; Hong, S.; Marcus, S. G.; Marks, N.; Mandegar, M.; Conklin, B. R.; Lee, L. P.; et al. Human IPSC-Based Cardiac Microphysiological System for Drug Screening Applications. *Sci. Rep.* **2015**, *5*, 8883.

(22) Lian, X.; Hsiao, C.; Wilson, G.; Zhu, K.; Hazeltine, L. B.; Azarin, S. M.; Raval, K. K.; Zhang, J.; Kamp, T. J.; Palecek, S. P. Robust Cardiomyocyte Differentiation from Human Pluripotent Stem Cells via Temporal Modulation of Canonical Wnt Signaling. *Proc. Natl. Acad. Sci.* **2012**, *109* (27).

(23) Ma, Z.; Wang, J.; Loskill, P.; Huebsch, N.; Koo, S.; Svedlund, F. L.; Marks, N. C.; Hua, E. W.; Grigoropoulos, C. P.; Conklin, B. R.; et al. Self-Organizing Human Cardiac Microchambers Mediated by Geometric Confinement. *Nat. Commun.* **2015**, *6*.

(24) Huebsch, N.; Loskill, P.; Deveshwar, N.; Spencer, C. I.; Judge, L. M.; Mandegar, M. A.; Fox, C. B.; Mohamed, T. M. A.; Ma, Z.; Mathur, A.; et al. Miniaturized IPS-Cell-Derived Cardiac Muscles for Physiologically Relevant Drug Response Analyses. *Sci. Rep.* **2016**, *6*.

(25) Ma, Z.; Huebsch, N.; Koo, S.; Mandegar, M. A.; Siemons, B.; Boggess, S.; Conklin, B. R.; Grigoropoulos, C. P.; Healy, K. E. Contractile Deficits in Engineered Cardiac Microtissues as a Result of MYBPC3 Deficiency and Mechanical Overload. *Nat. Biomed. Eng.* **2018**, *2* (12), 955–967.

(26) Laughner, J. I.; Ng, F. S.; Sulkin, M. S.; Arthur, R. M.; Efimov, I. R. Processing and Analysis of Cardiac Optical Mapping Data Obtained with Potentiometric Dyes. *Am. J. Physiol. Heart Circ. Physiol.* **2012**, *303* (7).

(27) Dempsey, G. T.; Chaudhary, K. W.; Atwater, N.; Nguyen, C.; Brown, B. S.; Mcneish, J. D.; Cohen, A. E.; Kralj, J. M. Cardiotoxicity Screening with Simultaneous Optogenetic

Pacing, Voltage Imaging and Calcium Imaging. *J. Pharmacol. Toxicol. Methods* **2016**, *81*, 240–250.

(28) Lu, H. R.; Hortigon-Vinagre, M. P.; Zamora, V.; Kopljar, I.; De Bondt, A.; Gallacher, D. J.; Smith, G. Application of Optical Action Potentials in Human Induced Pluripotent Stem Cells-Derived Cardiomyocytes to Predict Drug-Induced Cardiac Arrhythmias. *J. Pharmacol. Toxicol. Methods* **2017**, *87*, 53–67.

(29) Luo, S.; Michler, K.; Johnston, P.; Macfarlane, P. W. A Comparison of Commonly Used QT Correction Formulae: The Effect of Heart Rate on the QTc of Normal ECGs. *J. Electrocardiol.* **2004**, *37*, 81–90.

(30) Itzhaki, I.; Maizels, L.; Huber, I.; Zwi-Dantsis, L.; Caspi, O.; Winterstern, A.; Feldman, O.; Gepstein, A.; Arbel, G.; Hammerman, H.; et al. Modelling the Long QT Syndrome with Induced Pluripotent Stem Cells. *Nature* **2011**, *471* (7337), 225–230.

(31) Caspi, O.; Itzhaki, I.; Kehat, I.; Gepstein, A.; Arbel, G.; Huber, I.; Satin, J.; Gepstein, L. In Vitro Electrophysiological Drug Testing Using Human Embryonic Stem Cell Derived Cardiomyocytes. *Stem Cells Dev.* **2009**, *18* (1), 161–172.

(32) Crumb, W. J.; Vicente, J.; Johannesen, L.; Strauss, D. G. An Evaluation of 30 Clinical Drugs against the Comprehensive in Vitro Proarrhythmia Assay (CiPA) Proposed Ion Channel Panel. *J. Pharmacol. Toxicol. Methods* **2016**, *81*, 251–262.

(33) Redfern, W. S.; Carlsson, L.; Davis, A. S.; Lynch, W. G.; MacKenzie, I.; Palethorpe, S.; Siegl, P. K. S. S.; Strang, I.; Sullivan, A. T.; Wallis, R.; et al. Relationships between Preclinical Cardiac Electrophysiology, Clinical QT Interval Prolongation and Torsade de Pointes for a Broad Range of Drugs: Evidence for a Provisional Safety Margin in Drug Development. *Cardiovasc. Res.* **2003**, *58* (1), 32–45.

(34) Harris, K.; Aylott, M.; Cui, Y.; Louttit, J. B.; McMahon, N. C.; Sridhar, A. Comparison of Electrophysiological Data from Human-Induced Pluripotent Stem Cell-Derived Cardiomyocytes to Functional Preclinical Safety Assays. *Toxicol. Sci.* **2013**, *134* (2), 412–426.

(35) McKeithan, W. L.; Savchenko, A.; Yu, M. S.; Cerignoli, F.; Bruyneel, A. A. N.; Price, J. H.; Colas, A. R.; Miller, E. W.; Cashman, J. R.; Mercola, M. An Automated Platform for Assessment of Congenital and Drug-Induced Arrhythmia with Hipsc-Derived Cardiomyocytes. *Front. Physiol.* **2017**, *8*.

(36) Bedut, S.; Seminatore-Nole, C.; Lamamy, V.; Caignard, S.; Boutin, J. A.; Nosjean, O.; Stephan, J. P.; Coge, F. High-Throughput Drug Profiling with Voltage-and Calcium-Sensitive Fluorescent Probes in Human IPSC-Derived Cardiomyocytes. *Am. J. Physiol. - Hear. Circ. Physiol.* **2016**, *311* (1).

(37) McPheeters, MT; Wang, YT; Laurita KR; Jenkins, M. An Optical System for High-Throughput Screening of Cardiac Electrophysiology for Human Cardiomyocytes. *Physiology.* **2017**.

(38) Rohr, S.; Salzberg, B. M. Multiple Site Optical Recording of Transmembrane Voltage (MSORTV) in Patterned Growth Heart Cell Cultures: Assessing Electrical Behavior, with Microsecond Resolution, on a Cellular and Subcellular Scale. *Biophys. J.* **1994**, *67* (3), 1301–1315.

(39) Fery-Forgues, S.; Lavabre, D. Are Fluorescence Quantum Yields So Tricky to Measure? A Demonstration Using Familiar Stationery Products. *J. Chem. Educ.* **1999**, *76* (9), 1260.

(40) Edelstein, A. D.; Tsuchida, M. A.; Amodaj, N.; Pinkard, H.; Vale, R. D.; Stuurman, N. Advanced Methods of Microscope Control Using μManager Software. *J. Biol. Methods* **2014**, *1* (2).

(41) Edelstein, A.; Amodaj, N.; Hoover, K.; Vale, R.; Stuurman, N. Computer Control of Microscopes Using μManager. *Curr. Protoc. Mol. Biol.* **2010**.

(42) Boelens, H. F. M.; Dijkstra, R. J.; Eilers, P. H. C.; Fitzpatrick, F.; Westerhuis, J. A. New Background Correction Method for Liquid Chromatography with Diode Array Detection, Infrared Spectroscopic Detection and Raman Spectroscopic Detection. *J. Chromatogr. A* **2004**, *1057* (1–2), 21–30.

(43) Horrii, D.; Suematsu, S.; Tamamitsu, K.; Tanak, H.; Kuroboshi, M.; Koto, K. Phenyl-Terminated Oligofluorenes and Their Manufacture. JP2013107845A, 2011.

(44) Dong, M.; Babalhavaeji, A.; Hansen, M. J.; Kálmán, L.; Woolley, G. A. Red, Far-Red, and near Infrared Photoswitches Based on Azonium Ions. *Chem. Commun.* **2015**, *51* (65), 12981–12984.

(45) Marcin, L. R.; Thompson, L. A.; Boy, K. M.; Guernon, J. M.; Higgins, M. A.; Shi, J.; Wu, Y.-J.; Zhang, Y.; Macor, J. E. Preparation of Bicyclic Compounds, Especially Bicyclic Triazoles, for the Reduction of Beta-Amyloid Protein Production. WO199983141A1, 2010.

(46) Kramer, J.; Obejero-Paz, C. A.; Myatt, G.; Kuryshev, Y. A.; Bruening-Wright, A.; Verducci, J. S.; Brown, A. M. MICE Models: Superior to the HERG Model in Predicting Torsade de Pointes. *Sci. Rep.* **2013**, *3*.

(47) Fossa, A. A.; Wisialowski, T.; Wolfgang, E.; Wang, E.; Avery, M.; Raunig, D. L.; Fermini, B. Differential Effect of HERG Blocking Agents on Cardiac Electrical Alternans in the Guinea Pig. *Eur. J. Pharmacol.* **2004**, *486* (2), 209–221.

Chapter 3:

Vinyl-fluorene Molecular Wires with Enhanced Sensing Properties and Reduced Phototoxicity

Abstract

Fluorescent voltage indicators are an attractive alternative for studying the electrical activity of excitable cells, however the development of tools that are both highly sensitive and low in toxicity over long term experiments remains a challenge. Previously, we reported a fluorene-based PeT sensor that is much less phototoxic than previous voltage indicators in cardiomyocyte monolayers, but it suffers from low sensitivity to membrane potential changes. Here, we report that the addition of a single vinyl spacer in the fluorene molecular wire scaffold improves the voltage sensitivity of PeT indicator 1.5- to 3.5-fold over fluorene-based voltage probes. Furthermore, we demonstrate the improved ability of vinyl-fluorene VoltageFluors (v-fVFs) to monitor action potential kinetics in both mammalian neurons and human induced pluripotent stem cell derived cardiomyocytes (hiPSC-CMs). Addition of the vinyl spacer between the aniline donor and fluorene monomer results in indicators that are significantly less phototoxic in cardiomyocyte monolayers. These results demonstrate how structural modification to the voltage sensing domain have a large effect on improving the overall properties of PeT-based voltage indicators.

Portions of this work were performed in collaboration with the following person:

Initial synthesis of 7v-fVF 2 was performed by Shivaani Gandhi.

3.1 Motivation and design of a hybrid molecular wire for voltage sensing

Cells expend a huge proportion of their energy budget to maintain tight control over the electrical potential across the plasma membrane. This membrane potential (V_{mem}) can change quickly—giving rise to action potentials in excitable cells such as neurons and cardiomyocytes—which makes the study of these biophysical phenomena challenging. Patch-clamp electrophysiology is the gold-standard for measuring these electrical impulses in live cells, but these techniques are highly invasive and low throughput.[1] Dysregulation of electrical activity in these excitable cells is involved in many human diseases, such as epilepsy and long-QT syndrome, and continued development of methods to better understand this the cause of this activity will improve human health.

We have recently undertaken a program to develop small-molecule fluorescent indicators that measure rapid changes in V_{mem} in live cells.[2] Using fluorescence to monitor V_{mem} dynamics is attractive because it circumvents the issues associated with electrode-based. VoltageFluor indicators exhibit an increase in fluorescence in response to membrane depolarizations due to attenuation of fluorescence quenching by photoinduced electron transfer (PeT).[3] Within the VoltageFluor scaffold, the identity of the fluorescent reporter, the aniline electron donor, and the molecular wire can be modified to tune the spectral and voltage sensing properties of the probe.[4–6]

In a previous report, we demonstrated 9',9'-dimethylfluorene as a substitute for the phenylene-vinylene-based molecular wire in the VoltageFluor scaffold (Scheme 3-1).[7] These fluorene VoltageFluors (fVFs) are less phototoxic than other voltage indicators in cardiomyocyte monolayers, making them useful for reporting cardiac action potential kinetics over prolonged experiments. However, fVFs are much less sensitive to changes in V_{mem} than their phenylene vinylene-based counterparts. Still, reduced phototoxicity is a desirable feature for long-term recordings of voltage activity and the fluorene molecular wire presents a potential solution worth further exploration. We sought to improve the sensitivity of the fluorene molecular wire scaffold while harnessing its reduced phototoxicity characteristics.

The reduced voltage sensitivity of the fluorene molecular wire scaffold can be attributed to the increase in the electron attenuation value (0.09 $Å^{-1}$), or β factor, relative to the phenylene-vinylene scaffold (β = 0.04 $Å^{-1}$).[8–10] β is a parameter that describes the effectiveness of a scaffold as a molecular wire. Although β also depend on the identity of the electron donor and acceptor, efforts to improve the voltage sensitivity of a VoltageFluor scaffold should focus on incorporating molecular wires with lower β values.[11,12]

Wielopolski *et al.* demonstrated that combining structural features of fluorene and phenylene-vinylene based molecular wires allows for tuning of charge transfer kinetics.[13] In a donor-bridge-acceptor (DBA) system comprised of C_{60} fullerene electron acceptor and tetrathiafulvalene (TTF) donor, they found oligo-fluorenevinylene (oFV) wires have a measured β value of 0.075 $Å^{-1}$, an improvement over previous reports with pure oligo-fluorene wires. Given this study, we hypothesized incorporation of a vinylene spacer into the fluorene VoltageFluor scaffold would provide a boost in voltage sensitivity but would have little effect on phototoxicity (**Scheme 3-1**). These new indicators, vinylene-fluorene VoltageFluors (v-fVFs) represent a structural hybrid between the two wire scaffolds previously reported by our laboratory.

3.2 Synthesis and spectroscopic characterization of vinyl-fluorene VoltageFluors

We designed indicators with the vinyl spacer in two different regioisomeric locations: between the fluorene subunit and the dichlorofluoresein fluorophore (2v-fVFs, **Scheme 3-1**), and between the aniline donor and the fluorene (7v-fVFs, **Scheme 3-1**). The numbers 2 and 7 indicate the substituent position of the vinyl group on the fluorene ring. The synthesis of 2v-fVF indicators proceeds in the same manner as previously reported fVF indicators (**Scheme 3-5**)[7], then incorportating vinyl N-methyliminodiacetic acid (MIDA) boronate ester before addition to the fluorophore (**Scheme 3-2**). Cross-coupling using palladium(II) acetate and tri-*o*-tolylphosphine gives vinyl-fluorene MIDA boronate esters **1** and **2** in good yield. Suzuki-Miyaura coupling with modified conditions from Burke and coworkers[14] provides 2v-fVF indicators **3** (2v-fVF 1) and **4** (2v-fVF 2).

Construction of 7v-fVFs began by converting substituted 4-nitrobenzaldehydes to styrenes **7** and **8** by Wittig olefination (**Scheme 3-3**). Palladium-catalyzed cross-coupling with 2-bromo-7-iodo-9,9-dimethyl-9H-fluorene yields nitrostyryl-fluorene wires **9** and **10** as orange solids. Starting from the 4-nitrostyrenes (**Scheme 3-6**) was essential, as using 4-aminostyrenes in the cross-coupling reaction yields the branched isomer in a 1:2 ratio with the desired linear isomer and could not be separated by chromatography. Nitrostyryl-fluorene wires are converted to anilines **11** and **12** by reduction with tin(II) chloride, which is followed by reductive amination of formaldehyde to yield **13** and **14** as bright yellow solids (**Scheme 3-3**). Palladium catalyzed cross-coupling with bis(pinacolato)diboron provided pinacol boronic esters **15** and **16** for coupling with 2,7-dichlorosulfofluorescein. The following palladium catalyzed Suzuki-Miyaura reaction provided 7v-fVF indicators **17** (7v-fVF 1) and **18** (7v-fVF 2). To confirm that the effect of the structural changes on voltage sensing is due to changing PeT kinetics, we also constructed indicators that lack an aniline donor (**Scheme 3-4, 2v-fVF 0** and **7v-fVF 0**).

Spectroscopic characterization of these six indicators revealed that addition of the vinyl spacer had no effect on the absorption or emission of the xanthene fluorophore (**Figure 3-1, Figure 3-2**, **Table 3-1**). However, a bathochromic shift of the molecular wire absorbance is observed in the 2-vinyl indicators, and to a greater extent with 7-vinyl indicators **(Figure 3-1, Table 3-1**). This effect is due to the increased conjugation in the molecular wire system, which is electronically decoupled from the xanthene chromophore in the ground state. In agreement with a PeT mechanism, indicators lacking an aniline exhibit quantum yields two to three times higher than counterparts with aniline donor (**Table 3-1**).

3.3 Evaluation of voltage sensing properties in live cells

To test the effect of vinyl spacers on voltage sensitivity in the scaffold, we recorded the fluorescence signal of voltage-clamped HEK293T cells stained with vinyl-fluorene VoltageFluors. By altering V_{mem} from +100 to -100 mV in 20 mV increments, we evaluated the fractional change in fluorescence for each indicator. Indicators with the 2-vinyl spacer (**2v-fVF 1** and **2v-fVF 2**) exhibit a 7.4 and 15.2% F/F_o per 100 mV, respectively (**Figure 3-3, Table 3-2**)**.** When compared to the respective fluorene VoltageFluors, this structural modification produces a modest 1.6 and 1.4 fold improvement to sensitivity (fVF 1, 4.5%; fVF 2, 10.5% F/F_o per 100 mV change, **Figure 3-5**).[7] The 7-vinyl spacer improves voltage sensitivity to a much greater extent; **7v-fVF 1** has a 16.5% F/F_o (3.5 fold improvement) and **7v-fVF 2** exhibited a 30.6% F/F_o (2.9 fold improvement)

per 100 mV change in V_{mem}. Indicators lacking an aniline donor (**2v-fVF 0** and **7v-fVF 0**) were not sensitive the changes in V_{mem} as expected (**Figure 3-5g-i, p-r, Table 3-2**). These results suggest that increased conjugation and rigidity of the molecular wire improves voltage sensitivity but continuous conjugation between the aniline donor and molecular wire is the most effective for facilitating PeT. This is to be expected, as orbital overlap between the electron donor and molecular wire has been an important design consideration in donor-bridge-acceptor scaffolds with electron transfer mechanisms.[11]

We evaluated the four voltage sensitive indicators in mammalian neuron and cardiomyocyte cultures. All vinyl-fluorene indicators report neuronal action potentials with modest $\%F/F_o$ and good signal-to noise (SNR) in evoked activity experiments with rat hippocampal neurons (**Table 3-3**, **Figure 3-7**), and outperform fVF 2, the highest performing indicator in the fluorene VoltageFluor series.[7] **7v-fVF 1** performed the best of these new indicators in terms of SNR (18.5:1), while **7v-fVF 2** exhibit the highest $\Delta F/F_o$ (9%). Still, VF2.1.Cl outperforms vinyl-fluorene indicators in evoked activity experiments, with a measured SNR of 35:1, nearly double that of **7v-fVF 1** (**Table 3-3**, **Figure 3-7**). Comparison in spontaneously contracting human induced pluripotent stem cell derived cardiomyocyte (hiPSC-CM) monolayers demonstrates the ability of each vinyl-fluorene indicator to monitor cardiac action potential kinetics with high SNR. In these experiments, vinyl-fluorene VoltageFluors outperform both fVF 2 and VF2.1.Cl when comparing SNR, although with a lower $\%F/F_o$ than VF2.1.Cl (**Table 3-3, Figure 3-6, Figure 3-8**). We observe 2v-fVFs have the highest SNR (326-430:1) and $\%F/F_o$ (6-7.8%) of these new indicators, the opposite of what we observed in neurons.

3.4 Phototoxicity studies of VoltageFluors in hiPSC cardiomyocytes

Previously, we observed that substituting the phenylene-vinylene molecular wire with a fluorene monomer in the VF scaffold significantly reduces phototoxicity in cardiomyocytes, allowing for up to ten minutes of illumination without changes to recorded action potentials.[7] Thus, we were curious whether these vinyl-fluorene based voltage indicators would more like fVF 2 or previous VF dyes in terms of phototoxicity. We illuminated hiPSC-CM monolayers stained with the excitation LED for several minutes, making ten second recordings every minute to monitor action potential morphology over time. We were surprised to find that 2v-fVFs are extremely phototoxic—action potential morphology changes after just one (**2v-fVF 1**) to three (**2v-fVF 2**) minutes of illumination and cessation of spontaneous contraction was observed (**Figure 3-9, Figure 3-10**). This degree of toxicity was similar to VF2.1.Cl (**Figure 3-10**). However, placing the vinyl spacer at the 7-position results in indicators that were much less phototoxic, like fVF 2. Recordings can be made for up to 10 minutes with both **7v-fVF 1** and **7v-fVF 2** without observing any changes to action potential kinetics (**Figure 3-9, Figure 3-10**). While one can make recordings for longer with fVF 2, the low starting sensitivity and rapid decline of signal makes observation at these extended periods impractical (**Figure 3-10i-j**). SNR remains high for both **7v-fVF 1** and **7v-fVF 2** for the duration of these experiments—staying above 100:1 after illuminating **7v-fVF 2** for 9 minutes—permitting long-term recordings of electrical activity in cardiomyocyte monolayers (**Figure 3-10**).

The reason for these differences in phototoxicity amongst VoltageFluor indicators remains elusive. Before constructing vinyl-fluorene VoltageFluors, we believed phototoxicity was related

to the voltage sensitivity of the indicator, and that more sensitive indicators would exhibit greater toxicity. This assumes there is a trade-off between an indicator with better signal detection properties and an indicator that is less sensitive but less perturbative. However, results with v-fVFs suggest this is not the case, as the two most sensitive indicators in voltage-clamp experiments, **7v-fVF 1** and **7v-fVF 2**, were also the least toxic after prolonged illumination with light. Another explanation is that differences in the concentration of indicator in the cell membrane are the source of differences in phototoxicity. Although cells were incubated in solutions with the same concentration of indicator, bath application does not insure that the concentration in the membrane will be the same as this also relies on the membrane affinity of the indicator versus solubility in aqueous solution. For example, comparison of *in vitro* quantum yields (**Table 3-1**) and relative cell brightness (**Table 3-2**, **Figure 3-4**) of the non-sensitive probes **2v-fVF 0** and **7v-fVF 0** shows a discrepancy between indictors that are brighter in solution (**7v-fVF 0,** $\Phi_{Fl} = 0.23$) and indicators that are brighter in cells (**2v-fVF 0**, $\Phi_{Fl} = 0.16$). The difference in phototoxicity could be because the 2v-fVF indicators have a higher membrane affinity and are at a higher concentration than 7v-fVF indicators in the plasma membrane, and thus produce a higher concentration of reactive oxygen species (ROS). Indeed, phototoxicity of many voltage indicators can be decreased by lowering the concentration used to stain cells.[7,15–17] We also examined the rate of photobleaching as a possible source for the difference in phototoxicity. In HEK293T cells, 7v-fVFs photobleach less quickly than their 2v-fVF counterparts, which would align with their relative degree of phototoxicity if we assume higher rates of photobleaching would be more phototoxic (**Figure 3-11**). However, comparison to VF2.1.Cl and fVF 2 refutes this hypothesis, as fVF 2 photobleaches more rapidly than VF2.1.Cl but is less phototoxic. Furthermore, the photobleach rate in hiPSC-CMs is similar for all four v-fVFs. A final, speculative possibility for the difference in phototoxicity is relative positioning of VoltageFluor indicators in the cell membrane. In the 2v-fVFs and VF2.1.Cl, the vinyl group that attaches the molecular wire to the pendant ring of the chromophore sits closer to the aqueous environment outside the cell, and thus if the molecule crosses to the triplet state it can react with singlet oxygen and produce ROS.[18] However, in the case of the 7v-fVFs, the vinyl group is buried in the cell membrane and is exposed to lower concentrations of singlet oxygen, thus producing less ROS. This argument could also explain the reduced phototoxicity of fVF 2, which lacks vinyl spacers. Further studies are needed to provide support for any of the suggested hypotheses and should include time-resolved spectroscopy to obtain information about the excited states of these.

3.5 Conclusions and outlook

In summary, we developed four new voltage indicators with higher sensitivity to membrane potential changes than previous fluorene VoltageFluors by adding a vinyl spacer to the molecular wire scaffold. We present the synthesis and characterization of these indicators in HEK293T cells, mammalian neurons, and human iPSC derived cardiomyocytes to demonstrate the effect of this small structural change to the molecular wire on the performance of the voltage indicator. We found that adding a vinyl spacer between the electron donating aniline and the fluorene in the molecular wire (7v-fVFs) gave the largest boost in sensitivity (2.9-3.5 fold) compared to fluorene VoltageFluors. More importantly, these two indicators remained less phototoxic in cardiomyocytes relative to VF2.1.Cl, while maintaining higher SNR throughout extended recordings. Vinyl-fluorene VoltageFluors represent an improvement over the fluorene

VoltageFluor scaffold and are an attractive alternative to the traditional VoltageFluor scaffold for prolonged recordings of electrical activity in cells.

3.6 Materials and methods

3.6.1 General method for chemical synthesis and characterization

Palladium catalysts, phosphine ligands, and tin(II) chloride were purchased from Stream Chemical. Deuterated solvents used for NMR studies were purchased from Cambridge Isotope Laboratories. Anhydrous solvents and all other chemical reagents were purchased from Sigma Aldrich, Acros Chemical, or Oakwood Chemical (South Carolina, USA) and used without further purification. References to previously synthesized compounds are provided along with characterization data. Thin layer chromatography (TLC) (Silicycle, F254, 250 μm) and preparative thin layer chromatography (PTLC) (Silicycle, F254, 1000 μm) was performed on glass backed plates pre-coated with silica gel and were visualized by fluorescence quenching under UV light. Flash column chromatography was performed on Silicycle Silica Flash F60 (230–400 Mesh) using a forced flow of air at 0.5–1.0 bar. NMR spectra were measured on Bruker AVB-400 MHz, 100 MHz, AVQ-400 MHz, 100 MHz, Bruker AV-600 MHz, 150 MHz. NMR spectra measured on Bruker AVII-900 MHz, 225 MHz, equipped with a TCI cryoprobe accessory, were performed by Dr. Jeffrey Pelton (QB3). Chemical shifts are expressed in parts per million (ppm) and are referenced to $CDCl_3$ (7.26 ppm, 77.0 ppm), DMSO-d_6 (2.50 ppm, 40 ppm), or acetone-d_6 (2.04 ppm, 29.8 and 206.3 ppm). Coupling constants are reported as Hertz (Hz). Splitting patterns are indicated as follows: s, singlet; d, doublet; t, triplet; q, quartet; dd, doublet of doublet; m, multiplet. High-resolution mass spectra (HR-ESI-MS) were measured by the QB3/Chemistry mass spectrometry service at University of California, Berkeley. High performance liquid chromatography (HPLC) and low resolution ESI Mass Spectrometry were performed on an Agilent Infinity 1200 analytical instrument coupled to an Advion CMS-L ESI mass spectrometer. The column used for the analytical HPLC was Phenomenex Luna 5 μm C18(2) (4.6 mm I.D. × 75 mm) with a flow rate of 1.0 mL/min. The mobile phases were MQ-H2O with 0.05% trifluoroacetic acid (eluent A) and HPLC grade acetonitrile with 0.05% trifluoroacetic acid (eluent B). Signals were monitored at 254, 350 and 480 nm over 10 min with a gradient of 10-100% eluent B unless otherwise noted. Ultra-high performance liquid chromatography (UHPLC) for purification of final compounds was performed using a Waters Acquity Autopurificaiton system equipped with a Phenomenex Luna 10 μm C18(2) column (21.2 mm I.D. x 250 mm with a flow rate of 30.0 mL/min, made available by the Catalysis Facility of Lawrence Berkeley National Laboratory (Berkeley, CA). The mobile phases were MQ-H2O with 0.05% trifluoroacetic acid (eluent A) and HPLC grade acetonitrile with 0.05% trifluoroacetic acid (eluent B). Signals were monitored at 254 and 350 nm over 20 min with a gradient of 10-100% eluent B, unless otherwise noted.

3.6.2 Spectroscopic studies

Stock solutions of vinyl-fluorene VoltageFluors were prepared in DMSO (500 μM) and diluted with PBS (10 mM KH_2PO_4, 30 mM $Na_2HPO_4 \cdot 7H_2O$, 1.55 M NaCl, pH 7.2) solution containing 0.10 % (w/w) SDS (1:500 dilution). UV-Vis absorbance and fluorescence spectra were recorded using a Shimadzu 2501 Spectrophotometer (Shimadzu) and a Quantamaster Master 4 L-format scanning spectrofluorometer (Photon Technologies International). The fluorometer is equipped with an LPS-220B 75-W xenon lamp and power supply, A-1010B lamp housing with integrated

igniter, switchable 814 photon-counting/analog photomultiplier detection unit, and MD5020 motor driver. Samples were measured in 1-cm path length quartz cuvettes (Starna Cells).

Relative quantum yields (Φ_{Fl}) were calculated by comparison to fluorescein (Φ_{Fl} = 0.93 in 0.1 M NaOH) and rhodamine 6G (Φ_{Fl} = 0.95 in ethanol) as references.[19] Briefly, stock solutions of standards were prepared in DMSO (0.25-1.25 mM) and diluted with appropriate solvent (1:1000 dilution). Absorption and emission (excitation = 485 nm) were taken at 5 concentrations. The absorption value at the excitation wavelength (485 nm) was plotted against the integration of the area of fluorescence curve (495-675 nm). For fluorescein, the integration of the area of the fluorescence curve was also taken with an excitation at 450 nm. The area from 460-675 nm and 495-675 nm was used to extrapolate the area of the fluorescence curve with an excitation at 485 nm. This ensured the full fluorescence area of fluorescein excited at 485 nm was used for Φ_{Fl} calculations. The slope of the linear best fit of the data was used to calculate the relative Φ_{Fl} by the equation $\Phi_{Fl(X)} = \Phi_{Fl(R)}(S_R/S_X)(\eta_X/\eta_R)^2$, where S_R and S_X are the slopes of the reference compound and unknown, respectively, and η is the refractive index of the solution. This method was validated by cross-referencing the reported Φ_{Fl} values of fluorescein and rhodamine 6G to the calculated Φ_{Fl} using the one standard as a reference for the other and vice versa. Calculated Φ_{Fl} within 10% of the reported value for both standards ensured that Φ_{Fl} calculated for vinyl-fluorene VoltageFluors was reliable within 10% error.

3.6.3 Cell culture

All animal procedures were approved by the UC Berkeley Animal Care and Use Committees and conformed to the NIH Guide for the Care and Use and Laboratory Animals and the Public Health Policy.

Human embryonic kidney (HEK) 293T cells

HEK293T cells were acquired from the UC Berkeley Cell Culture Facility. Cells were passaged and plated onto 25 mm glass coverslips coated with Poly-D-Lysine (PDL; 1 mg/mL; Sigma-Aldrich) to a confluency of ~15% and 40% for electrophysiology and imaging, respectively. HEK293T cells were plated and maintained in Dulbecco's modified eagle medium (DMEM) supplemented with 4.5 g/L D-glucose, 10% fetal bovine serum (FBS), and 1% Glutamax.

Rat hippocampal neurons.

Hippocampi were dissected from embryonic day 18 Sprague Dawley rats (Charles River Laboratory) in cold sterile HBSS (zero Ca^{2+}, zero Mg^{2+}). All dissection products were supplied by Invitrogen, unless otherwise stated. Hippocampal tissue was treated with trypsin (2.5%) for 15 min at 37 °C. The tissue was triturated using fire polished Pasteur pipettes, in minimum essential media (MEM) supplemented with 5% fetal bovine serum (FBS; Thermo Scientific), 2% B-27, 2% 1M D-glucose (Fisher Scientific) and 1% glutamax. The dissociated cells were plated onto 12 mm diameter coverslips (Fisher Scientific) pre-treated with PDL (as above) at a density of 27,000 cells per coverslip in MEM supplemented media (as above). Neurons were maintained at 37 °C in a humidified incubator with 5 % CO2. At 1 day in vitro (DIV) half of the MEM supplemented media was removed and replaced with Neurobasal media containing 2% B-27 supplement and 1% glutamax. Electrophysiological experiments which were performed on 13-14 DIV neurons.

Differentiation of hiPSC into cardiomyocytes and culture

hiPSCs (WTC11)[20] were cultured on Matrigel (1:100 dilution; Corning)-coated 12 well-plates in StemFlex medium (Gibco). When the cell confluency reached 80–90%, which is referred as day 0, the medium was switched to RPMI 1640 medium (Life Technologies) containing B27 minus insulin supplement (Life Technologies) and 10 µM CHIR99021 GSK3 inhibitor (Peprotech). At day 1, the medium was changed to RPMI 1640 medium containing B27 minus insulin supplement only. At day 3, medium was replaced to RPMI 1640 medium containing B27 supplement without insulin, and 5 µM IWP4 (Peprotech) for 2 days without medium change. On day 5, medium was replaced to RPMI 1640 medium containing B27 minus insulin supplement for 2 days without medium change. On day 7, medium was replaced with RPMI 1640 containing B27 with insulin supplement. After day 7, the medium was changed every two days. Confluent contracting sheets of beating cells appear between days 7 to 15.[21]

Beating sheets were treated with collagenase II for 60-75 minutes. The collagenase solution was carefully transferred to cold DMEM, making sure cardiac sheets were not disturbed. Trypsin (0.25%) was added to dissociated sheets for 4-8 minutes and plated onto 6 well-plates coated with Matrigel (1:100 dilution) in RPMI 1640 medium containing B27 supplement plus ROCK inhibitor Y-27632. 24 hours later, the medium was replaced with fresh RMPI/B27 without ROCK inhibitor. Cardiomyocytes were maintained for 7 days, replacing media every other day, and then were switched to RPMI 1640 medium (-glucose) supplemented with 4 mM sodium lactate (Sigma Aldrich). Cells were maintained in this media for 7 days, replacing every other day, then switched back to RPMI/B27 containing glucose.[22] These purified cardiomyocytes were then used for imaging.

Lactate purified sheets were dissociated with 0.25% trypsin-EDTA (4-8 minutes, depending on density and quality of tissue) and plated onto Matrigel (1:100)-coated Ibidi ® 24 well µ-plates (cat no. 82406) in RPMI 1640 medium containing B27 supplement (containing insulin). Medium was changed every 3 days until imaging. For loading hiPSC cardiomyocytes, voltage dyes were diluted 1 in 1000 in RPMI 1640 with B27 supplement minus Phenol Red to the desired final concentration. Cardiomyocytes were incubated in this solution for 20 minutes at 37 °C, then exchanged with dye-free RPMI 1640 with B27 supplement minus Phenol Red.

3.6.4 Imaging parameters

For experiments with rat hippocampal neurons, Epifluorescence imaging was performed on an AxioExaminer Z-1 (Zeiss) equipped with a Spectra-X Light engine LED light (Lumencor), controlled with Slidebook (v6, Intelligent Imaging Innovations). Images were acquired with a W-Plan-Apo 20x/1.0 water objective (20x; Zeiss) and focused onto either an OrcaFlash4.0 sCMOS camera (sCMOS; Hamamatsu).

Inverted epifluorescence imaging of HEK293T cells and hiPSC cardiomyocytes was performed on an AxioObserver Z-1 (Zeiss), equipped with a Spectra-X Light engine LED light (Lumencor), controlled with µManager (V1.4, open-source, Open Imaging).[23,24] were acquired using a Plan-Apochromat 20/0.8 air objective (20x, Zeiss) or an EC-Plan-NEOFLUAR 40/1.3 oil immersion objective (40x; Zeiss). Images were focused onto an OrcaFlash4.0 sCMOS camera (sCMOS; Hamamatsu).

More detailed imaging information for each experimental application is expanded below.

Membrane staining and photostability in HEK293T cells

HEK293T cells were incubated with an imaging buffer (IB) solution (composition in mM: 139.5 NaCl, 10 HEPES, 5.6 D-glucose, 5.3 KCl, 1.3 $CaCl_2$, 0.49 $MgCl_2$, 0.44 KH_2PO_4, 0.41 $MgSO_4$, 0.34 Na_2HPO_4; 290 mOsm/kg, pH 7.25) containing vinyl-fluorene VoltageFluors (500 nM) at 37°C for 20 min prior to transfer to fresh IB (no dye) for imaging. Microscopic images were acquired with a 40X/1.3NA oil objective (Zeiss) and OrcaFlash4.0 sCMOS camera (Hamamatsu). For fluorescence images, the excitation light was delivered from a LED (9.5 mW/mm^2; 100 ms exposure time) at 475/34 (bandpass) nm and emission was collected with an emission filter (bandpass; 540/50 nm) after passing through a dichroic mirror (510 nm LP).

For photostability experiments HEK293T cells were loaded the same as above. Images (pixel size 0.16 μm × 0.16 μm) were taken every 1 second for 5 minutes with constant illumination of LED (30.4 mW/mm^2; 50 ms exposure for v-fVFs, 5 ms exposure for fVF 2 and VF2.1.Cl). The obtained fluorescence curves were normalized with the fluorescence intensity at t = 0 and averaged (three different cell rafts for each dye).

Voltage sensitivity in HEK293T cells

Functional imaging of the fluorene VoltageFluors was performed using a 40x/1.3 NA oil immersion objective paired with image capture from the sCMOS camera at a sampling rate of 0.5 kHz, focused onto a 100x100 $pixel^2$ ROI (binned 4x4, 66.5x66.5 μm^2). Fluorene VoltageFluors were excited using the 475 nm LED with an intensity of 9.5 mW/mm^2. For initial voltage characterization emission was collection with the emission filter and dichroic listed above.

Evoked and spontaneous activity in rat hippocampal neurons

Extracellular field stimulation was delivered by a Grass Stimulator connected to a recording chamber containing two platinum electrodes (Warner), with triggering provided through a Digidata 1440A digitizer and pCLAMP 10 software (Molecular Devices). Action potentials were triggered by 1 ms 80 V field potentials delivered at 5 Hz. To prevent recurrent activity the HBSS bath solution was supplemented with synaptic blockers 10 μM 2,3-Dioxo-6-nitro-1,2,3,4-tetrahydrobenzo[f]quinoxaline-7-sulfonamide (NBQX; Santa Cruz Biotechnology) and 25 μM DL-2-Amino-5-phosphonopentanoic acid (APV; Sigma-Aldrich). Functional imaging was performed using the sCMOS camera and a 20x water objective. fVF 2 and VF2.1.Cl (500 nM in HBSS) were excited with a 475/34 (bandpass) nm LED with an intensity of 6.9 mW/mm^2 and emission was collected with an emission filter (bandpass; 540/50 nm) after passing through a dichroic mirror (510 nm LP).

Voltage recordings of hiPSC cardiomyocytes and assessment of phototoxicity

Functional recordings of voltage indicators (0.5 μM) were performed using a 20x air objective paired with a sCMOS camera at a sampling rate of 0.2 kHz (4x4 binning and restricted to a 512x125 pixel frame for high-speed acquisition over long periods). Indicators were excited at 475/34 (bandpass) nm with an intensity of 11.1 mW/mm^2 and emission was collected with an emission filter (bandpass; 540/50 nm) after passing through a dichroic mirror (510 nm LP). Routine recordings were made for ten seconds.

Phototoxicity of VoltageFluor dyes was assessed in cardiomyocyte monolayers incubated with 0.5 μM of indicator. These were exposed to constant illumination from the excitation LED (475/34; bandpass) for up to 14 minutes, while typical ten second fluorescence recordings were made at the beginning of each minute.

3.6.5 Image analysis

Analysis of voltage sensitivity in HEK293T cells was performed using ImageJ (FIJI). Briefly, a region of interest (ROI) encompassing the cell body was selected and average fluorescence intensity was calculated for each frame. For background subtraction, a ROI encompassing a region without cells was selected and the average pixel intensity was calculated for each frame. A linear fit to the background trace was calculated and applied to the background, and this was used to subtract background signal from the fluorescence intensity trace. F/F_o values were calculated by dividing the background subtracted trace by the median value of fluorescence when the cell is held at -60 mV. ΔF/F values were calculated by plotting the change in fluorescence (ΔF) vs the applied voltage step and finding the slope of a linear best-fit. For analysis of voltage responses in neurons, regions of interest encompassing cell bodies were drawn in ImageJ and the mean fluorescence intensity for each frame extracted. ΔF/F values were calculated by first subtracting a mean background value from all raw fluorescence frames, bypassing the noise amplification which arises from subtracting background for each frame, to give a background subtracted trace. A baseline fluorescence value is calculated from the first several (10-20) frames of the experiment for evoked activity and was subtracted from each timepoint of the background subtracted trace to yield a ΔF trace. The ΔF was then divided by baseline fluorescence value to give ΔF/F traces. No averaging has been applied to any voltage traces.

Analysis of action potential (AP) data from hiPSC cardiomyocytes was performed using in-house MATLAB scripts based on previously developed software by the Efimov lab (Washington University, St. Louis, MO).[7,25] Scripts are available upon request. Briefly, raw OME-tiffs recorded in μManager was read directly into MATLAB for batch-processing of large datasets (>30 Gb per experiment). The mean pixel intensity of the entire image (512x125 pixels) was calculated for each frame and a mean fluorescence trace was extracted for the entire stack. Photobleach correction was performed by subtracting an asymmetric least-squares fit of the data from the mean trace.[26] No subtraction of background was possible due to staining of the entire monolayer. Individual AP events were identified through threshold detection based on a Schmidtt trigger. Action potential duration (APD) values were calculated for each AP by finding the activation time (time of the maximum derivative of the AP upstroke) and the time the signal returns to 70, 50, and 10% of the maximum depolarization (APD30, APD50, APD90, respectively). APD values were corrected for variation due to spontaneous beat rate by Fridericia's formula (Eq. 1). CL is the cycle length, calculated as the time period from the beginning of one beat to the beginning of the succeeding beat.[27]

$$\mathrm{APDc} = \frac{APD}{\sqrt[3]{CL}} \quad \textbf{[1]}$$

3.6.7 Electrophysiology

For electrophysiological experiments in HEK293T, pipettes were pulled from borosilicate glass with filament (Sutter Instruments, BF150-86-10) with a P-97 pipette puller (Sutter Instruments) to a resistance of 4-7 MΩ. Pipettes were filled with an internal solution (composition, in mM): 125 potassium gluconate, 10 HEPES, 10 KCl, 5 NaCl, 2 ATP disodium salt, 1 EGTA, 0.3 GTP sodium salt (pH 7.25, 285 mOsm). Pipettes were positioned with an MP-225 micromanipulator (Sutter Instruments). Electrophysiological recordings were obtained with an Axopatch 200B amplifier (Molecular Devices) at room temperature. The signals were digitized with a Digidata 1440A, sampled at 50 kHz, filtered at 5 kHz and recorded with pCLAMP 10 software (Molecular Devices).

Electrophysiology was performed in the whole cell voltage clamp configuration. After gigaseal formation and break-in, recordings were only pursued if series resistance in voltage clamp was less than 30 MΩ and the recording maintained a 30:1 ratio of membrane resistance to access resistance throughout all voltage steps. No series resistance compensation was applied. Fast capacitance was compensated in the cell attached configuration. All voltage clamp protocols were corrected for the calculated liquid junction (-14 mV, Liquid Junction Potential Calculator in pClamp). For tandem electrophysiology and fluorescence intensity recordings, cells were held at -60 mV and de- and hyper- polarizing steps were applied from +100 to -100 mV in 20 mV increments, with each step lasting 100 ms.

3.6.8 Synthesis

Preparation of fluorene-vinyl wires:

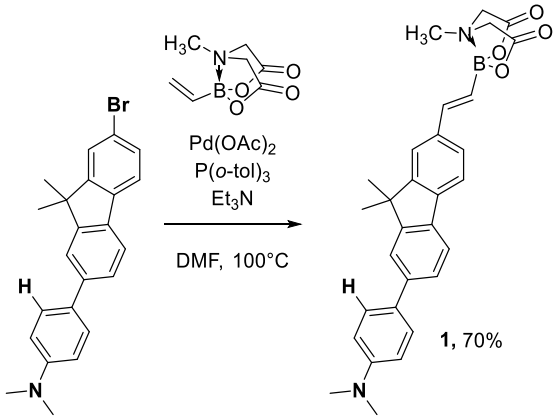

Synthesis of fluorene-ethylene MIDA boronate, 1

4-(7-bromo-9,9-dimethyl-9H-fluoren-2-yl)-N,N-dimethylaniline[7] (150 mg, 0.38 mmol) was combined with vinyl N-methyliminodiacetic acid (MIDA) boronate (209 mg, 1.1 mmol), $Pd(OAc)_2$ (1.7 mg, 7.6 µmol), and P(*o*-tol)$_3$ (4.6 mg, 15 µmol) in a flame-dried Schlenk flask. The flask was evacuated and backfilled with N_2 (3x). Anhydrous triethylamine (1 mL) and DMF (2 mL) was added, the flask was sealed, the stirred at 100°C. After 20 h, the reaction was cooled and diluted in ethyl acetate. This was washed with saturated ammonium chloride (2x) and with brine (2x). The organic fraction was collected, dried with magnesium sulfate, and concentrated onto silica *in vacuo*. Flash chromatography (ethyl acetate to 10% acetonitrile in ethyl acetate) was used to isolate **1** as a green-yellow solid (133 mg, 70%).

^{1}H NMR (600 MHz, Acetone-d_6) δ 7.80 (d, J = 7.9 Hz, 1H), 7.76 (s, 1H), 7.76 (d, J = 10.4 Hz, 1H), 7.72 (d, J = 1.5 Hz, 1H), 7.62 (d, J = 8.7 Hz, 2H), 7.58 (dd, J = 7.9, 1.7 Hz, 1H), 7.51 (dd, J = 7.9, 1.5 Hz, 1H), 7.04 (d, J = 18.1 Hz, 1H), 6.92 (s, 2H), 6.42 (d, J = 18.1 Hz, 1H), 4.27 (d, J = 17.0 Hz, 2H), 4.11 (d, J = 16.9 Hz, 2H), 3.08 (s, 3H), 3.01 (s, 6H), 1.55 (s, 6H).

^{13}C NMR (151 MHz, Acetone) δ 168.18, 154.69, 154.18, 142.39, 140.35, 138.95, 137.34, 136.84, 127.41, 126.00, 124.99, 120.82, 120.27, 120.14, 119.77, 61.56, 61.43, 46.57, 46.51, 38.78, 26.54, 24.23.

HRMS (ESI) m/z: $[M+H]^+$ calculated for $C_{30}H_{32}BN_2O_4$ 495.2450; found 495.2446

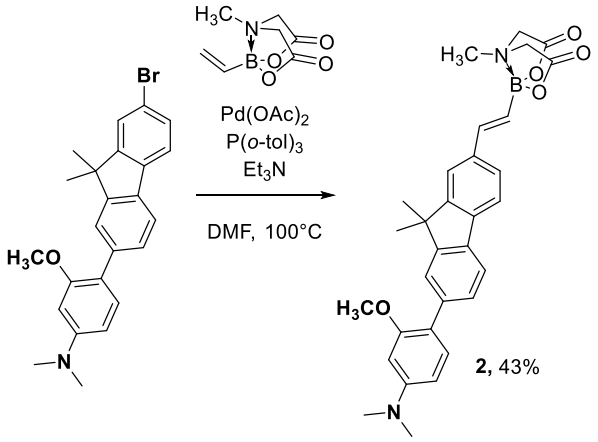

Synthesis of fluorene-ethylene MIDA boronate, 2

4-(7-bromo-9,9-dimethyl-9H-fluoren-2-yl)-3-methoxy-N,N-dimethylaniline[7] (60 mg, 0.14 mmol) was combined with vinyl N-methyliminodiacetic acid (MIDA) boronate (78 mg, 0.43 mmol), $Pd(OAc)_2$ (0.64 mg, 2.8 µmol), and P(*o*-tol)$_3$ (1.7 mg, 5.7 µmol) in a flame-dried Schlenk flask. The flask was evacuated and backfilled with N_2 (3x). Anhydrous triethylamine (0.5 mL) and DMF (1 mL) was added, the flask was sealed, the stirred at 100˚C. After 20 h, the reaction was cooled and diluted in ethyl acetate. This was washed with saturated ammonium chloride (2x) and with brine (2x). The organic fraction was collected, dried with magnesium sulfate, and concentrated onto silica *in vacuo*. Flash chromatography (ethyl acetate to 10% acetonitrile in ethyl acetate) was used to isolate **1** as a green-yellow solid (32 mg, 43%).

^{1}H NMR (600 MHz, Acetone-d_6) δ 7.74 (dd, J = 7.9, 4.3 Hz, 2H), 7.71 (s, 1H), 7.62 (s, 1H), 7.53 – 7.44 (m, 2H), 7.23 (d, J = 8.3 Hz, 1H), 7.04 (d, J = 18.2 Hz, 1H), 6.47 – 6.38 (m, 3H), 4.27 (d, J = 16.9 Hz, 2H), 4.11 (d, J = 16.9 Hz, 2H), 3.82 (d, J = 3.5 Hz, 3H), 3.07 (d, J = 3.6 Hz, 3H), 3.00 (s, 3H), 1.52 (d, J = 3.4 Hz, 6H).

^{13}C NMR (151 MHz, Acetone) δ 168.20, 157.50, 154.15, 153.53, 151.61, 142.44, 139.23, 138.65, 137.17, 136.22, 130.83, 128.45, 128.17, 125.97, 123.29, 120.79, 119.67, 119.24, 118.96, 105.05, 96.55, 61.42, 61.35, 59.59, 54.77, 46.50, 46.44, 39.73, 26.58, 19.89, 13.57.

HRMS (ESI) m/z: $[M+H]^+$ calculated for $C_{31}H_{34}BN_2O_5$ 525.2555; found 525.2552

Preparation of vinyl-fluorene wires

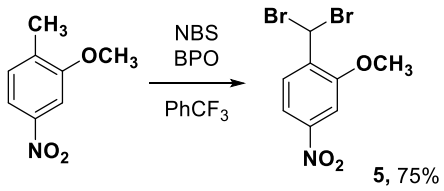

5, 75%

Synthesis of 1-(dibromomethyl)-2-methoxy-4-nitrobenzene, 5

2-methoxy-1-methyl-4-nitrobenzene (5.0 g, 29.9 mmol), N-bromosuccinimide (13.3 g, 74.8 mmol), and benzoyl peroxide (362 mg, 1.50 mmol) was added to a flame dried round bottom flask, to which 50 mL anhydrous trifluorotoluene was added. This was refluxed for 20 hours, then allowed to cool. Filtered to remove solid, then extracted out of filtrate using DCM. This was washed with 1 M KOH, 10% NaS_2O_3 solution, and finally brine. Dried with $MgSO_4$, then concentrated to recover a pale, off-white solid **5** (7.23 g, 75%) that was used without further purification.

^{1}H NMR (400 MHz, Chloroform-*d*) δ 8.21 (d, *J* = 8.6 Hz, 1H), 8.10 (dd, *J* = 8.6, 2.1 Hz, 1H), 7.90 (d, *J* = 2.1 Hz, 1H), 4.21 (s, 3H).

^{13}C NMR (101 MHz, $CDCl_3$) δ 154.00, 149.40, 136.44, 131.23, 116.44, 106.05, 56.64, 32.92.

HRMS (EI+) calculated for $C_8Br_2NO_0$ 322.8793; found 322.9790

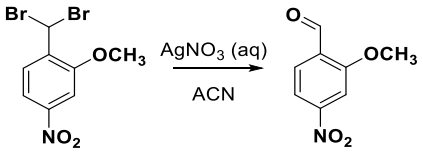

5 **6**, 75%

Synthesis of 2-methoxy-4-nitrobenzaldehyde, 6[28]

5 (6.0 g, 18.5 mmol) was suspended in 24 mL acetonitrile and stirred. To this, warm $AgNO_3$ solution (9.4 g, 55.4 mmol, 24 mL) was added. This was refluxed for 4 hours before quenching with saturated brine solution and filtering. The filtrate was extracted into ethyl acetate, washing with 10% NaS_2O_3 solution and brine. Drying with $MgSO_4$ and concentration *in vacuo* gave **6** as a white solid (2.5 g, 75%), which was used without further purification.

^{1}H NMR (400 MHz, Chloroform-*d*) δ 10.52 (s, 1H), 7.98 (d, *J* = 8.3 Hz, 1H), 7.90 – 7.85 (m, 2H), 4.06 (s, 3H).

^{13}C NMR (101 MHz, $CDCl_3$) δ 188.34, 161.83, 151.54, 129.60, 128.64, 115.62, 107.24, 56.48.

HRMS (EI+) calculated for $C_8H_7NO_4$ 181.0375; found 181.0373

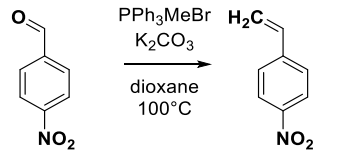

7, 91%

Synthesis of 1-nitro-4-vinylbenzene, 7

Following previously published methods,[29] **7** was isolated as a yellow oil (900 mg, 91%). NMR spectrum matched literature values and was used without further purification.

^{1}H NMR (300 MHz, Chloroform-*d*) δ 8.25 – 8.11 (m, 2H), 7.60 – 7.49 (m, 2H), 6.78 (dd, *J* = 17.6, 10.9 Hz, 1H), 5.93 (d, *J* = 17.6 Hz, 1H), 5.50 (d, *J* = 10.9 Hz, 1H).

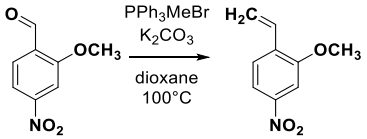

6 **8**, 63%

Synthesis of 2-methoxy-4-nitro-1-vinylbenzene, 8

PPh_3MeBr (845 mg, 2.4 mmol) and K_2CO_3 (490 mg, 3.5 mmol) were stirred in dioxane (4 mL) for 4 hours at room temperature. 2-methoxy-4-nitrobenzaldehyde, **6** (360 mg, 2.0 mmol) was added, and reaction was stirred at 100 °C for 12 hours. This was diluted with hexanes, then filtered over celite. Concentrated filtrate, then filtered over basic alumina as solution in ethyl acetate. This was repeated once, to give **8** as a yellow oil (220 mg, 63%).

^{1}H NMR (400 MHz, Chloroform-*d*) δ 7.83 (dt, *J* = 8.5, 1.7 Hz, 1H), 7.72 (d, *J* = 2.0 Hz, 1H), 7.58 (d, *J* = 8.4 Hz, 1H), 7.05 (dd, *J* = 17.7, 11.2 Hz, 1H), 5.90 (dd, *J* = 17.8, 1.6 Hz, 1H), 5.48 (dd, *J* = 11.2, 1.6 Hz, 1H), 3.95 (s, 3H).

^{13}C NMR (101 MHz, CDCl3) δ 156.82, 148.04, 133.37, 130.22, 126.64, 118.71, 116.01, 105.91, 56.02.

HRMS (EI+) calculated for $C_9H_9NO_3$ 179.0582; found 179.0584

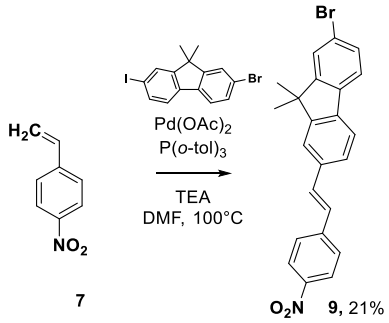

Synthesis of (E)-2-bromo-9,9-dimethyl-7-(4-nitrostyryl)-9H-fluorene, 9

2-bromo-7-iodo-9,9-dimethyl-9H-fluorene[7] (2.4 g, 6.0 mmol), 1-nitro-4-vinylbenzene **7** (890 mg, 6.0 mmol), palladium(II) acetate (27 mg, 0.12 mmol), and P(*o*-tol)$_3$ (73 mg, 0.24 mmol) were added to a flame dried Schlenk flask, then evacuated and backfilled with N_2 (3X). Anhydrous triethylamine (20 mL) was added, the flask sealed, and stirred at 100 °C for 18 hours. Extracted in ethyl acetate and washed with NH_4Cl (2X) and brine (1X). The organic layer was dried with $MgSO_4$ and concentrated onto silica gel. Purified by silica gel flash chromatography using 0-5% ethyl acetate in hexanes. The least polar orange band was collected and concentrated to give **9** as a light yellow powder (536 mg, 21%)

^{1}H NMR (600 MHz, Chloroform-*d*) δ 8.25 – 8.22 (m, 2H), 7.70 (d, *J* = 7.9 Hz, 1H), 7.66 (d, *J* = 8.6 Hz, 2H), 7.61 (s, 1H), 7.58 (d, *J* = 10.7 Hz, 1H), 7.58 (s, 1H), 7.53 (dd, *J* = 7.8, 1.5 Hz, 1H), 7.48 (dd, *J* = 8.0, 1.8 Hz, 1H), 7.35 (d, *J* = 16.2 Hz, 1H), 7.21 (d, *J* = 16.3 Hz, 1H), 1.52 (s, 6H).

^{13}C NMR (151 MHz, $CDCl_3$) δ 155.98, 153.92, 146.68, 143.89, 139.05, 137.53, 135.71, 133.48, 130.28, 126.74, 126.70, 126.21, 125.91, 124.16, 121.54, 121.52, 120.93, 120.45, 47.08, 26.99.

HRMS (EI+) calculated for $C_{23}H_{18}BrNO_2$ 419.0521; found 419.0529

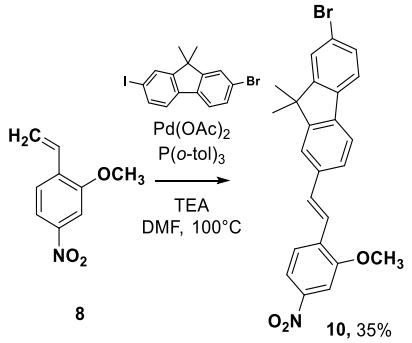

Synthesis of (E)-2-bromo-7-(2-methoxy-4-nitrostyryl)-9,9-dimethyl-9H-fluorene, 10

2-bromo-7-iodo-9,9-dimethyl-9H-fluorene[7] (1.1 g, 2.7 mmol), 2-methoxy-4-nitro-1-vinylbenzene **8** (445 mg, 2.5 mmol), palladium(II) acetate (11 mg, 0.05 mmol), and P(*o*-tol)$_3$ (30 mg, 0.10 mmol) were added to a flame dried Schlenk flask, then evacuated and backfilled with N_2 (3X). Anhydrous

triethylamine (10 mL) was added, the flask sealed, and stirred at 100 °C for 18 hours. Extracted in dichloromethane, and washed with NH_4Cl (2X) and brine (1X). The organic layer was dried with $MgSO_4$ and concentrated onto silica gel. Purified by silica gel flash chromatography using 5-10% ethyl acetate in hexanes. The least polar orange band was collected and concentrated to give **10** as a light yellow powder (390 mg, 35%)

^{1}H NMR (600 MHz, Chloroform-*d*) δ 7.88 (dd, *J* = 8.5, 2.2 Hz, 1H), 7.77 (d, *J* = 2.2 Hz, 1H), 7.73 (d, *J* = 8.5 Hz, 1H), 7.69 (d, *J* = 7.8 Hz, 1H), 7.61 (d, *J* = 1.5 Hz, 1H), 7.59 – 7.49 (m, 4H), 7.47 (dd, *J* = 8.0, 1.8 Hz, 1H), 7.35 (d, *J* = 16.4 Hz, 1H), 4.02 (s, 3H), 1.52 (s, 6H).

^{13}C NMR (151 MHz, $CDCl_3$) δ 156.72, 155.99, 153.84, 147.44, 138.72, 137.64, 136.46, 133.55, 133.33, 130.22, 126.69, 126.18, 126.09, 121.48, 121.37, 121.08, 120.96, 120.36, 116.24, 105.97, 56.05, 47.07, 27.00.

HRMS (EI+) calculated for 449.0627; found 449.0624

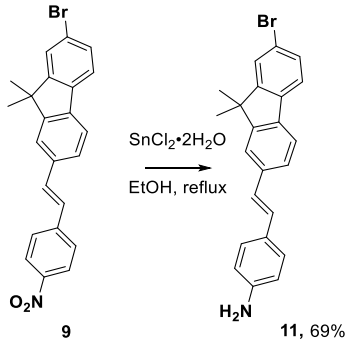

9 **11**, 69%

Synthesis of (E)-4-(2-(7-bromo-9,9-dimethyl-9H-fluoren-2-yl)vinyl)aniline, 11

9 (400 mg, 0.95 mmol) and tin(II) chloride (1.1 g, 4.8 mmol) was refluxed in ethanol (15 mL) for 1 hour. Saturated bicarbonate solution was added, and the solution was filtered over a basic alumina plug. This was washed with dichloromethane. This was concentrated to give **11** as an orange solid (255 mg, 69%). This was used without further purification.

^{1}H NMR (600 MHz, Chloroform-*d*) δ 7.64 (d, *J* = 7.9 Hz, 1H), 7.55 (dd, *J* = 4.9, 3.0 Hz, 2H), 7.53 (d, *J* = 1.5 Hz, 1H), 7.45 (ddd, *J* = 7.9, 2.9, 1.7 Hz, 2H), 7.39 – 7.35 (m, 2H), 7.10 (d, *J* = 16.2 Hz, 1H), 7.00 (d, *J* = 16.2 Hz, 1H), 6.71 – 6.68 (m, 2H), 3.76 (s, 2H), 1.51 (s, 6H).

^{13}C NMR (151 MHz, $CDCl_3$) δ 155.84, 153.70, 146.15, 138.05, 137.64, 137.05, 130.07, 128.52, 128.02, 127.73, 126.07, 125.60, 125.25, 121.17, 120.73, 120.22, 119.93, 115.20, 46.99, 27.06.

HRMS (ESI) m/z: $[M+H]^+$ calculated for $C_{23}H_{21}BrN$ 390.0852; found 390.0853

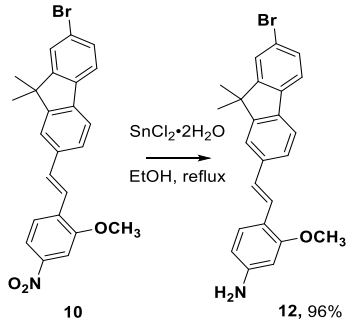

10 12, 96%

Synthesis of (E)-4-(2-(7-bromo-9,9-dimethyl-9H-fluoren-2-yl)vinyl)-3-methoxyaniline, 12

10 (380 mg, 0.84 mmol) and tin(II) chloride (950 mg, 4.3 mmol) were refluxed in ethanol (10 mL) for 2.5 hours. Saturated bicarbonate solution was added, and the solution was filtered over a basic alumina plug. This was washed with dichloromethane. This was concentrated to give **12** as a yellow solid (340 mg, 96%). This was used without further purification.

^{1}H NMR (600 MHz, Chloroform-*d*) δ 7.62 (d, *J* = 7.9 Hz, 1H), 7.57 – 7.52 (m, 3H), 7.45 (td, *J* = 8.4, 1.9 Hz, 3H), 7.42 (s, 1H), 7.03 (d, *J* = 16.4 Hz, 1H), 6.32 (dd, *J* = 8.2, 2.2 Hz, 1H), 6.26 (d, *J* = 2.2 Hz, 1H), 3.87 (s, 3H), 3.79 (s, 2H), 1.50 (s, 6H).

^{13}C NMR (151 MHz, $CDCl_3$) δ 158.10, 155.87, 153.63, 147.46, 138.35, 138.16, 136.77, 130.01, 127.53, 126.04, 125.74, 125.70, 123.37, 121.11, 120.58, 120.11, 119.95, 117.20, 107.56, 98.21, 55.40, 46.97, 27.06.

HRMS (ESI+) m/z: $[M+H]^+$ calculated for $C_{24}H_{23}BrNO$ 420.0958; found 420.0956

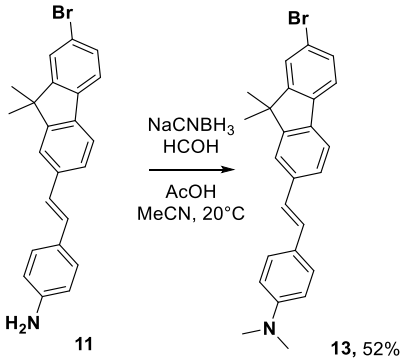

11 13, 52%

Synthesis of (E)-4-(2-(7-bromo-9,9-dimethyl-9H-fluoren-2-yl)vinyl)-N,N-dimethylaniline, 13

11 (200 mg, 0.5 mmol) was taken up in acetonitrile (5 mL). Formaldehyde solution (37% w/v, 0.19 mL) was added, and the solution was cooled to 0 °C and stirred for 30 minutes. Sodium cyanoborohydride (97 mg, 1.5 mmol) was added in 3 portions, and glacial acetic acid was added to bring pH to 5. The reaction was allowed to stir 12 hours, warming to room temperature. Reaction was poured into ice, then extracted with ethyl acetate. This was washed with sodium bicarbonate and brine, then dried with $MgSO_4$ and concentrated onto silica gel. Flash chromatography (5% ethyl acetate in hexanes) was used to purify **13** as a yellow solid (112 mg, 52%).

^{1}H NMR (600 MHz, Chloroform-*d*) δ 7.64 (d, *J* = 7.9 Hz, 1H), 7.56 – 7.54 (m, 3H), 7.47 – 7.44 (m, 4H), 7.13 (d, *J* = 16.2 Hz, 1H), 7.01 (d, *J* = 16.2 Hz, 1H), 6.74 (d, *J* = 8.3 Hz, 2H), 3.00 (s, 6H), 1.51 (s, 6H).

^{13}C NMR (151 MHz, $CDCl_3$) δ 155.87, 153.72, 150.11, 138.15, 137.92, 136.86, 130.08, 128.68, 127.59, 126.08, 125.79, 125.54, 124.54, 121.16, 120.67, 120.23, 119.86, 112.46, 47.01, 40.47, 27.10.

HRMS (ESI+) m/z: $[M+H]^+$ calculated for $C_{25}H_{25}BrN$ 418.1165; found 418.1162

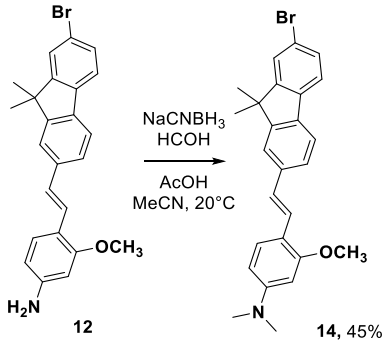

Synthesis of (E)-4-(2-(7-bromo-9,9-dimethyl-9H-fluoren-2-yl)vinyl)-3-methoxy-N,N-dimethylaniline, 14

12 (75 mg, 0.18 mmol) was taken up in acetonitrile (4 mL). Formaldehyde solution (37% w/v, 0.1 mL) was added, and the solution was cooled to 0 °C and stirred for 30 minutes. Sodium cyanoborohydride (34 mg, 0.5 mmol) was added and glacial acetic acid was added to bring pH to 5. The reaction was stirred 12 hours, warming to room temperature. Reaction was poured into ice, then extracted with ethyl acetate. This was washed with sodium bicarbonate and brine, then dried with $MgSO_4$ and concentrated onto silica gel. Flash chromatography (5-10% ethyl acetate in hexanes) was used to purify **14** as a yellow solid (44 mg, 45%).

^{1}H NMR (600 MHz, Chloroform-*d*) δ 7.62 (d, *J* = 7.9 Hz, 1H), 7.56 (d, *J* = 1.5 Hz, 1H), 7.54 (d, *J* = 6.3 Hz, 1H), 7.54 (d, *J* = 3.5 Hz, 1H), 7.50 (d, *J* = 8.6 Hz, 1H), 7.48 – 7.44 (m, 2H), 7.45 (dd, *J* = 14.5, 1.7 Hz, 1H), 7.04 (d, *J* = 16.4 Hz, 1H), 6.37 (dd, *J* = 8.6, 2.4 Hz, 1H), 6.25 (d, *J* = 2.4 Hz, 1H), 3.93 (s, 3H), 3.02 (s, 6H), 1.51 (s, 6H).

^{13}C NMR (151 MHz, $CDCl_3$) δ 158.07, 155.86, 153.62, 151.39, 138.58, 138.23, 136.55, 129.99, 127.23, 126.02, 125.61, 125.01, 123.49, 121.06, 120.49, 120.10, 119.84, 115.15, 105.14, 95.59, 55.43, 46.97, 40.50, 27.08.

HRMS (ESI+) m/z: $[M+H]^+$ calculated for $C_{26}H_{27}BrNO$ 448.1271; found 448.1268

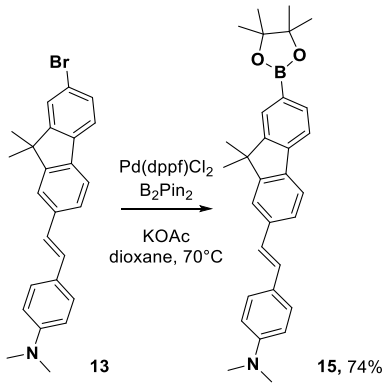

Synthesis of (E)-4-(2-(9,9-dimethyl-7-(4,4,5,5-tetramethyl-1,3,2-dioxaborolan-2-yl)-9H-fluoren-2-yl)vinyl)-N,N-dimethylaniline, 15

13 (68 mg, 0.16 mmol), Pd(dppf)Cl_2 (6 mg, 8.2 µmol), B_2pin_2 (62 mg, 0.25 mmol), and potassium acetate (48 mg, 0.49 mmol) were added to a flame dried Schlenk flash, evacuated and backfilled with N_2 (3X). Anhydrous dioxane (2 mL) was added, and the reaction was stirred for 16 hours at 70 °C. Reaction then diluted in ethyl acetate, then washed with NH_4Cl and brine. This was dried with $MgSO_4$, then concentrated onto silica. Purification by flash chromatography (5-10% ethyl acetate in hexanes) afforded **15** as a yellow powder (57 mg, 74%).

^{1}H NMR (600 MHz, Chloroform-*d*) δ 7.88 (s, 1H), 7.82 (dd, *J* = 7.6, 1.0 Hz, 1H), 7.72 – 7.69 (m, 2H), 7.56 (d, *J* = 1.5 Hz, 1H), 7.48 – 7.44 (m, 3H), 7.13 (d, *J* = 16.2 Hz, 1H), 7.02 (d, *J* = 16.2 Hz, 1H), 6.75 (d, *J* = 8.2 Hz, 2H), 3.00 (s, 6H), 1.54 (s, 6H), 1.39 (s, 12H).

^{13}C NMR (151 MHz, $CDCl_3$) δ 154.82, 152.99, 150.06, 142.15, 138.01, 137.82, 133.97, 128.71, 128.56, 127.61, 125.37, 124.86, 120.65, 119.95, 119.20, 112.57, 83.74, 46.78, 40.54, 29.72, 27.18, 24.93.

HRMS (ESI+) m/z: $[M+H]^+$ calculated for $C_{31}H_{37}BNO_2$ 466.2912; found 466.2911

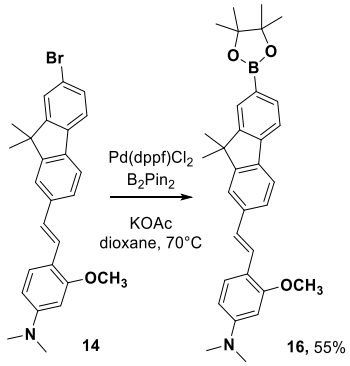

Synthesis of (E)-4-(2-(9,9-dimethyl-7-(4,4,5,5-tetramethyl-1,3,2-dioxaborolan-2-yl)-9H-fluoren-2-yl)vinyl)-3-methoxy-N,N-dimethylaniline, 16

14 (35 mg, 0.08 mmol), $Pd(dppf)Cl_2$ (2.9 mg, 3.9 µmol), B_2pin_2 (30 mg, 0.12 mmol), and potassium acetate (23 mg, 0.23 mmol) were added to a flame dried Schlenk flask, evacuated and backfilled with N_2 (3X). Anhydrous dioxane (1 mL) was added, and the reaction as stirred for 16 hours at 70 °C. Reaction was diluted in dichloromethane, then washed with NH_4Cl and brine. This was dried with $MgSO_4$, then concentrated onto silica. Purification by flash chromatography (10-20% ethyl acetate in hexanes) afforded **16** as a yellow powder (21 mg, 55%).

^1H NMR (600 MHz, Chloroform-*d*) δ 7.88 (s, 1H), 7.82 (d, *J* = 7.5 Hz, 1H), 7.70 (t, *J* = 8.1 Hz, 2H), 7.59 (d, *J* = 1.5 Hz, 1H), 7.52 (d, *J* = 8.6 Hz, 1H), 7.50 – 7.46 (m, 2H), 7.06 (d, *J* = 16.3 Hz, 1H), 6.38 (dd, *J* = 8.6, 2.4 Hz, 1H), 6.26 (d, *J* = 2.4 Hz, 1H), 3.93 (s, 3H), 3.02 (s, 6H), 1.54 (s, 6H), 1.39 (s, 12H).

^{13}C NMR (151 MHz, $CDCl_3$) δ 158.08, 154.69, 152.95, 151.36, 142.22, 138.67, 137.46, 133.89, 128.64, 127.22, 125.41, 125.23, 123.39, 120.50, 119.91, 119.08, 115.30, 105.17, 95.67, 83.66, 55.44, 46.72, 40.50, 29.68, 27.14, 24.89.

HRMS (ESI+) m/z: $[M+H]^+$ calculated for $C_{32}H_{39}BNO_3$ 496.3018; found 496.3021

Preparation of vinyl-fluorene VoltageFluors (v-fVFs):

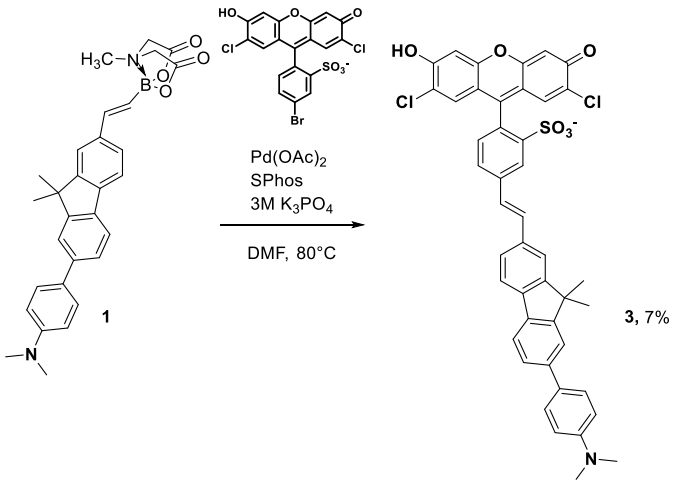

Synthesis of (E)-2-(2,7-dichloro-6-hydroxy-3-oxo-3H-xanthen-9-yl)-5-(2-(7-(4-(dimethylamino)phenyl)-9,9-dimethyl-9H-fluoren-2-yl)vinyl)benzenesulfonate, 3 (2v-fVF 1)

1 (50 mg, 0.1 mmol), 5-bromo-(2',7'-dichloro-sulfofluorescein (44 mg, 84 µmol), $Pd(OAc)_2$ (1 mg, 4.2 µmol) and SPhos (3.5 mg, 8.4 µmol) were combined in anhydrous DMF (1 mL). 3M K_3PO_4 solution was bubbled with N_2 for 30 minutes, then 100 µL was added, the flask was sealed, and the reaction was stirred at 60 °C for 18 hours. The reaction was then concentrated to dryness *in vacuo*, then the crude material was taken up in 1:1 dicholoromethane:methanol and precipitated in diethyl ether. The precipitate was purified by preparative-HPLC (10-100% MeCN in water + 0.05% trifluoroacetic acid) to afford **3** as a red-orange powder (4.5 mg, 7% yield).

^{1}H NMR (900 MHz, DMSO-d_6) δ 8.22 (d, *J* = 1.8 Hz, 1H), 7.96 (d, *J* = 1.5 Hz, 1H), 7.84 (dd, *J* = 7.8, 3.0 Hz, 2H), 7.82 (dd, *J* = 7.9, 1.8 Hz, 1H), 7.78 (d, *J* = 1.7 Hz, 1H), 7.66 (dd, *J* = 7.8, 1.5 Hz, 1H), 7.64 – 7.61 (m, 2H), 7.58 (dd, *J* = 7.8, 1.7 Hz, 1H), 7.55 (d, *J* = 16.4 Hz, 1H), 7.50 (d, *J* = 16.4 Hz, 1H), 7.27 (d, *J* = 7.7 Hz, 1H), 7.00 (s, 2H), 6.84 (d, *J* = 8.2 Hz, 2H), 6.57 (s, 2H), 2.96 (s, 6H), 1.55 (s, 6H).

^{13}C NMR (226 MHz, DMSO) δ 158.46, 158.31, 154.95, 154.56, 152.45, 150.18, 147.80, 140.18, 139.03, 138.95, 136.67, 136.23, 131.13, 130.57, 130.26, 128.00, 127.70, 127.08, 127.03, 126.82, 125.86, 125.10, 121.26, 121.03, 120.64, 120.32, 118.11, 116.80, 113.22, 103.75, 46.94, 40.61, 27.44.

HRMS (ESI-) m/z: $[M-H]^-$ calculated for $C_{44}H_{32}Cl_2NO_6S$ 772.1333; found 772.1323

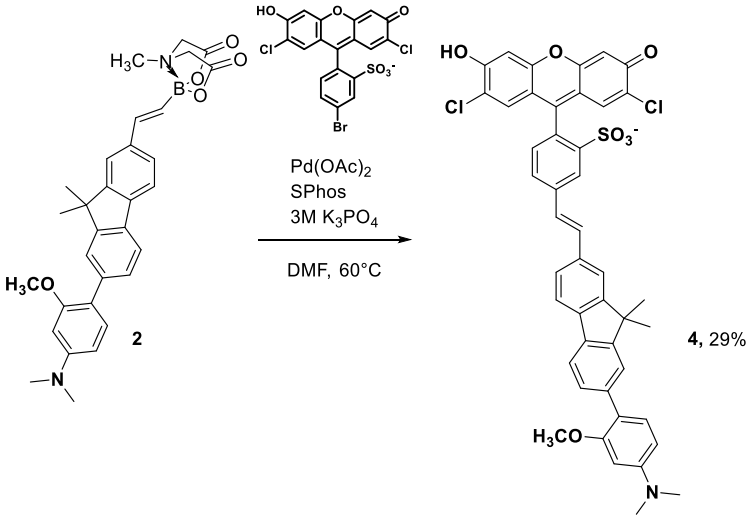

Synthesis of (E)-2-(2,7-dichloro-6-hydroxy-3-oxo-3H-xanthen-9-yl)-5-(2-(7-(4-(dimethylamino)-2-methoxyphenyl)-9,9-dimethyl-9H-fluoren-2-yl)vinyl)benzenesulfonate, 4 (2v-fVF 2)

2 (40 mg, 76 µmol), 5-bromo-(2',7'-dichloro-sulfofluorescein (26 mg, 51 µmol), $Pd(OAc)_2$ (0.6 mg, 2.6 µmol) and SPhos (2 mg, 5 µmol) were combined in anhydrous DMF (1 mL). 3M K_3PO_4 solution was bubbled with N_2 for 30 minutes, then 200 µL was added, the flask was sealed, and the reaction was stirred at 60 °C for 18 hours. The reaction was then concentrated to dryness *in vacuo*, then the crude material was taken up in 1:1 dicholoromethane:methanol and precipitated in diethyl ether. The precipitate was purified by preparative-TLC (15% MeOH in DCM + 5% acetic acid) to afford **4** as a red-orange powder (12 mg, 29% yield).

^{1}H NMR (900 MHz, DMSO-d_6) δ 8.20 (d, *J* = 1.7 Hz, 1H), 7.96 – 7.93 (m, 1H), 7.82 (d, *J* = 7.7 Hz, 1H), 7.79 (d, *J* = 7.8 Hz, 1H), 7.74 (dd, *J* = 7.8, 1.8 Hz, 1H), 7.66 – 7.63 (m, 1H), 7.58 (d, *J* = 1.6 Hz, 1H), 7.52 (d, *J* = 16.3 Hz, 1H), 7.46 (s, 1H), 7.45 – 7.42 (m, 1H), 7.23 – 7.20 (m, 1H), 7.13 (d, *J* = 7.7 Hz, 1H), 6.75 (s, 2H), 6.45 – 6.38 (m, 2H), 6.13 (s, 2H), 3.80 (s, 3H), 2.97 (s, 6H), 1.52 (s, 6H).

^{13}C NMR (226 MHz, DMSO) δ 175.82, 173.26, 157.13, 157.04, 156.40, 154.05, 153.37, 152.21, 151.26, 147.24, 138.59, 138.01, 137.57, 135.82, 130.70, 130.41, 130.10, 129.39, 128.63, 127.96, 126.82, 126.49, 126.01, 125.52, 123.07, 120.71, 120.09, 119.53, 118.19, 117.61, 108.96, 105.01, 104.02, 102.61, 96.49, 95.73, 55.32, 55.13, 46.35, 46.33, 27.02.

HRMS (ESI-) $[M-H]^-$ calculated for $C_{45}H_{34}O_7NCl_2S$ 802.1439; found 802.1430

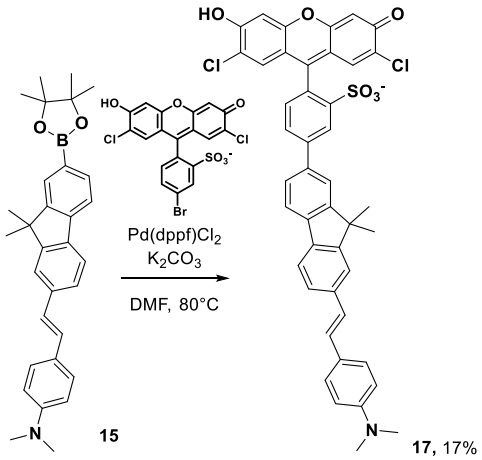

Synthesis of (E)-2-(2,7-dichloro-6-hydroxy-3-oxo-3H-xanthen-9-yl)-5-(7-(4-(dimethylamino)styryl)-9,9-dimethyl-9H-fluoren-2-yl)benzenesulfonate, 17 (7v-fVF 1)

15 (30 mg, 65 µmol), 5-bromo-(2',7'-dichloro-sulfofluorescein (28 mg, 54 µmol), and $Pd(dppf)Cl_2$ (2 mg, 2.7 µmol) were combined in anhydrous DMF (1 mL). 5M K_2CO_3 solution was bubbled with N_2 for 30 minutes, then 100 µL was added, the flask was sealed, and the reaction was stirred at 80 °C for 18 hours. The reaction was then concentrated to dryness *in vacuo*, then the crude material was taken up in 1:1 dicholoromethane:methanol, and precipitated in diethyl ether. The precipitate was purified by preparative-HPLC (10-100% MeCN in water + 0.05% trifluoroacetic acid) to afford **17** as a red-orange powder (7 mg, 17% yield).

^{1}H NMR (900 MHz, DMSO-d_6) δ 8.31 (d, J = 1.9 Hz, 1H), 7.99 (d, J = 1.6 Hz, 1H), 7.98 – 7.93 (m, 2H), 7.85 (d, J = 7.7 Hz, 1H), 7.81 – 7.77 (m, 2H), 7.53 (dd, J = 7.9, 1.5 Hz, 1H), 7.48 (d, J = 8.3 Hz, 2H), 7.37 (d, J = 7.6 Hz, 1H), 7.26 (d, J = 16.3 Hz, 1H), 7.09 (d, J = 16.2 Hz, 1H), 7.02 (s, 2H), 6.76 (d, J = 8.2 Hz, 2H), 6.57 (s, 2H), 2.95 (s, 6H), 1.58 (s, 6H).

^{13}C NMR (226 MHz, DMSO) δ 158.10, 157.96, 157.82, 157.68, 154.52, 154.34, 151.85, 149.84, 147.48, 141.43, 138.58, 137.74, 137.52, 136.71, 130.34, 129.78, 128.47, 127.65, 127.48, 127.21, 126.02, 125.55, 125.39, 124.03, 121.20, 120.60, 119.82, 117.65, 116.32, 112.38, 103.30, 59.72, 46.62, 26.90.

HRMS (ESI-) $[M-H]^-$ calculated for $C_{44}H_{32}O_6NCl_2S$ 772.1333; found 772.1327

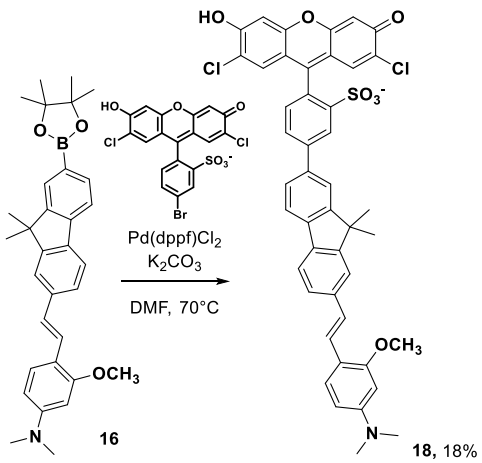

Synthesis of (E)-2-(2,7-dichloro-6-hydroxy-3-oxo-3H-xanthen-9-yl)-5-(7-(4-(dimethylamino)-2-methoxystyryl)-9,9-dimethyl-9H-fluoren-2-yl)benzenesulfonic acid, 18 (7v-fVF 2)

16 (30 mg, 61 µmol), 5-bromo-(2',7'-dichloro-sulfofluorescein (24 mg, 47 µmol), and Pd(dppf)Cl_2 (1.7 mg, 2.3 µmol) were combined in anhydrous DMF (1 mL). 5M K_2CO_3 solution was bubbled with N_2 for 30 minutes, then 50 µL was added, the flask was sealed, and the reaction was stirred at 80 °C for 18 hours. The reaction was then concentrated to dryness *in vacuo*, then the crude material was taken up in 1:1 dicholoromethane:methanol, and precipitated in diethyl ether. The precipitate was purified by preparative-HPLC (10-100% MeCN in water + 0.05% trifluoroacetic acid) to afford **18** as a red-orange powder (7 mg, 18% yield).

^{1}H NMR (900 MHz, DMSO-d_6) δ 8.31 (d, *J* = 1.9 Hz, 1H), 7.99 (d, *J* = 1.7 Hz, 1H), 7.97 – 7.94 (m, 2H), 7.84 (d, *J* = 7.7 Hz, 1H), 7.79 (dd, *J* = 7.7, 1.7 Hz, 1H), 7.72 – 7.70 (m, 1H), 7.51 – 7.49 (m, 2H), 7.40 (d, *J* = 16.4 Hz, 1H), 7.37 (d, *J* = 7.7 Hz, 1H), 7.09 (d, *J* = 16.3 Hz, 1H), 7.02 (s, 2H), 6.79 (s, 2H), 6.37 (dd, *J* = 8.6, 2.3 Hz, 1H), 6.32 (d, *J* = 2.4 Hz, 1H), 3.89 (s, 3H), 2.98 (s, 6H), 1.57 (s, 6H).

^{13}C NMR (226 MHz, DMSO) δ 157.88, 157.76, 154.52, 154.37, 151.85, 151.29, 147.49, 141.43, 138.60, 138.09, 137.68, 136.53, 130.34, 129.78, 127.64, 127.25, 127.20, 126.00, 125.38, 125.21, 124.34, 123.32, 121.18, 120.62, 120.55, 119.82, 117.75, 116.43, 113.91, 104.94, 103.30, 95.54, 55.26, 46.62, 40.05, 39.22, 29.27, 26.90.

HRMS (ESI-) m/z: $[M-H]^-$ calculated for $C_{45}H_{34}Cl_2NO_7S$ 802.1439; found 802.1429

Preparation of phenyl substituted wires and VoltageFluors:

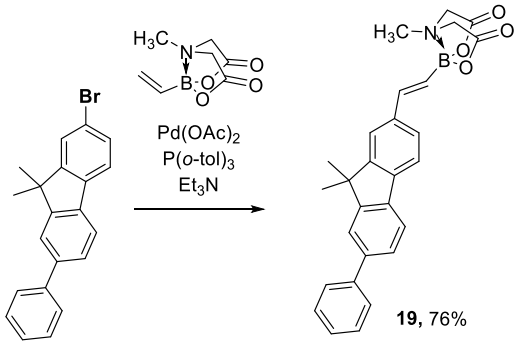

Synthesis of fluorene-ethylene MIDA boronate, 19

2-bromo-9,9-dimethyl-7-phenyl-9H-fluorene[7] (275 mg, 0.80 mmol), palladium(II) acetate (3.9 mg, 17 µmol), P(*o*-tol)$_3$ (11 mg, 34 µmol, and vinyl *N*-methyliminodiacetic acid (MIDA) boronate (315 mg, 1.6 mmol) were combined in a flame dried Schlenk flask, then evacuated and backfilled with N_2 (3X). Anhydrous DMF (3 mL) and triethylamine (1 mL) were added, and the reaction was stirred for 18 hours at 100 °C. Organics were extracted with ethyl acetate, then washed with NH_4Cl and brine. The organic layer was dried with $MgSO_4$, then concentrated onto silica. This was purified by flash chromatography (0-2% acetonitrile in ethyl acetate, affording **19** as a white powder (270 mg, 76%).

^{1}H NMR (600 MHz, Acetone-d_6) δ 7.87 (d, *J* = 7.9 Hz, 1H), 7.84 (d, *J* = 1.7 Hz, 1H), 7.80 (d, *J* = 7.8 Hz, 1H), 7.74 (s, 1H), 7.76 – 7.71 (m, 2H), 7.65 (dd, *J* = 7.9, 1.7 Hz, 1H), 7.54 (dd, *J* = 7.9, 1.5 Hz, 1H), 7.50 – 7.44 (m, 2H), 7.39 – 7.33 (m, 1H), 7.06 (d, *J* = 18.2 Hz, 1H), 6.44 (d, *J* = 18.2 Hz, 1H), 4.28 (d, *J* = 17.0 Hz, 2H), 4.12 (d, *J* = 16.9 Hz, 2H), 3.09 (s, 3H), 1.57 (s, 6H).

^{13}C NMR (151 MHz, Acetone) δ 168.25, 154.83, 154.41, 142.40, 141.31, 140.27, 138.69, 138.16, 137.77, 128.82, 127.17, 126.93, 126.09, 126.07, 121.28, 120.95, 120.43, 120.13, 61.49, 46.73, 46.57, 29.93, 26.52.

HRMS (ESI) m/z: $[M+Cl]^-$ calculated for $C_{28}H_{26}BClNO_4$ 486.1649; found 486.1649

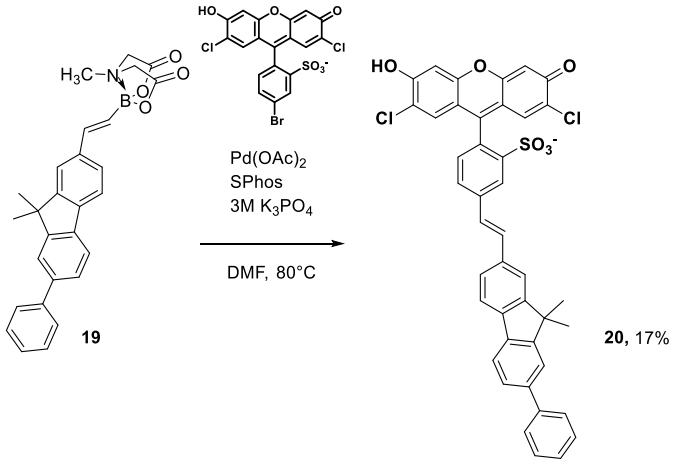

Synthesis of (E)-2-(2,7-dichloro-6-hydroxy-3-oxo-3H-xanthen-9-yl)-5-(2-(9,9-dimethyl-7-phenyl-9H-fluoren-2-yl)vinyl)benzenesulfonate, 20 (2v-fVF 0)

19 (50 mg, 0.11 mmol), 5-bromo-(2',7'-dichloro-sulfofluorescein (48 mg, 92 µmol), $Pd(OAc)_2$ (1 mg, 4.6 µmol) and SPhos (3.8 mg, 9.2 µmol) were combined in anhydrous DMF (1 mL). 3M K_3PO_4 solution was bubbled with N_2 for 30 minutes, then 300 µL was added, the flask was sealed, and the reaction was stirred at 60 °C for 18 hours. The reaction was then concentrated to dryness *in vacuo*, then the crude material was taken up in 1:1 dicholoromethane:methanol and precipitated in diethyl ether. The precipitate was purified by preparative-HPLC (50-95% MeCN in water + 0.05% trifluoroacetic acid) to afford **20** as a dark red powder (11 mg, 17% yield).

^{1}H NMR (900 MHz, DMSO-d_6) δ 8.23 (d, *J* = 1.8 Hz, 1H), 8.00 – 7.97 (m, 1H), 7.93 (d, *J* = 7.8 Hz, 1H), 7.91 – 7.87 (m, 2H), 7.83 (dd, *J* = 7.9, 1.8 Hz, 1H), 7.79 – 7.75 (m, 2H), 7.68 (ddd, *J* = 12.2, 7.8, 1.6 Hz, 2H), 7.57 (d, *J* = 16.4 Hz, 1H), 7.53 – 7.48 (m, 3H), 7.40 – 7.36 (m, 1H), 7.27 (d, *J* = 7.7 Hz, 1H), 7.00 (s, 2H), 6.77 (s, 2H), 1.57 (s, 6H).

^{13}C NMR (226 MHz, DMSO) δ 158.03, 157.89, 154.54, 154.28, 151.95, 147.33, 140.47, 139.47, 138.44, 138.23, 137.64, 136.18, 130.60, 130.11, 129.79, 128.88, 127.59, 127.29, 126.87, 126.78, 126.59, 126.39, 125.85, 125.43, 121.17, 120.86, 120.68, 120.53, 117.44, 115.84, 103.27, 46.59, 26.88.

HRMS (ESI-) m/z: $[M-H]^-$ calculated for $C_{42}H_{27}Cl_2O_6S$ 729.0911; found 729.0903

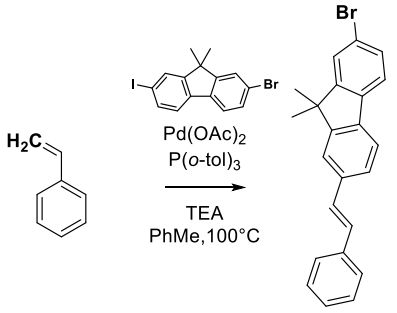

21, 50%

Synthesis of (E)-2-bromo-9,9-dimethyl-7-styryl-9H-fluorene, 21

2-bromo-7-iodo-9,9-dimethyl-9H-fluorene[7] (0.5 g, 1.25 mmol), palladium (II) acetate (5 mg, 2.3 µmol), and P(*o*-tol)$_3$ (14 mg, 46 µmol) were added to a flame dried Schlenk flash, then evacuated and backfilled with N_2 (3X). Anhydrous triethylamine (2 mL) and toluene (2 mL) were added, followed by styrene (120 mg, 1.1 mmol). The reaction was stirred 18 hours at 100 °C, then extracted into ethyl acetate. This was washed with NH_4Cl and brine, then dried with $MgSO_4$ and concentrated onto silica. Purified by flash chromatography (0-5% toluene in hexanes) to afford **21** as a white solid (215 mg, 50%).

^{1}H NMR (600 MHz, Chloroform-*d*) δ 7.67 (d, *J* = 7.9 Hz, 1H), 7.60 – 7.55 (m, 5H), 7.50 (dd, *J* = 7.9, 1.6 Hz, 1H), 7.47 (dd, *J* = 8.1, 1.7 Hz, 1H), 7.39 (t, *J* = 7.7 Hz, 2H), 7.31 – 7.27 (m, 1H), 7.20 (d, *J* = 2.2 Hz, 2H), 1.53 (s, 6H).

^{13}C NMR (151 MHz, $CDCl_3$) δ 155.97, 153.82, 137.95, 137.86, 137.42, 137.03, 130.20, 128.92, 128.75, 128.52, 127.65, 126.53, 126.18, 126.12, 121.38, 121.08, 120.46, 120.34, 47.09, 27.09.

HRMS (EI+) calculated for $C_{23}H_{19}Br$ 376.0670; found 376.0667

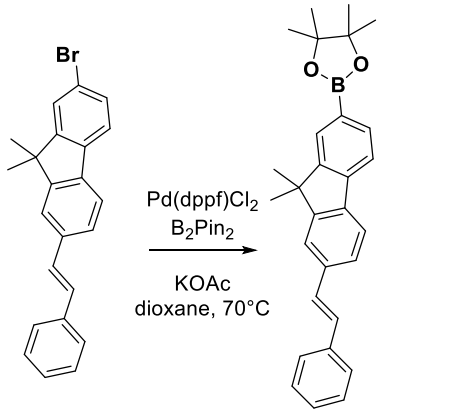

21 **22**, 39%

Synthesis of (E)-2-(9,9-dimethyl-7-styryl-9H-fluoren-2-yl)-4,4,5,5-tetramethyl-1,3,2-dioxaborolane, 22

21 (0.25 g, 0.67 mmol), B_2pin_2 (200 mg, 0.8 mmol), $Pd(dppf)Cl_2$ (24 mg, 33 µmol), and potassium acetate (200 mg, 2.0 mmol) were added to a flame dried Schlenk flask, then evacuated and backfilled with N_2 (3X). Anhydrous dioxane (5 mL) was added and the reaction stirred for 14 hours at 70 °C. This was extracted in ethyl acetate, then washed with NH_4Cl and brine. The organic layer was dried with $MgSO_4$ and concentrated onto silica. Purification by flash chromatography (1-5% ethyl acetate in hexanes) afforded **22** as an off-white foam (110 mg, 39%).

^{1}H NMR (600 MHz, Chloroform-*d*) δ 7.89 (s, 1H), 7.83 (dd, *J* = 7.5, 1.0 Hz, 1H), 7.73 (dd, *J* = 7.7, 4.7 Hz, 2H), 7.60 (d, *J* = 1.6 Hz, 1H), 7.57 – 7.53 (m, 2H), 7.51 (dd, *J* = 7.9, 1.6 Hz, 1H), 7.38 (t, *J* = 7.7 Hz, 2H), 7.28 (d, *J* = 7.4 Hz, 1H), 7.20 (d, *J* = 5.5 Hz, 2H), 1.55 (s, 6H), 1.39 (s, 12H).

^{13}C NMR (151 MHz, $CDCl_3$) δ 154.87, 153.07, 141.89, 138.74, 137.49, 137.07, 133.99, 129.10, 128.77, 128.71, 128.38, 127.56, 126.51, 125.90, 120.71, 120.51, 119.37, 83.78, 46.83, 29.72, 27.14, 24.93.

HRMS (EI+) calculated for $C_{29}H_{31}O_2B$ 422.2417; found 422.2412

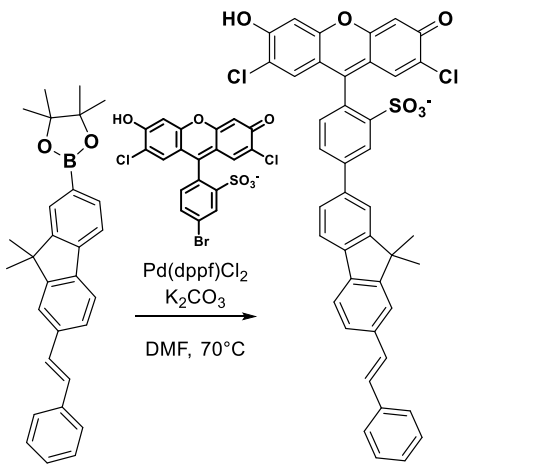

22 **23**, 13%

Synthesis of (E)-2-(2,7-dichloro-6-hydroxy-3-oxo-3H-xanthen-9-yl)-5-(9,9-dimethyl-7-styryl-9H-fluoren-2-yl)benzenesulfonate, 23 (7v-fVF 0)

22 (50 mg, 0.11 mmol), 5-bromo-(2',7'-dichloro-sulfofluorescein (51 mg, 98 µmol), and Pd(dppf)Cl_2 (3.6 mg, 4.9 µmol) were combined in anhydrous DMF (1 mL). 5M K_2CO_3 solution was bubbled with N_2 for 30 minutes, then 100 µL was added, the flask was sealed, and the reaction was stirred at 80 °C for 18 hours. The reaction was then concentrated to dryness *in vacuo*, then the crude material was taken up in 1:1 dicholoromethane:methanol, and precipitated in diethyl ether. The precipitate was purified by preparative-HPLC (50-95% MeCN in water + 0.05% trifluoroacetic acid) to afford **23** as a dark red powder (10 mg, 13% yield).

^{1}H NMR (900 MHz, DMSO-d_6) δ 8.32 (d, *J* = 2.0 Hz, 1H), 8.02 (d, *J* = 1.7 Hz, 1H), 7.99 (d, *J* = 7.7 Hz, 1H), 7.96 (dd, *J* = 7.7, 2.0 Hz, 1H), 7.92 – 7.88 (m, 2H), 7.81 (dd, *J* = 7.8, 1.7 Hz, 1H), 7.67 – 7.64 (m, 2H), 7.62 (dd, *J* = 7.8, 1.5 Hz, 1H), 7.40 (t, *J* = 7.5 Hz, 2H), 7.39 – 7.36 (m, 3H), 7.30 – 7.26 (m, 1H), 7.03 (s, 2H), 6.78 (s, 2H), 1.59 (s, 6H).

^{13}C NMR (226 MHz, DMSO) δ 158.09, 157.94, 154.65, 154.38, 151.83, 147.50, 141.40, 138.39, 138.06, 137.73, 137.24, 136.62, 130.35, 129.78, 128.81, 128.73, 128.08, 127.71, 127.53, 127.26, 126.42, 126.30, 126.08, 125.44, 121.27, 120.86, 120.68, 120.52, 115.88, 103.30, 46.69, 26.86.

HRMS (ESI-) m/z: $[M-H]^-$ calculated for $C_{42}H_{27}Cl_2O_6S$ 729.0911; found 729.0902

3.7 Figures and schemes

Scheme 3-1. *Vinyl-fluorene molecular wires are a hybrid between previous molecular wires used in VoltageFluor indicators*

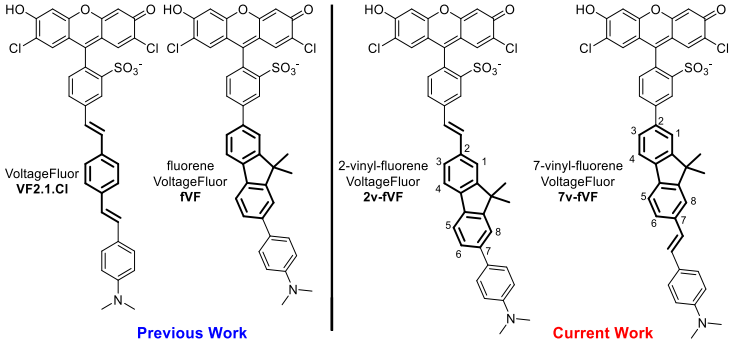

Scheme 3-2. *Synthesis of 2-vinyl fluorene VoltageFluors*

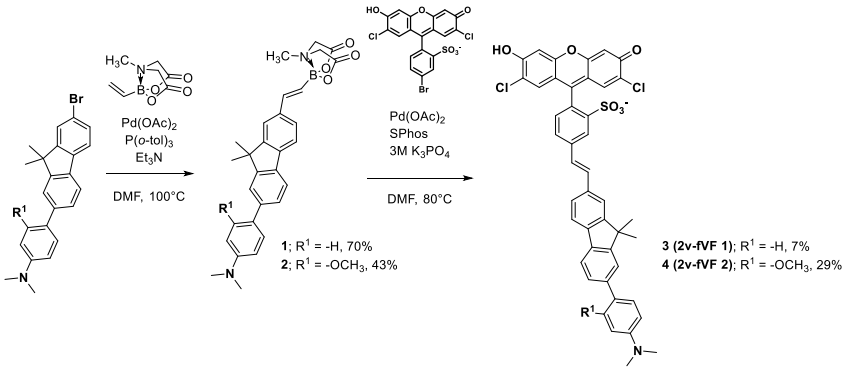

Scheme 3-3. *Synthesis of 7-vinyl fluorene VoltageFluors*

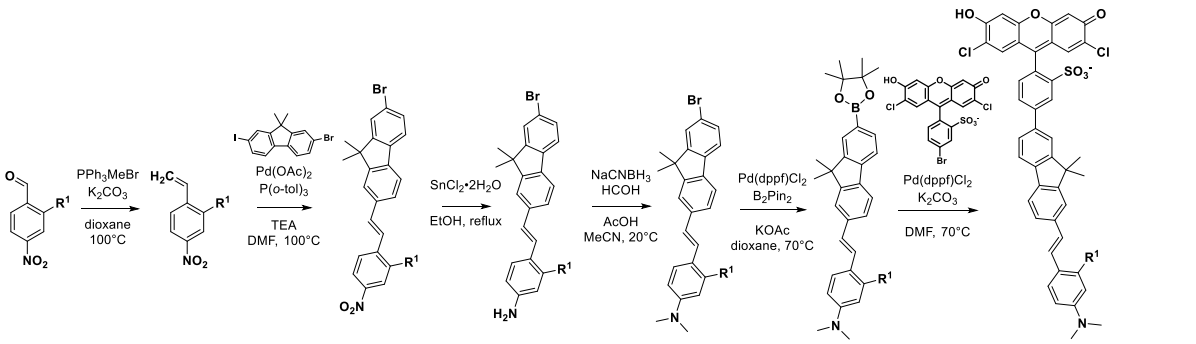

7; R^1 = -H, 91%
8; R^1 = -OCH_3, 63%

9; R^1 = -H, 21%
10; R^1 = -OCH_3, 35%

11; R^1 = -H, 69%
12; R^1 = -OCH_3, 96%

13; R^1 = -H, 52%
14; R^1 = -OCH_3, 45%

15; R^1 = -H, 74%
16; R^1 = -OCH_3, 55%

17 (7v-fVF 1); R^1 = -H, 17%
18 (7v-fVF 2); R^1 = -OCH_3, 18%

Scheme 3-4. *Synthesis of vinyl-fluorene VoltageFluors lacking an aniline donor*

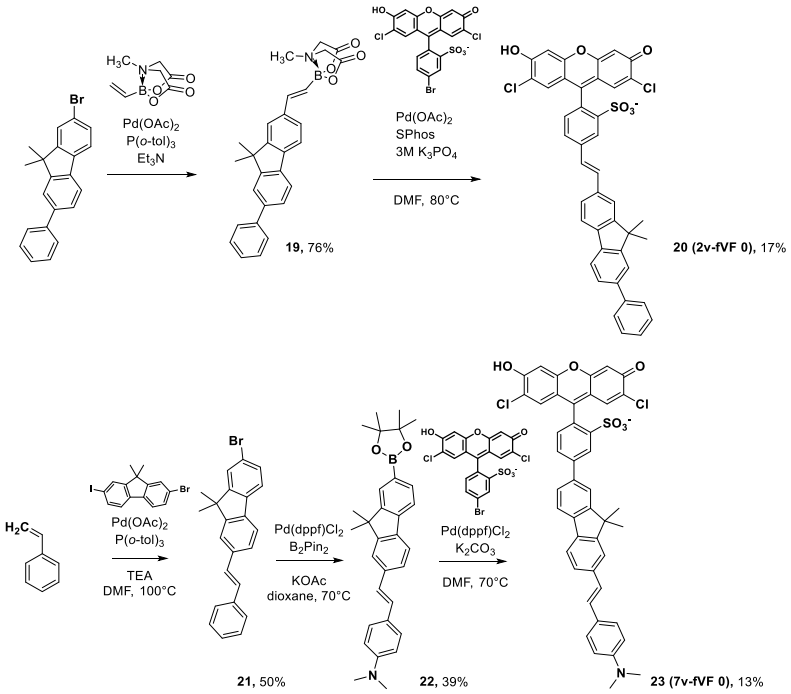

Scheme 3-5. *Synthesis of fluorene wire intermediates used in 2-vinyl fluorene VoltageFluors*

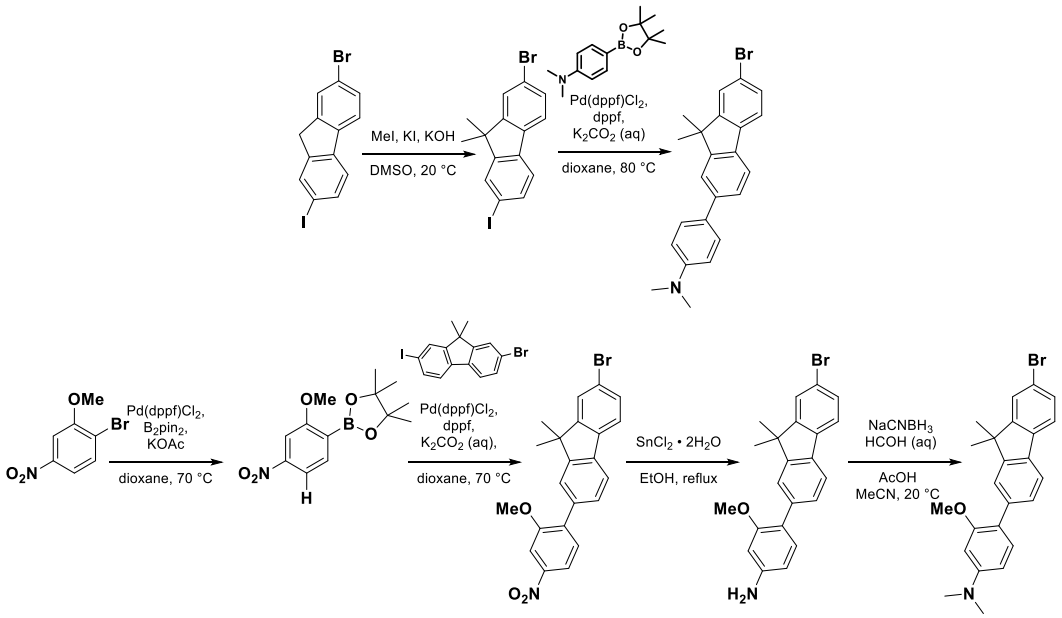

Scheme 3-6. *Synthesis of 4-nitro-2-methoxybenzaldehyde used in 7-vinyl fluorene VoltageFluor 2.*

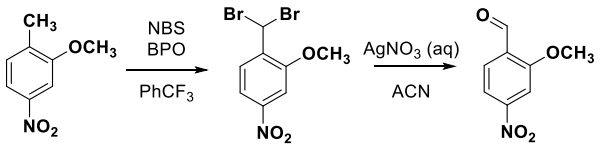

5, 75% **6**, 75%

Table 3-1. *Spectroscopic characterization of vinyl-fluorene VoltageFluors*

Entry	Absorbance [nm][a]	Wire Absorbance [nm][a]	Emission [nm][a]	QY[a]
2v-fVF 1 (**3**)	519	375	534	0.07
7v-fVF 1 (**4**)	520	384	535	0.06
2v-fVF 2 (**17**)	519	370	535	0.04
7v-fVF 2 (**18**)	519	390	535	0.07
2v-fVF 0 (**20**)	519	364	535	0.16
7v-fVF 0 (**23**)	520	357	535	0.23

[a] Measured in PBS + 0.1% SDS (pH = 7.2).

Table 3-2. *Brightness and sensitivity of vinyl-fluorene VoltageFluors in HEK293T cells*

Entry	Relative Brightness[a]	%F/F[b]	SNR
2v-fVF 1 (**3**)	1.6	7.4 ± 0.3	41 ± 10.5
7v-fVF 1 (**4**)	1.0	16.5 ±0.2	67 ± 8.5
2v-fVF 2 (**17**)	1.5	15.2 ± 0.2	49 ± 3.4
7v-fVF 2 (**18**)	0.4	30.6 ± 0.7	37 ± 5.6
2v-fVF 0 (**20**)	5.8	-0.3 ± 0.01	1.7 ± 0.2
7v-fVF 0 (**23**)	4.4	-0.3 ± 0.01	0.8 ± 0.2

[a] Measured in HEK 293T cells. [b] per 100 mV, recorded at 0.5 kHz optical sampling rate.

Table 3-3. *Performance of vinyl-fluorene VoltageFluors in neurons and cardiomyocytes*

Entry	$\%F/F_{neuron}$[c]	SNR_{neuron}	$\%F/F_{iCM}$[d]	SNR_{iCM}
2v-fVF 1 (**3**)	4.6 ± 0.2	16.5 ± 0.6	6.1 ± 0.5	326 ± 46
7v-fVF 1 (**4**)	4.5 ± 0.5	18.5 ± 0.9	3.6 ± 0.3	187 ± 23
2v-fVF 2 (**17**)	5.6 ± 0.4	16.9 ±1.1	7.8 ± 0.4	430 ± 37
7v-fVF 2 (**18**)	9.0 ± 2.6	15 ± 4.7	4.6 ± 0.4	263 ± 32
fVF 2[a]	3.5 ± 0.1	12.6 ± 0.8	2.2 ± 0.5	154 ± 12
VF2.1.Cl[b]	9.4 ± 0.3	35 ± 1.6	10.6 ± 0.8	169 ± 10

[a] Boggess et al. 2019 [b] Miller et al. 2014. [c] Recorded at 0.5 kHz optical sampling rate, error bars are ± SEM. [d] Recorded at 0.2 kHz optical sampling rate, error bars are ± SEM..

Figure 3-1. *Absorbance and emission of vinyl-fluorene VoltageFluors*

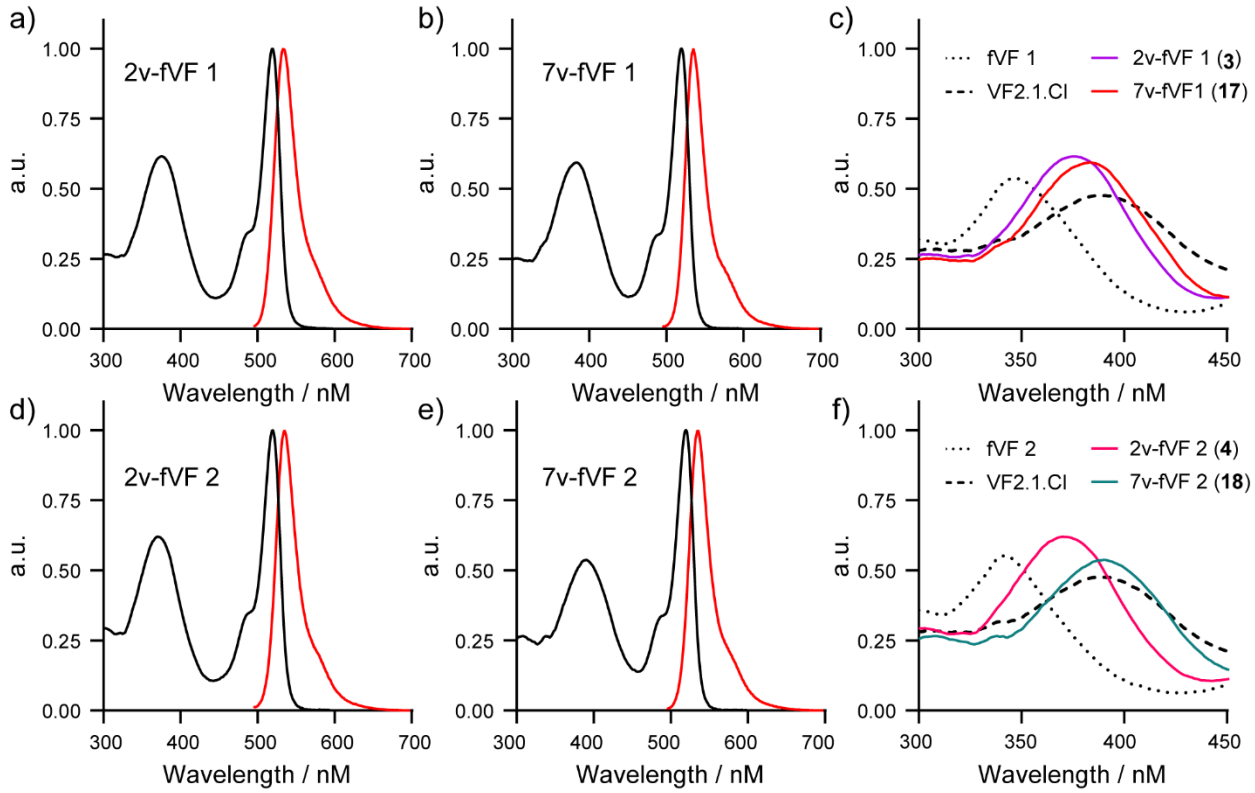

Figure 3-1. Normalized absorbance and emission of vinyl-fluorene VoltageFluors. (a) 2v-fVF 1 (**3**), (b) 2v-fVF 2 (**4**), (c) 7v-fVF 1 (**17**), and (e) 7v-fVF 2 (**18**) spectra were acquired at 1.25 µM in PBS (pH 7.2) with 0.1% SDS. Closer examination of wire absorbance signatures shows a bathochromic shift when a vinyl spacer is added to (c) fVF 1 or (f) fVF 2.

Figure 3-2. *Absorbance and emission of vinyl-fluorene VoltageFluors lacking an aniline donor*

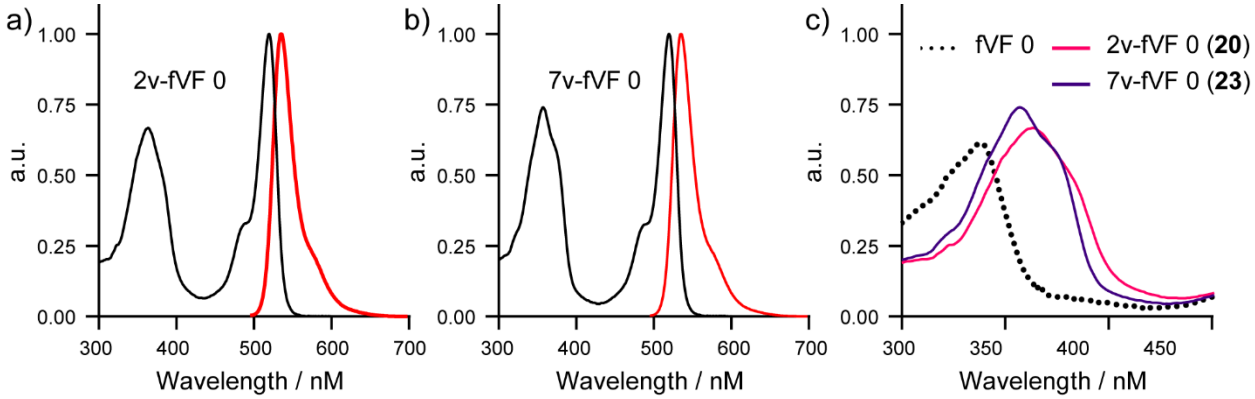

Figure 3-2. Absorbance and emission of vinyl-fluorene VoltageFluors lacking an aniline donor. (a) 2v-fVF 0 (**20**) and (b) 7v-fVF 0 (**23**) spectra were at 1.25 µM in PBS (pH 7.2) with 0.1% SDS. Closer examination of wire absorbance signatures shows a bathochromic shift when a vinyl spacer is added to (c) fVF 0

Figure 3-3. *Characterization of vinyl-fluorene VoltageFluors in HEK293T cells*

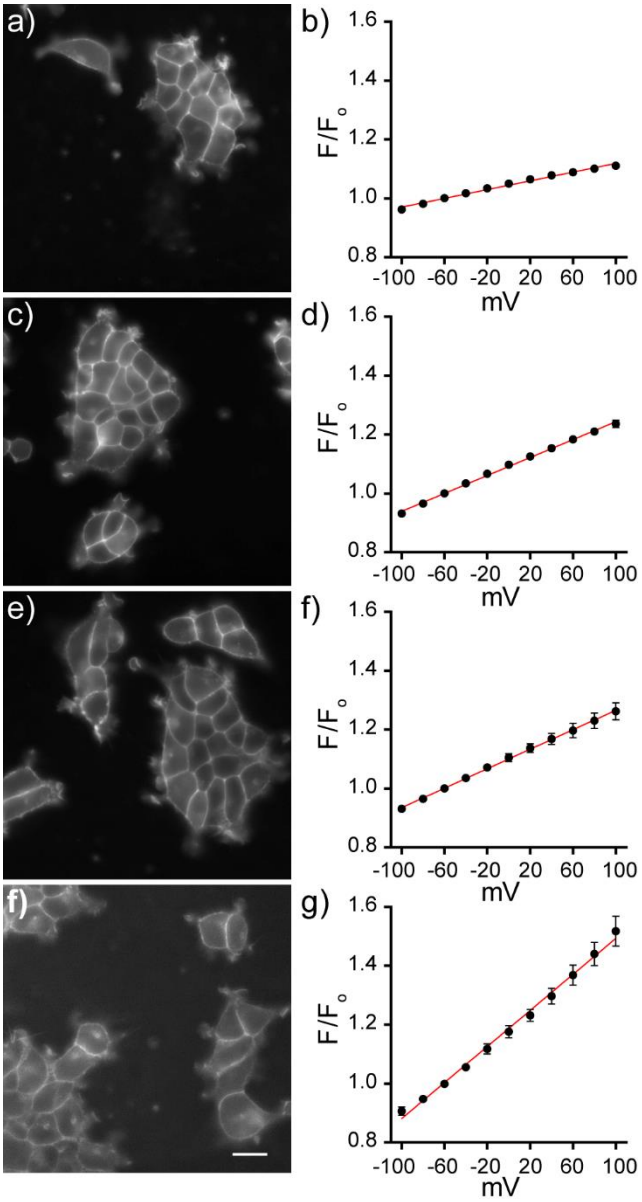

Figure 3-3. Characterization of vinyl-fluorene VoltageFluors in HEK293T cells. Live cell fluorescence images of (a) 2v-fVF 1, (c) 2v-fVF 2, (e) 7v-fVF 1, and (f) 7v-fVF 2 loaded at 0.5 µM in HEK 293T cells. Scale bar is 20 µm. Plots of F/F_o versus membrane potential (millivolts) in voltage-clamped HEK293T cells for (b) 2v-fVF 1, (d) 2v-fVF 2, (f) 7v-fVF1, and (g) 7v-fVF 2. The red line is the line of best fit, error bars are ± SEM for a minimum of 3 independent determinations.

Figure 3-4. *Brightness comparison of vinyl-fluorene VoltageFluors in HEK293T cells*

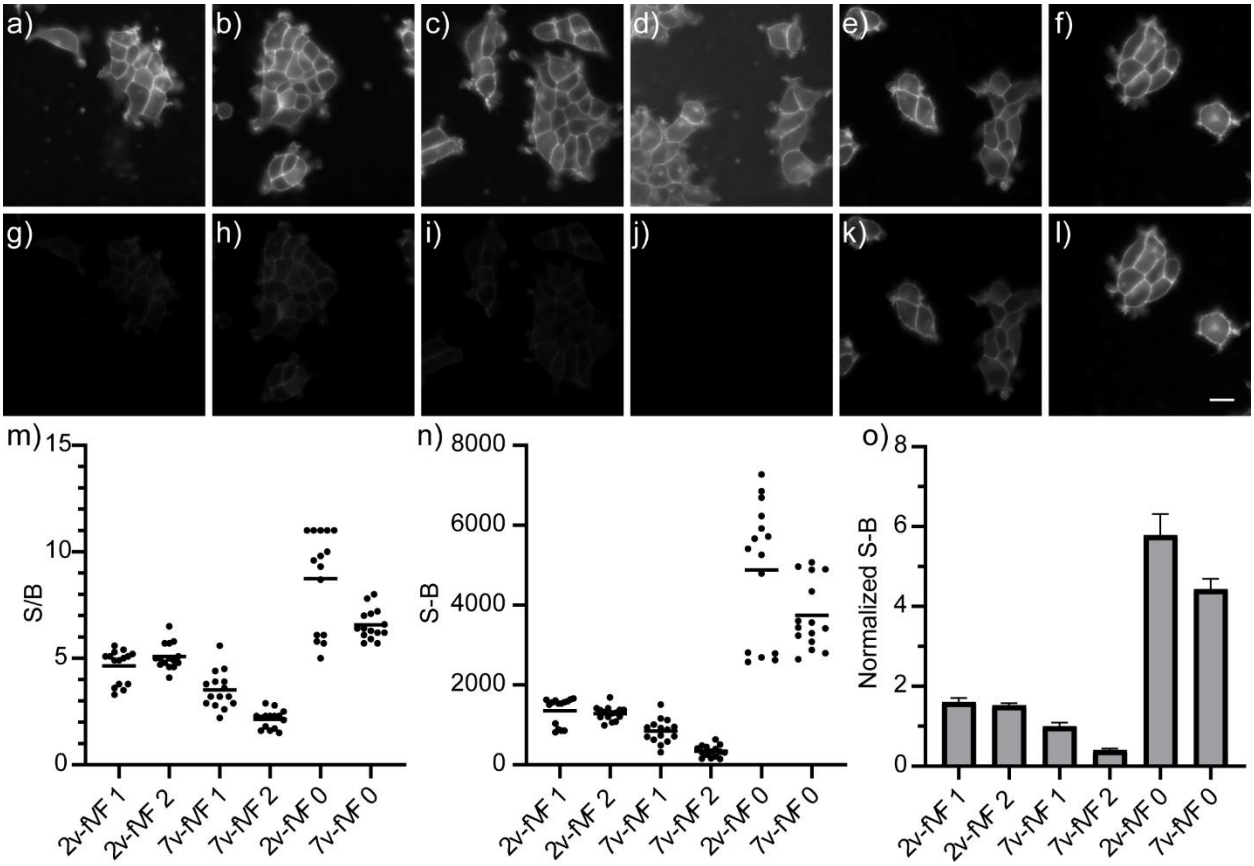

Figure 3-4. Brightness comparison of vinyl-fluorene VoltageFluors in HEK293T cells. Widefield epifluorescence micrographs of 2v-fVF 1 (**3**, a, e), 2v-fVF 2 (**4**, b, h), 7v-fVF 1 (**17,** c, i), 7v-fVF 2 (**18**, d, j), 2v-fVF 0 (**20**, e, k), and 7v-fVF 0 (**23**, f, l). Top row: pixel histograms adjusted to show max contrast for each indicator. Bottom row: pixel histograms matched to 7v-fVF 0 (l). Scale bar is 20 µm, all indicators were loaded at a concentration of 0.5 µM. (m) Scatter plot of measured signal over background for each indicator, where signal is fluorescence from cell rafts and background is the pixel intensity of areas where cells did not grow. Each dot is a single determination, bar represents the mean value, n = 15 ROIs per indicator. (n) Scatter plot of signal-background. (o) Bar plot of normalized average signal-background, where the 7v-fVF 1 is set to 1. Indicators lacking an aniline donor were approximately 4-5 times brighter than indicators possessing an aniline. Error bars are ± SEM.

Figure 3-5. *Comparison of voltage sensitivity to fluorene VoltageFluors*

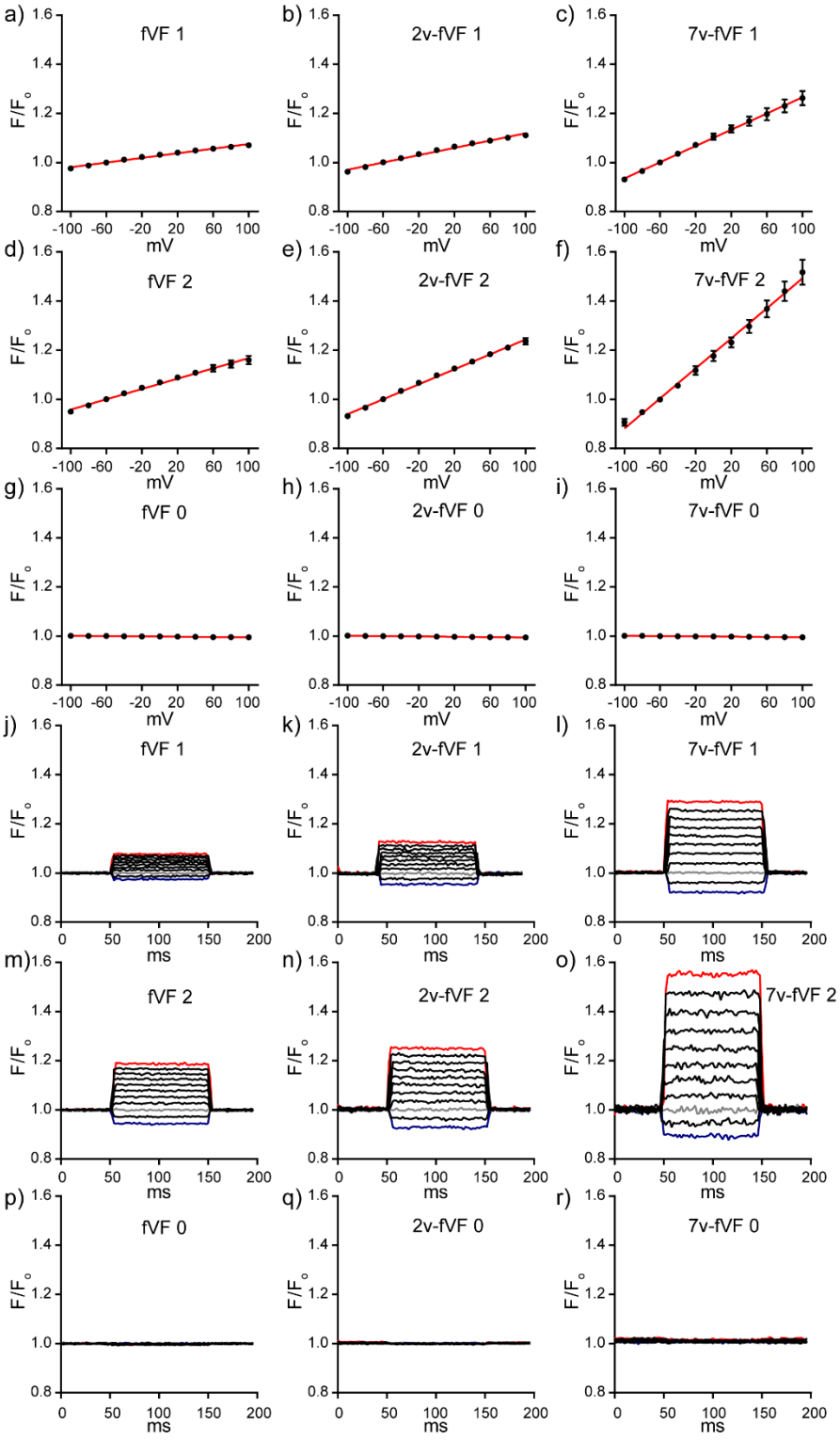

Figure 3-5. Comparison of voltage sensitivity to fluorene VoltageFluors. (a-c) Plots of F/F_o versus membrane potential comparing fVF 1 to its vinyl-fluorene derivatives, which are more sensitive. (d-f) comparison of fVF 2 derivatives, and (g-i) comparison of fVF 0 derivatives. These indicators lack an aniline donor and are not sensitive to changes in V_{mem}. Error bars are ± SEM, red line is the line of best fit, the slope of the line is used to calculate $\%\Delta F/F_o$. (j-r) show comparison of concatenated fluorescence traces of voltage steps (red: 100 mV, blue: -100 mV) during patch-clamp. The relative F/F_o and signal-to-noise can be visualized.

Figure 3-6. *Performance of vinyl-fluorene VoltageFluors in hiPSC-CM monolayers.*

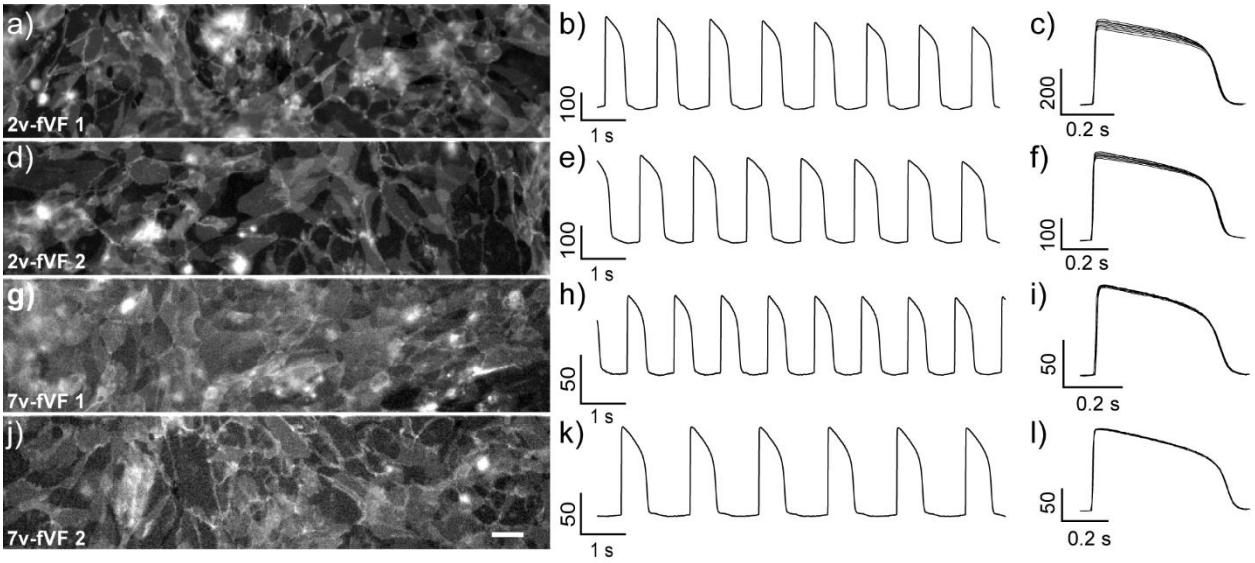

Figure 3-6. Performance of vinyl-fluorene VoltageFluors in hiPSC-CM monolayers. (a) Representative fluorescence micrograph of 2v-fVF (0.5 μM) in a hiPSC-CM monolayer. (b) Fluorescence trace of mean pixel intensity of (a) over ten seconds, acquired at a frame rate of 0.2 MHz. Ventricular action potentials are observed and maintain regular shape over the course of the recording (c). 2v-fVF 2 (d-f), 7v-fVF 1 (g-i), and 7v-fVF 2 (j-l) also report cardiac action potential morphology with high fidelity when loaded at 0.5 μM. Scale bar is 50 μm.

Figure 3-7. *Recordings of evoked activity in neurons with VoltageFluor indicators*

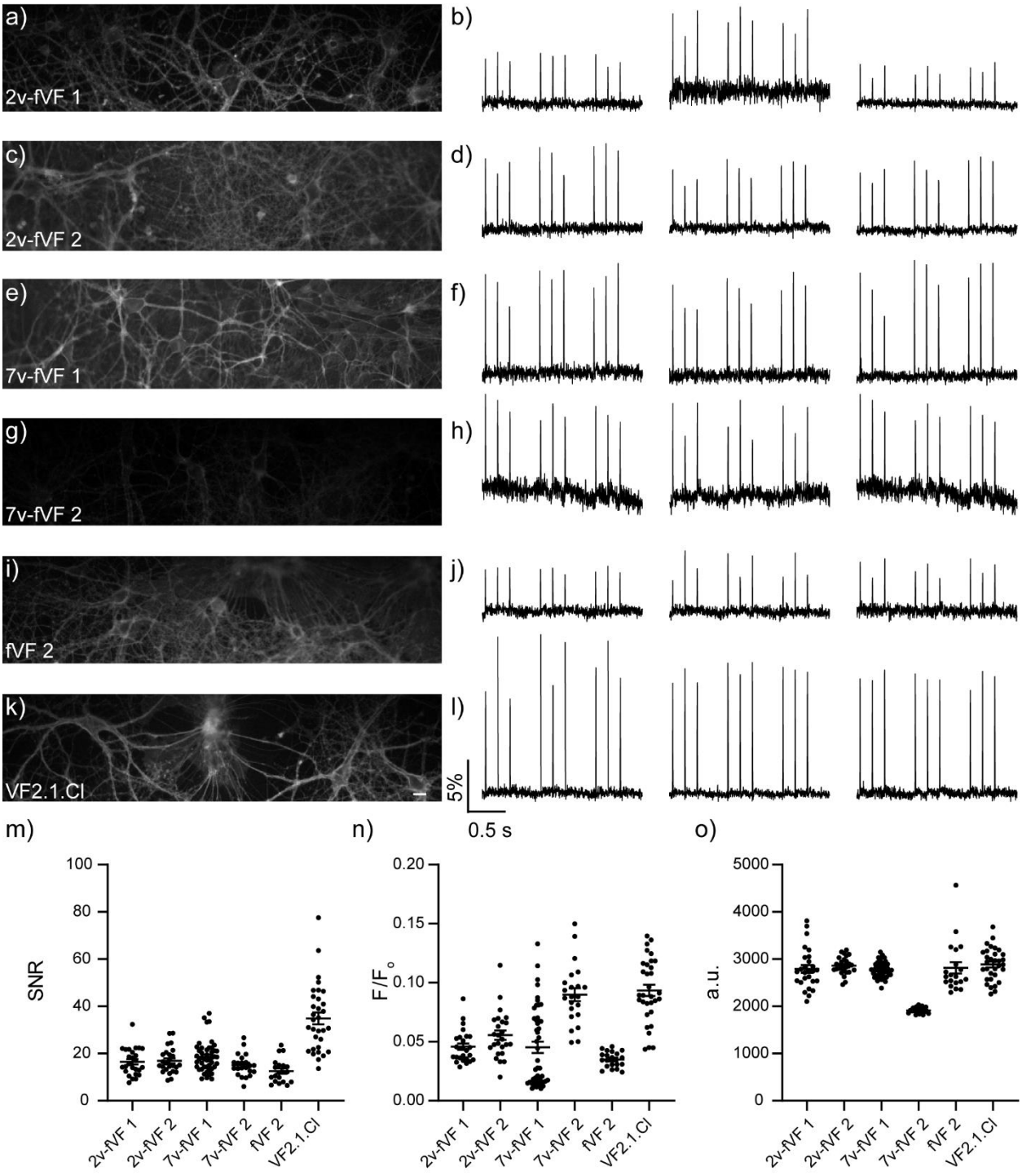

Figure 3-7. Recordings of evoked activity in neurons with VoltageFluor indicators. Live cell wide-field fluorescence images of 13-14 DIV rat hippocampal neurons stained with (a) 2v-fVF 1, (c) 2v-fVF 2, (e) 7v-fVF 1, (g) 7v-fVF2, (i) fVF 2, and (k) VF2.1.Cl at a concentration of 0.5 µM. Image pixel intensity histograms are adjusted to the same range to show relative brightness. Scale bar is 20 µm. Representative %$\Delta F/F_o$ plots of evoked neuronal activity recorded

optically with (b) 2v-fVF 1, (d) 2v-fVF 2, (f) 7v-fVF 1, (h) 7v-fVF2, (j) fVF 2, and (l) VF2.1.Cl. These traces come from three separate cells in different ROIs and are corrected for photobleach. Scatter plots comparing (m) signal-to-noise ratio, (n) $\Delta F/F_o$, and (o) baseline brightness of recordings made with VoltageFluors. Bars show the mean, error bars are ± SEM. Three coverslips were used per indicator, n = 26 (2v-fVF 1), 25 (2v-fVF 2), 47 (7v-fVF 1), 22 (7v-fVF 2), 20 (fVF 2), 32 (VF2.1.Cl) cells from which recordings were taken.

Figure 3-8. *Comparison VoltageFluor classes in hiPSC-CM monolayers.*

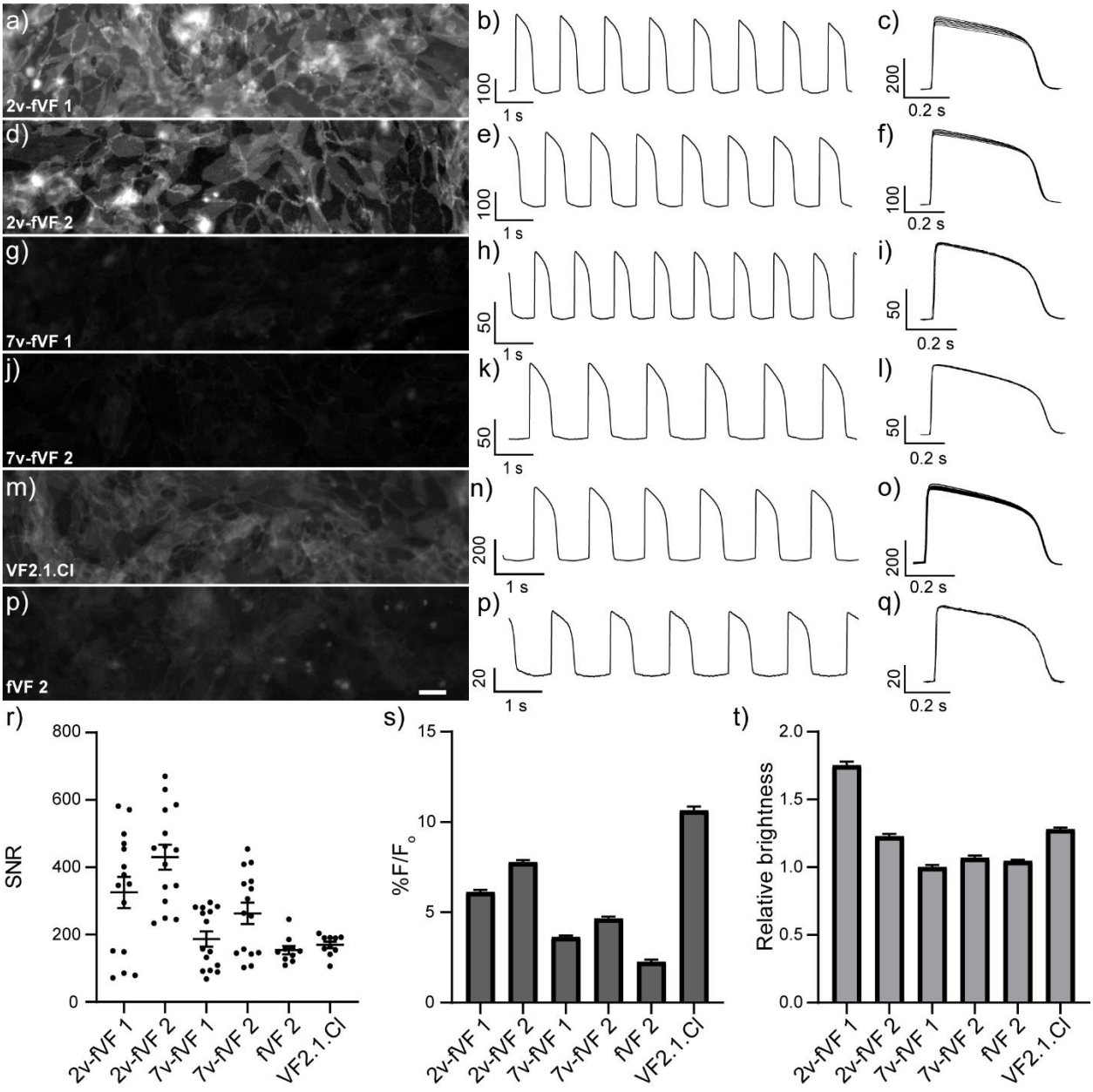

Figure 3-8. Comparison VoltageFluor classes in hiPSC-CM monolayers. (a-k) depict the same data available in Figure 3-6 but plotted alongside data acquired with (m-o) VF2.1.Cl and (p-q) fVF 2 at 0.5 µM. Pixel intensity histograms are the same in all fluorescence images to show relative brightness. Scale bar is 50 µm. Top middle column: Full ten second plots of fluorescence intensity are representative recordings made with each indicator, corrected for photobleaching. Right column: Overlaid recorded action potential events from recordings in the middle column, showing little to no change in morphology over the course of the ten second recording. (r) Scatter plot of signal-to-noise ratio of recording taken with VoltageFluor indicators. Middle bars show the mean, error bars are ± SEM. (s) Bar plot of mean $\Delta F/F_o$ (%) of recorded signals and (t) the normalized average baseline brightness of recordings, where 7v-fVF 1 is set to 1.0. n= 15 ROIs across three wells. Error bars are ± SEM.

Figure 3-9. *Phototoxicity of vinyl-fluorene VoltageFluors in hiPSC-iCM monolayers under constant illumination.*

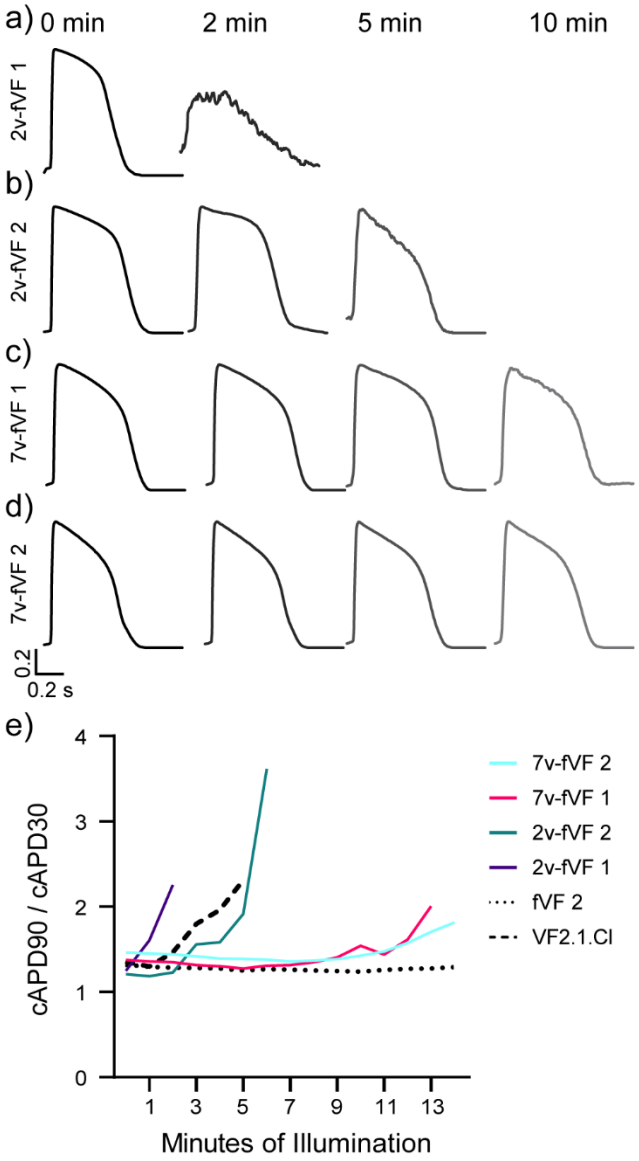

Figure 3-9. Phototoxicity of vinyl-fluorene VoltageFluors in hiPSC-iCM monolayers under constant illumination. Monolayers stained with (a) 2v-fVF 1, (b) 2v-fVF 2, (c) 7v-fVF 1, and (d) 7v-fVF 2 were illuminated with the excitation LED for up to 14 minutes. (a) Rapid degradation of signal and a drastic action potential morphology change is observed in monolayers staining with 2v-fVF 1; after 2 minutes of illumination cells cease spontaneous beating. (b) Recordings without changes to the action potential for about 3 minutes of illumination made using 2v-fVF 2, however action potential morphology changes quickly thereafter. (c-d) Long term recordings can be made with 7v-fVF 1 and 7v-fVF 2 up to 10 minutes without changes to action potential morphology. (e) Plot showing the ratio of cAPD90/cAPD30, which is the action potential duration at 90 and 30 percent of the repolarization, corrected for beat rate by Fridericia's formula. Initial recordings start with a ratio between 1.2 and 1.4, regardless of the indicator used. Increases in the ratio indicate a change in action potential morphology, caused by a decrease in cAPD30 or increase in cAPD90. 2v-fVFs are most like VF2.1.Cl, which deviates after just three minutes of illumination. 7v-fVFs behave more similarly to fVF 2, which does not deviate even after 14 minutes of illumination.

Figure 3-10. *Quantification of action potential morphology changes due to phototoxicity.*

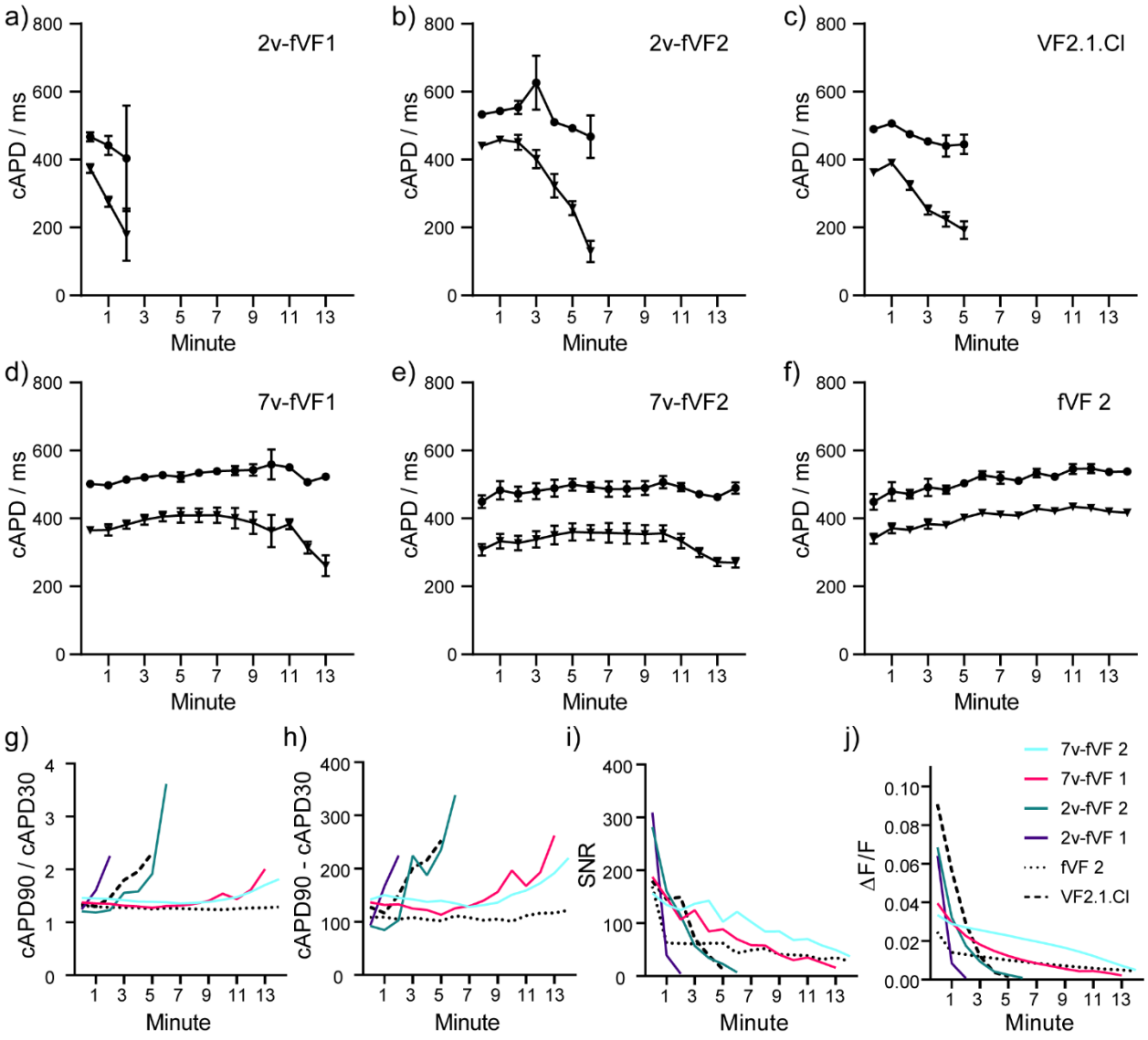

Figure 3-10. Quantification of action potential morphology changes due to phototoxicity. Average cAPD30 (black triangles) and cAPD90 (black circles) of cardiac action potential recordings during prolonged illumination. Deviations are quickly seen when (a) 2v-fVF 1, (b) 2v-fVF 2, or (c) VF2.1.Cl are used as indicators. cAPD measurements are steady for up to 10 minutes of illumination when (d) 7v-fVF 1 or (e) 7v-fVF 2 are used, while (f) fVF 2 can be used for 14 minutes without seeing a change. Error bars are ± SEM. The (g) ratio and (h) difference of cAPD90 and cAPD30 show when recorded action potentials start to deviate in morphology. (i) SNR and (j) $\Delta F/F_o$ decrease over prolonged illuminations due to photobleaching of the voltage indicator. 2v-fVFs and VF2.1.Cl lose signal rapidly, as the signal quality and tissue degrade under constant illumination. While action potential morphology is stable when using fVF 2 as an indicator, overall signal rapidly degrades, making these long-term recordings noisy. Because of increased sensitivity, 7v-fVFs are capable of reporting action potentials for long-term recordings and have reduced phototoxicity when compared to other voltage indicators.

Figure 3-11. *Photobleaching in HEK293T cells and hiPSC-CM monolayers.*

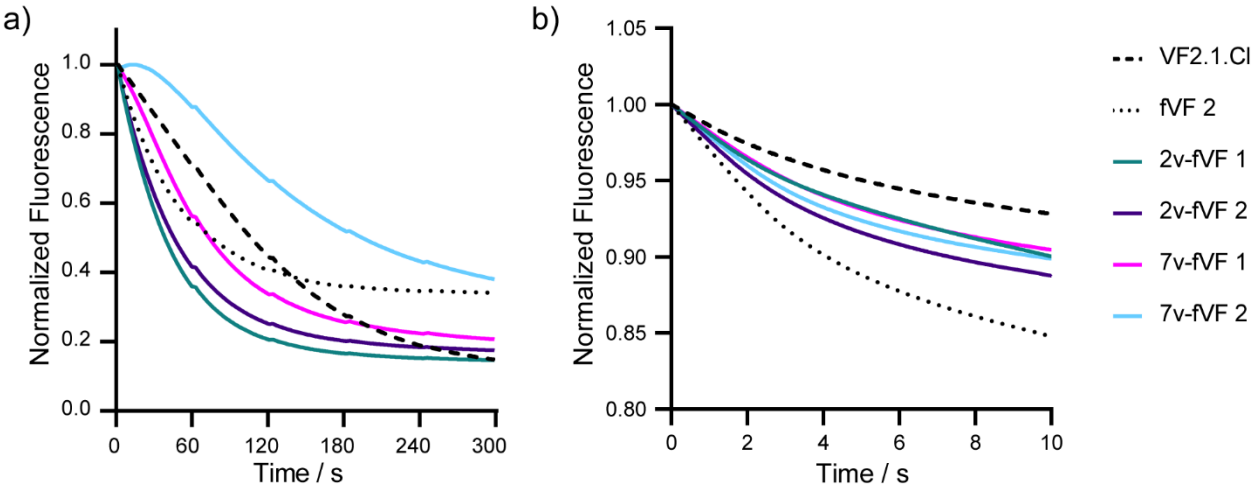

Figure 3-11. Photobleaching in HEK293T cells and hiPSC-CM monolayers. (a) Photobleach curve of vinyl-fluorene VoltageFluors compared to fVF 2 and VF2.1.Cl in HEK293T cells. Cells incubated with voltage indicator in imaging buffer were exposed to the excitation LED for 5 minutes, images were acquired at 1 Hz for analysis of membrane signal. Initial fluorescence values were normalized to 1.0 to show relative decay rates. 2v-fVF 1 and 2v-fVF 2 bleach the fastest of the indicators tested, decaying at a rate of 2.3 x 10^{-2} s^{-1} and 2.1 x 10^{-2} s^{-1}, respectively. fVF 2 decays at a rate of 1.9 x 10^{-2} s^{-1}, but then is constant after two minutes. 7v-fVF 1 decays slightly less quickly than 2v-fVF derivatives at a rate of 1.4 x 10^{-2} s^{-1}. Besides 7v-fVF 2, VF2.1.Cl bleaches less rapidly than fluorene-based indicators at a rate of 6.9 x 10^{-3} s^{-1}. 7v-fVF 2 initially photobrightens, but then decays at a rate of 4.4 x 10^{-3} s^{-1}, the slowest of indicators tested. (b) Splines used to correct for photobleach of traces acquire in hiPSC-CMs. These were calculated by an asymmetric least-squares fit of the baseline and averaged over three acquisitions. In cardiac monolayers, fVF 2 bleaches most rapidly, while VF2.1.Cl has the slowest rate of bleaching. All vinyl-fluorene VoltageFluors have intermediate rates of bleaching between previously described voltage indicators.

3.8 References

(1) Peterka, D. S.; Takahashi, H.; Yuste, R. Imaging Voltage in Neurons. *Neuron* **2011**, *69* (1), 9–21.

(2) Miller, E. W. Small Molecule Fluorescent Voltage Indicators for Studying Membrane Potential. *Curr. Opin. Chem. Biol.* **2016**, *33*, 74–80.

(3) Miller, E. W.; Lin, J. Y.; Frady, E. P.; Steinbach, P. A.; Kristan, W. B.; Tsien, R. Y. Optically Monitoring Voltage in Neurons by Photo- Induced Electron Transfer through Molecular Wires. *Proc. Natl. Acad. Sci. U. S. A.* **2011**, *109* (6), 2114–2119.

(4) Woodford, C. R.; Frady, E. P.; Smith, R. S.; Morey, B.; Canzi, G.; Palida, S. F.; Araneda, R. C.; Kristan, W. B.; Kubiak, C. P.; Miller, E. W.; et al. Improved PeT Molecules for Optically Sensing Voltage in Neurons. *J. Am. Chem. Soc.* **2015**, *137* (5), 1817–1824.

(5) Deal, P. E.; Kulkarni, R. U.; Al-Abdullatif, S. H.; Miller, E. W. Isomerically Pure Tetramethylrhodamine Voltage Reporters. *J. Am. Chem. Soc.* **2016**, *138* (29), 9085–9088.

(6) Ortiz, G.; Liu, P.; Naing, S. H. H.; Muller, V. R.; Miller, E. W. Synthesis of Sulfonated Carbofluoresceins for Voltage Imaging. *J. Am. Chem. Soc.* **2019**, *141* (16), 6631–6638.

(7) Boggess, S. C.; Gandhi, S. S.; Siemons, B. A.; Huebsch, N.; Healy, K. E.; Miller, E. W. New Molecular Scaffolds for Fluorescent Voltage Indicators. *ACS Chem. Biol.* **2019**, *14* (3), 390–396.

(8) Goldsmith, R. H.; Sinks, L. E.; Kelley, R. F.; Betzen, L. J.; Liu, W.; Weiss, E. a; Ratner, M. A.; Wasielewski, M. R. Wire-like Charge Transport at near Constant Bridge Energy through Fluorene Oligomers. *Proc. Natl. Acad. Sci. U. S. A.* **2005**, *102* (10), 3540–3545.

(9) Eng, M. P.; Albinsson, B. Non-Exponential Distance Dependence of Bridge-Mediated Electronic Coupling. *Angew. Chemie - Int. Ed.* **2006**, *45* (34), 5626–5629.

(10) Davis, W. B.; Svec, W. A.; Ratner, M. a; Wasielewski, M. R. Molecular-Wire Behaviour in p-Phenylenevinylene Oligomers. *Nature* **1998**, *396*, 60–63.

(11) Albinsson, B.; Mårtensson, J. Long-Range Electron and Excitation Energy Transfer in Donor-Bridge-Acceptor Systems. *J. Photochem. Photobiol. C Photochem. Rev.* **2008**, *9* (3), 138–155.

(12) Goldsmith, R. H.; Deleon, O.; Wilson, T. M.; Finkelstein-shapiro, D.; Ratner, M. A.; Wasielewski, M. R. Challenges in Distinguishing Superexchange and Hopping Mechanisms of Intramolecular Charge Transfer through Fluorene Oligomers. **2008**, 4410–4414.

(13) Wielopolski, M.; Santos, J.; Illescas, Beatriz, M.; Ortiz, A.; Insuasty, B.; Bauer, T.; Clark, T.; Guldi, D. M.; Martin, N. Vinyl Spacers—Tuning Electron Transfer through Fluorene-Based Molecular Wires. *Energy Environ. Sci.* **2011**, *4*, 765–771.

(14) Uno, B. E.; Gillis, E. P.; Burke, M. D. Vinyl MIDA Boronate: A Readily Accessible and Highly Versatile Building Block\nfor Small Molecule Synthesis. *Tetrahedron* **2009**, *65*

(16), 3130–3138.

(15) McKeithan, W. L.; Savchenko, A.; Yu, M. S.; Cerignoli, F.; Bruyneel, A. A. N.; Price, J. H.; Colas, A. R.; Miller, E. W.; Cashman, J. R.; Mercola, M. An Automated Platform for Assessment of Congenital and Drug-Induced Arrhythmia with Hipsc-Derived Cardiomyocytes. *Front. Physiol.* **2017**, *8*.

(16) McPheeters, MT; Wang, YT; Laurita KR; Jenkins, M. An Optical System for High-Throughput Screening of Cardiac Electrophysiology for Human Cardiomyocytes. *Physiology.* **2017**.

(17) Rohr, S.; Salzberg, B. M. Multiple Site Optical Recording of Transmembrane Voltage (MSORTV) in Patterned Growth Heart Cell Cultures: Assessing Electrical Behavior, with Microsecond Resolution, on a Cellular and Subcellular Scale. *Biophys. J.* **1994**, *67* (3), 1301–1315.

(18) Zheng, Q.; Jockusch, S.; Zhou, Z.; Blanchard, S. C. The Contribution of Reactive Oxygen Species to the Photobleaching of Organic Fluorophores. *Photochem. Photobiol.* **2014**, *90* (2), 448–454.

(19) Wall, K. P.; Dillon, R.; Knowles, M. K. Fluorescence Quantum Yield Measurements of Fluorescent Proteins: A Laboratory Experiment for a Biochemistry or Molecular Biophysics Laboratory Course. *Biochem. Mol. Biol. Educ.* **2015**, *43* (1), 52–59.

(20) Kreitzer, F. R.; Salomonis, N.; Sheehan, A.; Huang, M.; Park, J. S.; Spindler, M. J.; Lizarraga, P.; Weiss, W. A.; So, P.; Conklin, B. R. A Robust Method to Derive Functional Neural Crest Cells from Human Pluripotent Stem Cells. *Am. J. Stem Cell* **2013**, *2* (2), 119–131.

(21) Lian, X.; Zhang, J.; Azarin, S. M.; Zhu, K.; Hazeltine, L. B.; Bao, X.; Hsiao, C.; Kamp, T. J.; Palecek, S. P. Directed Cardiomyocyte Differentiation from Human Pluripotent Stem Cells by Modulating Wnt/β-Catenin Signaling under Fully Defined Conditions. *Nat. Protoc.* **2013**, *8* (1), 162–175.

(22) Tohyama, S.; Hattori, F.; Sano, M.; Hishiki, T.; Nagahata, Y.; Matsuura, T.; Hashimoto, H.; Suzuki, T.; Yamashita, H.; Satoh, Y.; et al. Distinct Metabolic Flow Enables Large-Scale Purification of Mouse and Human Pluripotent Stem Cell-Derived Cardiomyocytes. *Cell Stem Cell* **2013**, *12*, 127–137.

(23) Edelstein, A. D.; Tsuchida, M. A.; Amodaj, N.; Pinkard, H.; Vale, R. D.; Stuurman, N. Advanced Methods of Microscope Control Using μManager Software. *J. Biol. Methods* **2014**, *1* (2), 10. https://doi.org/10.14440/jbm.2014.36.

(24) Edelstein, A.; Amodaj, N.; Hoover, K.; Vale, R.; Stuurman, N. Computer Control of Microscopes Using μManager. *Curr. Protoc. Mol. Biol.* **2010**.

(25) Laughner, J. I.; Ng, F. S.; Sulkin, M. S.; Arthur, R. M.; Efimov, I. R. Processing and Analysis of Cardiac Optical Mapping Data Obtained with Potentiometric Dyes. *Am. J. Physiol. Heart Circ. Physiol.* **2012**, *303* (7).

(26) Boelens, H. F. M.; Dijkstra, R. J.; Eilers, P. H. C.; Fitzpatrick, F.; Westerhuis, J. A. New Background Correction Method for Liquid Chromatography with Diode Array Detection, Infrared Spectroscopic Detection and Raman Spectroscopic Detection. *J. Chromatogr. A* **2004**, *1057* (1–2), 21–30.

(27) Luo, S.; Michler, K.; Johnston, P.; Macfarlane, P. W. A Comparison of Commonly Used QT Correction Formulae: The Effect of Heart Rate on the QTc of Normal ECGs. *J. Electrocardiol.* **2004**, *37*, 81–90.

(28) Seto, M.; Aramaki, Y.; Imoto, H.; Aikawa, K.; Oda, T.; Kanzaki, N.; Iizawa, Y.; Baba, M.; Shiraishi, M. Orally Active CCR5 Antagonists as Anti-HIV-1 Agents 2: Synthesis and Biological Activities of Anilide Derivatives Containing a Pyridine N-Oxide Moiety. *Chem. Pharm. Bull.* **2004**, *52* (7), 818–829.

(29) Estrada, S. E.; Ochoa-Puentes, C.; Sierra, C. A. Phenylenevinylene Oligomers by Mizoroki-Heck Cross Coupling Reaction. Structural and Optoelectronic Characterization. *J. Mol. Struct.* **2017**, *1133*, 448–457.

Chapter 4:

Restricting Conformation of Aniline Donors in PeT Based Voltage Indicators Tunes Sensing Properties

Abstract

Effective reporting of fast biological changes in transmembrane potential (V_{mem}) demands measurement with high temporal resolution and signal-to-noise. To meet these demands, V_{mem} sensitivity and cell brightness must be optimized. To this end, we report the design and synthesis of four PeT-based voltage sensitive dyes with conformationally modified anilines as electron donors. With these indicators, as well as existing PeT-based voltage indicators, we construct a library of sensors with a range of conformations in the electron donating moiety. We find that measurements of fluorescence sensitivity and lifetime across this library span an order of magnitude and seek to understand how aniline conformation modulates PeT. By comparing in-depth photophysical characterization with performance at action potential detection, we establish a detailed link between the probe conformation and ability to report V_{mem} events with high fidelity.

Portions of this work were performed by the following persons:

Synthesis of VoltageFluors was assisted by Benjamin Raliski, Sam Mun, and Amy Li.

Steady-state spectroscopy and characterization in neurons was performed by Benjamin Raliski.

Fluorescence lifetime measurements were performed by Julia Lazzari-Dean.

Drafts of this chapter were co-written with Julia Lazzari-Dean and Benjamin Raliski.

4.1 Design of VoltageFluors with restricted aniline conformation

Cell membrane potential (V_{mem}) arises from an unequal distribution of ions across a semi-permeable lipid bilayer. In excitable cells such as neurons and cardiomyocytes, V_{mem} changes on the order of milliseconds create action potentials (APs). These APs facilitate electrochemical communication across synapses and coordinate the contraction of millions of cells across the chambers of the heart. Measuring this electrical activity is critical to understanding cell physiology in health and disease.

To study these rapid changes in V_{mem}, a technique must have exquisite temporal resolution and signal-to-noise. The gold standard for measuring V_{mem} is patch-clamp electrophysiology, a series of techniques that use an electrode in direct contact with the cell of interest, allowing very precise measurement of V_{mem}. However, the low-throughput, high invasiveness, and low spatial resolution[1,2] of patch-clamp electrophysiology render it an incomplete V_{mem} measurement technique.

To record electrical activity in a less invasive and more highly multiplexed manner, our lab and others have undertaken the development of fluorescent voltage indicators, either as genetically encoded voltage indicators (GEVIs) or small molecule voltage sensitive dyes. Development of voltage sensors with sufficiently fast kinetics, bright signal, and high sensitivity poses a significant challenge in sensor engineering. State-of-the-art V_{mem} sensors are capable of recording electrophysiological signatures from individual cells with high fidelity.[3,4] Additional optimization of sensor limit-of-detection could improve the reporting of subthreshold V_{mem} events, as well as enable simultaneous recording across larger neuronal ensembles.

To meet the precise needs of V_{mem} imaging, the rational tunability of small molecules versus fluorescent proteins is a major advantage. Rational tuning of small molecules has produced major advances in biological sensing: chemical probes for Ca^{2+} have been rationally tuned across a range of dissociation constants,[5,6] small molecule fluorophores can be turned to precise wavelengths via fluorination,[7] and reversible, intramolecular spirocyclization produces fluorophore blinking for super-resolution imaging.[8] Optimization of the brightness, sensitivity, color, and localization of small molecule voltage dyes has been fruitful,[4,9–11] but further investigation is required to obtain probes with sufficient signal-to-noise ratios for single-cell recordings in thick tissue.

Our lab has developed a class of small molecule voltage sensitive dyes (VoltageFluors, VFs) based on a photoinduced electron transfer (PeT)-based V_{mem} sensing trigger. Because PeT occurs from a membrane-localized electron donor, it is sensitive to the transmembrane electric field. We have previously demonstrated that the absorption and emission wavelength of VFs can be tuned through the incorporation of different chromophores,[9,12–14] and the sensitivity can be modulated via the electron density and attenuation of the molecular wire.[10,15]

To better understand the relationship between sensitivity and brightness, we investigated the coupling between the aniline donor and the molecular wire as a strategy for tuning VFs. Using VF2.1.Cl[16]. and VF2.0.Cl[10] as reference structures, we designed and synthesized four indicators with a range of dihedral angles between the aniline donor and the molecular wire (**Scheme 4-1**). With this library of six aniline-tuned VFs, we investigated the response of fluorescence intensity and fluorescence lifetime (τ_{fl}) to V_{mem}. We find that modifying the aniline conformation can

generate VFs that are both more and less PeT quenched than VF2.1.Cl, tuning both sensitivity and τ_{fl} across an order of magnitude. We identify a tradeoff between sensitivity and τ_{fl}, in which dyes with intermediate sensitivity and τ_{fl} have superior performance as voltage indicators. We compared the performance of the three best V_{mem} sensors in the series in the detection of both cardiac and neuronal action potentials. In doing so, we find that all three report APs with good signal to noise, and τ_{fl} is the best predictor of probe performance in detection of physiologically relevant V_{mem} signals.

4.2 Synthesis VoltageFluors with conformationally restricted anilines

To test these hypotheses, we synthesized phenylene-vinylene molecular wires with julolidine, N-methylindoline, N,N,2,6-tetramethylaniline, and N-methyl-N-isopropyl aniline donors (**Scheme 4-1**). Starting with julolidine, $POCl_3$ is used to obtain benzaldehyde **1** in high yield (**Scheme 4-2**). This is converted to the aminostyrene by Wittig olefination and promptly reacted with 4-bromobenzaldhyde in a palladium catalyzed cross coupling to provide molecular wire **2**. This series should be performed on the same day to prevent oxidation of the electron-rich julolidine scaffold. Another Wittig olefination and cross coupling with a sulfonated dichlorofluorescein provides voltage indicator **17** (JuloVF, **Scheme 4-4**).

A Wittig olefination with commercially available N-methylindolinecarbaldehyde provides **3** (**Scheme 4-2**), which is isolated as a yellow oil and is stable for a short time. Pd-catalyzed cross coupling with 4-bromobenzaldede provides wire **5** as an orange solid. Conversion to the olefin gave **6** as a yellow solid in moderate yield. The fluorophore is attached by a similar Pd-catalyzed cross coupling to JuloVF, and yields the voltage indicator **18** (IndoVF, **Scheme 4-4**).

Reductive amination of acetone with N-methylaniline using $NaCNBH_3$ produces **6** (**Scheme 4-3**), albeit in low yield. In a similar sequence to the synthesis of JuloVF (**17**), treatment with $POCl_3$ provides aldehyde **7** which is then converted to **8** through a Wittig olefination. **8** is then attached to 4-bromobenzaldehyde by Pd-catalyzed cross coupling to provide wire **9**. Wittig olefination, followed by a final Pd-catalyzed cross-coupling with sulfonated dichlorofluorescein provides **10** and voltage indicator **19** (^{i}PrVF, **Scheme 4-4**), respectively.

Iodination of 2,6-dimethylaniline provides **11** as an oil (**Scheme 4-3**), which is converted to the N,N,2,6-tetramethylaniline **12** by reductive amination of formaldehyde using $NaBH_4$ in excellent yield. Nucleophilic attack of dimethylformamide produces benzaldehyde **13**. Wittig olefination (**14**), followed by a Pd-catalyzed cross coupling (**15**), and a second Wittig olefination produces wire **16** as a light yellow solid. This is attached to sulfonated dichlorofluorescein with a final Pd-catalyzed cross coupling to yield voltage indicator **20** (NN26VF, **Scheme 4-4**).

4.3 Spectroscopic characterization

We first evaluated this VF library with UV-Vis spectroscopy in ethanol with 0.1 M KOH (ethanol-KOH). Modification of aniline conformation altered the absorbance of the molecular wire region of these indicators, but not the absorbance of the xanthene chromophore region (**Figure 4-1a**, **Figure 4-2**). The wire region of JuloVF displays an absorbance maximum at 406 nm, a red-shift of 17 nm relative to the wire region of VF2.1.Cl (**Table 4-1**). In contrast, the wire region of NN26VF displayed an absorbance maximum at 368 nm, a blue-shift of 21 nm relative to the wire region of VF2.1.Cl (**Table 4-1**). For comparison, the wire region of VF2.0.Cl, which completely

lacks an aniline, displays an absorbance maximum at 360 nm (**Table 4-1**). The wire regions of IndoVF and ^{i}PrVF display absorbance maxima very close to VF2.1.Cl (**Table 4-1**). Taken together, these data suggest that JuloVF contains an aniline with more sp^2 character than VF2.1.Cl, NN26VF contains an aniline with less sp^2 character than VF2.1.Cl, and IndoVF and ^{i}PrVF contain anilines with very similar sp^2 character to VF2.1.Cl. Furthermore, protonation of the aniline results in a hypsochromatic shift in the wire absorbance maxima all to 360-365 nm (**Figure 4-3**). We reason that these shifts in the wire absorbance maxima result from differences in the electronic coupling of the aniline with the rest of the molecular wire.

Next, we measured the emission, quantum yield (Φ_{fl}), and fluorescence lifetime (τ_{fl}) of our VoltageFluor series. We hypothesized that VoltageFluors containing aniline groups with more sp^2 character would experience more PeT and display reduced Φ_{fl} and τ_{fl}, whereas VoltageFluors containing aniline groups with less sp^2 character would experience less PeT and display higher Φ_{fl} and τ_{fl}. We observed consistent shapes of the emission spectra from the shared dichlorofluorescein chromophore, but there were clear differences in the Φ_{fl} and τ_{fl} (**Figure 4-1b, Figure 4-4**). VF2.0.Cl has the highest measured quantum yield in Ethanol-KOH, followed by NN26VF, ^{i}PrVF, IndoVF, JuloVF, and VF2.1.Cl respectively (**Table 4-1**). Apart from VF2.1.Cl, this decreasing trend in quantum yield matches our hypothesis regarding the sp^2 character of the aniline group.

We speculated that some of the differences between observed and hypothesized VF properties may be the result of solvent effects. To better mimic the lipid environment of the plasma membrane, we investigated τ_{fl} in vesicles of 1-palmitoyl-2-oleoyl-glycero-3-phosphocholine 16:0-18:1 PC (POPC) (**Table 4-1**, **Figure 4-1c**). The τ_{fl} trend in POPC matches more closely with our expectations, with VF2.1.Cl displaying an intermediate τ_{fl} like that of ^{i}PrVF. The lifetime of all aniline-containing VFs was longer in POPC, likely attributable to the effects of solvent dielectric constant on electron transfer rate.[17] Curiously, only VF2.1.Cl deviates from the τ_{fl} trend observed in Ethanol-KOH, suggesting that the dimethyl aniline has some additional mode of solvent dependence that is inaccessible to the other molecules. Minimal, if any, concentration dependence was seen for τ_{fl} in both Ethanol-KOH and POPC, suggesting that concentration quenching is not responsible for these trends (**Figure 4-4**).

Changes to the degree of electronic coupling between the wire and the aniline lone pair should be visible via ^{13}C NMR, with more electron dense molecular wires appearing upfield. Previous work found that the carbon *para* to the nitrogen display the strongest and clearest trends.[18] We analyzed the ^{13}C NMR chemical shifts of the benzaldehyde precursors to simplify identification of individual carbons in the spectrum (**Figure 4-5**). We observed a trend generally consistent with the expected aniline conformation; some deviations may be the result of inductive effects of methyl substitution on the benzene ring.

4.4 Characterization of fluorescence intensity and sensitivity

Having performed initial characterization of the VoltageFluor series of aniline donors *in vitro,* we next examined performance as a voltage sensor in cells. To measure voltage sensitivity of these indicators, we turned to whole-cell voltage clamp in HEK293T cells incubated in dye solution. By recording the changes in fluorescence intensity with epifluorescence microscopy when voltage steps from 100 to -100 mV are applied (in 20 mV increments), we observed a dramatic difference in voltage sensitivity based on the identity of the aniline donor. As previously reported, VF2.1.Cl

has modest sensitivity to V_{mem} changes (23-26% per 100 mV, **Figure 4-6j, Figure 4-7, Table 4-1**) and VF2.0.Cl, lacking an aniline donor, possesses little to no sensitivity (-0.2% per 100 mV, **Figure 4-6l, Figure 4-7, Table 4-1**).

When methyl groups are added *ortho* to the aniline nitrogen (NN26VF, **20**), voltage sensitivity drops to 2.2% per 100 mV (**Figure 4-6k, Figure 4-7, Table 4-1)**, an order of magnitude lower than VF2.1.Cl. This is likely attributable to steric inhibition of resonance, which decreases PeT by uncoupling the aniline lone pair and the molecular wire. Interestingly, ^{i}PrVF had a larger response to V_{mem} changes (34% per 100 mV, **Figure 4-6i, Figure 4-7, Table 4-1**) than VF2.1.Cl. This suggests that the added bulk of the isopropyl group had not decreased coupling between the aniline lone pair and the molecular wire. It is possible that a steric effect between the aromatic ring and isopropyl substituent inhibits rotation of the Ar-N bond, maintaining planarity between then aniline and molecular wire.

The indicators with ring-fused anilines also have larger fluorescence responses to voltage changes as expected; IndoVF is the most sensitive at 37% per 100 mV change and JuloVF averages 34% (**Figure 4-6g-h, Figure 4-7, Table 4-1)**. We observed a high degree of variability in the sensitivity of JuloVF (**Table 4-1**), which might be attributed to its overall dim signal in cells. For both indicators, the aniline lone pair is "locked" in a conformation that is in plane with the molecular wire, which accounts for an increase in PeT and greater sensitivity to V_{mem}.

4.5 Measurements of lifetime with fluorescence lifetime microscopy (FLIM)

We used fluorescence lifetime to investigate how these relative sensitivities (%ΔF/F) translated into absolute sensitivity of τ_{fl} to V_{mem}. %ΔF/F depends on both the starting fluorescence intensity of the probe and the change in fluorescence with a 100 mV V_{mem} change. Therefore, very dim probes with small V_{mem}-dependent fluorescence changes can appear highly sensitive in %ΔF/F. Fluorescence lifetime, on the other hand, allows for a more direct measure of the change in fluorescence with V_{mem}, as in does not depend on the initial fluorescence intensity of the sensor. By measuring the baseline τ_{fl}, as well as the V_{mem} dependent τ_{fl} change, we can determine differences in PeT in cells without confounding effects from probe brightness or loading.

We initially assessed the dependence of τ_{fl} on loading of each VF in HEK293T cells, testing probe concentrations ranging from 100 nM to 1 µM (**Figure 4-8**). As seen previously with VF2.1.Cl and VF2.0.Cl,[19] we observed concentration quenching[20] at high dye loading for all VFs, with concentration-independent τ_{fl} at lower dye loading. For IndoVF, ^{i}PrVF, and NN26VF, we were able to select working concentrations that avoided concentration quenching but retained enough signal for fluorescence lifetime imaging (300 nM). Interestingly, with these three dyes, we were able to load more probe before we observed concentration quenching than we were with either VF2.0.Cl or VF2.1.Cl.[19] One explanation for this difference is that, at the same nominal concentration of these new VFs, loading into the membrane is less efficient. Therefore, 300 nM of iPrVF may reflect a similar number of VF molecules in the membrane as 100 nM VF2.1.Cl. Nevertheless, concentration of VF molecules in a cell membrane is challenging to measure directly, so we cannot rule out the possibility that the propensity for concentration quenching differs across our library of VFs. Because JuloVF is rather dim in cells, we were not able to decrease loading below 500 nM. As a result, fluorescence lifetime data for JuloVF may contain contributions from autofluorescence and concentration quenching.

Using these optimized loading concentrations, we measured the dependence of fluorescence lifetime on V_{mem} in HEK293T cells with simultaneous fluorescence lifetime imaging and whole cell patch clamp electrophysiology (**Figure 4-9** through **4-15**). Our lifetime-V_{mem} calibrations for VF2.1.Cl and VF2.0.Cl are in good agreement with previous work (**Table 4-1**).[19] For processing of these τ_{fl}-V_{mem} calibrations, we selected exponential models for new VFs based on minimization of reduced chi squared without overfitting (**Methods, Figure 4-16, 4-17**). Shorter lifetime VFs (e.g. JuloVF, IndoVF), could not be well described with fewer than 3 exponential decay components, but use of a 3-component decay model for the other probes resulted in overfitting.

All the new aniline modified VFs show V_{mem} sensitive fluorescence lifetimes, with sensitivities (slope of lifetime-V_{mem} line of best fit) ranging from 0.50 to 2.97 ps/mV and 0 mV lifetimes ranging from 0.31 to 3.32 ns (**Table 4-1**). Good agreement is observed between the $\%\Delta F/F$ and $\%\Delta\tau/\tau$ per 100 mV (**Figure 4-18**), which is consistent with a PeT-based V_{mem} sensing trigger and suggests that our selected fit models described the underlying data adequately. The 0 mV lifetimes (y-intercepts, in ns) observed are generally consistent with the expected degree of electronic coupling between the aniline lone pair and the molecular wire. JuloVF displays the shortest fluorescence lifetime at 0 mV (0.31 ± 0.01 ns). NN26VF displays the longest fluorescence lifetime (3.32 ± 0.01 ns), as expected with the steric inhibition of resonance between the aniline lone pair and the wire. IndoVF is most similar to JuloVF, with its slightly longer lifetime perhaps attributable to its increased flexibility. ^{i}PrVF exhibits a slightly shorter τ_{fl} than VF2.1.Cl, suggesting that it experiences increased PeT, either via increased substitution at the aniline or increasing planarity of the aniline resulting from steric inhibition of rotation.

Curiously, JuloVF, IndoVF, and ^{i}PrVF all display shorter τ_{fl} than VF2.1.Cl, implying that these molecular wires produce faster rates of PeT than the dimethyl aniline containing wire in VF2.1.Cl. JuloVF, IndoVF, and ^{i}PrVF are all more substituted at the aniline and bottom ring of the molecular wire than VF2.1.Cl. This methyl substitution could slightly increase electron density on the wire, but the magnitude of the lifetime change seems hard to attribute to an inductive effect. Another possible explanation is that the dimethyl aniline in VF2.1.Cl is rotated partially out of the plane of the wire in the membrane, but the fused rings or steric bulk of JuloVF, IndoVF, and ^{i}PrVF prevents them from accessing this conformation. The difference in VF2.1.Cl τ_{fl} in POPC vesicles and Ethanol-KOH adds further support to the idea of a solvent-dependent conformational change in the C-C-N-C dihedral angle, although additional studies are required to validate this.

4.6 Evaluation of indicator performance in excitable cells

We evaluated our three best aniline modified VFs for their ability to monitor spontaneous electrical activity in human induced pluripotent stem cell derived cardiomyocytes (hiPSC-CMs) and dissociated rat hippocampal neurons. We selected VF2.1.Cl, iPrVF, and IndoVF for these studies, as they displayed the best combination of sensitivity and brightness in HEK293T. All three indicators faithfully record action potential waveforms in spontaneously contracting monolayers of cardiomyocytes (**Figure 4-19a-f**) and evoked action potentials in dissociated rat hippocampal neurons (**Figure 4-19h-m**). The average signal-to-noise ratio (SNR) of activity recordings in cardiomyocyte monolayers is high in all cases, with ^{i}PrVF and VF2.1.Cl having the highest SNR values in excess of 400:1 when loaded at a concentration of 300 nM (**Figure 4-19g, Table 4-2**). IndoVF exhibits an average SNR that is similar to VF2.1.Cl loaded at lower concentrations but is

still capable of reporting cardiac action potential kinetics (**Figure 4-20i**). Differences in SNR seem to be loosely correlated to brightness in hiPSC-CMs but are more related to measured %ΔF/F (**Figure 4-20j**). VF2.1.Cl exhibits the highest average SNR of evoked activity recordings in dissociated rat hippocampal neurons at 13:1 when loaded at a concentration of 300 nM followed by ^{i}PrVF (9.7:1) and IndoVF (5.6:1) respectively (**Figure 4-19n, Table 4-2**). Interestingly, ^{i}PrVF displays the highest sensitivity to V_{mem} in dissociated rat hippocampal neurons but the second-highest average SNR due to its dimness relative to VF2.1.Cl (**Figure 4-21**). This further demonstrates the trade-off between brightness and sensitivity in VoltageFluors and the need for a better predictor of dye performance in physiologically relevant systems.

We also investigated the phototoxicity and photostability of these three derivatives, as we have previously observed difference in the phototoxicity of PeT-based voltage indicators with different wire structures.[15] We compared the phototoxicity of ^{i}PrVF and IndoVF to VF2.1.Cl during prolonged measurements of activity in iPSC-CM monolayers. With all three sensors, we were able to record action potentials (APs) without alterations to the AP waveform for up to 4 minutes (**Figure 4-22**). IndoVF appeared slightly less phototoxic than ^{i}PrVF or VF2.1.Cl, as AP kinetics remain unchanged for approximately 6 minutes of illumination in tissue. The initial photobleaching rates for all three indicators are similar in HEK293T cells, iPSC-CMs, and dissociated rat hippocampal neurons (**Figure 4-23**). Taken together, these data suggest that modifying the aniline conformation has minimal effect on probe photobleaching and phototoxicity, and IndoVF, ^{i}PrVF, and VF2.1.Cl are all capable of reporting on cardiac and neuronal electrophysiology with high SNR.

4.7 Discussion of VoltageFluor design and predictive measures

From the τ_{fl} electrophysiology data, we noticed a tradeoff between the absolute sensitivity and 0 mV τ_{fl} of the VFs (**Figure 4-24a**). Because all the VFs are based on the dichlorofluorescein chromophore and have the same extinction coefficient, 0 mV τ_{fl} should reflect the inherent brightness of the VFs. Dimmer VFs such as JuloVF and IndoVF have a high relative V_{mem} sensitivity (%ΔF/F or %Δτ/τ, **Figure 4-6**, **Figure 4-18**), but a lower absolute change in τ per mV. We observe the highest absolute sensitivity for VF2.1.Cl, which has an intermediate 0 mV lifetime. Very long lifetimes, such as those in NN26VF, are associated with both low %ΔF/F and low absolute sensitivity. Taken together, these data suggest that the performance of VFs hinges on a balance between fluorescence and PeT, and that the intermediate levels of both PeT and fluorescence produce the largest sensitivities.

We found that fluorescence intensity of the VFs in HEK293T cells did not correlate strongly with the fluorescence lifetime (**Figure 4-24b**), suggesting that VF loading into membranes plays a major role in dictating fluorescence intensity. The differences we observed in the onset of concentration quenching of τ_{fl} are consistent with this notion (**Figure 4-8**). Although the aniline modified VFs are structurally similar, changes in the basicity of the aniline could lead to protonation in buffer, forming a charged, quaternary nitrogen that could disfavor incorporation into the membrane. Taken together, the substantial differences between fluorescence intensity and fluorescence lifetime suggest that caution should be used in interpreting probe brightness in cells in terms of fundamental photophysics. As an alternative to fluorescence intensity, the τ_{fl} in POPC (**Figure 4-1**, **Table 4-1**) matches the trends observed in 0 mV lifetime in HEK293T cell

membranes qualitatively, suggesting that characterization in POPC vesicles is a reasonable strategy for predicting VF properties.

From this multidimensional characterization, we sought to identify a property that would predict performance (signal-to-noise ratio, SNR) in V_{mem} event detection. We observed strong correlation between the absolute sensitivity ($\Delta\tau$/mV) and the SNR of a 100 mV step in HEK293T (**Figure 4-24c**)**.** It stands to reason that the total change in the probe fluorescence lifetime reflects how much V_{mem}-sensitive PeT is modulating the fluorescence. To evaluate whether SNR in HEK293T translates to applications in excitable cell culture, we analyzed the relationship between the SNR for a V_{mem} step in HEK293T and the SNR for per action potential (AP) in cardiomyocytes and neurons (**Figure 4-24d**). We observed strong correlation between the SNR in HEK293T and neurons, with slightly weaker correlation between results in HEK293T and iPSC-CMs. Therefore, the absolute sensitivity of τ_{fl} to Vmem is a good predictor of probe SNR in diverse contexts.

4.8 Conclusions and outlook

In summary, we present the design and synthesis of a library of PeT-based voltage-sensitive dyes with conformationally modified electron donating moieties. We performed extensive characterization of VF properties in vitro, in a model cell culture system, and in excitable cells. The large range of brightness and sensitivity observed in our library suggests that synthetic modification of the aniline electron donor is an effective way to tune PeT-based V_{mem} sensing domains across a wide variety of electron donor strengths. We identify that τ_{fl} and the magnitude of V_{mem} induced changes in τ_{fl}, give a more accurate picture of VF photophysics than fluorescence intensity alone. We anticipate that similar τ_{fl} information would be useful for many novel probe libraries, not limited to those designed for V_{mem} sensing.

4.9 Materials and methods

4.9.1 General method for chemical synthesis and characterization

Chemical reagents and solvents (dry) were purchased from commercial suppliers and used without further purification. References to previously synthesized compounds are provided along with characterization data. Thin layer chromatography (TLC) (Silicycle, F254, 250 μm) and preparative thin layer chromatography (PTLC) (Silicycle, F254, 1000 μm) was performed on glass backed plates pre-coated with silica gel and were visualized by fluorescence quenching under UV light. Flash column chromatography was performed on Silicycle Silica Flash F60 (230–400 Mesh) using a forced flow of air at 0.5–1.0 bar. NMR spectra were measured on Bruker AVB-400 MHz, 100 MHz, AVQ-400 MHz, 100 MHz, Bruker AV-600 MHz, 150 MHz. NMR spectra measured on Bruker AVII-900 MHz, 225 MHz, equipped with a TCI cryoprobe accessory, were performed by Dr. Jeffrey Pelton (QB3). Chemical shifts are expressed in parts per million (ppm) and are referenced to CDCl3 (7.26 ppm, 77.0 ppm) or DMSO (2.50 ppm, 40 ppm). Coupling constants are reported as Hertz (Hz). Splitting patterns are indicated as follows: s, singlet; d, doublet; t, triplet; q, quartet; dd, doublet of doublet; m, multiplet. High-resolution mass spectra (HR-ESI-MS) were measured by the QB3/Chemistry mass spectrometry service at University of California, Berkeley. High performance liquid chromatography (HPLC) and low resolution ESI Mass Spectrometry were performed on an Agilent Infinity 1200 analytical instrument coupled to an Advion CMS-L ESI mass spectrometer. The column used for the analytical HPLC was Phenomenex Luna 5 μm

C18(2) (4.6 mm I.D. × 75 mm) with a flow rate of 1.0 mL/min. The mobile phases were MQ-H2O with 0.05% trifluoroacetic acid (eluent A) and HPLC grade acetonitrile with 0.05% trifluoroacetic acid (eluent B). Signals were monitored at 254, 350 and 480 nm over 10 min with a gradient of 10-100% eluent B unless otherwise noted. Ultra-high performance liquid chromatography (UHPLC) for purification of final compounds was performed using a Waters Acquity Autopurificaiton system equipped with a Phenomenex Luna 10 µm C18(2) column (21.2 mm I.D. x 250 mm) with a flow rate of 30.0 mL/min, made available by the Catalysis Facility of Lawrence Berkeley National Laboratory (Berkeley, CA). The mobile phases were MQ-H2O with 0.05% trifluoroacetic acid (eluent A) and HPLC grade acetonitrile with 0.05% trifluoroacetic acid (eluent B). Signals were monitored at 254 and 350 nm over 20 min with a gradient of 10-100% eluent B, unless otherwise noted.

4.9.2 Spectroscopic studies

Stock solutions of VoltageFluors were prepared in DMSO (500 µM-1 mM) by comparing the absorbance of the chloro-fluorescein peak of each VoltageFluor with the known extinction coefficient for this dye head.[16] These stock solutions were then diluted (1:1000) in the indicated solvent for each spectroscopic analysis. UV-Vis absorbance and fluorescence spectra were recorded using a Shimadzu 2501 Spectrophotometer (Shimadzu) and a Quantamaster Master 4 L-format scanning spectrofluorometer (Photon Technologies International). The fluorometer is equipped with an LPS-220B 75-W xenon lamp and power supply, A-1010B lamp housing with integrated igniter, switchable 814 photon-counting/analog photomultiplier detection unit, and MD5020 motor driver. Samples were measured in 1-cm path length quartz cuvettes (Starna Cells).

Relative quantum yields (Φ_{Fl}) were calculated by comparison to fluorescein (Φ_{Fl} = 0.93 in 0.1 M NaOH, Φ_{Fl} = 0.92 in Ethanol w/ 0.1 M KOH)[21,22] and rhodamine 6G (Φ_{Fl} = 0.95 in ethanol)[23] as references.[24] Stock solutions of standards were prepared in DMSO (0.25-1.25 mM) and diluted with appropriate solvent (1:1000 dilution). Absorption and emission (excitation = 485 nm) were taken at 5 concentrations. The absorption value at the excitation wavelength (485 nM) was plotted against the integration of the area of fluorescence curve (495-675 nm). For fluorescein, the integration of the area of the fluorescence curve was also taken with an excitation at 450 nm. The area from 460-675 nm and 495-675 nm was used to extrapolate the area of the fluorescence curve with an excitation at 485 nm. This ensured the full fluorescence area of fluorescein excited at 485 nm was used for Φ_{Fl} calculations. The slope of the linear best fit of the data was used to calculate the relative Φ_{Fl} by the equation $\Phi_{Fl(X)} = \Phi_{Fl(R)}(S_X/S_R)(\eta_X/\eta_R)^2$, where S_R and S_X are the slopes of the reference compound and unknown, respectively, and η is the refractive index of the solution. This method was validated by cross-referencing the reported Φ_{Fl} values of fluorescein and rhodamine 6G to the calculated Φ_{Fl} using the one standard as a reference for the other and vice versa. Calculated Φ_{Fl} within 10% of the reported value for both standards ensured that Φ_{Fl} calculated for fluorene VoltageFluors was reliable within 10% error.

4.9.3 Preparation of POPC Vesicles

1-palmitoyl-2-oleoyl-glycero-3-phosphocholine (16:0-18:1 PC, POPC) was purchased as $CHCl_3$ solution from Avanti Polar Lipids (Alabaster, AL). Stocks were aliquoted and stored at -80°C; all lipid solutions were handled in glassware cleaned with copious amounts of $CHCl_3$. For preparation of vesicles, 1-15 mg of POPC (at 4 mg/mL in $CHCl_3$) was dried down on a rotary

evaporator at 45°C and 35 RPM to produce a film. The film was dried under vacuum at room temperature overnight and then rehydrated for 30-60 minutes with slow rotation (10-15 RPM) at room temperature in 1x Dulbecco's Phosphate Buffered Saline (dPBS, Gibco, composition in mM: 138 NaCl, 8 NaH_2PO4, 2.7 KCl, 1.5 KH_2PO_4, pH approx. 7.1). Unilamellar vesicles were formed by extrusion through a 0.1 µm pore size polycarbonate membrane with the Mini Extruder Set at room temperature (Avanti) as per the manufacturer's protocol. Vesicles were kept at room temperature and used within a few hours of formation.

Vesicle formation was verified by dynamic light scattering (DLS) with a Zetasizer Nano ZS (Malvern Instruments). Vesicle diameters ranged from 125.9-160.3 nm between batches; all batches were monodisperse, with one primary size peak. For DLS measurements, vesicle suspensions were used directly or diluted 1:1 in dPBS before measurement. 100-200 µL of vesicle suspension was placed into a Zen 0040 cuvette. Refractive indices of 1.450 (material) and 1.332 (dispersant) were used in the Zetasizer software to obtain size distributions. Vesicle size distributions were measured in both naïve POPC vesicles and in POPC vesicles incubated with VoltageFluor; results were indistinguishable.

4.9.3 Cell culture

All animal procedures were approved by the UC Berkeley Animal Care and Use Committees and conformed to the NIH Guide for the Care and Use and Laboratory Animals and the Public Health Policy.

Human embryonic kidney (HEK) 293T cells

HEK293T cells were acquired from the UC Berkeley Cell Culture Facility and were verified by STR (short tandem repeat) profiling. Cells were routinely checked for mycoplasma contamination. HEK293T cells were maintained in Dulbecco's modified eagle medium (DMEM, Gibco) supplemented with 4.5 g/L D-glucose, 10% fetal bovine serum (FBS, Seradigm), and 2 mM GlutaMAX (Gibco). Cells were passaged every few days into fresh media following dissociation with 0.05% Trypsin-EDTA (Gibco). All cells were discarded after 30 passages. For imaging experiments, 25 mm glass coverslips (Electron Microscopy Sciences) were prepared by acid washing (1 M HCl, approx. 5 hours), followed by three overnight washes in ethanol and three overnight washes in water. Coverslips were sterilized by heating at 150°C for 2-4 hours. To facilitate cell attachment, sterilized coverslips were coated with Poly-D-Lysine (PDL; 1 mg/mL; Sigma-Aldrich) for 1-24 hours at 37°C, followed by two washes with water and two washes with phosphate-buffered saline. For general imaging, cells were seeded onto prepared coverslips in complete DMEM at a 42,000 cells/cm^2 and used approximately 24 hours after plating. For electrophysiology, cells were seeded at a density of 21,000 cells/cm^2 in low glucose DMEM (1 g/L glucose, 10% FBS, 1 mM pyruvate, 2 mM GlutaMAX) and used approximately 16 hours after plating.

Rat hippocampal neurons.

Hippocampi were dissected from embryonic day 18 Sprague Dawley rats (Charles River Laboratory) in cold sterile HBSS (zero Ca^{2+}, zero Mg^{2+}). All dissection products were supplied by Invitrogen, unless otherwise stated. Hippocampal tissue was treated with trypsin (2.5%) for 15 min at 37 °C. The tissue was triturated using fire polished Pasteur pipettes, in minimum essential media

(MEM) supplemented with 5% fetal bovine serum (FBS; Thermo Scientific), 2% B-27, 2% 1M D-glucose (Fisher Scientific) and 1% glutamax. The dissociated cells were plated onto 12 mm diameter coverslips (Electron Microscopy Sciences, prepared as above) at a density of 27,000 cells per coverslip in MEM supplemented media. Neurons were maintained at 37 °C in a humidified incubator with 5 % CO_2. At 1 day in vitro (DIV) half of the MEM supplemented media was removed and replaced with Neurobasal media containing 2% B-27 supplement and 1% glutamax. Functional imaging was performed on 14-17 DIV neurons.

Differentiation of hiPSC into cardiomyocytes and culture.

hiPSCs (WTC11)[25] were cultured on Matrigel (1:100 dilution; Corning)-coated 12 well-plates in StemFlex medium (Gibco). When the cell confluency reached 80–90%, which is referred as day 0, the medium was switched to RPMI 1640 medium (Life Technologies) containing B27 minus insulin supplement (Life Technologies) and 10 μM CHIR99021 GSK3 inhibitor (Peprotech). At day 1, the medium was changed to RPMI 1640 medium containing B27 minus insulin supplement only. At day 3, medium was replaced to RPMI 1640 medium containing B27 supplement without insulin, and 5 μM IWP4 (Peprotech) for 2 days without medium change. On day 5, medium was replaced to RPMI 1640 medium containing B27 minus insulin supplement for 2 days without medium change. On day 7, medium was replaced with RPMI 1640 containing B27 with insulin supplement. After day 7, the medium was changed every two days. Confluent contracting sheets of beating cells appear between days 7 to 15.[26]

Beating sheets were treated with collagenase II for 60-75 minutes. The collagenase solution was carefully transferred to cold DMEM, making sure cardiac sheets were not disturbed. Trypsin (0.25%) was added to dissociated sheets for 4-8 minutes and plated onto 6 well-plates coated with Matrigel (1:100 dilution) in RPMI 1640 medium containing B27 supplement plus ROCK inhibitor Y-27632. 24 hours later, the medium was replaced with fresh RMPI/B27 without ROCK inhibitor. Cardiomyocytes were maintained for 7 days, replacing media every other day, and then were switched to RPMI 1640 medium (-glucose) supplemented with 4 mM sodium lactate (Sigma Aldrich). Cells were maintained in this media for 7 days, replacing every other day, then switched back to RPMI/B27 containing glucose.[27] These purified cardiomyocytes were then used for imaging.

Lactate purified sheets were dissociated with 0.25% trypsin-EDTA (4-8 minutes, depending on density and quality of tissue) and plated onto Matrigel (1:100)-coated Ibidi ® 24 well μ-plates (cat no. 82406**)** in RPMI 1640 medium containing B27 supplement (containing insulin). Medium was changed every 3 days until imaging. For loading hiPSC cardiomyocytes, voltage dyes were diluted 1 in 1000 in RPMI 1640 with B27 supplement minus Phenol Red to the desired final concentration. Cardiomyocytes were incubated in this solution for 20 minutes at 37 °C, then exchanged with dye-free RPMI 1640 with B27 supplement minus Phenol Red.

4.9.4 VoltageFluor stocks and cellular loading

VoltageFluors were stored as 0.5-1 mM DMSO stocks at -20°C or as a solid at room temperature. For cellular loading in HEK293T, DMSO stocks were diluted to the indicated concentration in imaging buffer (IB; composition in mM: 139.5 NaCl, 10 HEPES, 5.6 D-glucose, 5.3 KCl, 1.3 $CaCl_2$, 0.49 $MgCl_2$, 0.44 KH_2PO_4, 0.41 $MgSO_4$, 0.34 Na_2HPO_4; 290 mOsm/kg, pH

7.25). HEK293T cells were incubated in the VF-IB solution for 20-25 minutes in a humidified incubator at 37°C. Cells were washed once in IB and transferred to fresh IB for imaging. Hippocampal neurons were loaded with VoltageFluor at the indicated concentration in HBSS and incubated in the VF-HBSS solution for 20 minutes in a humidified incubator at 37°C. For imaging evoked activity, the hippocampal neurons were then transferred to a HBSS solution containing the synaptic blockers 10 μM 2,3-Dioxo-6-nitro-1,2,3,4-tetrahydrobenzo[f]quinoxaline-7-sulfonamide (NBQX; Santa Cruz Biotechnology) and 25 μM DL-2-Amino-5-phosphonopentanoic acid (APV; Sigma-Aldrich) to prevent recurrent activity. Cardiomyocytes were loaded with VoltageFluor in RPMI-B27 with no phenol red (instead of IB). The loading solution was exchanged for fresh RPMI-B27 without phenol red (and without VF) before imaging. All imaging was conducted under ambient atmosphere; no imaging samples were used for longer than an hour.

For assessment of the concentration dependence of fluorescence lifetime, the indicated concentration of VoltageFluor was used (**Fig. S6**). From these data, an optimal working concentration that minimized concentration quenching but retained adequate signal was selected. This concentration was used for all other experiments in HEK293T unless indicated. Optimal concentrations for VF2.1.Cl and VF2.0.Cl were previously determined;[19] where indicated, we also include some data at 300 nM (3x higher concentration) for comparison. Working concentration values are tabulated below (**Table 4-3**):

4.9.5 Fluorescence intensity imaging parameters

For all experiments, excitation light for epifluorescence intensity image was generated by Spectra-X Light engine LED (Lumencor) using the cyan LED (475/34 nm bandpass filter). Light was collected with an emission filter (bandpass 540/50 nm) after passing through a dichroic mirror (510 nm LP). Images were captured with an OrcaFlash4.0 sCMOS camera (Hamamatsu). More detailed imaging information for each fluorescence intensity application is expanded below.

Membrane staining and photostability in HEK293T cells

HEK293T cells were imaged on an inverted Zeiss AxioObserver Z-1. Fluorescence was collected with a 40x oil immersion objective (EC-Plan-NEOFLUAR 40/1.3; Zeiss). For membrane staining, images (2048x2048 px^2, pixel size 0.16 x 0.16 μm^2). For voltage sensitivity experiments, images (100x100 px^2, pixel size 0.64 x 0.64 μm^2) were collected continuously with constant LED illumination (9.53 mW/mm^2) and a sampling rate of 0.5 kHz. For photostability experiments, images (2048 x 2048 px^2, pixel size 0.16 x 0.16 μm^2) were taken every 1 second for 5 minutes with constant illumination of LED (30.4 mW/mm^2; 100 ms exposure time).

Evoked activity in rat hippocampal neurons

Evoked activity imaging was performed on an upright AxioExaminer Z-1 (Zeiss), equipped with a Spectra-X light engine LED light (Lumencor), and controlled with μManager (V1.4, open-source, Open Imaging).[28] Images were acquired using a W-Plan-Apo/1.0 NA 20x water immersion objective (Zeiss). Images (2048x400 px^2, pixel size: 0.325 x 0.325 μm) were collected continuously on an OrcaFlash4.0 sCMOS camera (sCMOS; Hamamatsu) at a sampling rate of 0.5 kHz with 4x4 binning and cyan excitation light power of 13.22 mW/mm^2. Extracellular field stimulation was delivered by a Grass Stimulator connected to a recording chamber containing two

platinum electrodes (Warner), with triggering provided through a Digidata 1440A digitizer and pCLAMP 10 software (Molecular Devices). Action potentials were triggered by 1 ms 80 V field potentials delivered at 5 Hz.

Spontaneous activity in human induced pluripotent stem cell derived cardiomyocytes (iCMs)

Functional recordings of VoltageFluors were performed on an inverted AxioObserver Z-1 (Zeiss), equipped with a Spectra-X Light engine LED light (Lumencor), controlled with µManager (V1.4, open-source, Open Imaging).[28] Images were acquired using a Plan-Apochromat 20/0.8 air objective (20x, Zeiss). Images were focused onto an OrcaFlash4.0 sCMOS camera (sCMOS; Hamamatsu). Images (512 x 125 px^2, pixel size 0.64 x 0.64 µm) were taken continuously at 0.2 kHz for ten seconds with constant LED illumination (11.1 mW/mm^2).

Phototoxicity of VoltageFluor dyes was assessed in cardiomyocyte monolayers exposed to constant illumination from the excitation LED (9.53 mW/mm^2) for up to ten minutes (or until automaticity was lost), while typical ten second fluorescence recordings were made at the beginning of each minute.

4.9.6 Fluorescence intensity image analysis

Voltage sensitivity in HEK293T cells (%ΔF/F)

Analysis of voltage sensitivity in HEK293T cells was performed using ImageJ (FIJI). Briefly, a region of interest (ROI) encompassing the cell body was selected and average fluorescence intensity was calculated for each frame. For background subtraction, a ROI encompassing a region without cells was selected and the average pixel intensity was calculated for each frame. A linear fit to the background trace was calculated and applied to the background, and this was used to subtract background signal from the fluorescence intensity trace. F/F_o values were calculated by dividing the background subtracted trace by the median value of fluorescence when the cell is held at -60 mV. ΔF/F values were calculated by plotting the change in fluorescence (ΔF) vs the applied voltage step and finding the slope of a linear best-fit.

Spontaneous activity in iCMs

Analysis of action potential (AP) data from hiPSC cardiomyocytes was performed using in-house MATLAB scripts based on previously developed software by the Efimov lab (Washington University, St. Louis, MO).[15,29] Scripts are available upon request. Briefly, raw OME-tiffs recorded in µManager was read directly into MATLAB for batch-processing of large datasets (>30 Gb per experiment). The mean pixel intensity of the entire image was calculated for each frame and a mean fluorescence trace was extracted for the entire stack. Photobleach correction was performed by subtracting an asymmetric least-squares fit of the data from the mean trace.[30] This spline was used to estimate and compare the rate of photobleaching of VoltageFluors in cardiomyocytes (**Figure S19b**). No subtraction of background was possible due to staining of the entire monolayer. Individual AP events were identified through threshold detection based on a Schmidtt trigger. Action potential duration (APD) values were calculated for each AP by finding the activation time (time of the maximum derivative of the AP upstroke) and the time the signal returns to 70 and 10% of the maximum depolarization (APD30 and APD90, respectively). APD values were corrected for variation due to spontaneous beat rate by Fridericia's formula (Eq. 4-1).

CL is the cycle length, calculated as the time period from the beginning of one beat to the beginning of the succeeding beat.[31]

$$\text{cAPD} = \frac{APD}{\sqrt[3]{CL}} \quad [4\text{-}1]$$

Evoked activity in rat hippocampal neurons

For analysis of evoked voltage responses in neurons, regions of interest encompassing cell bodies were drawn in ImageJ and the mean fluorescence intensities for each frame were extracted. ΔF/F values were calculated in the following manner. First, a mean background value was subtracted from all raw fluorescence frames, bypassing the noise amplification which arises from subtracting background for each frame, to give a background subtracted trace. A least squares regression was then fit to the background subtracted trace. A bleaching curve, derived from the slope of the regression, was then subtracted from the background subtracted trace to correct for photobleaching and yield a bleach-corrected trace. The median of the bleach-corrected trace was subtracted from each timepoint of the bleach-corrected trace to yield a ΔF trace. The ΔF trace was then divided by the median of the bleach-corrected trace to give a ΔF/F trace. No averaging has been applied to any voltage traces. Signal-to-noise ratios were calculated by dividing the ΔF/F value for the frame containing the first spike of evoked activity by the standard deviation of the previous 10 frames in the ΔF/F trace.

Photobleaching studies

For photostability experiments HEK293T cells were loaded the same as above. Images (pixel size 0.16 μm × 0.16 μm) were taken every 1 second for 5 minutes with constant illumination of LED (30.4 mW/mm^2; 50 ms exposure). The obtained fluorescence curves were normalized with the fluorescence intensity at t = 0 and averaged (three different cell rafts for each dye).

Phototoxicity of VoltageFluor dyes was assessed in cardiomyocyte monolayers incubated with 0.3 μM of indicator (and 0.1 μM for VF2.1.Cl). These were exposed to constant illumination from the excitation LED (475/34; bandpass) for up to 10 minutes, while typical ten second fluorescence recordings were made at the beginning of each minute. Initial photobleach was compared using splines calculated from asymmetric least squares fit of the baseline (**Figure 4-23**).

Bleach rate of VoltageFluors in neurons was assessed according to the analysis above. These were compared in **Figure 4-23**.

4.9.7 Fluorescence lifetime data acquisition

Microscopy configuration

Fluorescence lifetime data were obtained as described previously.[19] Briefly, fluorescence lifetime data were acquired on an inverted LSM 510 (Zeiss) scanning confocal microscope equipped with a Becker and Hickl SPC-150N photon counting card. Pulsed excitation light was

supplied by a MaiTai HP Ti:Sapphire laser (SpectraPhysics) tuned to 958 nm and frequency doubled to 479 nm. Average power at the sample ranged from 5-25 μW. Photons were collected with a 40x oil immersion objective (1.3 NA Plan-Neofluar, Zeiss) and detected with an HPM-100-40 hybrid detector (Becker and Hickl) after passing through a 488 nm long pass dichroic (Zeiss) and a 550/49 nm bandpass emission filter (Semrock, Rochester, NY). Fluorescence lifetime data were acquired using SPCM software (Becker and Hickl). To maximize photon signal but retain some optical sectioning, the confocal pinhole was set to 2.5-3.5 AU (~2.5 μm optical section). Proper functioning of the fluorescence lifetime imaging system was routinely measured with the standards erythrosin B and fluorescein in 0.1 N NaOH. The instrument response function (IRF) was recorded at least hourly during data acquisition from a solution of quenched fluorescein (500 μM fluorescein, 12 M NaI, 0.1 N NaOH).[32]

Data acquisition – solution phase measurements

POPC vesicles in 1x dPBS were incubated with VoltageFluor at the indicated concentration at room temperature for 20-30 minutes. The final concentration of DMSO was kept at or below 0.2%. After incubation, vesicle suspensions with dye were transferred to a clean 25 mm coverslip in an Attofluor imaging chamber (Thermo Fisher Scientific). Fluorescence lifetime images were acquired for 60 seconds and generally contained $>10^6$ photons per recording. Data from the image were combined into a global decay with 256 time channels in the fluorescence decay before analysis (see below).

4.9.7c. Data acquisition – cellular measurements

HEK293T loaded with VF were transferred to an Attofluor imaging chamber containing imaging buffer. Fluorescence lifetime images were recorded with 256x256 px^2 of spatial resolution (112 x 112 μm^2 image size; see below for binning during lifetime fitting) and 256 time channels. Images for evaluating concentration dependence were acquired for 75-90 seconds; results are the sum of approximately 12 scans across the field of view. For tandem electrophysiology and fluorescence lifetime imaging, data were recorded with 64x64 px^2 of spatial resolution (56.3 x 56.3 μm^2 image size) and 256 time channels. Images with concurrent electrophysiology were acquired for 30 seconds, summing multiple frames recorded from the same field of view.

4.9.8 Fluorescence lifetime data analysis

Time-resolved fluorescence decays I(t) of VoltageFluors were fit to a single exponential decay or to a sum of two or three exponential decays (eqn. 2, n=1, 2, or 3). Fits were optimized in custom MATLAB code (MathWorks, Natick, MA) using the weighted least squares method to minimize the reduced chi squared χ^2 (eqn. 4-3). The interior-point algorithm from the built-in MATLAB optimization routine fmincon was used for optimization. Code is available upon request.

$$I(t) = \sum_{i=1}^{n} a_i e^{-t/\tau_i} \qquad [4\text{-}2]$$

To calculate χ^2, the difference between the observed value y_m and the calculated value z_m for each time channel m was determined, with Poisson weighting based on the square root of the calculated number of counts in each channel. χ^2 was adjusted for the total number of time channels *N* included in the fit, as well as the number of parameters *p* in the model (coefficients a_i and decay constants τ_i).

$$\chi^2 = \sum_{m=1}^{N} \frac{(y_m - z_m)^2}{z_m(N-p)} \quad [4\text{-}3]$$

Where only one fluorescence decay term was used, the reported τ_{fl} is simply the decay constant τ. Where more than one exponential decay term was used, τ_{fl} data are presented as the amplitude weighted average of the two (eqn. 4-4) or three (eqn. 4-5) coefficients a_i and decay constants τ_i.

$$\tau_{fl} = \frac{a_1\tau_1 + a_2\tau_2}{a_1 + a_2} \quad [4\text{-}4]$$

$$\tau_{fl} = \frac{a_1\tau_1 + a_2\tau_2 + a_3\tau_3}{a_1 + a_2 + a_3} \quad [4\text{-}5]$$

The number of fluorescence decay terms was chosen to balance the reduction in χ^2 against the need to minimize fit noise (**Fig. 4-16, 4-17**). The number of terms selected for each probe is indicated below (**Table 4-4**).

4.9.9 Electrophysiology

For electrophysiological experiments in HEK293T, pipettes were pulled from borosilicate glass with filament (Sutter Instruments, BF150-86-10) with a P-97 pipette puller (Sutter Instruments) to a resistance of 4-7 MΩ. Pipettes were filled with an internal solution (composition, in mM): 125 potassium gluconate, 10 HEPES, 10 KCl, 5 NaCl, 2 ATP disodium salt, 1 EGTA, 0.3 GTP sodium salt (pH 7.25, 285 mOsm). Pipettes were positioned with an MP-225 micromanipulator (Sutter Instruments). Electrophysiological recordings were obtained with an Axopatch 200B amplifier (Molecular Devices) at room temperature. The signals were digitized with a Digidata 1550B sampled at 50 kHz, filtered at 5 kHz and recorded with pCLAMP 10 software (Molecular Devices).

Electrophysiology was performed in the whole cell voltage clamp configuration. After gigaseal formation and break-in, recordings were only pursued if series resistance in voltage clamp was less than 30 MΩ and the recording maintained a 30:1 ratio of membrane resistance to access

resistance throughout all voltage steps. No series resistance compensation was applied. Fast capacitance was compensated in the cell attached configuration. All voltage clamp protocols were corrected for the calculated liquid junction (-14 mV, Liquid Junction Potential Calculator in pClamp).[33] For tandem electrophysiology and fluorescence intensity recordings, cells were held at -60 mV and de- and hyper- polarizing steps were applied from +100 to -100 mV in 20 mV increments, with each step lasting 100 ms. For tandem electrophysiology and fluorescence lifetime recordings, the potentials -80, -40, 0, and +40 mV were randomly applied in four sequential 30 second recordings, followed by a 30 second recording at +80 mV. Cells were only included if the aforementioned patch quality criteria were retained throughout the first 4 steps; the 5th step to +80 mV was included if it also met the quality criteria (true for ~3/4 of cells).

4.9.10 Synthesis

Preparation of molecular wires

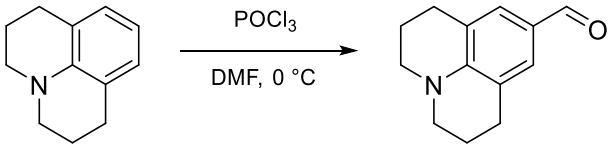

1, 88%

Synthesis of 2,3,6,7-tetrahydro-1H,5H-pyrido[3,2,1-ij]quinoline-9-carbaldehyde, 1

$POCl_3$ (1.2 mL, 12.7 mmol) was slowly added to ice-cold anhydrous DMF (20 mL) and set to stir for 30 minutes at room temperature. This solution was added to 2,3,6,7-tetrahydro-1H,5H-pyrido[3,2,1-ij]quinoline (2.0 g, 11.5 mmol) and stirred at 90° C under N_2 for 16 hours. The reaction mixture was cooled to room temperature, added to ice cold water, neutralized with saturated $NaHCO_3$ and extracted with EtOAc (3x). The organic layers were collected, dried with Na_2SO_4, and concentrated to dryness *in vacuo*. The residue was taken up in 1:1 EtOAc:hexanes and run through a silica plug to afford **1** as an orange powder (2.0 g, 88**%** yield).

^{1}H NMR (400 MHz, Chloroform-d) δ 9.58 (s, 1H), 7.28 (s, 2H), 3.28 (t, J = 5.9 Hz, 4H), 2.75 (t, J = 6.3 Hz, 4H), 1.95 (p, J = 6.1 Hz, 4H).

^{13}C NMR (101 MHz, Chloroform-d) δ 190.22, 147.98, 129.60, 124.05, 120.39, 50.11, 27.74, 21.33.

HRMS (ESI+) Calculated for $C_{13}H_{16}ON$ $[M+H]^+$ 202.1226; Found 202.1225.

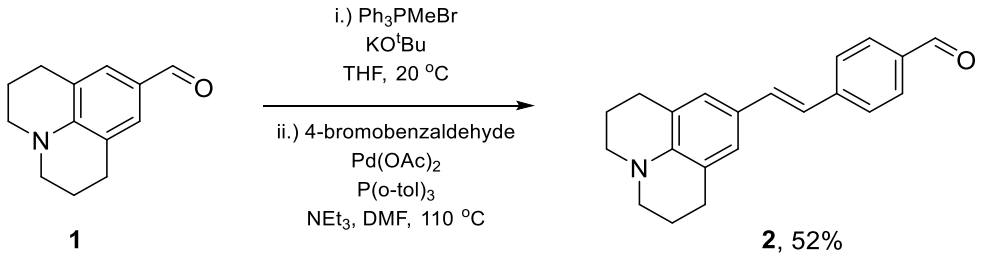

1 **2**, 52%

Synthesis of (E)-4-(2-(2,3,6,7-tetrahydro-1H,5H-pyrido[3,2,1-ij]quinolin-9-yl)vinyl)benzaldehyde, 2

PPh_3MeBr (2.44 g, 6.82 mmol) and KO^tBu (920 mg, 8.19 mmol) were combined with anhydrous THF (38 mL) and set to stir at room temperature for one hour. Compound **1** (1.1 g, 5.46 mmol) was then dissolved in anhydrous THF (10 mL), added to the reaction mixture, and set to stir at room temperature for four hours. The reaction was then added to water and extracted with EtOAc (3X). The organic layers were collected, washed twice with brine, dried with Na_2SO_4, and concentrated to dryness *in vacuo* to give an orange solid. This crude material was combined with 4-bromobenzaldehyde (957 mg, 5.46 mmol), $Pd(OAc)_2$ (61 mg, 0.27 mmol), and $P(o\text{-}tol)_3$ (167 mg, 0.55 mmol) in a flame-dried Schlenk flask. The flask was evacuated/backfilled with N_2 (3X). Anhydrous DMF (11 mL) and anhydrous triethylamine (11 mL) were added, the flask was sealed, and the solution was stirred at 110° C for 40 hours. The reaction was then cooled to room temperature, diluted with EtOAc, and filtered. The filtrate was concentrated to dryness *in vacuo*. The residue was purified by flash chromatography (10% EtOAc in hexanes), affording **2** as an orange powder (1.7 g, 52% yield).

^1H NMR (400 MHz, Chloroform-d) δ 9.94 (s, 1H), 7.81 (d, J = 8.4 Hz, 2H), 7.56 (d, J = 8.2 Hz, 2H), 7.12 (d, J = 16.2 Hz, 1H), 7.01 (s, 2H), 6.86 (d, J = 16.2 Hz, 1H), 3.20 (t, J = 5.6 Hz, 4H), 2.78 (t, J = 6.4 Hz, 4H), 1.98 (p, J = 6.3 Hz, 4H).

^{13}C NMR (101 MHz, Chloroform-d) δ 191.73, 144.96, 143.56, 134.30, 133.00, 130.38, 126.16, 126.13, 123.80, 121.76, 121.39, 50.05, 27.85, 21.95.

HRMS (ESI+) Calculated for $C_{21}H_{22}O_1N_1$ $[M+H]^+$ 304.1696; Found 304.1693.

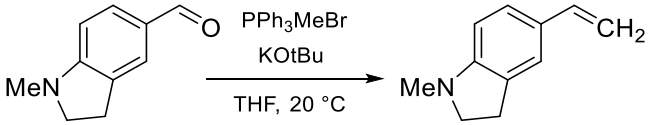

3, 59%

Synthesis of 1-methyl-5-vinylindoline, 3

KO^tBu (3.3 g, 9.1 mmol) and Ph_3PMeBr (3.3 g, 9.1 mmol) were combined in anhydrous THF (10 mL) stirred at 20 °C for 30 minutes. N-methylindoline carbaldehyde (0.82 g, 5.1 mmol) was added and stirred for 12 hours. This was then suspended in hexanes and filtered over celite. Filtrate was concentrated onto celite, then was purified by flash column chromatography with basic alumina as a support (1-5% ethyl acetate in hexanes). 3 was isolated as a yellow oil (0.48 g, 59%).

^1H NMR (400 MHz, Chloroform-d) δ 7.22 (q, J = 1.3 Hz, 1H), 7.14 – 7.10 (m, 1H), 6.63 (dd, J = 17.5, 10.9 Hz, 1H), 6.42 (d, J = 8.0 Hz, 1H), 5.52 (dd, J = 17.5, 1.0 Hz, 1H), 5.00 (dd, J = 10.9, 1.1 Hz, 1H), 3.33 (t, J = 8.2 Hz, 2H), 2.95 (t, J = 8.1 Hz, 2H), 2.77 (s, 3H).

^{13}C NMR (101 MHz, $CDCl_3$) δ 153.33, 137.05, 130.73, 127.82, 126.57, 121.66, 109.10, 106.64, 56.12, 36.07, 28.54.

HRMS (ESI+) m/z: $[M+H]^+$ calculated for $C_{11}H_{14}N$: 160.1121; found 160.1121

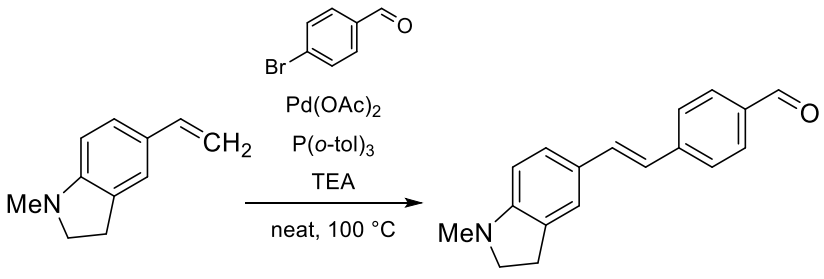

3 **4**, 34%

Synthesis of (E)-4-(2-(1-methylindolin-5-yl)vinyl)benzaldehyde, 4

$Pd(OAc)_2$ (19 mg, 0.084 mmol) and P(*o*-tol)$_3$ (51 mg, 0.17 mmol) and 4-bromo-benzaldehyde (0.31 g, 1.7 mmol) were added into flame dried Schlenk flask. This was evacuated and backfilled with N_2 (3x). Anhydrous triethylamine (3 mL) and **3** (0.4 g, 2.5 mmol) were then added and stirred at 95°C. After 18 hours, the reaction was cooled and diluted in dichloromethane, washed with sat. ammonium chloride (1X) and brine (1X). This was dried with $MgSO_4$, and concentrated. This was triturated with hexanes and filtered, affording **4** as an orange solid (153 mg, 34%).

^{1}H NMR (600 MHz, Chloroform-*d*) δ 9.95 (s, 1H), 7.82 (dd, 2H), 7.58 (d, *J* = 8.2 Hz, 2H), 7.34 (d, *J* = 1.8 Hz, 1H), 7.24 (dd, *J* = 8.0, 1.8 Hz, 1H), 7.19 (d, *J* = 16.2 Hz, 1H), 6.91 (d, *J* = 16.1 Hz, 1H), 6.43 (d, *J* = 8.1 Hz, 1H), 3.39 (t, *J* = 8.2 Hz, 2H), 2.99 (t, *J* = 8.2 Hz, 2H), 2.81 (s, 3H).

^{13}C NMR (151 MHz, $CDCl_3$) δ 191.59, 153.96, 144.64, 134.46, 132.99, 130.97, 130.27, 128.13, 126.33, 126.21, 122.39, 122.26, 106.44, 55.74, 35.50, 28.35

HRMS (ESI+) calculated for $C_{18}H_{18}NO$ $[M+H)^+$ m/z: 264.1383; found: 264.1383

.

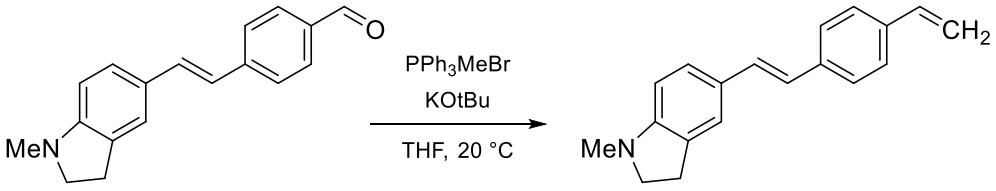

4 **5**, 38%

Synthesis of (E)-1-methyl-5-(4-vinylstyryl)indoline, 5

Potassium tert-butoxide (0.28 g, 2.5 mmol) and Ph_3PMeBr (0.32 g, 0.89 mmol) was stirred in anhydrous THF (3 mL) at 20 °C for 30 minutes. **4** (0.13 g, 0.49 mmol) was then added and stirred

for 12 hours. The reaction was then concentrated to dryness, resuspended in dichloromethane, and filtered over basic alumina. Filtrate was concentrated onto silica and purified by flash chromatography (10% ethyl acetate in hexanes) affording **5** a yellow solid (49 mg, 38%)

^{1}H NMR (600 MHz, Chloroform-*d*) δ 7.44 (d, *J* = 8.3 Hz, 2H), 7.39 (d, *J* = 8.3 Hz, 2H), 7.33 (s, 1H), 7.23 (dd, *J* = 8.0, 1.8 Hz, 1H), 7.06 (d, *J* = 16.2 Hz, 1H), 6.90 (d, *J* = 16.2 Hz, 1H), 6.72 (dd, *J* = 17.6, 10.9 Hz, 1H), 6.45 (d, *J* = 8.0 Hz, 1H), 5.78 – 5.72 (m, 1H), 5.25 – 5.21 (m, 1H), 3.37 (t, *J* = 8.1 Hz, 2H), 2.99 (t, *J* = 8.2 Hz, 2H), 2.80 (s, 3H).

^{13}C NMR (151 MHz, $CDCl_3$) δ 153.29, 137.89, 136.64, 135.96, 130.91, 129.29, 127.36, 127.21, 126.51, 126.13, 123.74, 121.96, 113.09, 106.73, 55.98, 35.88, 28.51.

HRMS (ESI+) m/z $[M+H]^+$ calculated for $C_{19}H_{20}N$: 262.1590; found 262.1591

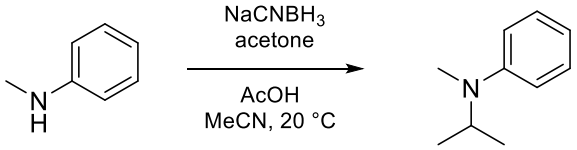

6, 18%

Synthesis of N-isopropyl-N-methylaniline, 6

N-methylaniline (1.0 g, 9.3 mmol) was stirred in ACN (10 mL). Reagent grade acetone (5.4 g, 93 mmol) was added and stirred for 4 hours at 0°C. $NaCNBH_3$ (2.3 g, 37 mmol) was then added in four portions and the pH and glacial acetic acid (1.5 mL) was added. After two hours of stirring at 0°C, more glacial acetic acid (1 mL) was added, and the reaction was stirred for 12 hours and allowed to warm to 20 °C. The reaction was poured into ice and diluted with saturated $NaHCO_3$. This was then extracted in ethyl acetate, washed with brine, dried with $MgSO_4$, and concentrated onto celite. This was purified by flash chromatography on basic alumina (5% EtOAc in hexanes), affording 6 as a yellow oil (0.24 g, 18%).

^{1}H NMR (400 MHz, Chloroform-*d*) δ 7.23 (dd, *J* = 8.9, 7.2 Hz, 2H), 6.83 – 6.76 (m, 2H), 6.69 (tt, *J* = 7.1, 1.1 Hz, 1H), 4.10 (hept, *J* = 6.6 Hz, 1H), 2.73 (s, 3H), 1.16 (d, *J* = 6.6 Hz, 6H).

^{13}C NMR (101 MHz, $CDCl_3$) δ 150.28, 129.15, 116.45, 113.39, 48.96, 29.81, 19.35

HRMS (ESI+) m/z $[M+H]^+$ calculated for $C_{10}H_{16}N$: 150.1277; found 150.1277

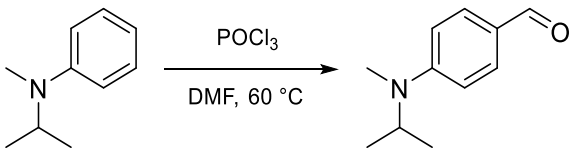

6 **7,** 83%

Synthesis of 4-(isopropyl(methyl)amino)benzaldehyde, 7

N,N-Dimethylformamide (2 mL) was stirred at 0°C and phosphorus oxychloride (0.4 mL) was added dropwise, then stirred for 15 minutes. **6** (0.24 g, 1.6 mmol) was then added into solution and stirred 15 hours at 60 °C. The reaction was then poured into ice. This was extracted with ethyl acetate, washed with 1M KOH and brine, and dried with $MgSO_4$. Concentrated *in vaccuo* to yield compound **7** as a yellow oil (0.24 g, 83%).

^{1}H NMR (400 MHz, Chloroform-*d*) δ 9.72 (s, 1H), 7.72 (dd, *J* = 8.9 Hz, 2H), 6.76 (dd, 2H), 4.23 (hept, *J* = 6.6 Hz, 1H), 2.85 (s, 3H), 1.22 (d, *J* = 6.6 Hz, 6H).

^{13}C NMR (101 MHz, $CDCl_3$) δ 190.10, 154.15, 132.14, 125.08, 111.27, 48.42, 29.94, 19.66.

HRMS (ESI+) m/z $[M+H]^+$ calculated for $C_{11}H_{16}NO$: 178.1226; found 178.1228

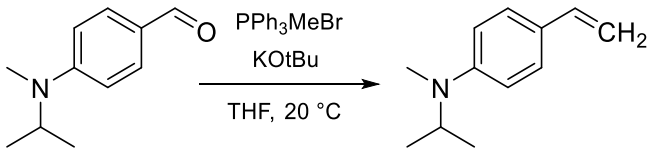

7 **8**, 56%

Synthesis of N-isopropyl-N-methyl-4-vinylaniline, 8

KO^tBu (0.73 g, 6.5 mmol) and Ph_3PMeBr (0.83 g, 2.3 mmol) were combined in anhydrous THF (4 mL) stirred at 20 °C for 30 minutes. **7** (0.23 g, 1.3 mmol) was added and stirred for 12 hours. This was then suspended in hexanes and filtered over celite. Filtrate was taken up in ethyl acetate, then filtered again over basic alumina, repeating once more. **8** was isolated as a yellow oil (0.13 g, 56%).

^{1}H NMR (400 MHz, Chloroform-*d*) δ 7.33 – 7.27 (m, 2H), 6.77 – 6.71 (m, 2H), 6.63 (dd, *J* = 17.6, 10.9 Hz, 1H), 5.53 (dd, *J* = 17.6, 1.1 Hz, 1H), 5.01 (dd, *J* = 10.9, 1.1 Hz, 1H), 4.11 (hept, *J* = 6.6 Hz, 1H), 2.74 (s, 3H), 1.17 (d, *J* = 6.6 Hz, 6H).

^{13}C NMR (101 MHz, $CDCl_3$) δ 149.88, 136.62, 127.23, 126.03, 112.91, 109.17, 48.81, 29.81, 19.37.

HRMS (ESI+) m/z $[M+H]^+$ calculated for $C_{12}H_{18}N$: 176.1434; found 176.1433

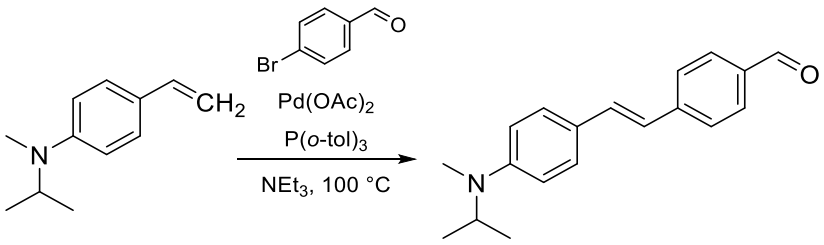

8 **9**, 63%

Synthesis of (E)-4-(4-(isopropyl(methyl)amino)styryl)benzaldehyde, 9

4-bromobenzaldehyde (120 mg, 0.66 mmol), $Pd(OAc)_2$ (7.4 mg, 33 µmol), and P(*o*-tol)$_3$ (20 mg, 66 µmol) were added to a flame dried Schlenk flash, then evacuated and backfilled with N_2 (3X). **8** (115 mg, 0.66 mmol) was added as a solution in anhydrous triethylamine (3 mL). This was stirred for 18 hours at 100 °C, then diluted in dichloromethane. This was washed with NH_4Cl and brine before drying with $MgSO_4$. This was concentrated to a yellow solid, taken up in a small portion of dichloromethane, and triturated. Filtration afforded **9** as a yellow solid (115 mg, 63%).

^{1}H NMR (600 MHz, Chloroform-*d*) δ 9.96 (s, 1H), 7.83 (d, *J* = 8.3 Hz, 2H), 7.59 (d, *J* = 8.2 Hz, 2H), 7.46 – 7.42 (m, 2H), 7.20 (d, *J* = 16.2 Hz, 1H), 6.93 (d, *J* = 16.2 Hz, 1H), 6.77 (d, *J* = 8.9 Hz, 2H), 4.16 (hept, *J* = 6.6 Hz, 1H), 2.79 (s, 3H), 1.20 (d, *J* = 6.6 Hz, 6H).

^{13}C NMR (151 MHz, $CDCl_3$) δ 191.56, 150.25, 144.59, 134.39, 132.49, 130.22, 128.25, 126.17, 124.47, 122.42, 112.65, 77.21, 77.00, 76.79, 48.54, 29.74, 19.45.

HRMS (ESI+) m/z $[M+H]^+$ calculated for $C_{19}H_{22}NO$: 280.1696; found 280.1695

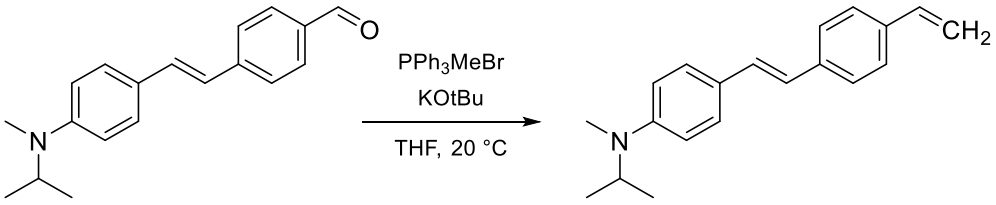

9 **10**, 44%

Synthesis of (E)-N-isopropyl-N-methyl-4-(4-vinylstyryl)aniline, 10

Potassium tert-butoxide (0.2 g, 1.8 mmol) and methyltriphenylphosphonium bromide (0.23 g, 0.64 mmol) was stirred in anhydrous THF (4 mL) at 20 °C for 30 minutes. **9** (0.1 g, 0.36 mmol) was then added and stirred for 12 hours. The reaction was diluted in hexanes, then filtered over celite. This was concentrated, then suspended in ethyl acetate and filtered over basic alumina. This was concentrated to afford **10** as a yellow solid (44 mg, 44%).

^{1}H NMR (600 MHz, Chloroform-*d*) δ 7.45 – 7.42 (m, 2H), 7.41 – 7.35 (m, 4H), 7.04 (d, *J* = 16.2 Hz, 1H), 6.89 (d, *J* = 16.2 Hz, 1H), 6.79 – 6.75 (m, 2H), 6.71 (dd, *J* = 17.6, 10.9 Hz, 1H), 5.74 (dd, *J* = 17.6, 0.9 Hz, 1H), 5.21 (dd, *J* = 10.8, 0.9 Hz, 1H), 4.14 (p, *J* = 6.6 Hz, 1H), 2.77 (s, 3H), 1.19 (d, *J* = 6.6 Hz, 6H).

^{13}C NMR (151 MHz, $CDCl_3$) δ 149.78, 137.89, 136.62, 135.92, 128.82, 127.67, 126.48, 126.10, 125.53, 123.77, 113.05, 112.96, 48.73, 29.78, 19.41.

HRMS (ESI+) m/z $[M+H]^+$ calculated for $C_{20}H_{24}N$: 278.1903; found 278.1902

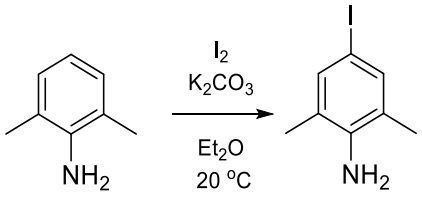

11, 67%

Synthesis of 4-iodo-2,6-dimethylaniline, 11

2,6-dimethylaniline (1.5 g, 12.4 mmol), iodine (3.3 g, 13.0 mmol), and K_2CO_3 (3.4 g, 24.8 mmol) were combined with diethyl ether (22 mL) and set to stir under N_2 in the absence of light for 16 hours. The reaction mixture was then diluted with diethyl ether and washed with water, an aqueous solution of $Na_2S_2O_3 \cdot 5H_2O$ (3.2 g, 13.0 mmol), water, and brine. The organic layer was then dried with Na_2SO_4 and concentrated to dryness *in vacuo*. The residue was purified by flash chromatography (silica deactivated with Et_3N, 15% to 20% EtOAc in hexanes) to afford **11** as a purple oil (2.0 g, 67% yield).

^{1}H NMR (500 MHz, Chloroform-d) δ 7.24 (s, 2H), 3.58 (s, 2H), 2.13 (s, 6H).

^{13}C NMR (126 MHz, Chloroform-d) δ 142.67, 136.54, 124.21, 79.23, 17.36.

HRMS (ESI+) Calculated for $C_8H_{11}NI$ $[M+H]^+$ 247.9931; Found 247.9930.

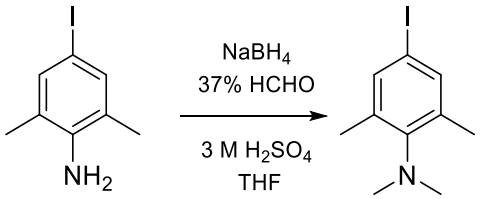

11 **12**, 95%

Synthesis of 4-iodo-N,N,2,6-tetramethylaniline, 12

11 (1 g, 4 mmol), 37 wt.% aqueous HCHO (1.3 mL, 12 mmol), 3 M H_2SO_4 (2.4 mL), and THF (10.76 mL) were combined and set to stir in an ice bath. $NaBH_4$ (605 mg, 16 mmol) was added portion wise to the solution with strong stirring. After one hour, the reaction was quenched with a saturated aqueous solution of $NaHCO_3$ and basified to a pH of 8. The reaction mixture was extracted with EtOAc (3X). The organic layers were washed with brine, dried with Na_2SO_4, and concentrated to dryness *in vacuo* to afford **12** as a brown oil with an orange hue (1.06 g, 95% yield).

^{1}H NMR (500 MHz, Chloroform-d) δ 7.32 (s, 2H), 2.78 (s, 6H), 2.23 (s, 6H).

^{13}C NMR (126 MHz, Chloroform-d) δ 149.77, 139.70, 137.55, 89.31, 42.45, 18.89.

HRMS (ESI+) Calculated for $C_{10}H_{15}NI$ $[M+H]^+$ 276.0244; Found 276.0242.

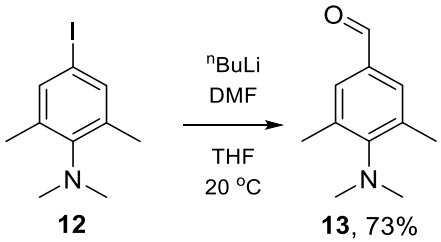

12 **13**, 73%

Synthesis of 4-(dimethylamino)-3,5-dimethylbenzaldehyde, 13

A solution of **12** (510 mg, 1.87 mmol) in anhydrous THF (11.2 mL) was added to a flame-dried Schlenk flask under inert atmosphere and cooled to -78 °C using a bath of dry ice in acetone. A solution of 1.6 M ^{n}BuLi in hexane (1.73 mL, 2.8 mmol)) was added dropwise to the flask. After 1 hr, anhydrous DMF (217 μL, 2.8 mmol) was added dropwise to the flask. After 15 minutes, the reaction mixture was brought to room temperature and quenched with saturated aqueous NH_4Cl (~10 mL). This solution was extracted with EtOAc (3X). The organic layers were washed with brine, dried with Na_2SO_4, and concentrated to dryness *in vacuo*. The residue was purified by flash chromatography (silica deactivated with Et_3N, 10% EtOAc in hexanes) to afford **13** as a clear, yellow oil (242 mg, 73% yield).

^{1}H NMR (500 MHz, Chloroform-d) δ 9.86 (s, 1H), 7.50 (s, 2H), 2.87 (s, 6H), 2.34 (s, 6H).

^{13}C NMR (126 MHz, Chloroform-d) δ 191.99, 156.38, 136.70, 132.28, 130.83, 42.55, 19.66.

HRMS (ESI+) Calculated for $C_{11}H_{16}ON$ $[M+H]^+$ 178.1226; Found 178.1224.

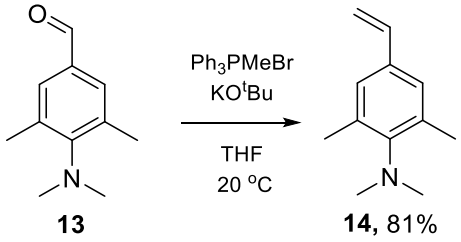

13 **14**, 81%

Synthesis of N,N,2,6-tetramethyl-4-vinylaniline, 14

Ph_3PMeBr (917 mg, 2.57 mmol) and KO^tBu (345 mg, 3.081 mmol) were added to a flask and the flask was evacuated/backfilled with N_2 (3x). Anhydrous THF (14 mL) was added to the reaction mixture and the solution was set to stir at room temperature for 30 minutes. **13** (364 mg, 2.05 mmol) was then dissolved in anhydrous THF (4 mL) and added to the flask. The mixture was set

to stir at room temperature for 16 hours. The reaction was then added to water and extracted with EtOAc (3x). The organic layers were washed with brine, dried with Na_2SO_4, and concentrated to dryness *in vacuo*. The residue was purified by flash chromatography (silica deactivated with Et_3N, 10% to 20% EtOAc in hexanes) to afford **14** as a clear, yellow oil (291 mg, 81% yield).

^{1}H NMR (500 MHz, Chloroform-d) δ 7.05 (s, 2H), 6.62 (dd, J = 17.6, 10.9 Hz, 1H), 5.64 (d, J = 17.6 Hz, 1H), 5.14 (d, J = 10.9 Hz, 1H), 2.81 (s, 6H), 2.29 (s, 6H).

^{13}C NMR (126 MHz, Chloroform-d) δ 137.14, 136.67, 133.94, 126.77, 112.70, 42.64, 19.34.

HRMS (ESI+) Calculated for $C_{12}H_{18}N$ $[M+H]^+$ 176.1434; Found 176.1432.

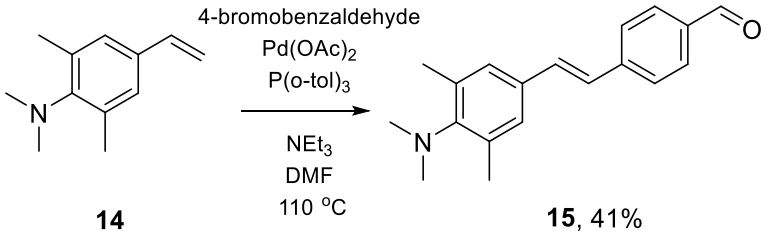

Synthesis of (E)-4-(4-(dimethylamino)-3,5-dimethylstyryl)benzaldehyde, 15

14 (98 mg, 0.56 mmol), 4-bromobenzaldehyde (104 mg, 0.56 mmol), $Pd(OAc)_2$ (6.3 mg, 0.03 mmol), and $P(o\text{-tol})_3$ (17 mg, 0.06 mmol) were combined in a flame-dried Schlenk flask. The flask was evacuated/backfilled with N_2 (3x). Triethylamine (1.1 mL) and DMF (1.1 mL) were then added to the flask. The reaction was set to stir at 110 °C for 16 hours. The mixture was then concentrated to dryness *in vacuo* and purified by flash chromatography (silica deactivated with Et_3N, 5% to 8% EtOAc in hexanes to afford **15** as a yellow solid (64 mg, 41% yield).

^{1}H NMR (400 MHz, Chloroform-d) δ 9.98 (s, 1H), 7.85 (d, J = 8.2 Hz, 2H), 7.62 (d, J = 8.2 Hz, 2H), 7.22 – 7.00 (m, 4H), 2.84 (s, 6H), 2.33 (s, 6H).

^{13}C NMR (101 MHz, Chloroform-d) δ 191.72, 150.60, 143.98, 137.28, 135.10, 132.71, 132.17, 130.34, 127.57, 126.78, 126.10, 42.63, 19.43.

HRMS (ESI+) Calculated for $C_{19}H_{22}ON$ $[M+H]^+$ 280.1696; Found 280.1694.

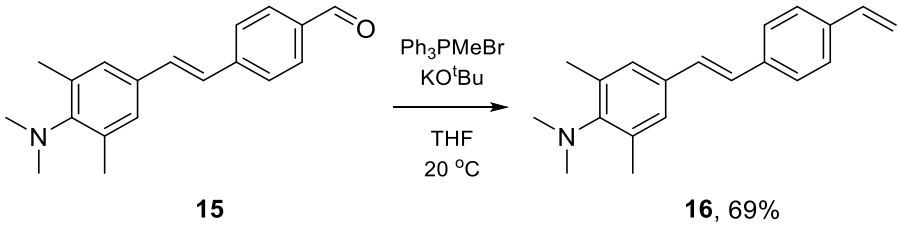

Synthesis of (E)-N,N,2,6-tetramethyl-4-(4-vinylstyryl)aniline, 16

PPh_3MeBr (256 mg, 0.72 mmol) and KO^tBu (96.5, 0.86 mmol) were added to a flask and the flask was evacuated/backfilled with N_2 (3x). Anhydrous THF (4 mL) was added to the reaction mixture and the solution was set to stir at room temperature for 30 minutes. **15** (160 mg, 0.573 mmol) was then dissolved in anhydrous THF (1 mL) and added to the flask. The mixture was set to stir at room temperature for 16 hours. The reaction was then added to water and extracted with EtOAc (3x). The organic layers were washed with brine, dried with Na_2SO_4, and concentrated to dryness *in vacuo*. The residue was purified by flash chromatography (silica deactivated with Et_3N, 15% EtOAc in hexanes) to afford **16** as an orange solid (109 mg, 69% yield).

^1H NMR (500 MHz, Chloroform-d) δ 7.48 – 7.38 (m, 4H), 7.16 (s, 2H), 7.01 (d, J = 3.0 Hz, 2H), 6.72 (dd, J = 17.6, 10.9 Hz, 1H), 5.76 (d, J = 17.6 Hz, 1H), 5.24 (d, J = 10.9 Hz, 1H), 2.83 (s, 6H), 2.32 (s, 6H).

^{13}C NMR (126 MHz, Chloroform-d) δ 149.76, 137.41, 137.26, 136.63, 128.54, 127.18, 127.11, 126.65, 126.62, 113.64, 42.68, 19.42.

HRMS (ESI+) Calculated for $C_{20}H_{24}N$ $[M+H]^+$ 278.1903; Found 278.1900.

Preparation of voltage indicators

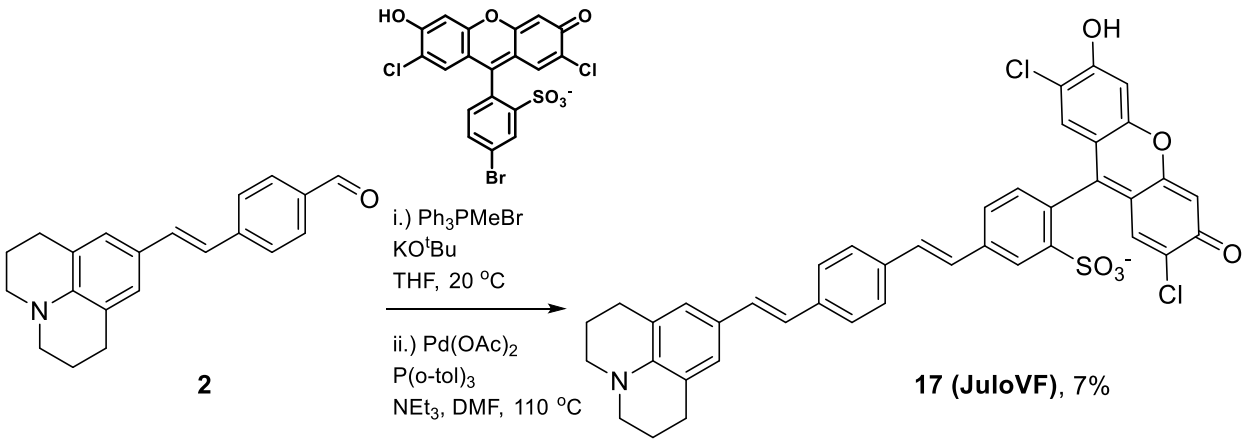

Synthesis of 17 (Julolidine VF)

Ph_3PMeBr (146 mg, 0.41 mmol) and KO^tBu (56 mg, 0.5 mmol) were combined with anhydrous THF (2 mL) and set to stir at room temperature for one hour. Compound **2** (100 mg, 0.33 mmol) was then dissolved in anhydrous THF (1 mL), added to the reaction mixture, and set to stir at room temperature for 16 hours. The reaction was then added to water and extracted with EtOAc (3x). The organic layers were collected, washed with brine, dried with Na_2SO_4, and concentrated to dryness *in vacuo* to give a red-orange solid. This crude material was combined with 5-bromo-(2',7'-dichloro-sulfofluorescein (155 mg, 0.30 mmol), $Pd(OAc)_2$ (3 mg, 0.015 mmol), and $P(o\text{-}tol)_3$ (9 mg, 0.030 mmol) in a flame-dried Schlenk flask. The flask was evacuated/backfilled with N_2 (3x). Anhydrous DMF (1.4 mL) and anhydrous triethylamine (339 μL) were added, the flask was sealed, and the solution was stirred at 110° C for 16 hours. The reaction was then cooled to room temperature and concentrated to dryness *in vacuo*. The crude residue was taken up in 1:1

MeOH/ACN (100 mL) and filtered through Celite. The filtrate was concentrated to dryness *in vacuo*. The residue was taken up in a minimal amount of 1:1 MeOH/ACN and precipitated in ether. The precipitate was purified by preparative-HPLC (Water/MeCN + 0.05% TFA) to afford **17** as a red-orange powder (15 mg, 7% yield).

^{1}H NMR (400 MHz, DMSO-d_6) δ 8.17 (s, 1H), 7.79 (d, *J* = 8.0 Hz, 1H), 7.66 (d, *J* = 7.7 Hz, 2H), 7.54 (d, *J* = 7.8 Hz, 2H), 7.48 – 7.35 (m, 2H), 7.25 (d, *J* = 7.9 Hz, 1H), 7.18 – 6.82 (m, 6H), 6.77 (s, 2H), 3.28 – 3.01 (m, 4H), 2.87 – 2.58 (m, 4H), 1.99 – 1.78 (m, 4H).

^{13}C NMR (226 MHz, DMSO-d_6) δ 158.33, 158.16, 154.87, 152.18, 147.37, 138.40, 137.82, 134.90, 130.07, 129.83, 127.52, 127.19, 126.44, 126.05, 125.39, 122.46, 121.10, 115.89, 103.28, 49.34, 27.11, 21.43.

HRMS (ESI-) Calculated for $C_{41}H_{30}O_6NCl_2S$ $[M-H]^-$ 734.1176; Found 734.1168.

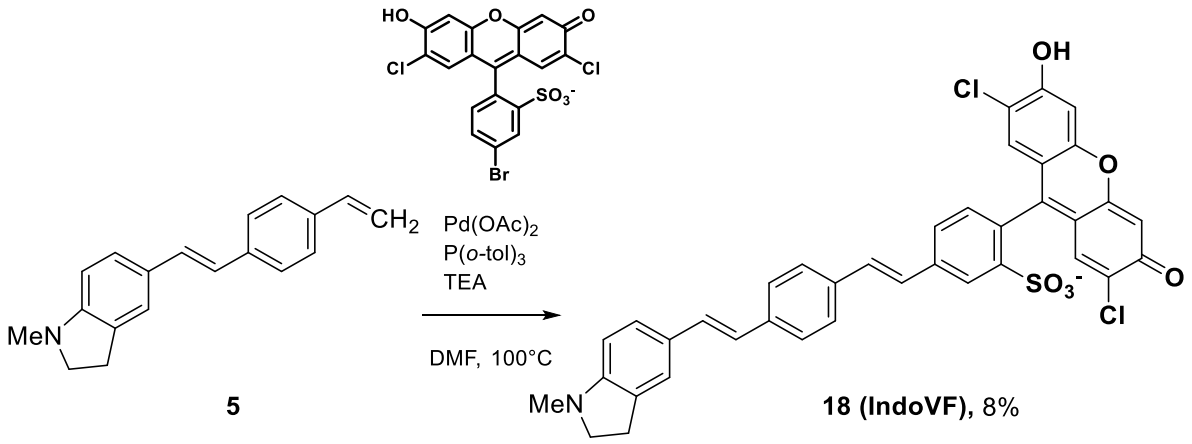

Synthesis of 18 (IndoVF)

5 (30 mg, 0.11 mmol), 5-bromo-(2',7'-dichloro-sulfofluorescein (54 mg, 0.1 mmol), $Pd(OAc)_2$ (0.5 mg, 2 µmol), and P(*o*-tol)$_3$ (1.5 mg, 5 µmol) were combined in anhydrous DMF (2 mL). Anhydrous triethylamine (0.21 g, 2.1 mmol) was added, the flask was sealed, and the reaction was stirred at 110 °C for 18 hours. The reaction was then concentrated to dryness *in vacuo*, then the crude material was taken up in 1:1 dicholoromethane:methanol and precipitated in ether. The precipitate was purified by preparative-HPLC (Water/MeCN + 0.05% TFA) to afford **18** as a red-orange powder (6 mg, 8% yield).

^{1}H NMR (400 MHz, DMSO-d_6) δ 8.15 (s, 1H), 7.76 (d, *J* = 7.8 Hz, 1H), 7.64 (d, *J* = 8.0 Hz, 2H), 7.53 (d, *J* = 7.9 Hz, 2H), 7.42 – 7.32 (m, 3H), 7.22 (dd, *J* = 8.1, 4.2 Hz, 2H), 7.16 (d, *J* = 16.5 Hz, 1H), 6.97 (d, *J* = 10.3 Hz, 3H), 6.73 (s, 2H), 6.47 (d, *J* = 8.0 Hz, 1H), 3.29 (t, *J* = 8.2 Hz, 3H), 2.89 (t, *J* = 8.3 Hz, 2H), 2.71 (s, 3H).

^{13}C NMR (226 MHz, DMSO) δ 157.97, 157.83, 157.69, 157.55, 153.24, 151.99, 147.33, 138.41, 137.78, 135.03, 130.55, 130.06, 129.78, 129.41, 128.87, 128.17, 127.55, 127.31, 127.17, 126.55,

126.41, 126.14, 125.36, 122.87, 121.72, 118.93, 117.73, 116.40, 115.08, 106.47, 55.25, 35.33, 27.82.

HRMS (ESI-) m/z: $[M-H]^-$ calculated for $C_{38}H_{26}Cl_2NO_6S$ 694.0863; found 694.0859.

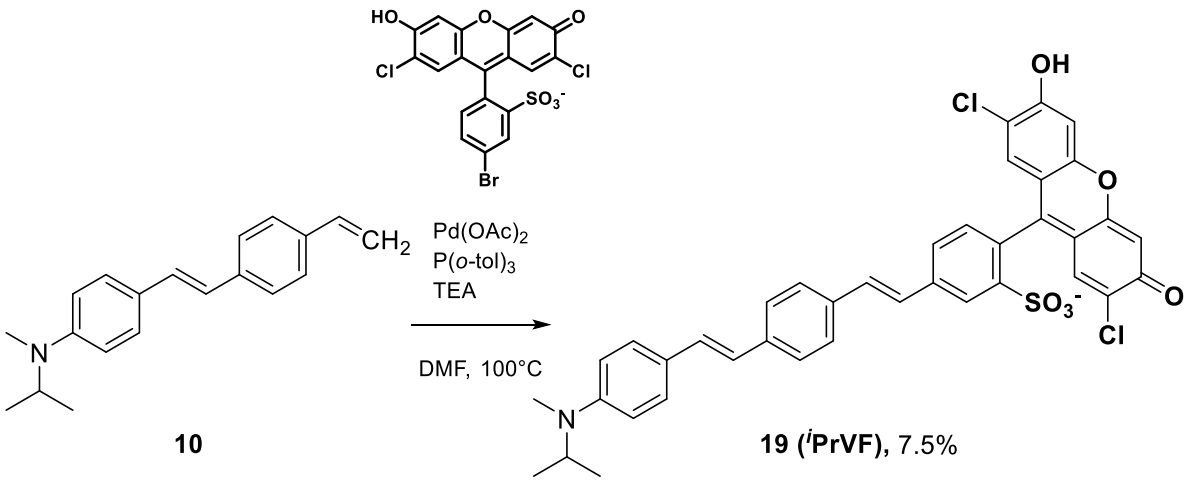

Synthesis of 19 (^{i}PrVF)

10 (40 mg, 0.14 mmol), 5-bromo-(2',7'-dichloro-sulfofluorescein (68 mg, 0.13 mmol), $Pd(OAc)_2$ (0.6 mg, 3 µmol), and P(*o*-tol)$_3$ (1.6 mg, 5 µmol) were combined in anhydrous DMF (1 mL). Anhydrous triethylamine (0.27 g, 2.6 mmol) was added, the flask was sealed, and the reaction was stirred at 100 °C for 18 hours. The reaction was then concentrated to dryness *in vacuo*, then the crude material was taken up in 1:1 dicholoromethane:methanol and precipitated in ether. The precipitate was purified by preparative-TLC (15% methanol in dichloromethane + 1% acetic acid) to afford **19** as a red solid (7 mg, 7.5% yield).

^{1}H NMR (900 MHz, DMSO-d_6) δ 8.16 (d, *J* = 1.9 Hz, 1H), 7.71 (dd, *J* = 7.9, 1.9 Hz, 1H), 7.66 (d, *J* = 7.9 Hz, 2H), 7.56 (d, *J* = 8.0 Hz, 2H), 7.44 (d, *J* = 8.3 Hz, 2H), 7.41 (d, *J* = 16.3 Hz, 1H), 7.37 – 7.34 (m, 1H), 7.18 (d, *J* = 16.3 Hz, 1H), 7.12 (d, *J* = 7.7 Hz, 1H), 6.99 (d, *J* = 16.3 Hz, 1H), 6.79 (d, *J* = 8.5 Hz, 2H), 6.74 (s, 2H), 6.12 (s, 2H), 4.16 (q, *J* = 6.6 Hz, 1H), 2.72 (s, 3H), 1.13 (d, *J* = 6.5 Hz, 6H).

^{13}C NMR (226 MHz, DMSO) δ 173.21, 156.41, 152.19, 149.47, 147.22, 137.63, 137.49, 135.17, 130.38, 129.46, 128.86, 128.60, 127.71, 127.10, 126.81, 126.48, 126.15, 126.08, 125.52, 124.82, 124.18, 123.05, 112.67, 112.35, 108.91, 102.57, 69.76, 47.82, 29.54, 22.04, 19.12.

HRMS (ESI-) m/z: $[M-H]^-$ calculated for $C_{39}H_{30}Cl_2NO_6$ 710.1176; found 710.1172.

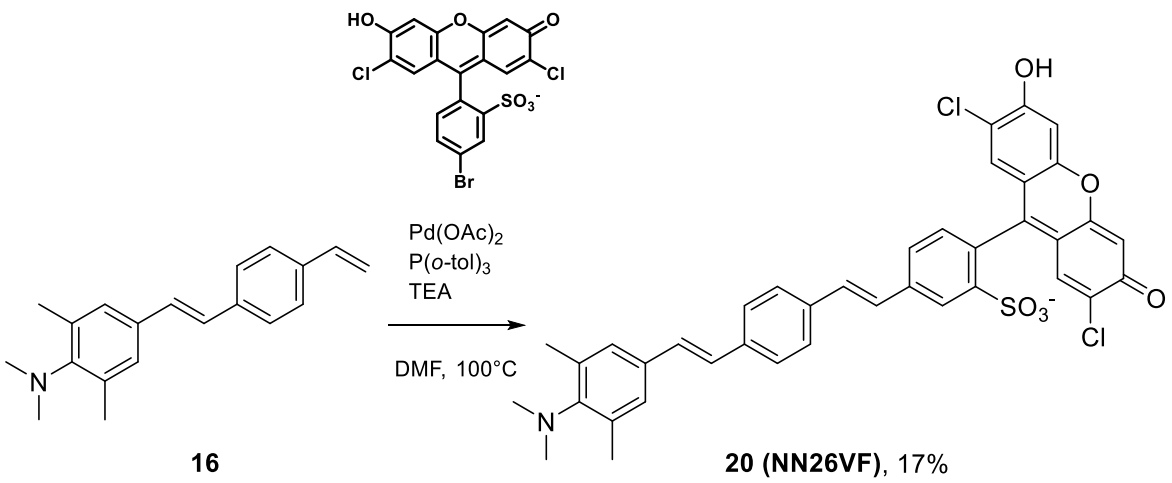

16 **20 (NN26VF)**, 17%

Synthesis of 20 (*N*,*N*,2,6-tetramethyl VF)

16 (18 mg, 0.065 mmol), 5-bromo-(2',7'-dichloro-sulfofluorescein) (20 mg, 0.039 mmol), $Pd(OAc)_2$ (0.5 mg, 0.002 mmol), and $P(o\text{-}tol)_3$ (1.2 mg, 0.004 mmol) were combined in a flame-dried Schlenk flask. The flask was evacuated/backfilled with N_2 (3x). Anhydrous DMF (750 µL) and anhydrous triethylamine (187.5 µL) were added, the flask was sealed, and the solution was stirred at 110° C for 16 hours. The reaction was then cooled to room temperature, diluted with 1:1 MeOH/DCM (10 mL), and filtered through Celite. The filtrate was concentrated to dryness *in vacuo*. The residue was purified by preparative-TLC ((silica deactivated with Et_3N, 10% MeOH in DCM) to afford **20** as a red-orange powder (4.6 mg, 17% yield).

^{1}H NMR (900 MHz, DMSO-d_6) δ 8.17 (d, *J* = 1.8 Hz, 1H), 7.73 (dd, *J* = 7.8, 1.8 Hz, 1H), 7.69 (d, *J* = 7.9 Hz, 2H), 7.61 (d, *J* = 7.9 Hz, 2H), 7.44 (d, *J* = 16.4 Hz, 1H), 7.37 (d, *J* = 16.4 Hz, 1H), 7.24 (s, 2H), 7.19 – 7.15 (m, 2H), 7.13 (d, *J* = 7.8 Hz, 1H), 6.75 (s, 2H), 6.16 (s, 2H), 2.78 (s, 6H), 2.28 (s, 6H).

^{13}C NMR (226 MHz, DMSO-d_6) δ 156.38, 152.30, 149.13, 147.26, 137.48, 136.96, 136.23, 135.96, 133.12, 130.39, 129.48, 129.41, 128.67, 128.22, 127.29, 127.15, 127.01, 126.80, 126.66, 126.17, 125.61, 109.18, 102.70, 42.45, 19.01.

HRMS (ESI-) Calculated for $C_{39}H_{30}O_6NCl_2S$ $[M\text{-}H]^-$ 710.1176; Found 710.1172.

4.10 Schemes, tables, and figures

Scheme 4-1. *Design of VoltageFluors with restricted aniline donors*

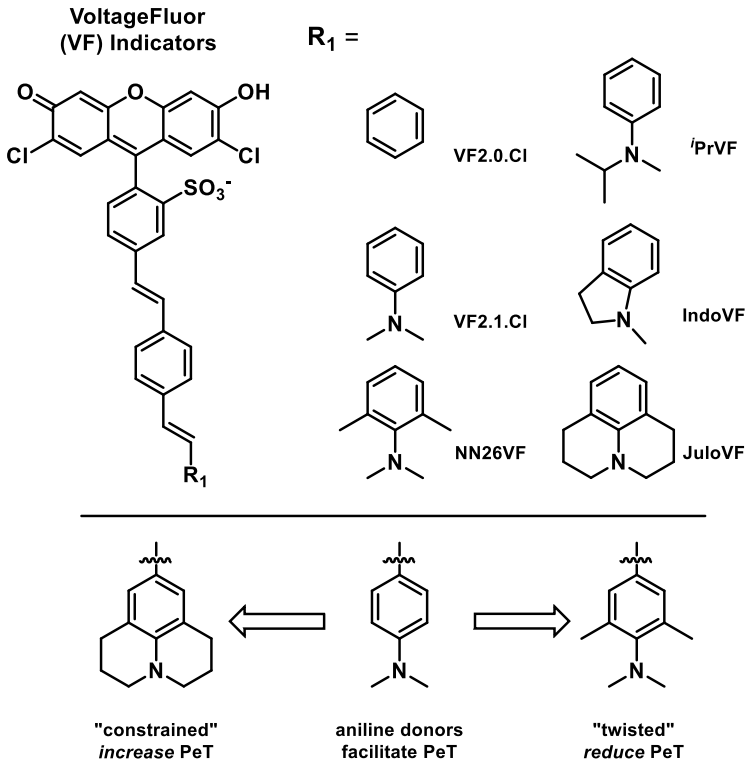

***Scheme 4-2**. Synthesis of ring-constrained aniline donors.*

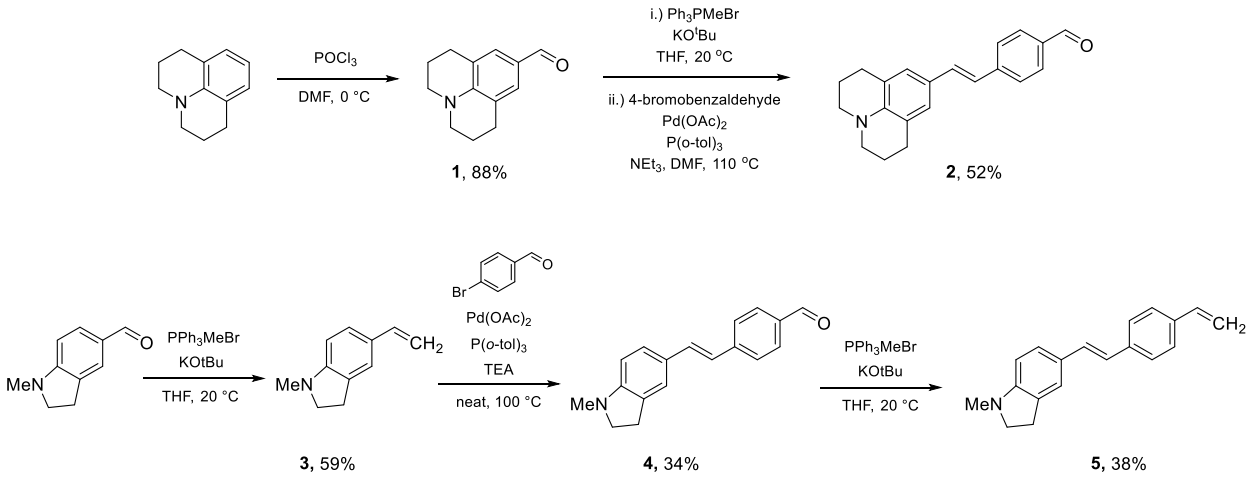

Scheme 4-3. *Synthesis of sterically hindered aniline donors*

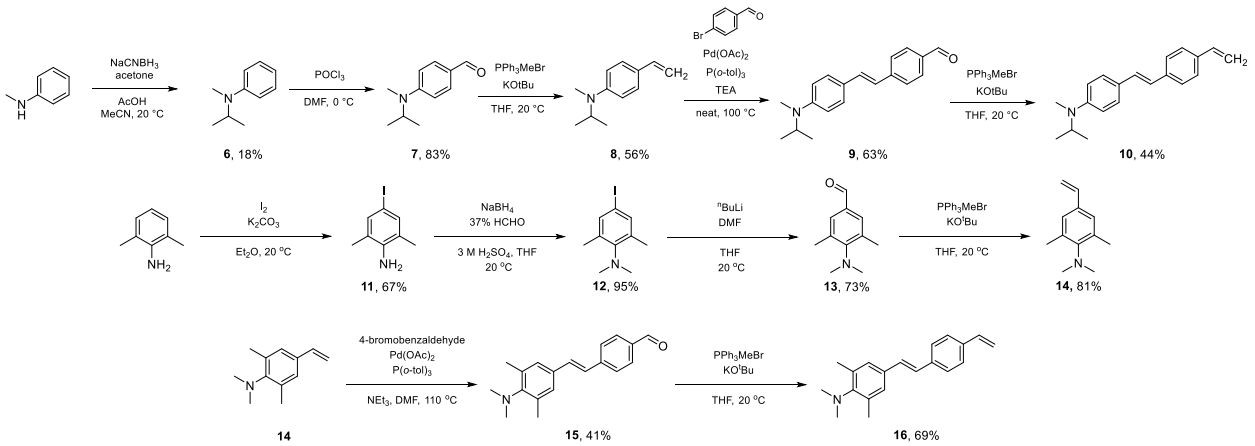

Scheme 4-4. *Synthesis of VoltageFluors with constrained aniline donors*

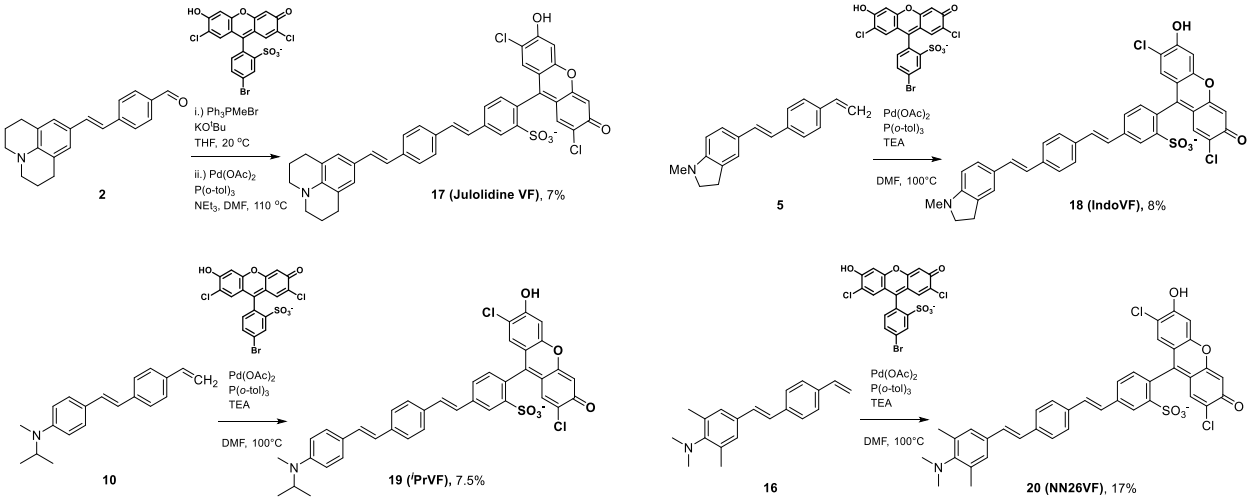

Table 4-1. *Summarized properties of conformationally restricted VFs.*

Voltage Fluor	Wire λ_{abs} (nm)	Φ_F	τ_{fl} (ns, in EtOH-KOH)	τ_{fl} (ns, in POPC)	Rel. brightness (HEK293T)	%ΔF/F, 100 mV	$\Delta\tau_{fl}$ per mV (ps)	τ_{fl} at 0 mV (ns)
JuloVF (**17**)	406	0.10	0.63 ± 0.08	0.81 ± 0.05	0.021 ± 0.003 (300nM)	34 ± 6 (500 nM)	0.73 ± 0.03 (500 nM)	0.31 ± 0.01 (500 nM)
					0.037 ± 0.004 (500 nM)			
IndoVF (**18**)	390	0.14	0.52 ± 0.03	0.98 ± 0.02	0.28 ± 0.02	37 ± 2.4	1.49 ± 0.04	0.48 ± 0.02
^{i}PrVF (**19**)	392	0.28	1.04 ± 0.04	1.67 ± 0.03	0.29 ± 0.03	34 ± 1.6	2.97 ± 0.04	1.28 ± 0.01
NN26VF (**20**)	368	0.44	1.66 ± 0.03	2.55 ± 0.06	0.44 ± 0.05	2.2 ± 0.05	0.50 ± 0.02	3.32 ± 0.01
VF2.1.Cl	389	0.12	0.53 ± 0.02	1.58 ± 0.05	0.361 ± 0.01 (100 nM)	23 ± 3 (100 nM)	3.11 ± 0.04 (100 nM)	1.68 ± 0.04 (100 nM)
					1.0 ± 0.1 (300 nM)	26 ± 3 (300 nM)	3.05 ± 0.08 (300 nM)	1.57 ± 0.03 (300 nM)
VF2.0.Cl	360	0.83	3.18 ± 0.02	3.13 ± 0.10	0.62 ± 0.06 (100 nM)	-0.3 ± 0.02 (100 nM)	0.02 ± 0.03 (100 nM)	3.44 ± 0.01 (100 nM)
					1.8 ± 0.2 (300 nM)	-0.2 ± 0.01 (300 nM)	0.00 ± 0.03 (300 nM)	3.36 ± 0.03 (100 nM)

Table 4-2. *Probe performance at detection of electrical activity in excitable cells*

VoltageFluor	HEK293T SNR	iCM SNR	Neuron SNR
JuloVF (**17**)	26 ± 1.8 (500 nM)	-	-
IndoVF (**18**)	87 ± 6.5	141 ± 4.4	5.6 ± 0.3
^{i}PrVF (**19**)	125 ± 1.7	451 ± 11	9.7 ± 0.5
NN26VF (**20**)	8.6 ± 0.2	-	-
VF2.1.Cl	103 ± 4.6 197 ± 12	130 ± 5.3 (100 nM) 441 ± 14 (300 nM)	7.8 ± 0.6 (100 nM) 13 ± 1 (300 nM)
VF2.0.Cl	1.8 ± 0.06 2.4 ± 1.4	-	-

Table 4-3. *Optimized working concentrations for the VoltageFluors used in this study*

VoltageFluor	**Optimized Concentration**
JuloVF	500 nM
IndoVF	300 nM
^{i}PrVF	300 nM
VF2.1.Cl	100 nM
NN26VF	300 nM
VF2.0.Cl	100 nM

Table 4-4. *Number of exponential terms selected to describe VF time-resolved fluorescence decays*

VoltageFluor	Number of exponential decay terms
JuloVF	3
IndoVF	3
^{i}PrVF	2
VF2.1.Cl	2
NN26VF	1
VF2.0.Cl	1

Figure 4-1. *UV-VIS and fluorescence spectroscopy suggests conformational restriction in aniline modified VoltageFluors*

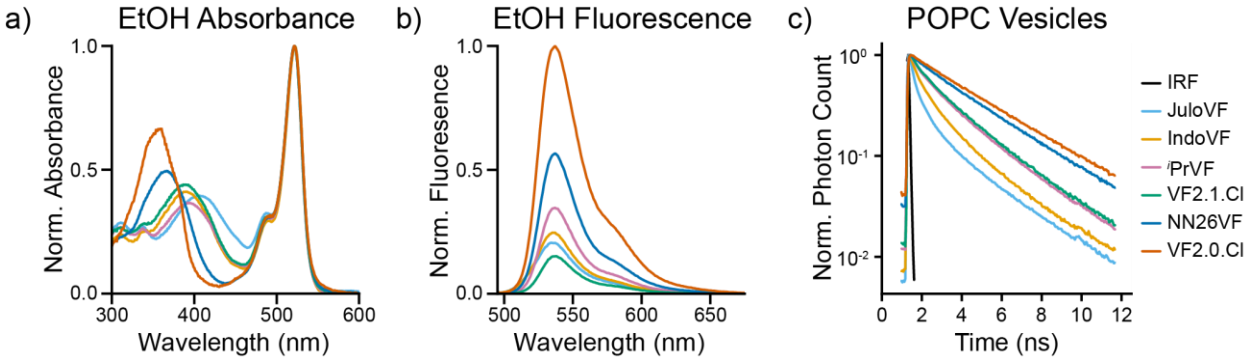

Figure 4-1. UV-VIS and fluorescence spectroscopy suggests conformational restriction in aniline modified VoltageFluors. a) Absorbance spectra of VoltageFluors at 500 nM in Ethanol with 0.1 M KOH (Ethanol-KOH) normalized to their absorbance maxima. b) Emission spectra of VoltageFluors at 500 nM in Ethanol-KOH adjusted to their respective absorbance values at 485 nm and normalized to the VF2.0.Cl trace. c) Time-resolved fluorescence decays of VFs at 500 nM in POPC vesicles. Decays were normalized to the time channel with maximum photon counts. Black line indicates the instrument response function (IRF).

Figure 4-2. *Absorbance, Emission, and Excitation Spectra of Aniline VFs*

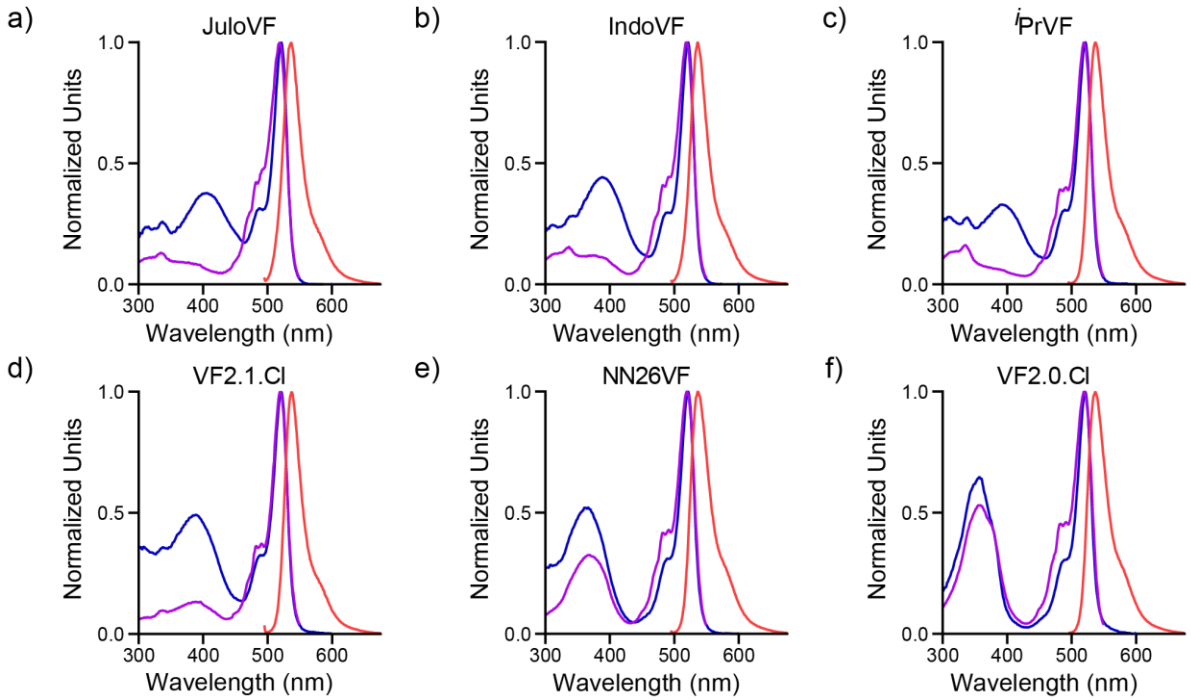

Figure 4-2. Absorbance, Emission, and Excitation Spectra of Aniline VFs**.** Absorbance spectra (blue), emission spectra (red), and excitation spectra (purple) for JuloVF (a), IndoVF (b), ^{i}PrVF (c), VF2.1.Cl (d), NN26VF(e), and VF2.0.Cl (f) in ethanol with 0.1 M KOH. The VoltageFluors were diluted from DMSO stocks (500 µM-1 mM) to either 1 µM (JuloVF, IndoVF, ^{i}PrVF, VF2.1.Cl, NN26VF) or 500 nM (VF2.0.Cl) in ethanol with 0.1 M KOH. VF2.0.Cl was measured at 500 nM as the emission of 1 mM VF2.0.Cl was higher than the range of the detector for wavelengths near the emission maximum. Spectra were taken using the equipment described above in section **2**. Absorbance measurements were recorded at 1 nm intervals from 300 nm to 600 nm. Emission measurements were recorded at 1 nm intervals from 495 nm to 675 nm while exciting the VoltageFluors with 485 nm light. Excitation measurements were recorded by measuring the emission of each VoltageFluor at 570 nm while the excitation light was varied from 300 nm to 550 nm. 2 nm slit widths were used for each measurement. Each absorbance, emission, and excitation trace was normalized to the maximum value of absorbance, emission, or excitation respectively.

Figure 4-3. *Absorption and emission measurements of different pH*

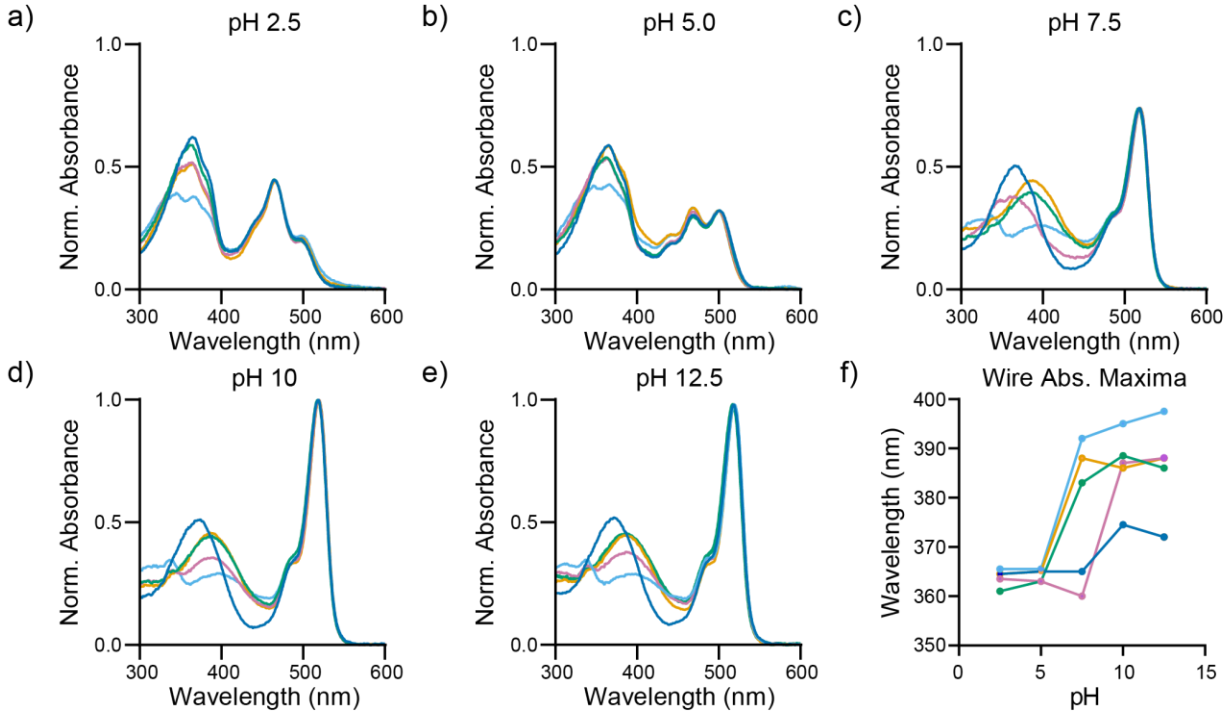

Figure 4-3. Absorption and emission measurements of different pH. Absorbance spectra for JuloVF (light blue), IndoVF (orange), ^{i}PrVF (pink), VF2.1.Cl (green), and NN26VF (dark blue) in buffered solutions with defined pH. All buffer solutions contain 0.1% w/v SDS to help solubilize the VoltageFluors. The VoltageFluors were diluted from DMSO stocks (500 µM-1 mM) to 500 nM in the following solutions. a) Absorbance spectra in 10 mM phosphate buffer which was adjusted to pH 2.5 with HCl/NaOH and adjusted to 56 mOsm with NaCl. b) Absorbance spectra in 10 mM acetate buffer which was adjusted to pH 5.0 with HCl/NaOH and adjusted to 56 mOsm with NaCl. c) Absorbance spectra in 10 mM phosphate buffer which was adjusted to pH 7.5 with HCl/NaOH and adjusted to 56 mOsm with NaCl. d) Absorbance spectra in 10 mM carbonate buffer which was adjusted to pH 10.0 with HCl/NaOH and adjusted to 56 mOsm with NaCl. e) Absorbance spectra in 10 mM KCl/NaOH buffer which was adjusted to pH 12.5 with HCl/NaOH and adjusted to 56 mOsm with NaCl. f) Plot of the wavelength of maximum absorbance for the wire peak of each VoltageFluor versus the pH of the solution. Spectra were taken using the equipment described above in section **2**. Absorbance measurements were recorded at 0.5 nm intervals from 300 nm to 600 nm. 2 nm slit widths were used for each measurement. The absorbance traces were first normalized to their respective absorbance values at 519 nm (pH 7.5, 10.0, and 12.5), 500 nm (pH 5.0), or 470 nm (pH 2.5). The absorbance of chloro-fluorescein varies as a function of pH and these wavelengths are the absorbance maxima for the chloro-fluorescein peaks at the respective pH values. Finally, the absorbance traces were multiplied by the ratio of the average raw absorbance values at the chloro-fluorescein peak for a given pH to the average raw absorbance values at 519 nm for the pH 10 traces. The pH 10 traces had the highest raw absorbance values at 519 nm.

Figure 4-4. *Concentration dependence of VoltageFluor fluorescence lifetimes in vesicles and in basic ethanol*

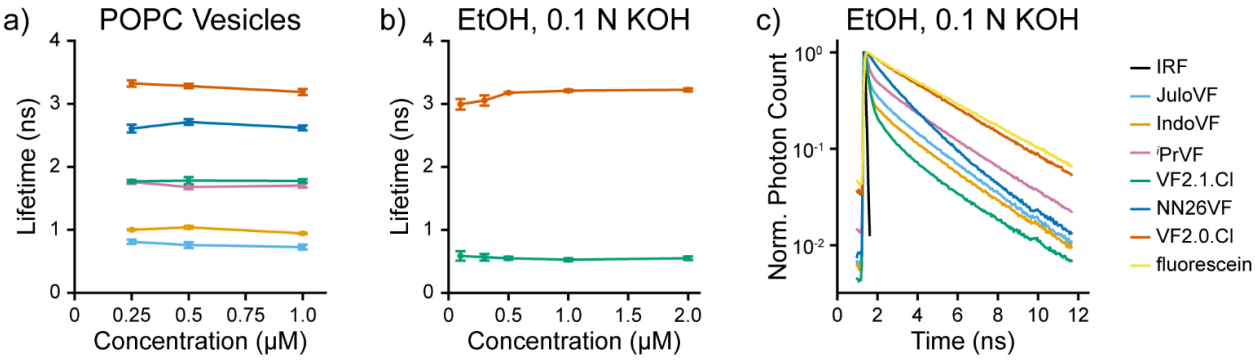

Figure 4-4. Concentration dependence of VoltageFluor fluorescence lifetimes in vesicles and in basic ethanol. Fluorescence lifetime data for VoltageFluors in POPC vesicles and in ethanol with 0.1 N KOH (EtOH-KOH). In all cases, 500 nM was selected as the optimal working concentration. The fluorescence lifetime of VF2.0.Cl was modeled as a sum of two exponential components; all other probes were modeled with three exponential components (see **Methods**). a) Concentration dependence of VF fluorescence lifetime in POPC vesicles. Data were tested for homoscedasticity (Levene's test on the median, $p>0.05$ for 5/6 probes, $p>0.01$ for ^{i}PrVF). Differences between concentrations for each probe were evaluated with Fisher's one-way ANOVA. No significant differences were found between groups for 5 of the 6 probes ($p>0.05$). For IndoVF, significant differences were observed between groups ($F(2,24)=9.00$, $p<0.01$). Tukey-Kramer post hoc tests revealed significant differences between 500 nM IndoVF and 1μM IndoVF ($p<0.05$), as well as between 250 nM IndoVF and 1 μM IndoVF ($p<0.001$). b) Concentration dependence of the fluorescence lifetime of VF2.0.Cl and VF2.1.Cl in EtOH-KOH. The data for each probe were tested for homoscedasticity (Levene's test on the median, $p>0.05$ in both cases). Differences between concentrations were assessed via Fisher's one-way ANOVA. No significant differences were observed between VF2.1.Cl concentrations ($F(4,32)=0.254$, $p=0.91$). Significant differences were observed between VF2.0.Cl concentrations ($F(4,20)=3.61$, $p=0.023$). Tukey-Kramer post hoc tests revealed significant differences between 100 nM and 1 μM VF2.0.Cl and between 100 nM and 2 μM VF2.0.Cl ($p<0.05$); all other comparisons did not yield significant differences ($p>0.05$). c) Representative time-resolved fluorescence intensity of the library of VFs at 500 nM VF in EtOH-KOH. Color coding for VF identity is consistent throughout all plots. IRF= instrument response function. Data in (a) and (b) represent are displayed as the mean ± SEM of data taken on 3 or 4 independent samples, each with 1-3 technical replicates.

Figure 4-5. *^{13}C NMR shifts of the para-carbon in aniline series precursors.*

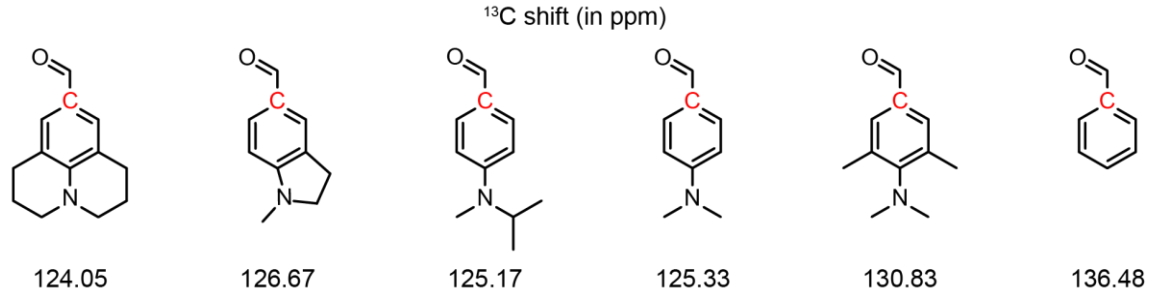

Figure 4-5. ^{13}C NMR shifts of the para-carbon in aniline series precursors. ^{13}C NMR shifts (in ppm) for the carbons labeled above in red. All spectra were taken in $CDCl_3$ (chloroform peak referenced to 77.16 ppm). In order from left to right: Compound **1**, 1-methylindoline-5-carbaldehyde, Compound **7**, 4-(dimethylamino)benzaldehyde, Compound **13**, and benzaldehyde.

Figure 4-6. *Aniline modifications modulate voltage sensitivity of the fluorescence intensity in HEK293T cells.*

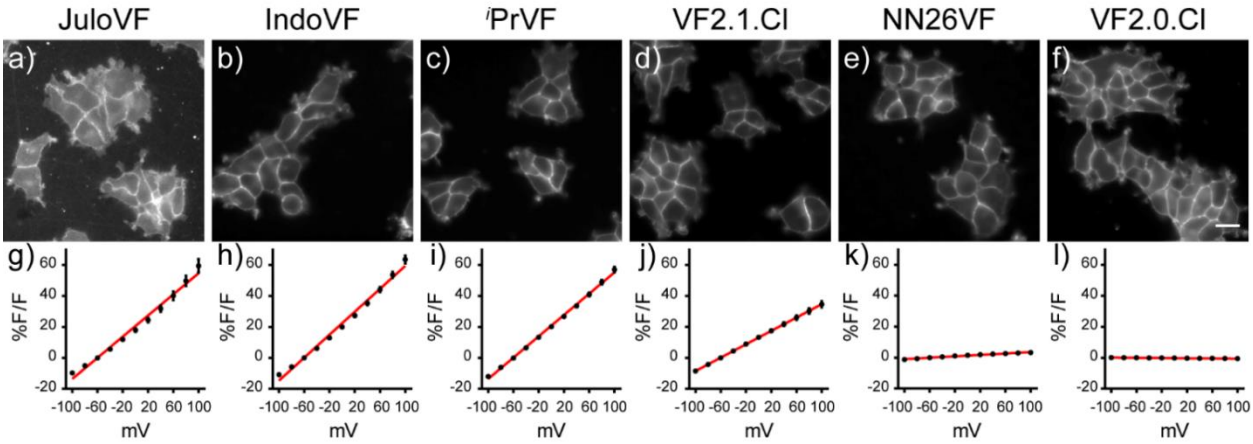

Figure 4-6. Aniline modifications modulate voltage sensitivity of the fluorescence intensity in HEK293T cells. (a-f) Epifluorescence micrographs of HEK293T cells staining with VoltageFluor. Scale bar is 20 µm. (g-l) Linear plots used to calculated voltage sensitivity values listed in Table 4-1.

Figure 4-7. *HEK293T intensity patching and relative brightness*

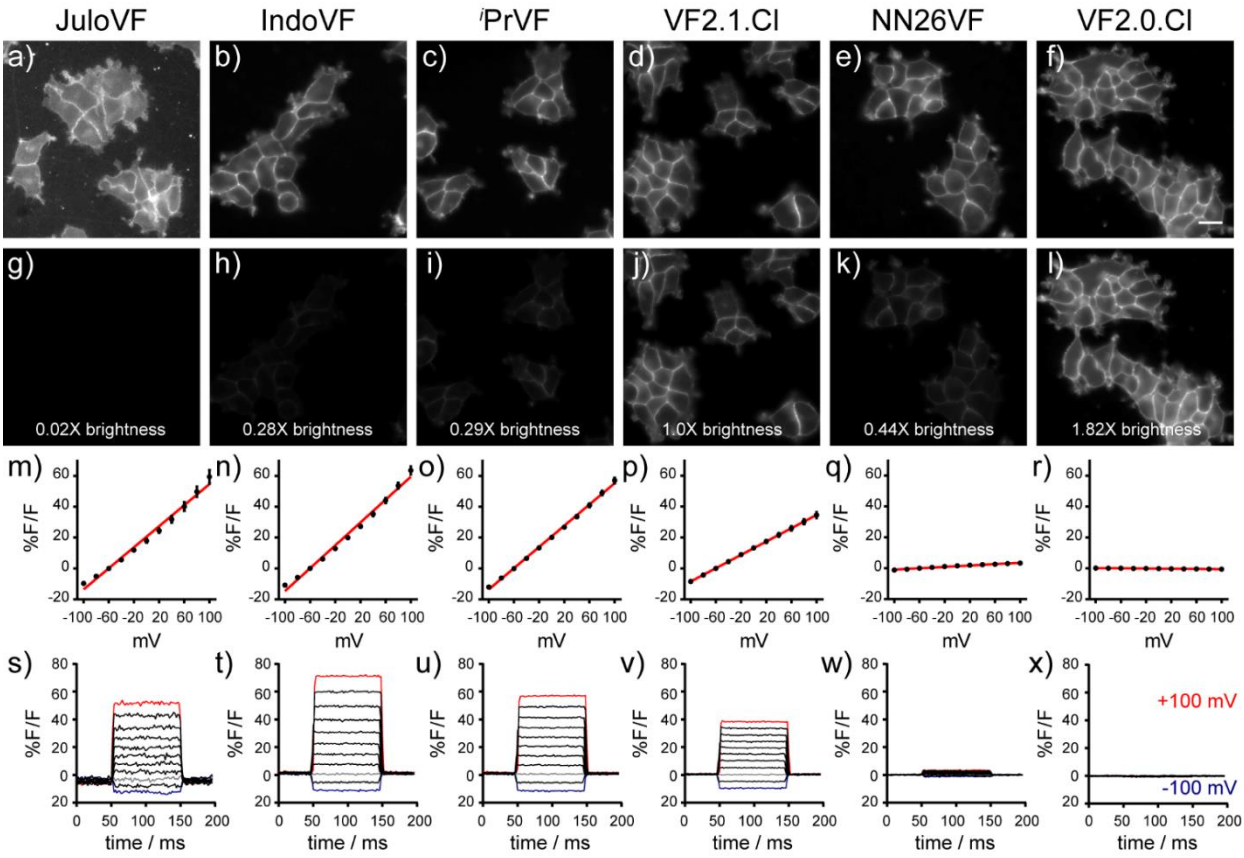

Figure 4-7. HEK293T intensity patching and relative brightness. Voltage sensitivity and relative brightness comparison of VoltageFluor indicators in HEK293T cells with intensity-based imaging. Relative brightness was compared at a working concentration of 300 nM for all dyes. All brightness values are relative to VF2.1.Cl (d,j, 1.0X brightness), and were calculated as the difference between cell signal and the surrounding background (signal-background). Scale bar represents 20 µm. Top row (a-f) images are the same as Figure 2a-f, and display membrane localization for each indicator. The second row (g-l) features the same images, but with consistent pixel histograms across each image to illustrate the relative brightness of membrane staining. Linear plots (m-r) of the percent change in fluorescence versus V_{mem} from whole-cell voltage clamp (m, n=8 cells; n, n=4 cells; o, n=4 cells; p, n=8 cells; q, n=3 cells; r, n=5 cells). For whole-cell voltage clamp experiments, cells were loaded at optimized concentration for each indicator (JuloVF, 500 nM; IndoVF, 300 nM; ^{i}PrVF, 300 nM; VF2.1.Cl, 100 nM; NN26VF, 300 nM; VF2.0.Cl, 100 nM). Representative concatenated traces from a single patched cell (s-x) show the percent change in fluorescence over time as the holding potential is changed from +100 mV (red) to -100 mV (blue) in 20 mV increments.

Figure 4-8. *Concentration dependence of τ_{fl} for four new VFs in HEK293T cells*

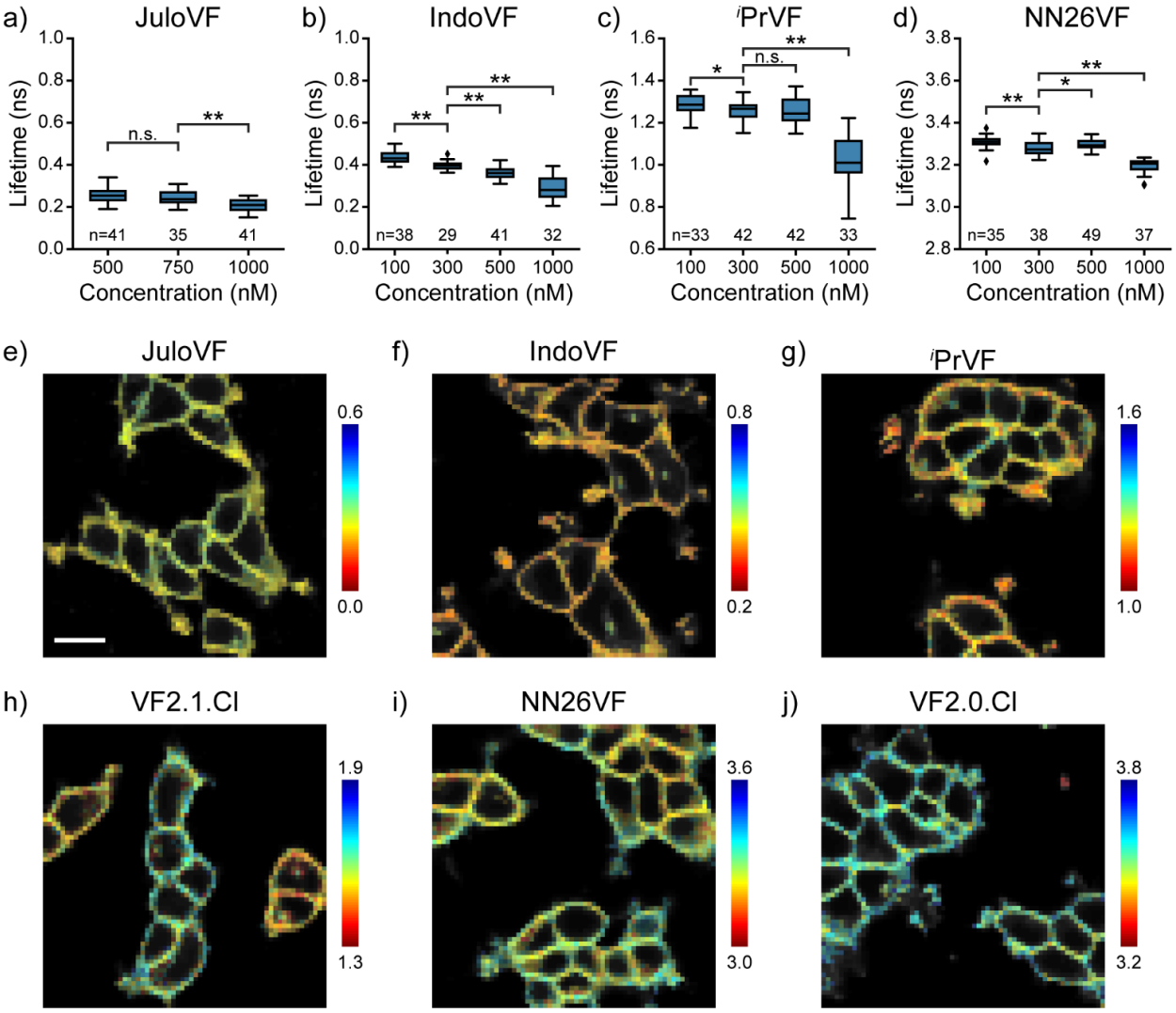

Figure S6. Concentration dependence of τ_{fl} for four new VFs in HEK293T cells. (a-d) Box plots showing the effect of JuloVF, IndoVF, ^{i}PrVF, or NN26VF concentration on fluorescence lifetime in HEK293T cells at rest in imaging buffer. Diamonds represent datapoints more than 1.5 times the interquartile range past an edge of the box. Data were tested for homoscedasticity (Levene's test on the median, many with $p<0.05$). The statistical significance of differences between concentrations were evaluated with Welch's ANOVA; in all cases resulting in $p<0.05$. Asterisks indicate the significance level of Games-Howell post hoc tests (n.s. $p>0.05$, * $p<0.05$, ** $p<0.01$, *** $p<0.001$). For clarity, only the significance level of post hoc comparisons involving the concentration used in this study is shown (300 nM for all probes except JuloVF, where 500 nM was used). e-j) Representative fluorescence lifetime images overlaid on the fluorescence intensity for all six VFs used in this study. Lifetimes are scaled across the same range for electrophysiological studies. Scale bar represents 20 µm.

***Figure 4-9**. Fluorescence lifetime captures absolute sensitivity of VFs*

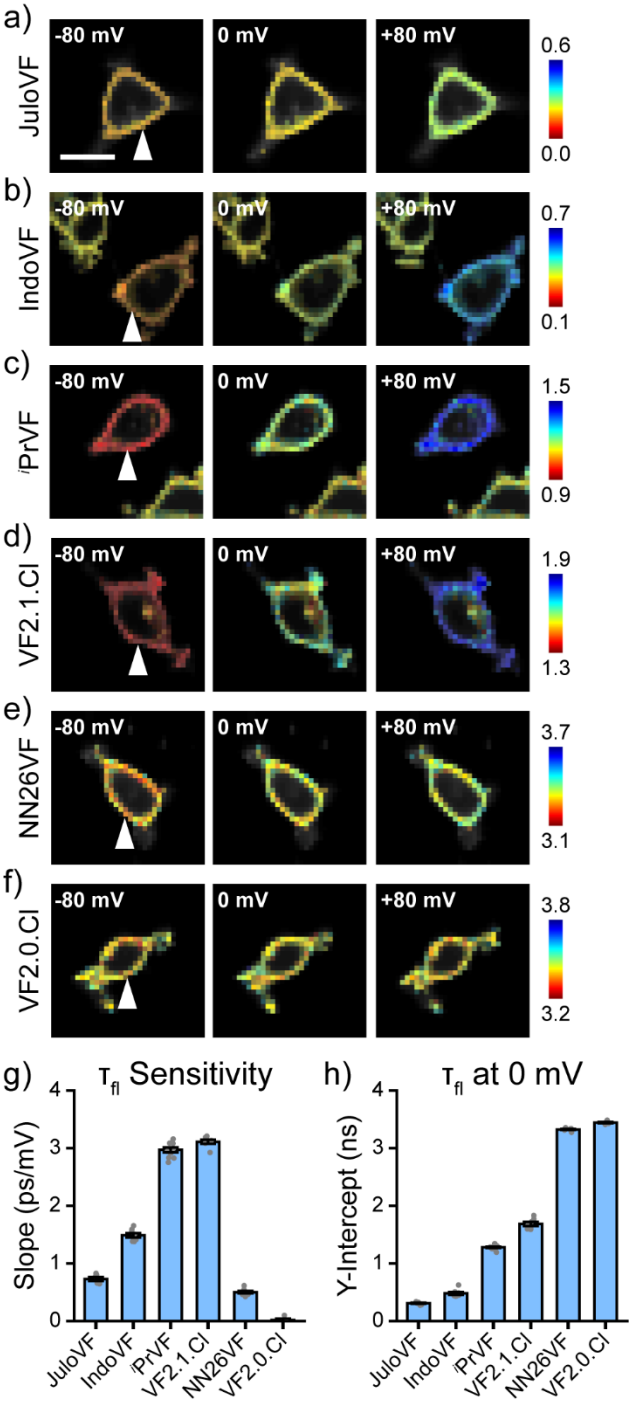

Figure 4-9. Fluorescence lifetime captures absolute sensitivity of VFs. a-f) Lifetime intensity overlay images for HEK293T cells at different V_{mem} stained with JuloVF, IndoVF, ^{i}PrVF, VF2.1.Cl, NN26VF, and VF2.0.Cl, respectively. V_{mem} was held at the indicated value with whole cell voltage clamp electrophysiology. Lifetimes are scaled across the same lifetime range (0.6 ns) with different start and ending values. White arrow indicates voltage-clamped cell. Scale bar represents 20 µm. g) Slope of the line of best fit for the lifetime-V_{mem} calibration for the aniline

modified VF library. Gray points represent measurements from individual cells. h) Y-intercept (0 mV lifetime) from the same lines of best fit as in g. Data are shown as mean ± SEM for the following number of patched cells: JuloVF 6, IndoVF 8, ^{i}PrVF 10, VF2.1.Cl 7, NN26VF 8, VF2.0.Cl 5.

Figure 4-10. *V_{mem} sensitivity of the fluorescence lifetime of JuloVF.*

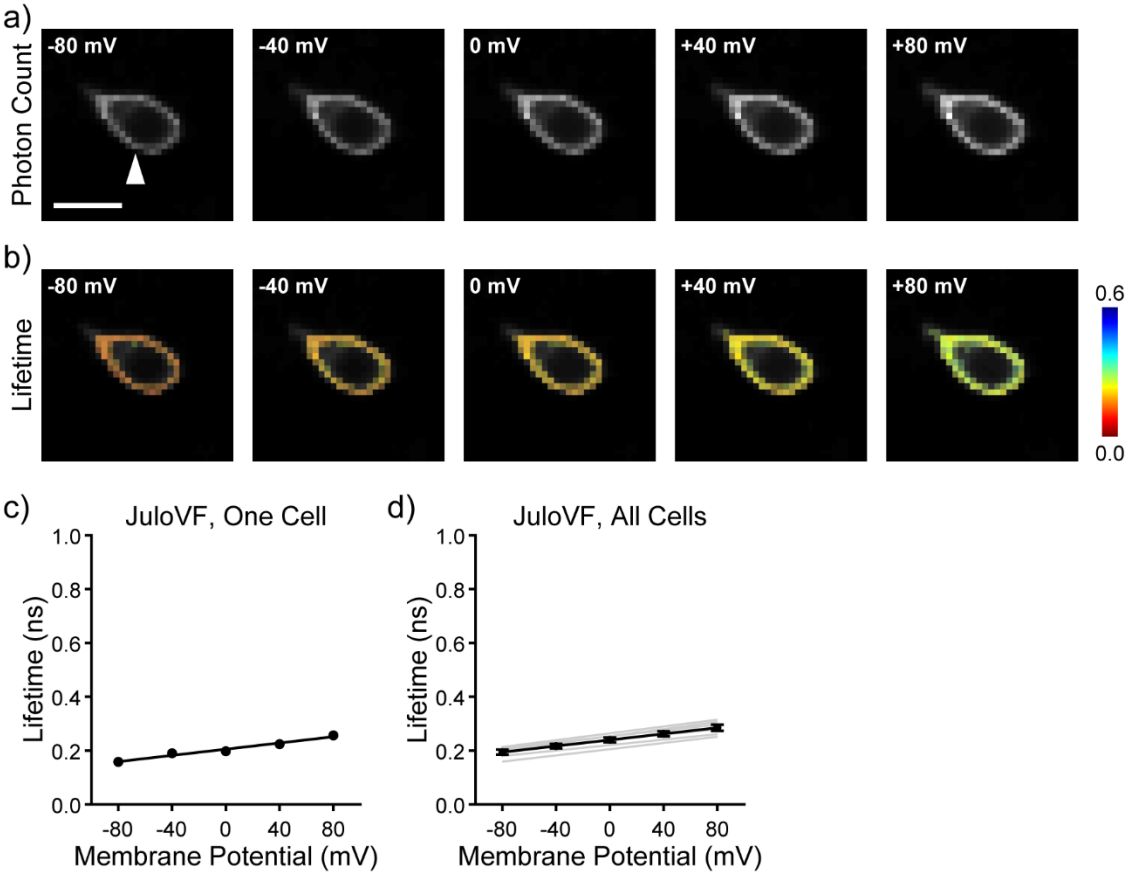

Figure 4-10. V_{mem} sensitivity of the fluorescence lifetime of JuloVF. (a) Photon count images of JuloVF in a HEK293T cell held at the indicated V_{mem} by whole cell patch clamp electrophysiology. The white arrow indicates the patch pipette; scale bar represents 20 µm. b) Lifetime-intensity overlay images of JuloVF as in (a). The time-resolved fluorescence decay for JuloVF was modeled as a sum of three exponential terms; the weighted average is shown here. Lifetime scale is in ns. c) Quantification of average lifetime at the plasma membrane for the individual cell shown in (a-b). The line of best fit for τ_{fl} vs. V_{mem} is shown in black. d) The average τ_{fl}-V_{mem} relationship for JuloVF (black line), as well as lines of best fit for each individual patched cell (gray, n=6 cells).

Figure 4-11. *V_{mem} sensitivity of the fluorescence lifetime of IndoVF.*

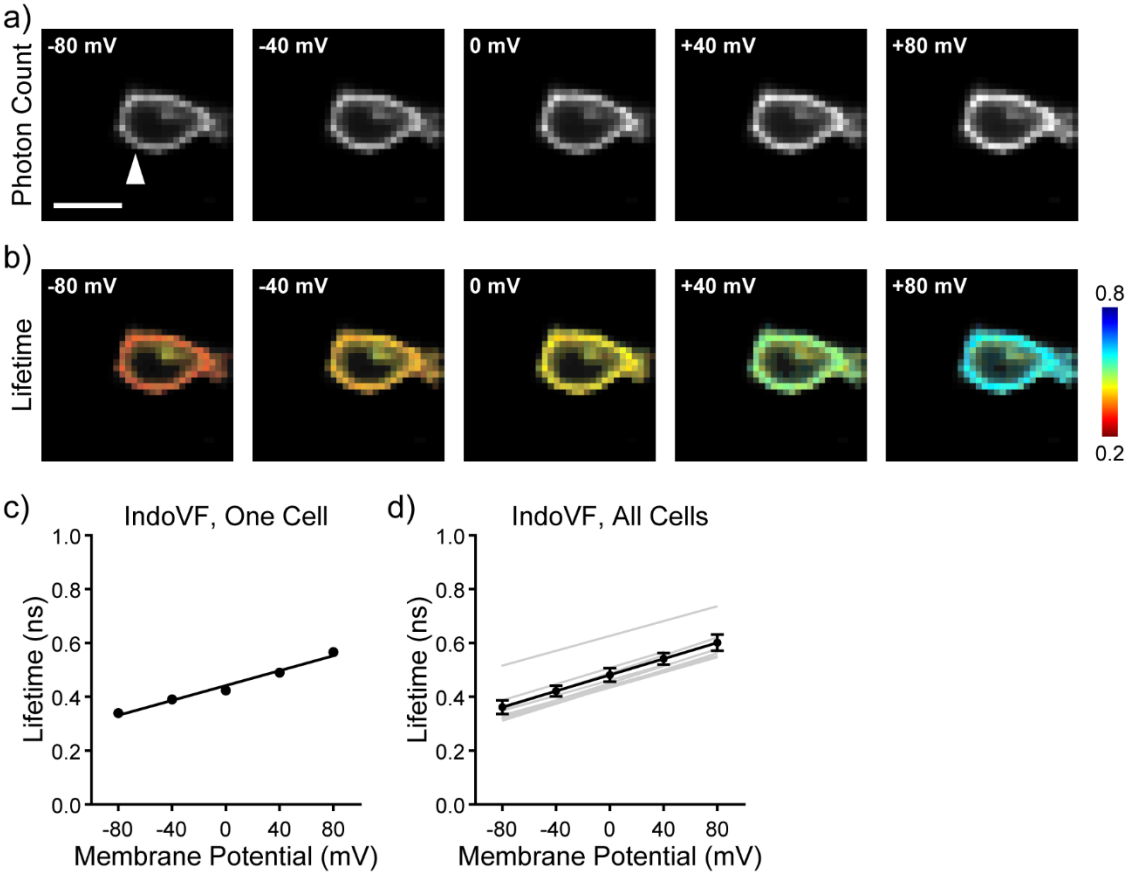

Figure 4-11. V_{mem} sensitivity of the fluorescence lifetime of IndoVF. (a) Photon count images of IndoVF in a HEK293T cell held at the indicated V_{mem} by whole cell patch clamp electrophysiology. The white arrow indicates the patch pipette; scale bar represents 20 µm. b) Lifetime-intensity overlay images of IndoVF as in (a). The time-resolved fluorescence decay for IndoVF was modeled as a sum of three exponential terms; the weighted average is shown here. Lifetime scale is in ns. c) Quantification of average lifetime at the plasma membrane for the individual cell shown in (a-b). The line of best fit for τ_{fl} vs. V_{mem} is shown in black. d) The average τ_{fl}-V_{mem} relationship for IndoVF (black line), as well as lines of best fit for each individual patched cell (gray, n=8 cells).

Figure 4-12. *V_{mem} sensitivity of the fluorescence lifetime of ^{i}PrVF.*

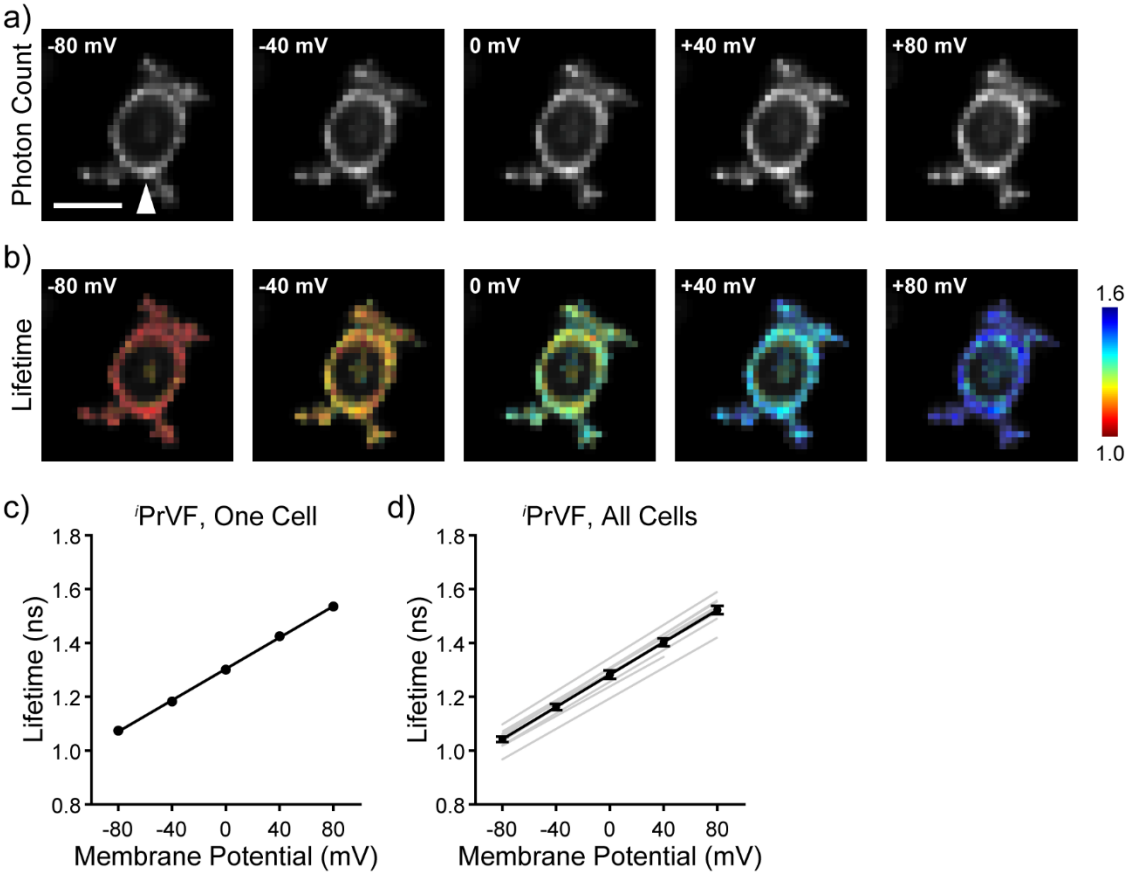

Figure 4-12. V_{mem} sensitivity of the fluorescence lifetime of ^{i}PrVF. (a) Photon count images of ^{i}PrVF in a HEK293T cell held at the indicated V_{mem} by whole cell patch clamp electrophysiology. The white arrow indicates the patch pipette; scale bar represents 20 µm. b) Lifetime-intensity overlay images of ^{i}PrVF as in (a). The time-resolved fluorescence decay for ^{i}PrVF was modeled as a sum of two exponential terms; the weighted average is shown here. Lifetime scale is in ns. c) Quantification of average lifetime at the plasma membrane for the individual cell shown in (a-b). The line of best fit for τ_{fl} vs. V_{mem} is shown in black. d) The average τ_{fl}-V_{mem} relationship for ^{i}PrVF (black line), as well as lines of best fit for each individual patched cell (gray, n=10 cells).

Figure 4-13. *V_{mem} sensitivity of the fluorescence lifetime of VF2.1.Cl*

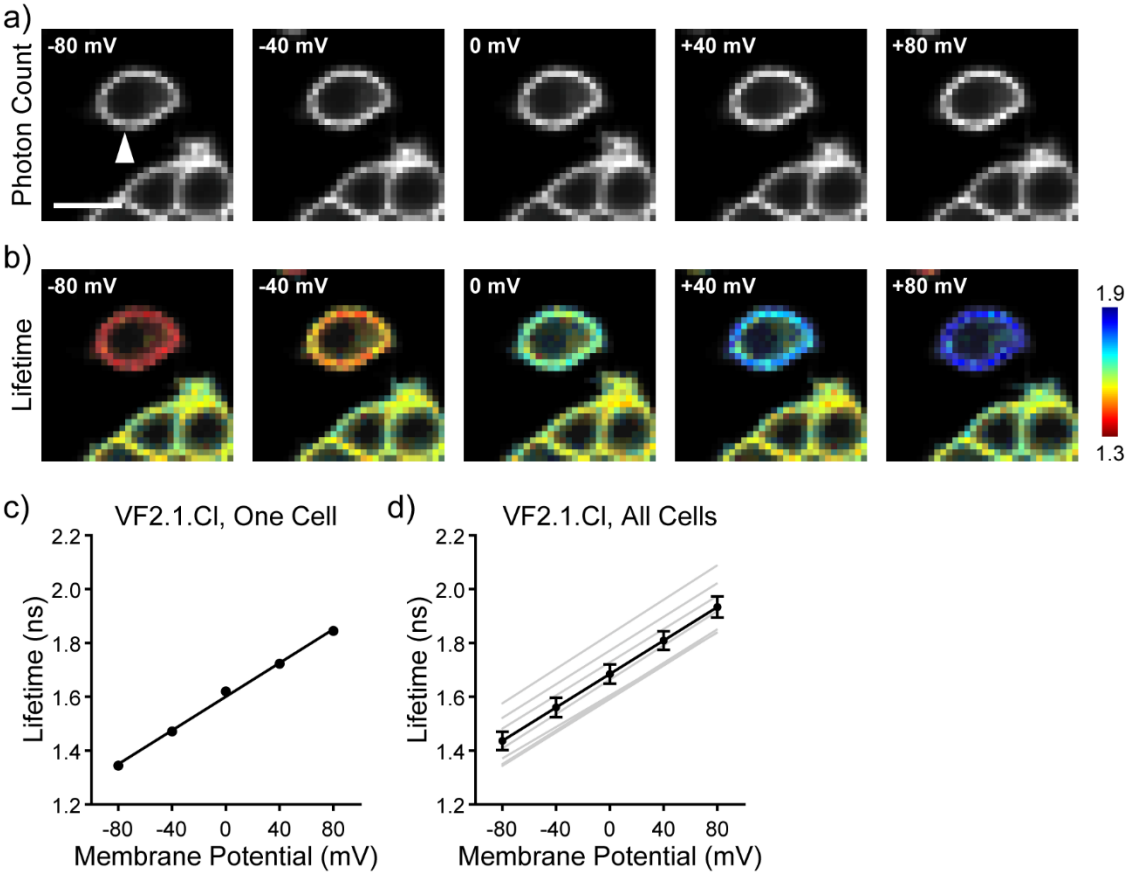

Figure 4-13. V_{mem} sensitivity of the fluorescence lifetime of VF2.1.Cl. The relationship between fluorescence lifetime and V_{mem} for VF2.1.Cl was previously reported by our lab;[19] we repeated the experiment independently here for maximum comparability with the rest of the VF series presented here. These results are in good agreement with our previous work. a) Photon count images of VF2.1.Cl in a HEK293T cell held at the indicated V_{mem} by whole cell patch clamp electrophysiology. The white arrow indicates the patch pipette; scale bar represents 20 µm. b) Lifetime-intensity overlay images of VF2.1.Cl as in (a). The time-resolved fluorescence decay for ^{i}PrVF was modeled as a sum of two exponential terms; the weighted average is shown here. Lifetime scale is in ns. c) Quantification of average lifetime at the plasma membrane for the individual cell shown in (a-b). The line of best fit for τ_{fl} vs. V_{mem} is shown in black. d) The average τ_{fl}-V_{mem} relationship for VF2.1.Cl (black line), as well as lines of best fit for each individual patched cell (gray, n=7 cells).

Figure 4-14. *V_{mem} sensitivity of the fluorescence lifetime of NN26VF*

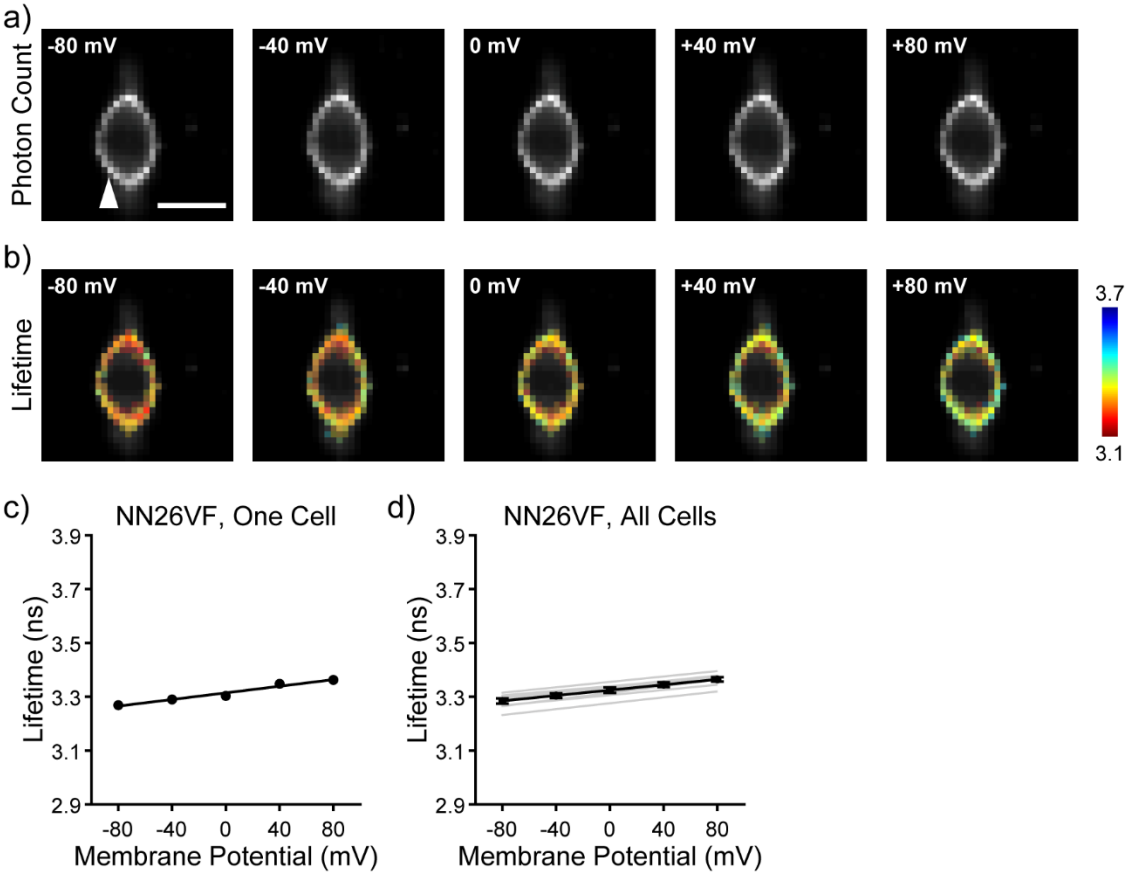

Figure 4-14. V_{mem} sensitivity of the fluorescence lifetime of NN26VF. (a) Photon count images of NN26VF in a HEK293T cell held at the indicated V_{mem} by whole cell patch clamp electrophysiology. The white arrow indicates the patch pipette; scale bar represents 20 µm. b) Lifetime-intensity overlay images of NN26VF as in (a). The time-resolved fluorescence decay for NN26VF was described by a single exponential decay term. Lifetime scale is in ns. c) Quantification of the NN26VF fluorescence lifetime at the plasma membrane for the individual cell shown in (a-b). The line of best fit for τ_{fl} vs. V_{mem} is shown in black. d) The average τ_{fl}-V_{mem} relationship for NN26VF (black line), as well as lines of best fit for each individual patched cell (gray, n=8 cells).

Figure 4-15. *The fluorescence lifetime of VF2.0.Cl is not sensitive to* V_{mem}

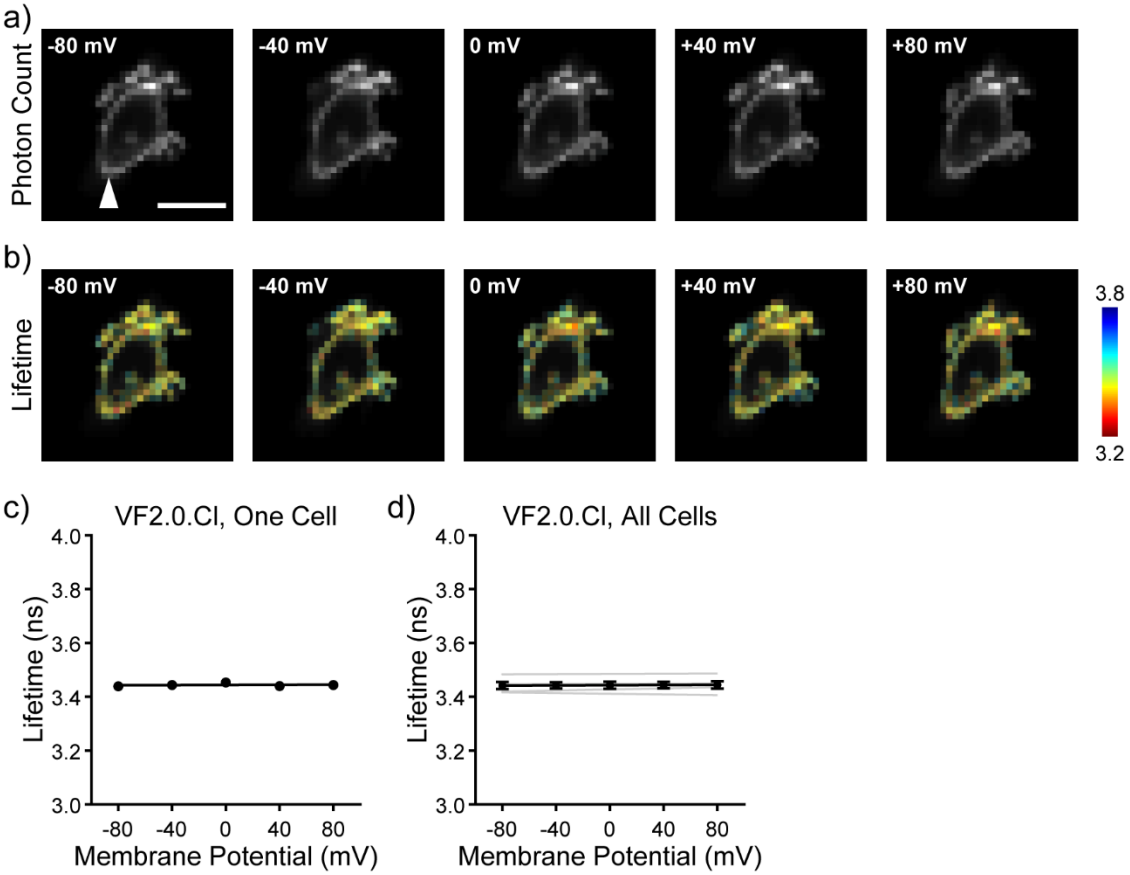

Figure 4-15. The fluorescence lifetime of VF2.0.Cl is not sensitive to V_{mem}. The voltage-insensitivity of the fluorescence lifetime of VF2.0.Cl was previously reported by our lab;[19] we repeated the experiment independently here for maximum comparability with the rest of the VF series presented here. These results are in good agreement with our previous work. a) Photon count images of VF2.0.Cl in HEK293T cells held at the indicated V_{mem} by whole cell patch clamp electrophysiology. The white arrow indicates the patch pipette; scale bar represents 20 µm. b) Lifetime-intensity overlay images of VF2.1.Cl as in (a). The time-resolved fluorescence decay for VF2.0.Cl was modeled with a single exponential term. Lifetime scale is in ns. c) Quantification of average lifetime at the plasma membrane for the individual cell shown in (a-b). The line of best fit for τ_{fl} vs. V_{mem} is shown in black. d) The average τ_{fl}-V_{mem} relationship for VF2.0.Cl (black line), as well as lines of best fit for each individual patched cell (gray, n=7 cells).

Figure 4-16. *Effect of fit model on the value and the V_{mem} sensitivity of the VF2.1.Cl fluorescence lifetime.*

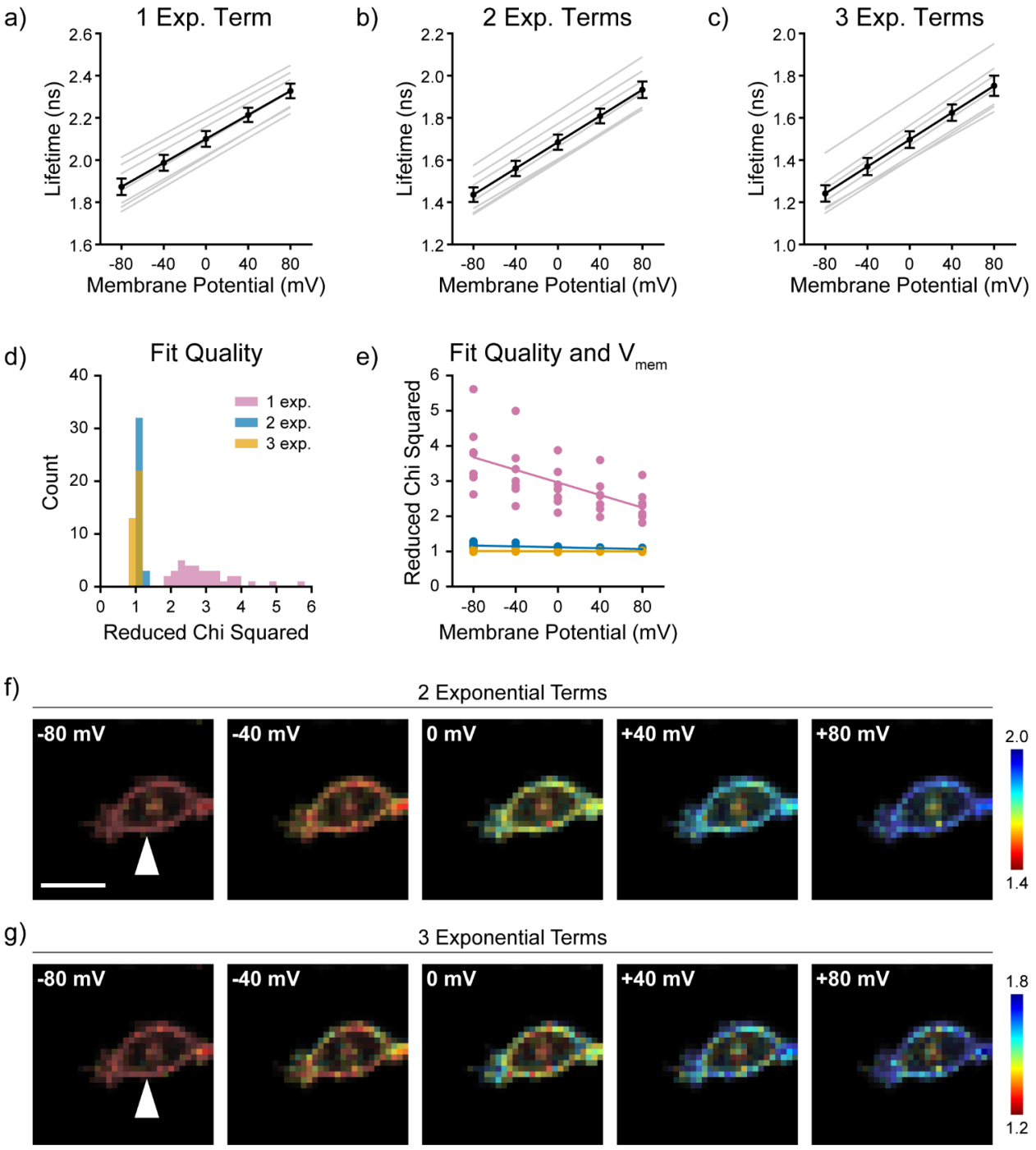

Figure 4-16. Effect of fit model on the value and the V_{mem} sensitivity of VF2.1.Cl fluorescence lifetime. The relationship between Vmem and τ_{fl} of VF2.1.Cl in HEK293T was confirmed by whole cell patch clamp electrophysiology in HEK293T cells. V_{mem} was set with whole cell voltage clamp electrophysiology; the patch electrode is indicated by the white arrow. Previously reported τ_{fl} data for VF2.1.Cl was modeled with two exponential components;[19] here we show in details the process of selecting a satisfactory number of terms in a fluorescence lifetime

decay model. a-c) The relationship between τ_{fl} and V_{mem} for VF2.1.Cl in HEK293T when VF2.1Cl τ_{fl} is described by a sum of one, two, or three exponential components (n=7 cells). The overall relationship is preserved, although the 0 mV lifetime shifts considerably across the three models. d) The quality of the exponential fit, as described by the reduced chi squared (χ^2, see **Methods**). Each value in the histogram is an individual measurement at a particular V_{mem}; therefore, each patch is represented by 4 or 5 values in the histogram). e) V_{mem} dependence of the fit quality of the exponential fit. Each point represents an individual measurement as in (d); each line represents the line of best fit for χ^2 vs V_{mem}. If a fit model adequately describes the V_{mem} sensitivity of a VoltageFluor, there should be no V_{mem} dependence in χ^2. f-g) Representative images of the fluorescence lifetime of VF2.1.Cl fit pixel-by-pixel in a HEK293T cell. Increased variability between nearby pixels is observed when a third exponential component is added. Scale bar represents 20 μm.

Figure 4-17. *Fluorescence lifetime fit model selection for all VF derivatives*

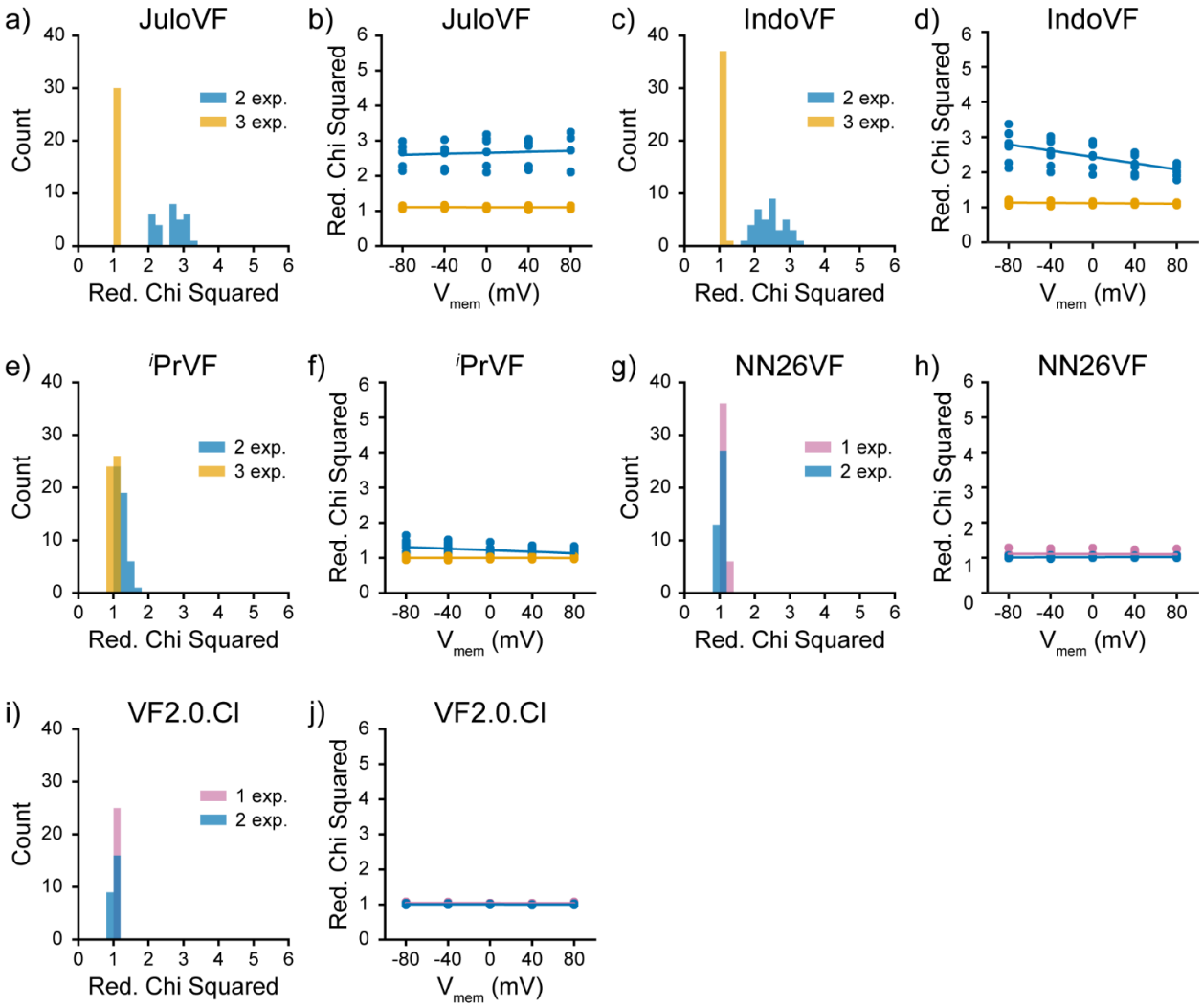

Figure 4-17 Fluorescence lifetime fit model selection for all VF derivatives. Selection of the appropriate number of exponential terms in the fluorescence lifetime decay model was based on minimization of reduced chi squared χ^2 and avoidance of V_{mem} dependence in χ^2. a) Comparison of χ^2 when the time resolved fluorescence decay of JuloVF is modeled as a sum of two or three exponential components b) Relationship between V_{mem} χ^2 for JuloVF. Measurements from individual cells are shown as markers; for closely spaced results, markers may overlap. The line of best fit for χ^2 vs. V_{mem} for each fit model is shown. c-d) Evaluation of χ^2 overall and as it relates to V_{mem} for IndoVF when its fluorescence lifetime is modeled as a sum of two or three exponential terms. e-f) Evaluation of χ^2 overall and as it relates to V_{mem} for ^{i}PrVF when modeled as a sum of two or three exponential terms. g-h) Evaluation of χ^2 overall and as it relates to V_{mem} for NN26VF when modeled as a single exponential decay or as a sum of two exponential terms. i-j) Evaluation of χ^2 overall and as it relates to V_{mem} for VF2.0.Cl when the fluorescence lifetime of VF2.0.Cl is modeled as a single exponential decay or as a sum of two exponential terms. Each measurement on each cell at a given potential is represented individually (i.e. each patch has 4 or 5 values in the histogram, one for each recorded V_{mem}). Sample sizes (number of HEK293T cells patched): JuloVF 6, IndoVF 8, ^{i}PrVF 10, NN26VF 8, VF2.0.Cl 5.

Figure 4-18. *Percent change in τ_{fl} and goodness of linear fit for V_{mem}-τ_{fl} calibrations*

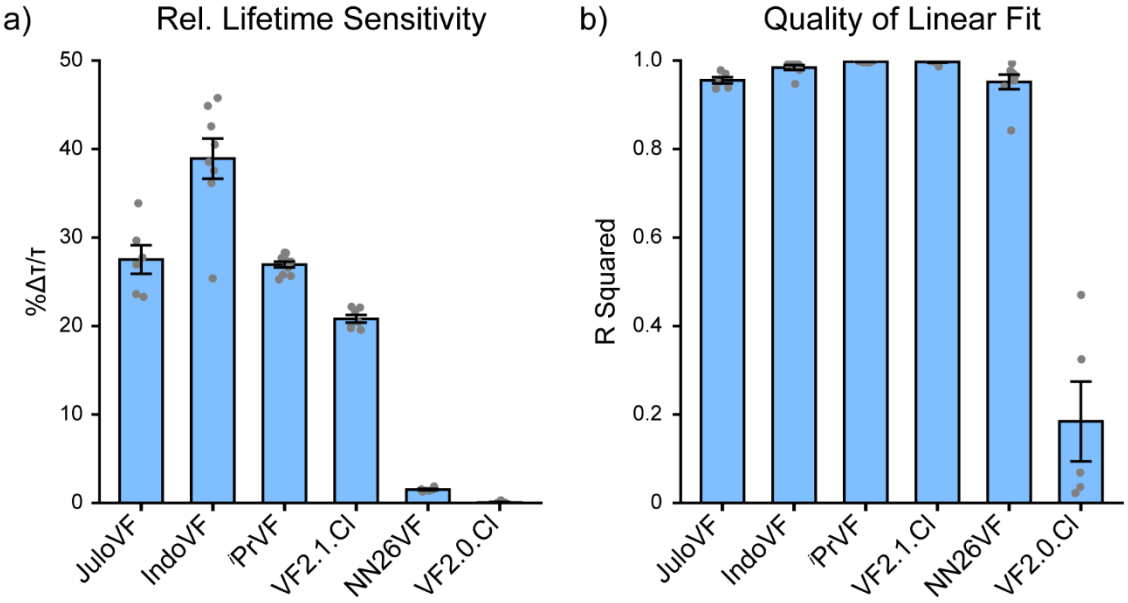

Figure 4-18. Percent change in τ_{fl} and goodness of linear fit for V_{mem}-τ_{fl} calibrations. a) Percent change in τ_{fl} per 100 mV change, relative to the lifetime at -60 mV. b) Quality of the linear fit (as evaluated by the squared correlation coefficient, r^2) for the V_{mem}-τ_{fl} relationship of each VF. Each gray dot represents an individual patched HEK293T cell; bars represent mean ± SEM. Sample sizes (number of individual HEK293T cells): JuloVF 6, IndoVF 8, ^{i}PrVF 10, VF2.1.Cl 7, NN26VF 8, VF2.0.Cl 5.

***Figure 4-19**. Performance at signal detection in excitable cells*

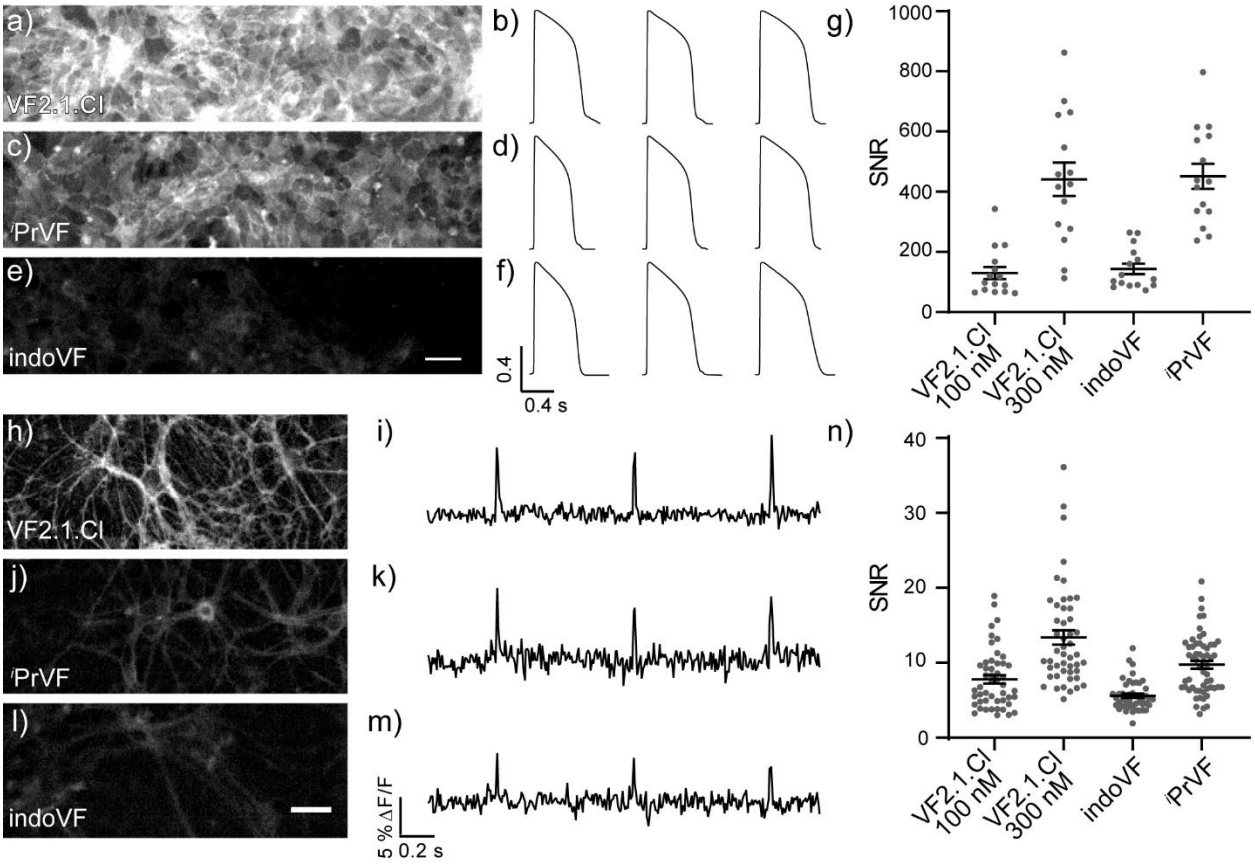

Figure 4-19. Performance at signal detection in excitable cells. Representative field of view (FOV) used for recordings of electrical activity in iPSC-CMs using (a) VF2.1.Cl, (c) *i*PrVF, and (e) IndoVF. Scale bar represents 50 µm. Average action potentials from single ten second acquisitions (3 total traces) sampled at 0.2 kHz taken with 300 nM (b) VF2.1.Cl, (d) *i*PrVF, and (f) IndoVF. (g) Plot of signal-to noise ratio (SNR) shows the difference in signal detection using different VoltageFluor indicators. Dots are the SNR for a single acquisition, bars are mean ± SEM. N = 15 traces. Images in dissociate rat hippocampal neuron culture using (h) VF2.1.Cl, (j) *i*PrVF, and (l) IndoVF. Scale bar is 40 µm. Single epochs of activity showing three evoked spikes from a single cell using (i) VF2.1.Cl, (k) *i*PrVF, and (m) IndoVF. (n) SNR plot of evoked spikes using each indicator, dots indicate a single spike. Bars are the mean ± SEM.

Figure 4-20. *Functional comparison of VoltageFluor indicators in hiPSC-CMs*

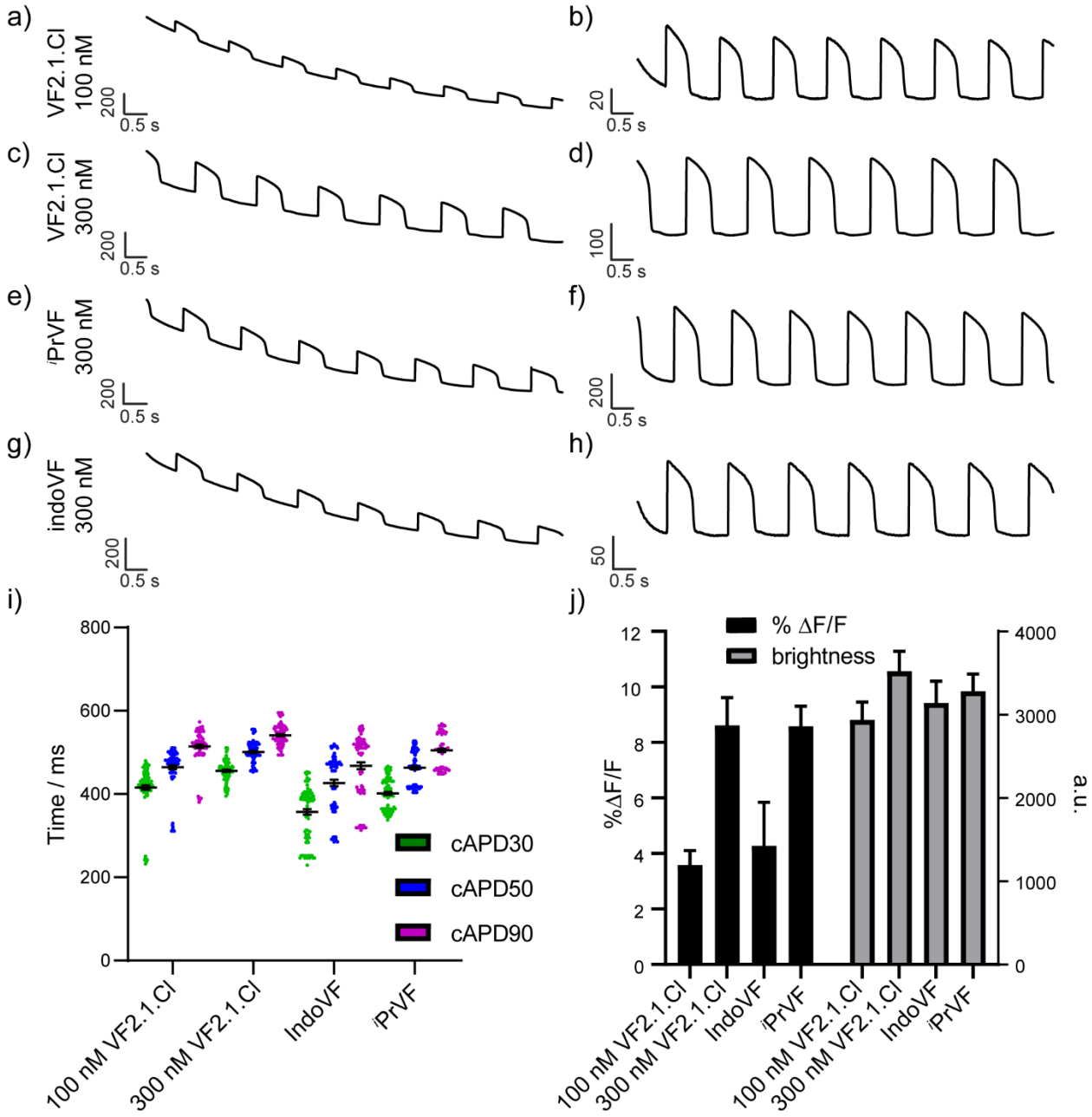

Figure 4-20. Functional comparison of VoltageFluor indicators in hiPSC-CMs. Representative uncorrected (a, c, e, g) and bleach-corrected (b, d, f, h) functional recordings of spontaneous activity in hiPSC-CMs. Recordings were made for 10 seconds; bleach correction was made by subtracting the exponential decay calculated by an asymmetric least-squares fit to the raw trace. Of the VoltageFluors tested, each has a similar photobleach decay (see **Figure 4-23**). i) Scatter plot of corrected action potential duration (cAPD) values at 30, 50, and 90% of the repolarization recorded with VoltageFluors. cAPD, and action potential morphology, was not affected by the identity of VoltageFluor used in these studies. Bars represent mean ± SEM. Samples were taken from 3 wells per condition, with 5 fields of view per well for a total of 15 recordings per condition. Sample size (number of individual action potentials recorded): 100 nM – VF2.1.Cl 100, 300 nM – VF.2.1.Cl 103, IndoVF 89, ^{i}PrVF 102. j) Bar plot of mean %ΔF/F (left y-axis, black bars),

and mean brightness (right y-axis, grey bars). Brightness was calculated as the average pixel intensity of the baseline of the fluorescence trace. IndoVF and ^{i}PrVF were loaded at a concentration of 300 nM. As with SNR, IndoVF performs similarly in %ΔF/F and has a similar brightness to VF2.1.Cl loaded at 100 nM, and ^{i}PrVF performs similarly to VF2.1.Cl loaded at 300 nM.

Figure 4-21. *Functional comparison of VoltageFluor indicators in rat hippocampal neurons*

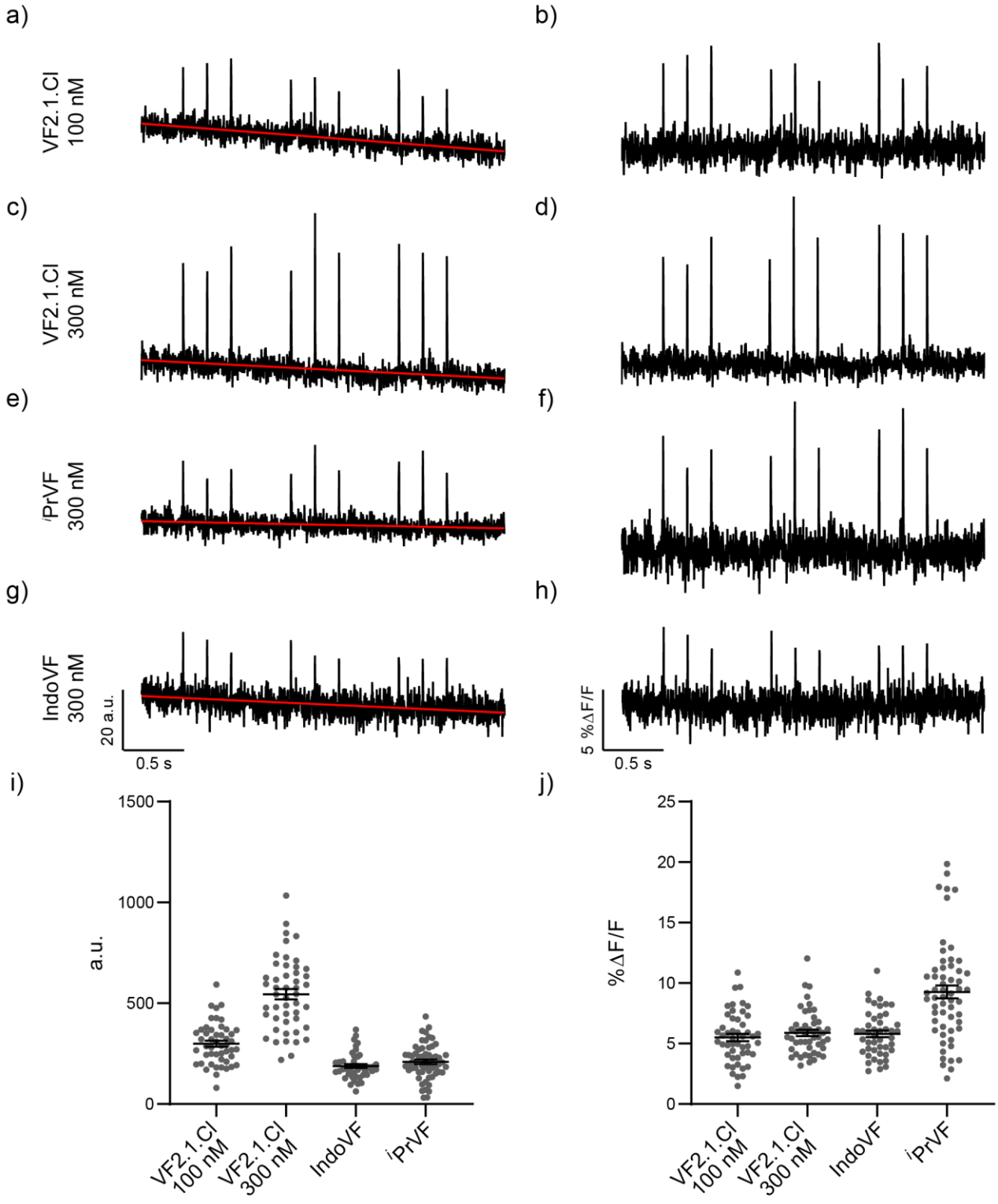

Figure 4-21. Functional comparison of VoltageFluor indicators in rat hippocampal neurons. **(**a, c, e, g) Representative background-corrected traces (black) of evoked activity in rat hippocampal neurons and regression lines (red) fit to the respective traces for VF2.1.Cl 100 nM (a), VF2.1.Cl 300 nM (c), ^{i}PrVF 300 nM (e), and IndoVF 300 nM (g). b, d, f, h) %ΔF/F traces (black) of evoked activity in rat hippocampal neurons for VF2.1.Cl 100 nM (b), VF2.1.Cl 300 nM (d), ^{i}PrVF 300 nM (f), and IndoVF 300 nM (h). %ΔF/F traces were obtained from the background-corrected traces using the methodology described in **Methods**. Evoked activity in rat hippocampal neurons. i) Plot of the raw fluorescence values of each dye in rat hippocampal neurons. Each grey dot represents a background-corrected first frame fluorescence value for one measurement of evoked activity; bars represent mean ± SEM. j) Plot of the %ΔF/F values for evoked activity in rat hippocampal neurons. Each grey dot represents the %ΔF/F value of the first action potential in one measurement of evoked activity; bars represent mean ± SEM.

Figure 4-22. *Cardiotoxicity with prolonged illumination of VoltageFluors*

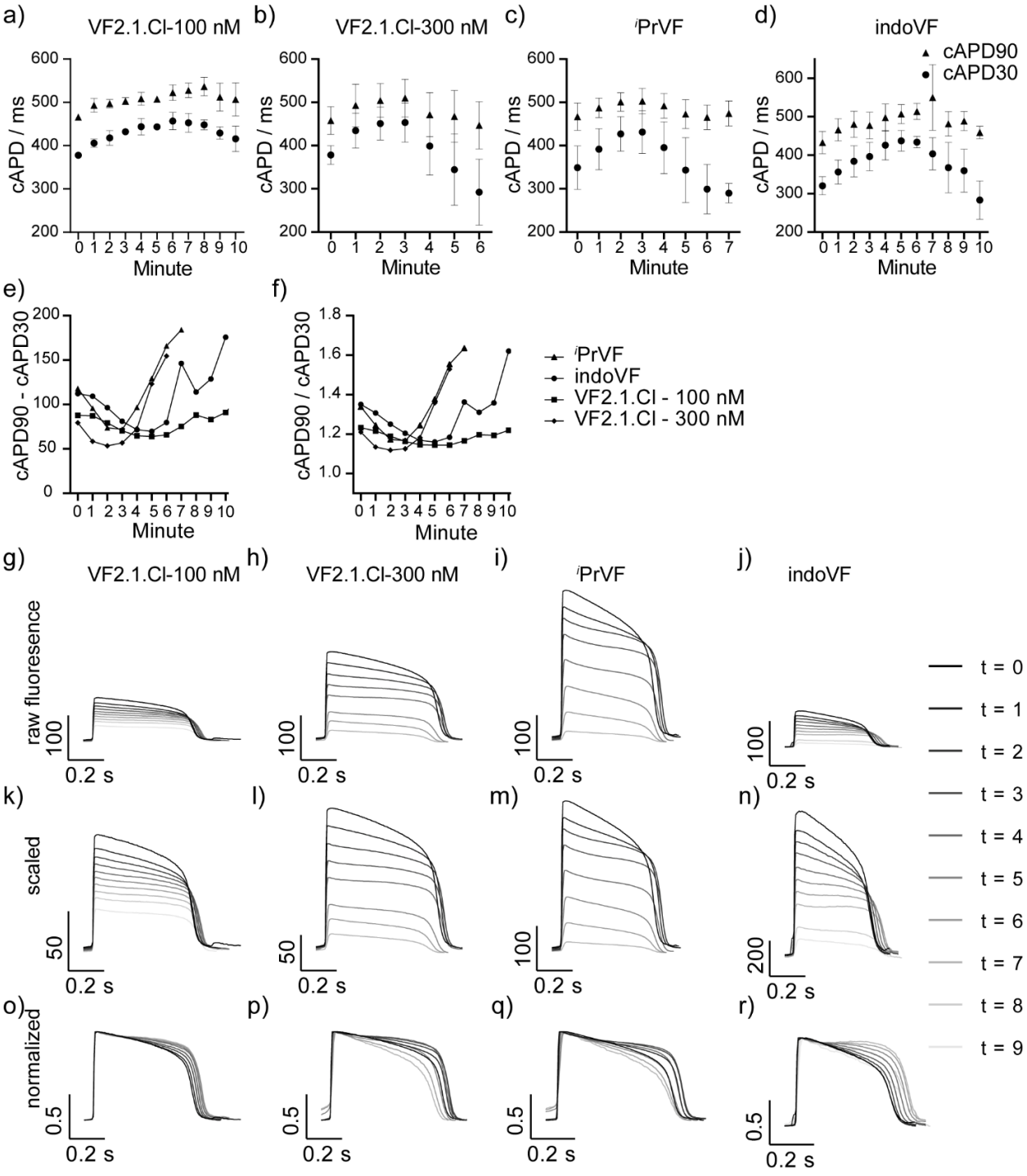

Figure 4-22. Cardiotoxicity with prolonged illumination of VoltageFluors. The phototoxicity of VoltageFluors was examined in hiPSC-CMs by prolonged, continuous exposure to the excitation LED. Action potential morphology was monitored through 10 second recordings made each minute (a-d) and quantified using cAPD. Deviations in cAPD from starting values (recording made at 0 minutes) can be interpreted as an action potential morphology change, which is indicative of potential phototoxic effects. As previously observed,[15] decreasing the concentration of VF2.1.Cl to

100 nM (a) from 300 nM (b) permits recordings over extended times with minimal change to action potential morphology. ^{i}PrVF (c, 300 nM) performs similarly to VF2.1.Cl loaded at 300 nM (b), permitting recordings for 3 minutes of constant illumination before AP morphology changes are seen. IndoVF (d, 300 nM) resembles VF2.1.Cl loaded at a lower concentration (a, 100 nM), as AP morphology changes are not observed until extended illumination periods. AP morphology changes were also quantified by the difference (e) and ratio (f) of cAPD90 and cAPD30. Deviations from initial values indicate changes to AP morphology. In the case of the VoltageFluors tested, both the difference and ratio of cAPD90 and cAPD30 increases over prolonged exposure to excitation light, indicating a prolongation of phase 2 in the cardiac AP and an overall increase in duration. (g-j) Representative fluorescence traces from a single trial, each action potential is the mean trace from a single 10 second recording. As time progresses (purple to cream), the amplitude of the cardiac action potential decreases regardless of VoltageFluor used due to photobleaching. (k-n) Scaled fluorescence traces more clearly show the decrease in amplitude for each VoltageFluor. (o-r) Normalized fluorescence traces show the change in action potential morphology with increased illumination.

Figure 4-23. *Comparison of VF bleach rate in HEK293T, iCMs, and rat hippocampal neurons*

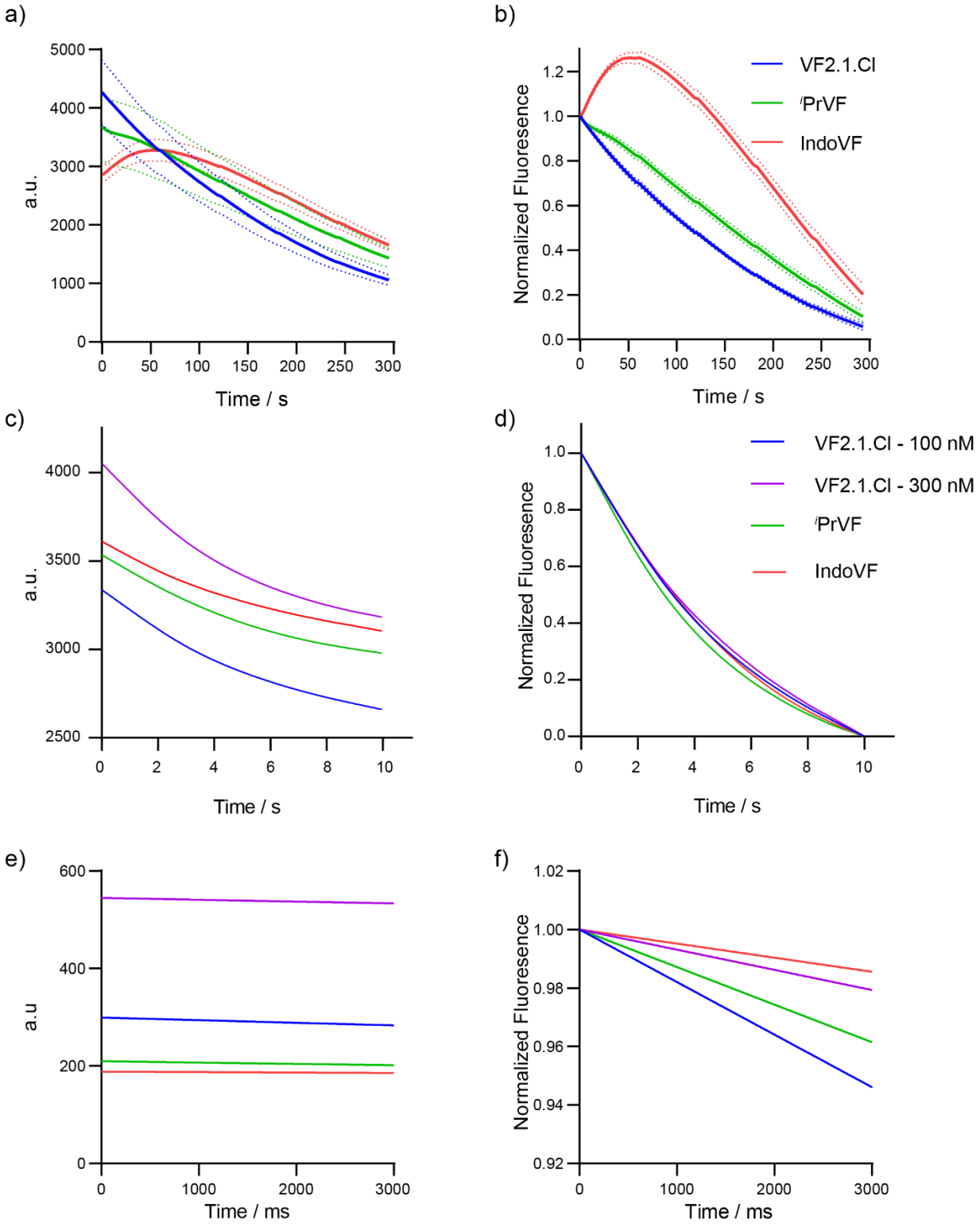

Figure 4-23. Comparison of VF bleach rate in HEK293T, iCMs, and rat hippocampal neurons. (a) Photobleaching in HEK293T cells, sampled at 1 Hz for five minutes. (b) Normalized values in HEK293T cells. (c) Average splines used for photobleach correction by asymmetric least-square fit (Methods) of the first ten seconds of recording in iPSC-CMs. (d) Average bleach splines from (c) normalized to show relative rates of decay. (e) Average bleaching traces for evoked activity experiments in neurons. The y-intercept is the average fluorescence value of the first frame of the background-subtracted traces for each dye. The slope is the average slope of the regression lines which were fit to the background-corrected traces for each dye and used to correct for bleaching. f) Each trace from (e) normalized.

***Figure 4-24**. Fluorescence lifetime change dictates VF performance*

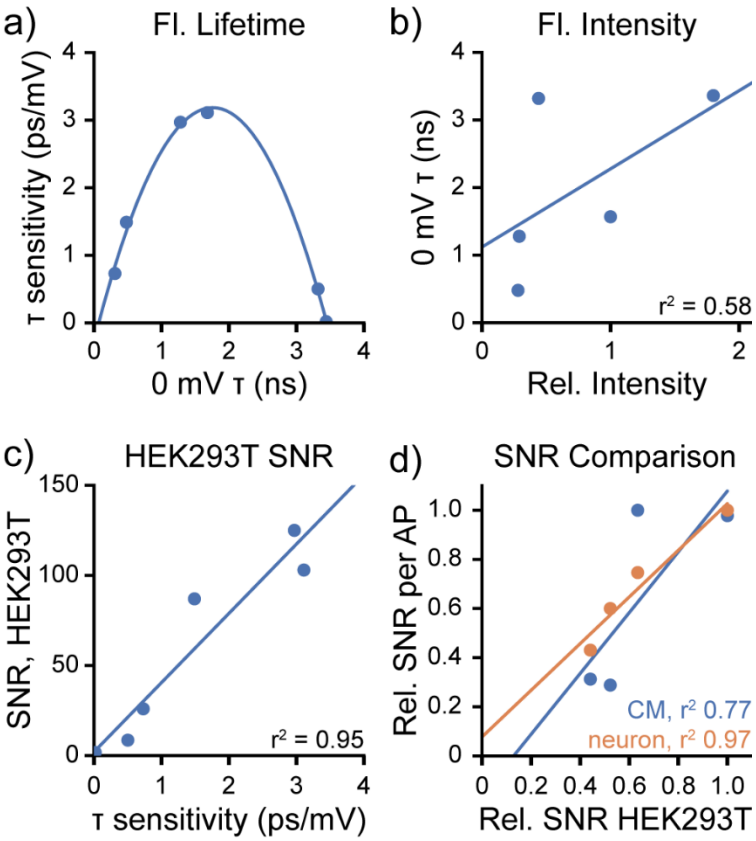

Figure 4-24. Fluorescence lifetime change dictates VF performance. Data shown here are aggregated to highlight properties of the VF library. a) The sensitivity (ps/mV) and 0 mV lifetime (ns) of VF fluorescence lifetimes in HEK293T exhibit a parabolic relationship. b) The relative fluorescence intensity of VFs does not display the same trend as τ_{fl}. Fluorescence intensity of VFs at 300 nM in HEK293T is shown here; JuloVF is omitted because no lifetime data were taken at 300 nM. c) Correlation between the signal to noise ratio (SNR) of a 100 mV V_{mem} step (-60 to +40 mV) with the SNR for detection spontaneous action potentials (APs) in cardiomyocytes (CM, blue) or neurons (orange). The SNR for each probe in each system was normalized to the maximum SNR seen in that system for ease of comparison. d) Correlation between the SNR in HEK293T (as in c) and the sensitivity of τ_{fl} to V_{mem}. Data are represented as the mean; error bars are omitted for clarity.

4.11 References

(1) Armstrong, C. M.; Gilly, W. F. Access Resistance and Space Clamp Problems Associated with Whole-Cell Patch Clamping. *Methods Enzymol.* **1992**, *207*, 100–122.

(2) Williams, S. R.; Mitchell, S. J. Direct Measurement of Somatic Voltage Clamp Errors in Central Neurons. *Nat. Neurosci.* **2008**, *11* (7), 790–798.

(3) Knöpfel, T.; Song, C. Optical Voltage Imaging in Neurons: Moving from Technology Development to Practical Tool. *Nat. Rev. Neurosci.* **2019**, *20* (12), 719–727.

(4) Miller, E. W. Small Molecule Fluorescent Voltage Indicators for Studying Membrane Potential. *Curr. Opin. Chem. Biol.* **2016**, *33*, 74–80.

(5) Tsien, R. Y. New Calcium Indicators and Buffers with High Selectivity Against Magnesium and Protons: Design, Synthesis, and Properties of Prototype Structures. *Biochemistry* **1980**, *19* (11), 2396–2404.

(6) Paredes, R. M.; Etzler, J. C.; Watts, L. T.; Zheng, W.; Lechleiter, J. D. Chemical Calcium Indicators. *Methods* **2008**, *46* (3), 143–151.

(7) Grimm, J. B.; Muthusamy, A. K.; Liang, Y.; Brown, T. A.; Lemon, W. C.; Patel, R.; Lu, R.; Macklin, J. J.; Keller, P. J.; Ji, N.; et al. A General Method to Fine-Tune Fluorophores for Live-Cell and in Vivo Imaging. **2017**, *14* (10).

(8) Uno, S.; Kamiya, M.; Yoshihara, T.; Sugawara, K.; Okabe, K.; Tarhan, M. C.; Fujita, H.; Funatsu, T.; Okada, Y.; Tobita, S.; et al. A Spontaneously Blinking Fluorophore Based on Intramolecular Spirocyclization for Live-Cell Super-Resolution Imaging. *Nat. Chem.* **2014**, *6* (8), 681–689.

(9) Kulkarni, R. U.; Kramer, D. J.; Pourmandi, N.; Karbasi, K.; Bateup, H. S. Voltage-Sensitive Rhodol with Enhanced Two-Photon Brightness. **2017**, No. 22.

(10) Woodford, C. R.; Frady, E. P.; Smith, R. S.; Morey, B.; Canzi, G.; Palida, S. F.; Araneda, R. C.; Kristan, W. B.; Kubiak, C. P.; Miller, E. W.; et al. Improved PeT Molecules for Optically Sensing Voltage in Neurons. *J. Am. Chem. Soc.* **2015**, *137* (5), 1817–1824.

(11) Fluhler, E.; Burnham, V. G.; Loew, L. M. Spectra , Membrane Binding , and Potentiometric Reponses of New Charge Shift Probes. *Biochemistry* **1985**, *24*, 5749–5755.

(12) Deal, P. E.; Kulkarni, R. U.; Al-Abdullatif, S. H.; Miller, E. W. Isomerically Pure Tetramethylrhodamine Voltage Reporters. *J. Am. Chem. Soc.* **2016**, *138* (29), 9085–9088.

(13) Huang, Y.-L.; Walker, A. S.; Miller, E. W. A Photostable Silicon Rhodamine Platform for Optical Voltage Sensing. *J. Am. Chem. Soc.* **2015**, *137*, 10767–10776.

(14) Ortiz, G.; Liu, P.; Naing, S. H. H.; Muller, V. R.; Miller, E. W. Synthesis of Sulfonated Carbofluoresceins for Voltage Imaging. *J. Am. Chem. Soc.* **2019**, *141* (16), 6631–6638.

(15) Boggess, S. C.; Gandhi, S. S.; Siemons, B. A.; Huebsch, N.; Healy, K. E.; Miller, E. W. New Molecular Scaffolds for Fluorescent Voltage Indicators. *ACS Chem. Biol.* **2019**, *14*

(3), 390–396.

(16) Miller, E. W.; Lin, J. Y.; Frady, E. P.; Steinbach, P. A.; Kristan, W. B.; Tsien, R. Y. Optically Monitoring Voltage in Neurons by Photo-Induced Electron Transfer through Molecular Wires. *Proc. Natl. Acad. Sci. U. S. A.* **2012**, *109* (6), 2114–2119.

(17) Rehm, D.; Albert, W. Kinetics of Fluorescence Quenching by Electron and H-Atom Transfer. *Isr. J. Chem.* **1970**, *8* (2), 259–271.

(18) Ahlbrecht, H.; Düber, E. O.; Epsztajn, J.; Marcinkowski, R. M. K. Delocalisation, Conformation and Basicity of Anilines. *Tetrahedron* **1984**, *40* (7), 1157–1165.

(19) Lazzari-Dean, J. R.; Gest, A. M. M.; Miller, E. W. Optical Estimation of Absolute Membrane Potential Using Fluorescence Lifetime Imaging. *Elife* **2019**, *8*, e44522.

(20) Chen, R. F.; Knutson, J. R. Mechanism of Fluorescence Concentration Quenching of Carboxyfluorescein in Liposomes: Energy Transfer to Nonfluorescent Dimers. *Anal. Biochem.* **1988**, *172* (1), 61–77.

(21) Magde, D.; Wong, R.; Seybold, P. G. Fluorescence Quantum Yields and Their Relation to Lifetimes of Rhodamine 6G and Fluorescein in Nine Solvents: Improved Absolute Standards for Quantum Yields¶. *Photochem. Photobiol.* **2002**, *75* (4), 327.

(22) Zhang, X. F.; Zhang, J.; Liu, L. Fluorescence Properties of Twenty Fluorescein Derivatives: Lifetime, Quantum Yield, Absorption and Emission Spectra. *J. Fluoresc.* **2014**, *24* (3), 819–826.

(23) Fischer, M.; Georges, J. Fluorescence Quantum Yield of Rhodamine 6G in Ethanol as a Function of Concentration Using Thermal Lens Spectrometry. *Chem. Phys. Lett.* **1996**, *260*, 115–118.

(24) Wall, K. P.; Dillon, R.; Knowles, M. K. Fluorescence Quantum Yield Measurements of Fluorescent Proteins: A Laboratory Experiment for a Biochemistry or Molecular Biophysics Laboratory Course. *Biochem. Mol. Biol. Educ.* **2015**, *43* (1), 52–59.

(25) Kreitzer, F. R.; Salomonis, N.; Sheehan, A.; Huang, M.; Park, J. S.; Spindler, M. J.; Lizarraga, P.; Weiss, W. A.; So, P.; Conklin, B. R. A Robust Method to Derive Functional Neural Crest Cells from Human Pluripotent Stem Cells. *Am. J. Stem Cell* **2013**, *2* (2), 119–131.

(26) Lian, X.; Zhang, J.; Azarin, S. M.; Zhu, K.; Hazeltine, L. B.; Bao, X.; Hsiao, C.; Kamp, T. J.; Palecek, S. P. Directed Cardiomyocyte Differentiation from Human Pluripotent Stem Cells by Modulating Wnt/β-Catenin Signaling under Fully Defined Conditions. *Nat. Protoc.* **2013**, *8* (1), 162–175.

(27) Tohyama, S.; Hattori, F.; Sano, M.; Hishiki, T.; Nagahata, Y.; Matsuura, T.; Hashimoto, H.; Suzuki, T.; Yamashita, H.; Satoh, Y.; et al. Distinct Metabolic Flow Enables Large-Scale Purification of Mouse and Human Pluripotent Stem Cell-Derived Cardiomyocytes. *Cell Stem Cell* **2013**, *12*, 127–137.

(28) Edelstein, A. D.; Tsuchida, M. A.; Amodaj, N.; Pinkard, H.; Vale, R. D.; Stuurman, N. Advanced Methods of Microscope Control Using μManager Software. *J. Biol. Methods* **2014**, *1* (2).

(29) Laughner, J. I.; Ng, F. S.; Sulkin, M. S.; Arthur, R. M.; Efimov, I. R. Processing and Analysis of Cardiac Optical Mapping Data Obtained with Potentiometric Dyes. *Am. J. Physiol. Heart Circ. Physiol.* **2012**, *303* (7).

(30) Boelens, H. F. M.; Dijkstra, R. J.; Eilers, P. H. C.; Fitzpatrick, F.; Westerhuis, J. A. New Background Correction Method for Liquid Chromatography with Diode Array Detection, Infrared Spectroscopic Detection and Raman Spectroscopic Detection. *J. Chromatogr. A* **2004**, *1057* (1–2), 21–30.

(31) Luo, S.; Michler, K.; Johnston, P.; Macfarlane, P. W. A Comparison of Commonly Used QT Correction Formulae: The Effect of Heart Rate on the QTc of Normal ECGs. *J. Electrocardiol.* **2004**, *37*, 81–90.

(32) Liu, M.; Jia, M.; Pan, H.; Li, L.; Chang, M.; Ren, H.; Argoul, F.; Zhang, S.; Xu, J. Instrument Response Standard in Time-Resolved Fluorescence Spectroscopy at Visible Wavelength: Quenched Fluorescein Sodium. *Appl. Spectrosc.* **2014**, *68* (5), 577–583.

(33) Barry, P. H. JPCalc, a Software Package for Calculating Liquid Junction Potential Corrections in Patch-Clamp, Intracellular, Epithelial and Bilayer Measurements and for Correcting Junction Potential Measurements. *J. Neurosci. Methods* **1994**, *51* (1), 107–116.

Appendix 1:

Design of Alternative Fluorene-based Molecular Wires for Voltage Imaging

A1.1 Synopsis

The fluorene VoltageFluor (fVF) series of voltage indicators were the first example of a PeT based voltage indicator with a molecular wire other than the most frequently sued phenylene-vinylene architecture.[1] However, many other methods and modifications to the fluorene wire that affect voltage sensing properties exist. In this Appendix, I briefly explain the rational for three modifications to the fluorene scaffold, based off structures presented in Chapters 2 and 3.

Others in our laboratory have noted that the attachment position of the molecular wire on the pendant ring (either *para* or *meta* to the xanthene) of the fluorophore can have a large effect on the voltage sensitivity and brightness of the fluorophore.[2] Also, fluorene wires were initially attractive as wire alternatives because additional fluorene units to the conjugated system were shown to have little effect on the HOMO of the wire, thus enabling long-range electron transfer without a significant effect to the rate of PeT.[3] In the case of VoltageFluors, a longer molecular wire should be more sensitive to changes in the electric field if the overall dipole in the charge separation state is larger. Finally, initial results with vinyl-fluorene molecular wires (Chapter 3) demonstrated a massive effect caused by the addition of single vinyl groups to either end of fluorene in the scaffold. I was curious if the effect of adding a vinyl group would have an additive effect on the voltage sensing properties previously reported. Herein, I report the synthesis and sensitivity characterization of four fluorene-based VoltageFluor indicators that explore these potential modifications (**Scheme A1**).

To investigate the effect of moving the fluorene molecular wire to the *iso* (meta) position relative to the xanthene fluorophore, I synthesized indicators **1** and **2** (***iso*fVF 1** and **2**) using previously described wire precursors[1] and the 4-bromo isomer of 2,7-dicholorofluorescein (**Scheme A2**). Initially, results from patch-clamp experiments in HEK293T cells with these indicators were surprising, as voltage sensitivity was lower than their respective isomers (**Figure A1**). ***iso*fVF 1** was hardly voltage sensitive (2.4%F/F_0 per 100 mV) and ***iso*fVF 2** was half as sensitive (5.5%F/F_o) as fVF 2. It may be reasoned that the boost in voltage sensing properties seen in *iso*VoltageFluors with phenylene-vinylene wires is a result of direct conjugation with the sulfonate, which could significantly alter the rate of PeT. The insulating nature of the fluorene molecular wire would not benefit as significantly from these effects.

Longer molecular wires that intercalate deeper into the cell membrane would have a larger dynamic range. I synthesized di-fluorenyl wire **3** in relatively low yield by Suzuki cross-coupling with previously described fluorene wires and fluorene monomer (**Scheme A3**). Conversion to boron pinacol ester **4** then permitted attachment to the fluorophore to yield **5** (**Fl_2-fVF 2**) which was purified by HPLC. Experiments in HEK293T cells showed low signal at the cell membrane, despite loading at the same concentration as previous fVFs (0.5 μM). Presumably, this loss of signal would be caused by the decreased aqueous solubility of this indicator, which is unsurprising given its size. Still, this was slightly sensitive to changes in membrane potential at 4.2% F/F_o per 100 mV change. Future studies with this indicator would benefit from the use of more soluble chromophores, such as disulfonated derivatives.[4]

Synthesis of a divinyl-fluorene molecular wire started from the 7v-fluorene molecular wire described in Chapter 3. Cross coupling with vinyl MIDA boronate ester instead of B_2pin_2 provided wire **6** in excellent yield (**Scheme A4**). This was attached to the fluorescein chromophore with a

subsequent palladium-catalyzed cross coupling to provide **7** (**dv-fVF 2**). I initially expected an additive effect from both the 2v and 7v modifications together, however I measured a sensitivity of 8.0% $F/F_{o,}$ which was lower than the original fVF 2 (10.5%). This probe also suffered from poor solubility and might also benefit from more water-soluble chromophores. Still, it is puzzling that the effect of adding vinyl groups is overwhelmingly beneficial if added to either end of fluorene, but addition on both ends results in a less sensitive probe. Computational and advanced spectroscopic approaches, such as lifetime and transient absorption measurements, could provide more insight to this observation.

A1.2 Experimental section

A1.2.1 General methods for chemical synthesis and characterization

Palladium acetate was purchased from Strem Chemicals. Deuterated solvents were purchased from Cambridge Isotope Laboratories. All other reagents, including anhydrous solvents, were purchased from Sigma-Aldrich and used without further purification. References to previously synthesized compounds are provided along with characterization data. Thin layer chromatography (TLC) (Silicycle, F254, 250 μm) and preparative thin layer chromatography (PTLC) (Silicycle, F254, 1000 μm) was performed on glass backed plates pre-coated with silica gel and were visualized by fluorescence quenching under UV light. Flash column chromatography was performed on Silicycle Silica Flash F60 (230–400 Mesh) using a forced flow of air at 0.5–1.0 bar. NMR spectra were measured on Bruker AV-300 MHz, AVB-400 MHz, AVQ-400 MHz, and Bruker AV-600 MHz. Chemical shifts are expressed in parts per million (ppm) and are referenced to $CDCl_3$ (7.26 ppm, 77.0 ppm), d_6-DMSO (2.50 ppm, 40 ppm), or d_4-MeOD (3.35 ppm). Coupling constants are reported as Hertz (Hz). Splitting patterns are indicated as follows: s, singlet; d, doublet; t, triplet; q, quartet; dd, doublet of doublet; m, multiplet. High performance liquid chromatography (HPLC) and low resolution ESI Mass Spectrometry were performed on an Agilent Infinity 1200 analytical instrument coupled to an Advion CMS-L ESI mass spectrometer. The column used for the analytical HPLC was Phenomenex Luna 5 μm C18(2) (4.6 mm I.D. × 125 mm) with a flow rate of 1.0 mL/min. The mobile phases were MQ-H2O with 0.05% trifluoroacetic acid (eluent A) and HPLC grade acetonitrile with 0.05% trifluoroacetic acid (eluent B). Signals were monitored at 254, 350 and 480 nm over 10 min with a gradient of 10-100% eluent B unless otherwise noted. Semi-preparative high-performance liquid chromatography (HPLC) was performed on the same system with a semi-preparative Phenomenex Luna C18(2) column. Preparative HPLC was performed using a Waters Acquity Autopurificaiton system equipped with a Waters XBridge BEH 5 μm C18 column (19 mm I.D. x 250 mm) with a flow rate of 30.0 mL/min, made available by the Catalysis Facility of Lawrence Berkeley National Laboratory (Berkeley, CA). The mobile phases were MQ-H2O with 0.05% trifluoroacetic acid (eluent A) and HPLC grade acetonitrile with 0.05% trifluoroacetic acid (eluent B). Signals were monitored at 254 and 350 nm over 20 min with a gradient of 10-100% eluent B, unless otherwise noted.

A1.2.2 Imaging, cell culture, and electrophysiology

For HEK293T cells, epifluorescence imaging was performed on an AxioExaminer Z-1 (Zeiss) equipped with a Spectra-X Light engine LED light (Lumencor), controlled with Slidebook (v6, Intelligent Imaging Innovations). Images were acquired with either a W-Plan-Apo 20x/1.0 water objective (20x; Zeiss. Images were focused onto an eVolve 128 EMCCD camera (EMCCD;

Photometrix). Functional imaging of the fluorene VoltageFluors was performed at a sampling rate of 0.5 kHz, all dyes were loaded at approximately 0.5 µM. Excitation was supplied a 475 nm LED with an intensity of 20.9 mW/mm^2.

Human embryonic kidney (HEK) 293T cells were acquired from the UC Berkeley Cell Culture Facility. Cells were passaged and plated onto 12 mm glass coverslips coated with Poly-D-Lysine (PDL; 1 mg/mL; Sigma-Aldrich) to a confluency of ~15% and 50% for electrophysiology and imaging, respectively. HEK293T cells were plated and maintained in Dulbecco's modified eagle medium (DMEM) supplemented with 4.5 g/L D-glucose, 10% fetal bovine serum (FBS), and 1% Glutamax.

For electrophysiological experiments in HEK293T cells and rat hippocampal neurons, pipettes were pulled from borosilicate glass (Sutter Instruments, BF150-86-10), with a resistance of 5–6 MΩ, and were filled with an internal solution; 125 mM potassium gluconate, 1 mM EGTA, 10 mM HEPES, 5 mM NaCl, 10 mM KCl, 2 mM ATP disodium salt, 0.3 mM GTP trisodium salt (pH 7.25, 285 mOsm). Recordings were obtained with an Axopatch 200B amplifier (Molecular Devices) at room temperature. The signals were digitized with a Digidata 1440A, sampled at 50 kHz and recorded with pCLAMP 10 software (Molecular Devices) on a PC. Fast capacitance was compensated in the on-cell configuration. For all electrophysiology experiments, recordings were only pursued if series resistance in voltage clamp was less than 30 MΩ. For whole-cell, voltage clamp recordings in HEK293T cells, cells were held at -60 mV and hyper- and de- polarizing steps applied from -100 to +100 mV in 20 mV increments.

A1.2.3 Synthetic methods

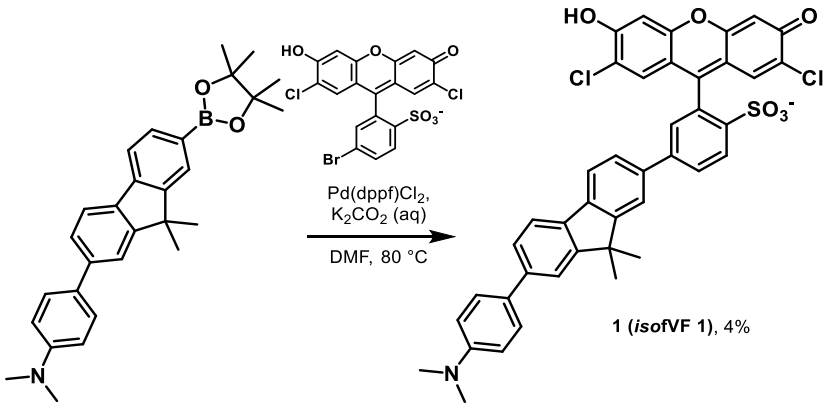

Synthesis of *iso*VF 1, 1

Molecular wire[1] (26 mg, 0.06 mmol), 4-bromo-2',7'-dichloro-sulfofluorescein (25 mg, 0.05 mmol), and Pd(dppf)Cl_2 (1.8 mg, 2 µmol) were added to a flame dried Schlenk flask. Flask was evacuated and backfilled (3X), then anhydrous DMF (1 mL) and bubbled 5 M K_2CO_3 solution (0.1 mL) was added. Reaction was stirred at 80 °C for 16 hours. Reaction was concentrated *in vacuo* to dryness, then taken up in a small amount of 1:1 dichlormethane:methanol, then precipitated in diethyl ether. 29 mg of orange precipitate was collected after filtration. This was purified further

by semi-preparative HPLC (10-100% MeCN + 0.1% TFA) to obtain **1** as an orange solid (1.5 mg, 4%).

Analytical HPLC retention time, 4.96 min; MS (ESI+) m/z for $C_{42}H_{32}Cl_2NO_6S$ $[M+H]^+$ 748.1; found 747.7. Estimated purity: 98%.

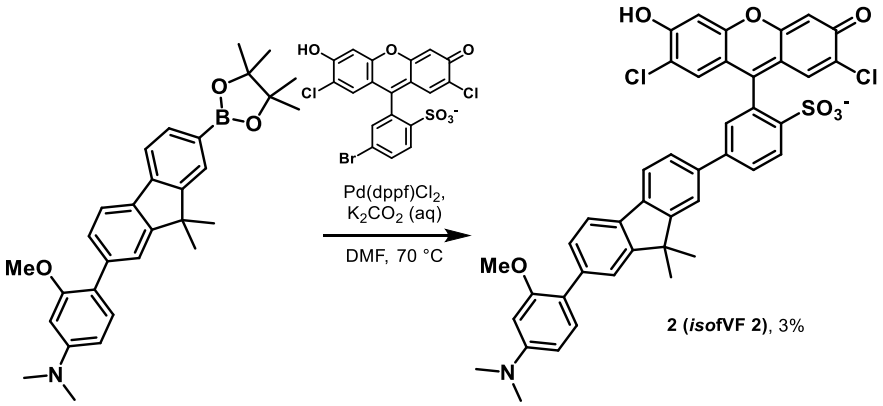

Synthesis of *iso*fVF 2

Molecular wire[1] (44 mg, 0.09 mmol), 4-bromo-2',7'-dichloro-sulfofluorescein (40 mg, 0.08 mmol), and $Pd(dppf)Cl_2$ (2.8 mg, 4 µmol) were added to a flame dried Schlenk flask. Flask was evacuated and backfilled (3X), then anhydrous DMF (2 mL) and bubbled 5 M K_2CO_3 solution (0.2 mL) was added. Reaction was stirred at 70 °C for 16 hours. Reaction was concentrated *in vacuo* to dryness, then taken up in a small amount of 1:1 dichlormethane:methanol, then precipitated in diethyl ether. 64 mg of brown precipitate was collected after filtration. This was purified further by semi-preparative HPLC (30-80% MeCN + 0.1% TFA) to obtain **2** as an orange solid (2 mg, 3%).

Analytical HPLC retention time (10-100% MeCN), 8.31 min; MS (ESI+) m/z for $C_{42}H_{32}Cl_2NO_6S$ $[M+H]^+$ 778.1; found 778.1. Estimated crude purity: 70%.

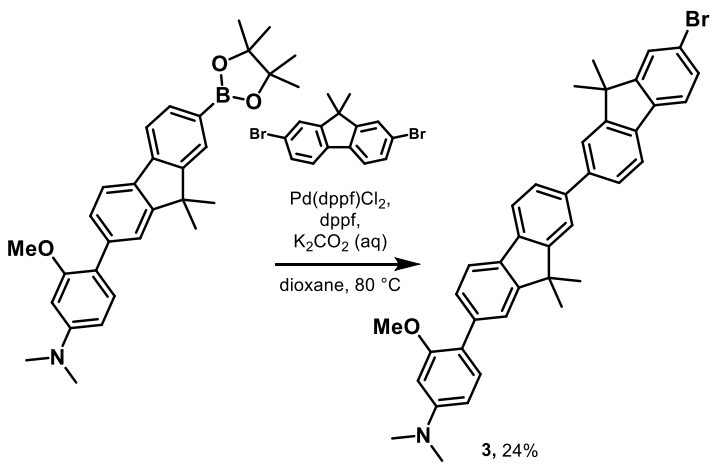

Synthesis of 4-(7'-bromo-9,9,9',9'-tetramethyl-9H,9'H-[2,2'-bifluoren]-7-yl)-3-methoxy-N,N-dimethylaniline, 3

Molecular wire[1] (105 mg, 0.22 mmol), 2,7-dibromo-9,9-dimethyl-9H-fluorene (157 mg, 0.45 mmol), and $Pd(dppf)Cl_2$ (8 mg, 0.01 mmol) were added to a flame dried Schlenk flask. Flask was evacuated and backfilled (3X), then anhydrous dioxane (1 mL) and bubbled 5 M K_2CO_3 solution (0.1 mL) was added. Reaction was stirred at 80 °C for 16 hours. This was diluted in dichloromethane, then washed with NH_4Cl and brine. Dried with $MgSO_4$, then concentrated onto silica. Purification by flash chromatography (10-50% dichloromethane in hexanes) gave **3** as a yellow solid (33 mg, 24%).

^{1}H NMR (400 MHz, Chloroform-d) δ 7.83 – 7.76 (m, 3H), 7.73 – 7.69 (m, 2H), 7.69 – 7.65 (m, 1H), 7.65 – 7.60 (m, 3H), 7.57 (dd, J = 7.8, 1.6 Hz, 1H), 7.51 – 7.49 (m, 1H), 7.33 (d, J = 8.4 Hz, 1H), 7.20 (d, J = 7.7 Hz, 1H), 6.47 (dt, J = 8.5, 2.1 Hz, 1H), 6.41 (d, J = 2.4 Hz, 1H), 3.89 (s, 3H), 3.05 (d, J = 1.7 Hz, 6H), 1.61 (s, 6H), 1.58 (d, J = 1.6 Hz, 6H).

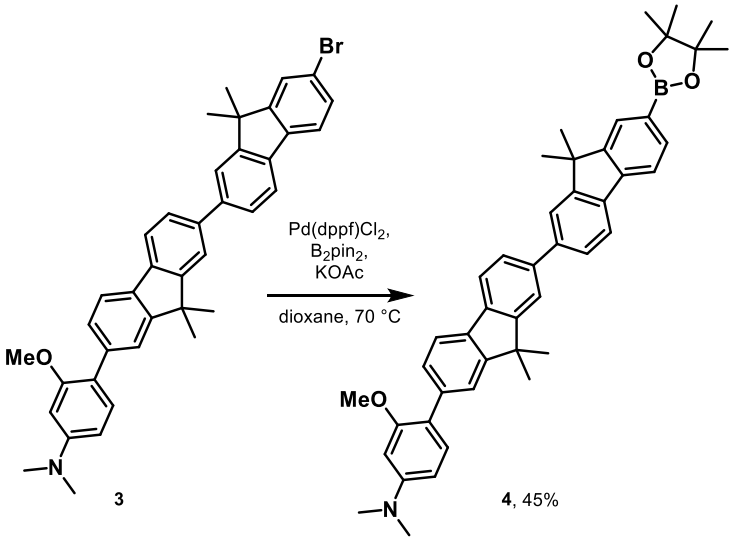

Synthesis of 3-methoxy-N,N-dimethyl-4-(9,9,9',9'-tetramethyl-7'-(4,4,5,5-tetramethyl-1,3,2-dioxaborolan-2-yl)-9H,9'H-[2,2'-bifluoren]-7-yl)aniline, 4

Molecular wire **3** (33 mg, 0.05 mmol), B_2pin_2 (20 mg, 0.08 mmol), potassium acetate (16 mg, 0.16 mmol), and Pd(dppf)Cl_2 were combined in a flame dried Schlenk flask. The flask was evacuated and backfilled with N_2 (3X) before addition of anhydrous dioxane (2 mL). This was stirred for 16 hours at 70 °C. Extracted in dichloromethane, washed with NH_4Cl and brine, then dried with $MgSO_4$ and concentrated onto silica. **4** was purified by flash chromatography (50-100% dichloromethane in hexanes, followed by 10% ethyl acetate in dichloromethane) as a yellow solid (16 mg, 45%).

^{1}H NMR (300 MHz, Chloroform-d) δ 7.91 (d, J = 0.9 Hz, 1H), 7.86 – 7.80 (m, 3H), 7.79 – 7.73 (m, 3H), 7.70 (dd, J = 6.8, 1.5 Hz, 2H), 7.65 (dd, J = 7.7, 1.7 Hz, 2H), 7.60 (d, J = 1.5 Hz, 1H), 7.54 (dd, J = 7.9, 1.6 Hz, 1H), 7.31 (d, J = 8.4 Hz, 1H), 6.45 (dd, J = 8.5, 2.4 Hz, 1H), 6.38 (d, J = 2.4 Hz, 1H), 3.86 (s, 3H), 3.02 (s, 6H), 1.58 (s, 12H), 1.39 (s, 12H).

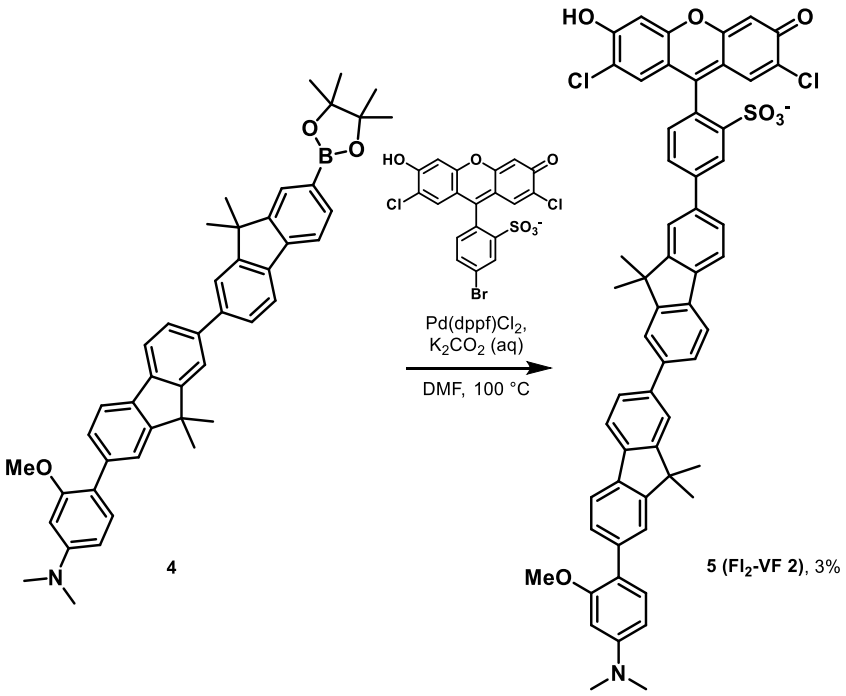

Synthesis of Fl_2-VF 2, 5

Molecular wire **4** (15 mg, 0.02 mmol), 5-bromo-2',7'-dichloro-sulfofluorescein (10 mg, 0.02 mmol), and Pd(dppf)Cl_2 (0.7 mg, 1 µmol) were added to a flame dried Schlenk flask. Flask was evacuated and backfilled (3X), then anhydrous DMF (1 mL) and bubbled 5 M K_2CO_3 solution (0.1 mL) was added. This was stirred for 36 hours at 100 °C. Reaction was concentrated *in vacuo* to dryness, then taken up in a small amount of 1:1 dichlormethane:methanol, then precipitated in diethyl ether. 8 mg of violet precipitate was collected after filtration. This was purified further by preparative HPLC (40-70% MeCN + 0.05% TFA) to obtain **5** as an orange solid (0.5 mg, 3%).

Analytical HPLC retention time 6.68 min (40-70% MeCN in water + 0.05% TFA); MS (ESI+) m/z for $C_{58}H_{46}Cl_2NO_7S$ $[M+H]^+$ 970.2; found 970.2. Estimated purity, 80%

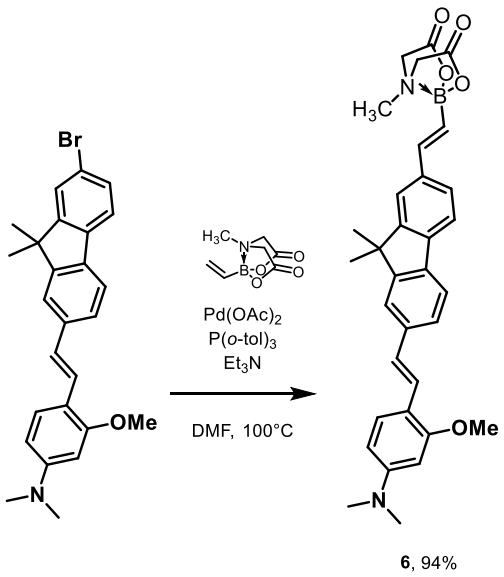

6, 94%

Synthesis of MIDA boronate ester, 6

Molecular wire (Chapter 3, compound 14; 125 mg, 0.28 mmol), vinyl MIDA boronate (153 mg, 0.84 mmol), palladium (II) acetate (1.9 mg, 8 µmol), and P(*o*-tol)$_3$ were combined in a flame dried Schlenk flask. The flask was evacuated and backfilled with N_2 (3X), then anhydrous DMF (0.5 mL) and triethylamine (2 mL) were added. The was sealed and stirred for 18 hours at 100 °C. This was diluted in ethyl acetate, then washed with NH_4Cl (2X) and brine. Dried with $MgSO_4$, then concentrated onto silica. **6** was purified by flash chromatography (75-100% ethyl acetate in hexanes) as a yellow solid (144 mg, 94%).

^{1}H NMR (400 MHz, Chloroform-d) δ 7.65 (dd, J = 7.9, 2.6 Hz, 1H), 7.58 – 7.53 (m, 1H), 7.53 – 7.47 (m, 2H), 7.47 – 7.41 (m, 2H), 7.17 – 7.10 (m, 1H), 7.05 (d, J = 16.3 Hz, 1H), 6.37 (d, J = 8.4 Hz, 1H), 6.31 – 6.17 (m, 2H), 5.88 (d, J = 8.1 Hz, 2H), 3.85 (d, J = 20.1 Hz, 2H), 3.65 (d, J = 20.9 Hz, 2H), 3.02 (s, 6H), 2.93 (d, J = 1.9 Hz, 3H), 2.86 (s, 3H), 1.57 (s, 3H), 1.53 (s, 3H).

Analytical HPLC retention time 7.43 min; MS (ESI+) m/z calculated for $C_{33}H_{36}BN_2O_5$ $[M+H]^+$ 551.2 ; found 551.3

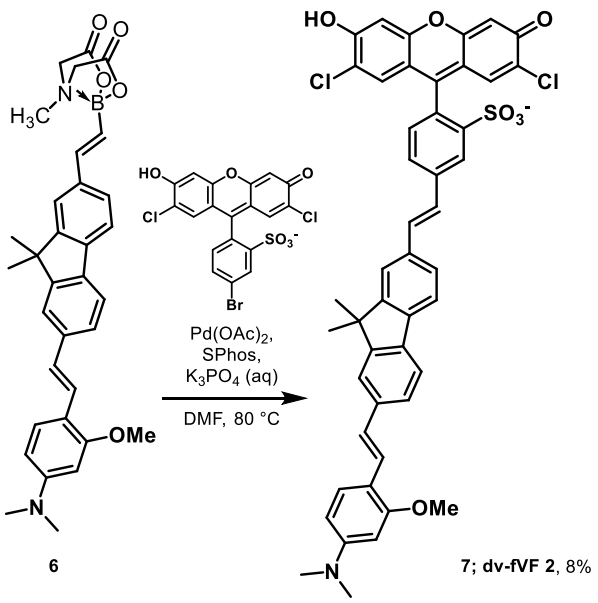

Synthesis of dv-fVF 2, 7

Molecular wire **6** (64 mg, 0.11 mmol), 5-bromo-2',7'-dichloro-sulfofluorescein (50 mg, 0.10 mmol), palladium (II) acetate (1.1 mg, 5 µmol), and SPhos (4 mg, 0.01 mmol) were combined in a flame dried Schlenk flask. The flask was evacuated and backfilled with N_2 (3X) before addition of anhydrous DMF (1 mL) and bubbled 3M K_3PO_4 solution (0.2 mL). This was stirred at 80 °C for 20 hours. Reaction was concentrated *in vacuo* to dryness, then taken up in a small amount of 1:1 dichlormethane:methanol, then precipitated in diethyl ether. 42 mg of brown precipitate was collected after filtration. This was purified further by preparative HPLC (30-80% MeCN + 0.05% TFA) to obtain **7** as an orange solid (4.5 mg, 8%).

Analytical HPLC retention time 6.56 min; MS (ESI+) m/z calculated for $C_{47}H_{38}Cl_2NO_7S$ $[M+H]^+$ 830.2; found: 829.8. Estimated purity: 81%

A1.3 Schemes and figures

Scheme A1. *Alternative fluorene-based voltage sensing scaffolds*

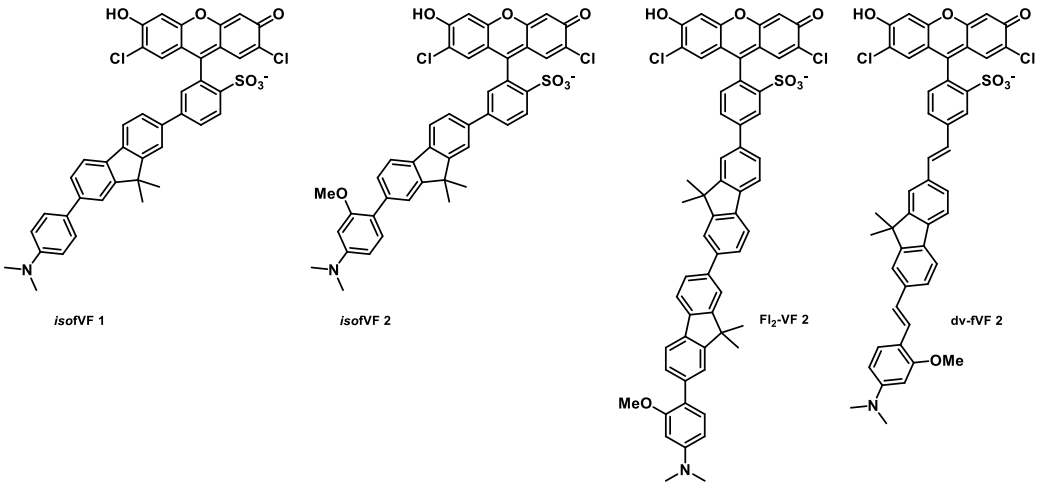

Scheme A2. *Synthesis of iso-fluorene VoltageFluors (isofVFs)*

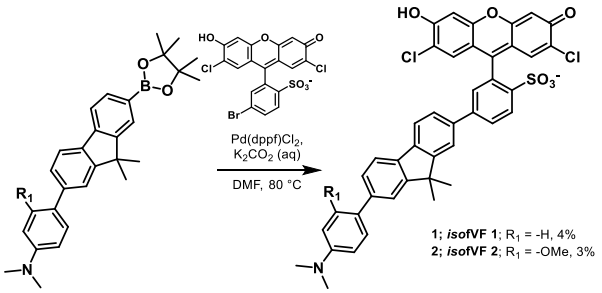

Scheme A3. *Synthesis of an extended fluorene molecular wire*

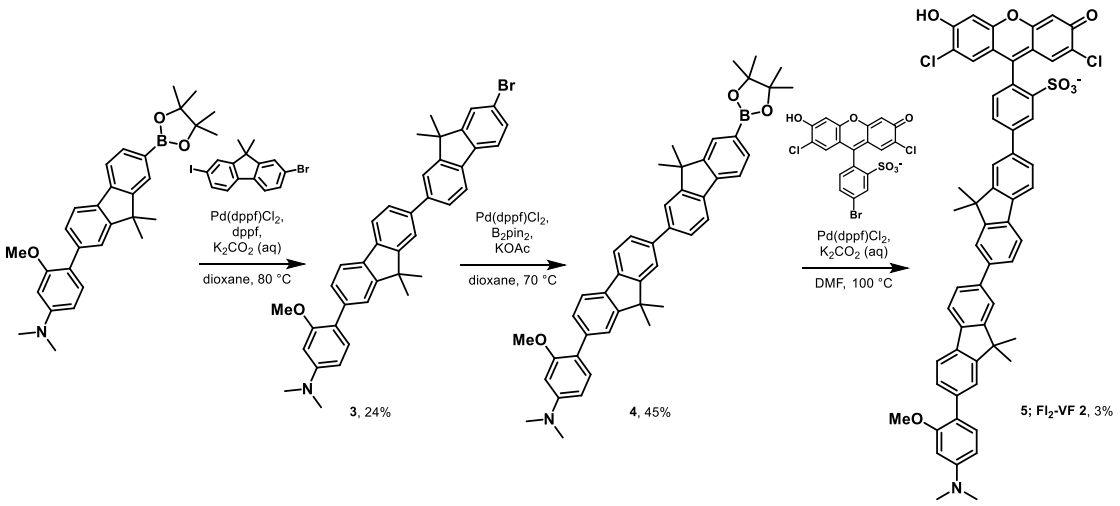

Scheme A4. *Synthesis of divinyl-fluorene VoltageFluor*

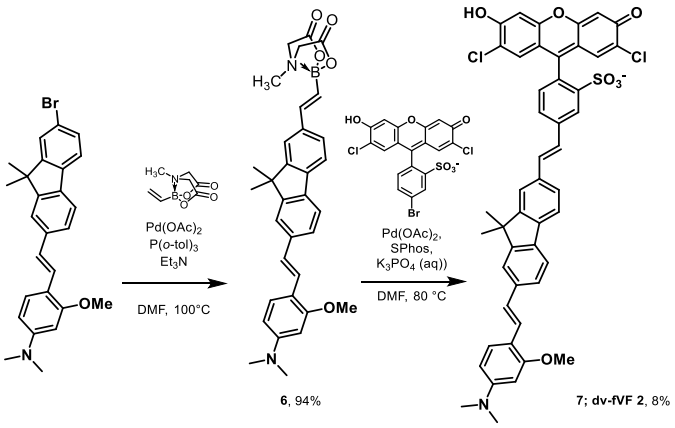

Figure A1. *Sensitivity measurements of alternative fluorene VoltageFluors*

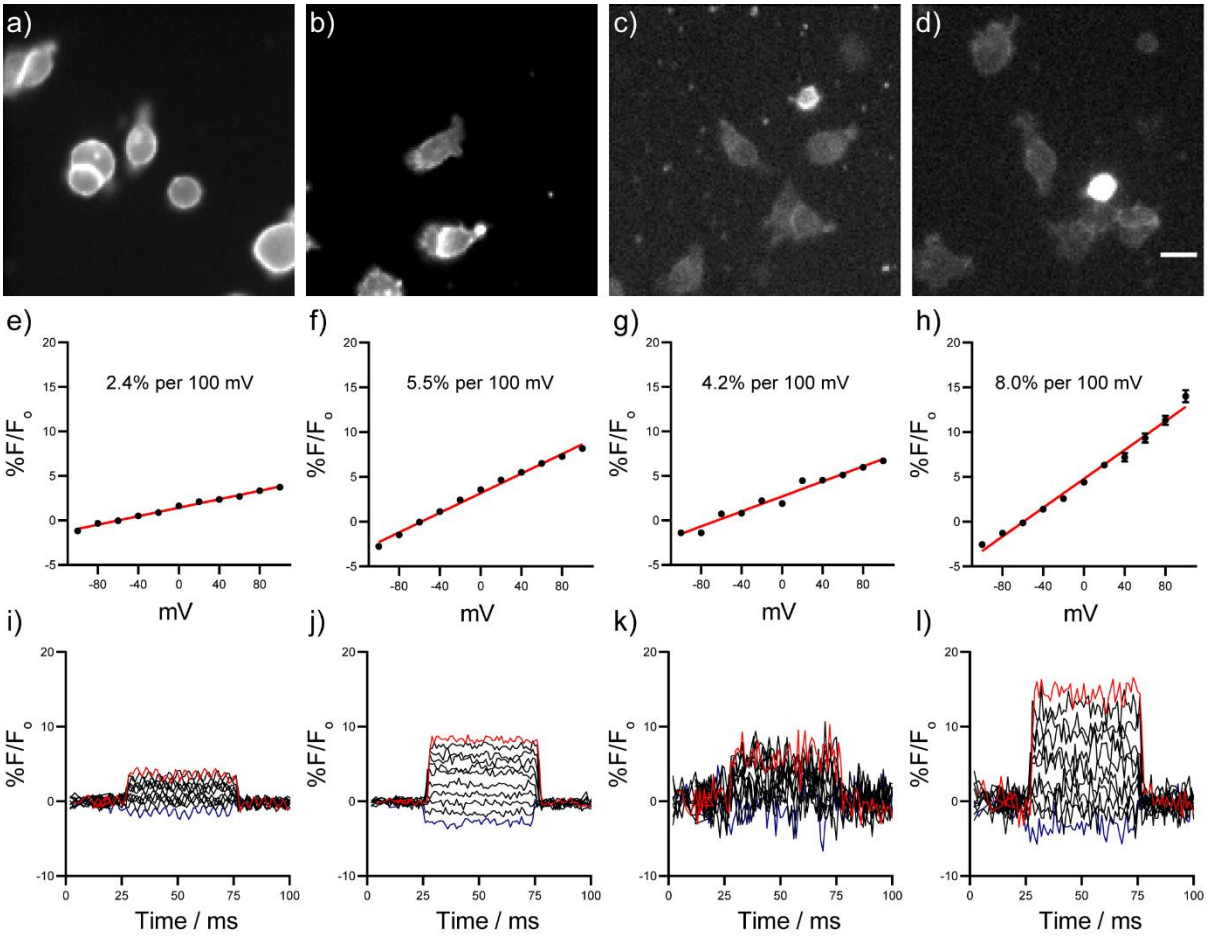

Figure A1. Sensitivity measurements of alternative fluorene VoltageFluors. Epifluorescence micrograph of (a) *iso*VF 1, (b) *iso*VF 2, (c) Fl_2-fVF 2, and (d) dv-fVF 2 loaded at 0.5 µM in HEK293T cells. Pixel intensity histograms adjusted to show membrane staining regardless of fluorescence intensity. Scale bar is 20 µm. Plots below (e-h) show the linear response to voltage of the above indicators. Error bars are SEM, where applicable, n=3 cells (f, h). Concatenated fluorescence traces of voltage steps (i-l) show the $\%F/F_o$ response from a single cell recording of the above indicators.

A1.4 References

(1) Boggess, S. C.; Gandhi, S. S.; Siemons, B. A.; Huebsch, N.; Healy, K. E.; Miller, E. W. New Molecular Scaffolds for Fluorescent Voltage Indicators. *ACS Chem. Biol.* **2019**, *14* (3), 390–396.

(2) Deal, P. E.; Kulkarni, R. U.; Al-Abdullatif, S. H.; Miller, E. W. Isomerically Pure Tetramethylrhodamine Voltage Reporters. *J. Am. Chem. Soc.* **2016**, *138* (29), 9085–9088.

(3) Goldsmith, R. H.; Sinks, L. E.; Kelley, R. F.; Betzen, L. J.; Liu, W.; Weiss, E. a; Ratner, M. A.; Wasielewski, M. R. Wire-like Charge Transport at near Constant Bridge Energy through Fluorene Oligomers. *Proc. Natl. Acad. Sci. U. S. A.* **2005**, *102* (10), 3540–3545.

(4) Kulkarni, R. U.; Yin, H.; Pourmandi, N.; James, F.; Adil, M. M.; Schaffer, D. V.; Wang, Y.; Miller, E. W. A Rationally Designed, General Strategy for Membrane Orientation of Photoinduced Electron Transfer-Based Voltage-Sensitive Dyes. *ACS Chem. Biol.* **2017**, *12* (2), 407–413.

Appendix 2:

Red-shifted Voltage Indicators with Fluorene-based Molecular Wires

Rhodamine coupling partners were provided by Rishikesh Kulkarni.

Carbofluorescein coupling partners were provided by Gloria Ortiz.

A2.1 Synopsis

Development of red-shifted fluorophores and probes has been a longstanding goal of the Chemical Biology community in order to access tools that can be used in more complex tissue systems. Red-shifted excitation penetrates deeper into tissue, causes less photodamage to the sample, and reduces autofluorescence from endogenous chromophores.[1] Our laboratory has developed numerous voltage sensitive dyes that absorb at red-shifted wavelengths, permitting multiplexing with other optical tools such as GCaMP and channelrhodopsins.[2–4] While these indicators have high sensitivities and excellent signal to noise, further optimization is hampered by the lack of available voltage sensing modalities. The development of fluorene based molecular wires presents a potential method for building new red-shifted chromophores with desirable properties such as greater brightness and lower phototoxicity.[5] In this appendix, I present the initial attempts at applying fluorene wire voltage sensing domains to red-shifted fluorophores (**Scheme A2-1**).

The first red-shifted VoltageFluors which incorporated a fluorene molecular wire were synthesized by Pd-catalyzed cross coupling of the fluorene molecular wire from fVF 2[5] with either 5 or 4-bromo-tetramethylsulfonorhodamine derivatives to provide indicators **1** and **2** (**Scheme A2-2**).[6] Optimization of purification steps could help improve the poor yields of these reactions. When examined in HEK293T cells, membrane localized staining was observed for these regioisomeric indicators (**Figure A2-1**). Dual fluorescence microscopy and patch clamp electrophysiology experiments showed these indicators had low sensitivity (4.9%, 5.5%, **Figure A2-2**). While the signal-to-noise of these measurements was relatively good given the low sensitivity, these probes are less practically useful than other rhodamine based indicators.[2]

In an attempt to boost the voltage sensitivity of aforementioned red-shifted fluorene-based voltage indicators, a 7-vinyl-fluorene molecular wire (Chapter 3) was used in hopes the previously observed characteristics would persist with a rhodamine dye-head. Compound **3** was produced by the same cross-coupling strategy (**Scheme A2-2**). However, I was disappointed to find that this indicator rapidly internalizes in cells, prohibiting measurement of voltage changes on the cell membrane (**Figure A2-1**). While overall neutral, the partial positive charge of the rhodamine aniline would direct the observed localization to the mitochondria. The increased lipophilicity may have negated the localizing effect of the sulfonate, which normally prohibits internalization of RhoVRs.[6]

Believing the rhodamine anilines were the source of internalization issues, I incorporated carbofluoresceins with vinyl-fluorene molecular wires (**Scheme A2-3**).[4] Compounds **4** and **5** were produced by Suzuki cross-coupling, however only **4** could be isolated as **5** decomposed upon HPLC purification. Gratifyingly, evaluation in HEK293T cells demonstrated compound **4** localizes to the cell membrane and does not internalize (**Figure A2-1**). While the measured voltage sensitivity of compound **4** was low (3.2%, **Figure A2-2**), further optimization of fluorophore identity could serve to tune a red-shifted indicator.[4]

A2.2 Experimental section

A2.2.1 General methods for chemical synthesis and characterization

Palladium acetate was purchased from Strem Chemicals. Deuterated solvents were purchased from Cambridge Isotope Laboratories. All other reagents, including anhydrous solvents, were purchased from Sigma-Aldrich and used without further purification. References to previously synthesized compounds are provided along with characterization data. High performance liquid chromatography (HPLC) and low resolution ESI Mass Spectrometry were performed on an Agilent Infinity 1200 analytical instrument coupled to an Advion CMS-L ESI mass spectrometer. The column used for the analytical HPLC was Phenomenex Luna 5 μm C18(2) (4.6 mm I.D. × 125 mm) with a flow rate of 1.0 mL/min. The mobile phases were MQ-H2O with 0.05% trifluoroacetic acid (eluent A) and HPLC grade acetonitrile with 0.05% trifluoroacetic acid (eluent B). Signals were monitored at 254, 350 and 480 nm over 10 min with a gradient of 10-100% eluent B unless otherwise noted. Semi-preparative high-performance liquid chromatography (HPLC) was performed on the same system with a semi-preparative Phenomenex Luna C18(2) column. Preparative HPLC was performed using a Waters Acquity Autopurificaiton system equipped with a Waters XBridge BEH 5 μm C18 column (19 mm I.D. x 250 mm) with a flow rate of 30.0 mL/min, made available by the Catalysis Facility of Lawrence Berkeley National Laboratory (Berkeley, CA). The mobile phases were MQ-H2O with 0.05% trifluoroacetic acid (eluent A) and HPLC grade acetonitrile with 0.05% trifluoroacetic acid (eluent B). Signals were monitored at 254 and 350 nm over 20 min with a gradient of 10-100% eluent B, unless otherwise noted.

A2.2.2 Imaging, cell culture, and electrophysiology

For HEK293T cells, epifluorescence imaging was performed on an AxioExaminer Z-1 (Zeiss) equipped with a Spectra-X Light engine LED light (Lumencor), controlled with Slidebook (v6, Intelligent Imaging Innovations). Images were acquired with either a W-Plan-Apo 20x/1.0 water objective (20x; Zeiss. Images were focused onto an eVolve 128 EMCCD camera (EMCCD; Photometrix). Functional imaging of the fluorene VoltageFluors was performed at a sampling rate of 0.5 kHz, all dyes were loaded at approximately 0.5 μM. Excitation was supplied a 475 nm LED with an intensity of 20.9 mW/mm^2.

Human embryonic kidney (HEK) 293T cells were acquired from the UC Berkeley Cell Culture Facility. Cells were passaged and plated onto 12 mm glass coverslips coated with Poly-D-Lysine (PDL; 1 mg/mL; Sigma-Aldrich) to a confluency of ~15% and 50% for electrophysiology and imaging, respectively. HEK293T cells were plated and maintained in Dulbecco's modified eagle medium (DMEM) supplemented with 4.5 g/L D-glucose, 10% fetal bovine serum (FBS), and 1% Glutamax.

For electrophysiological experiments in HEK293T cells and rat hippocampal neurons, pipettes were pulled from borosilicate glass (Sutter Instruments, BF150-86-10), with a resistance of 5–6 MΩ, and were filled with an internal solution; 125 mM potassium gluconate, 1 mM EGTA, 10 mM HEPES, 5 mM NaCl, 10 mM KCl, 2 mM ATP disodium salt, 0.3 mM GTP trisodium salt (pH 7.25, 285 mOsm). Recordings were obtained with an Axopatch 200B amplifier (Molecular Devices) at room temperature. The signals were digitized with a Digidata 1440A, sampled at 50 kHz and recorded with pCLAMP 10 software (Molecular Devices) on a PC. Fast capacitance was compensated in the on-cell configuration. For all electrophysiology experiments, recordings were only pursued if series resistance in voltage clamp was less than 30 MΩ. For whole-cell, voltage

clamp recordings in HEK293T cells, cells were held at -60 mV and hyper- and de- polarizing steps applied from -100 to +100 mV in 20 mV increments.

A2.2.3 Synthetic methods

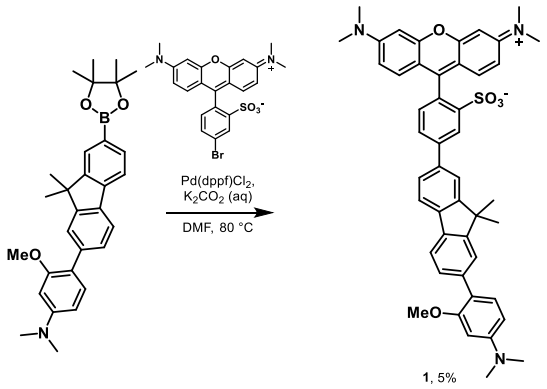

Synthesis of rhodamine-fluorene indicator, 1

5-bromo-tetramethylsulfonorhodamine[6] (25 mg, 0.05 mmol), fluorene molecular wire[5] (28 mg, 0.06 mmol), and Pd(dppf)Cl_2 (1.8 mg, 2 µmol) were combined in a flame dried Schlenk flask. The flask was evacuated and backfilled with N_2 (3X) before addition of anhydrous DMF (1 mL) and bubbled 5 M K_2CO_3 solution (0.1 mL). This was stirred at 80 °C for 14 hours, then concentrated to dryness under reduced pressure. A small amount of 1:1 dichloromethane:methanol was used to solubilize, then was precipitated in diethyl ether, which provided a violet solid (29 mg) after filtration. **1** was purified further by semi-preparative HPLC (10-100% MeCN in water + 0.1% TFA) to provide a purple solid (1.5 mg, 5%).

Analytical HPLC retention time 5.76 min; MS (ESI+) calculated for $C_{47}H_{46}N_3O_5S$ m/z $[M+H]^+$ 764.3; found 763.9. Estimated purity >99%.

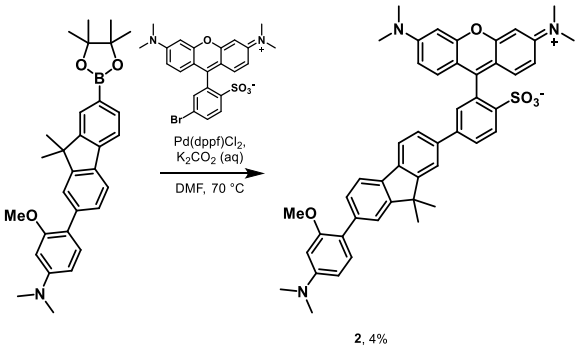

Synthesis of isorhodamine-fluorene indicator, 2

4-bromo-tetramethylsulfonorhodamine[6] (35 mg, 0.07 mmol), fluorene molecular wire[5] (39 mg, 0.08 mmol), and Pd(dppf)Cl_2 (2.5 mg, 3 µmol) were combined in a flame dried Schlenk flask. The

flask was evacuated and backfilled with N_2 (3X) before addition of anhydrous DMF (1 mL) and bubbled 5 M K_2CO_3 solution (0.1 mL). This was stirred at 70 °C for 14 hours, then concentrated to dryness under reduced pressure. A small amount of 1:1 dichloromethane:methanol was used to solubilize, then was precipitated in diethyl ether, which provided a red solid (39 mg) after filtration. **2** was purified further by semi-preparative HPLC (10-100% MeCN in water + 0.1% TFA) to provide a purple solid (2 mg, 4%).

Analytical HPLC retention time 6.20 min; MS (ESI+) calculated for $C_{47}H_{46}N_3O_5S$ m/z $[M+H]^+$ 764.3; found 764.1. Estimated purity >95%.

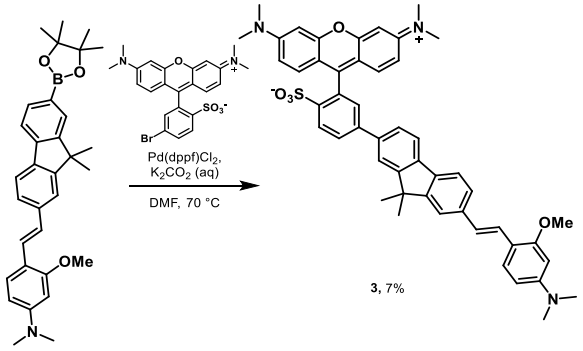

Synthesis of rhodamine-vinylfluorene indicator, 3

4-bromo-tetramethylsulfonorhodamine[6] (17 mg, 0.03 mmol), 7-vinyl-fluorene molecular wire (Chapter3, 19 mg, 0.04 mmol), and $Pd(dppf)Cl_2$ (1.2 mg, 2 µmol) were combined in a flame dried Schlenk flask. The flask was evacuated and backfilled with N_2 (3X) before addition of anhydrous DMF (1 mL) and bubbled 5 M K_2CO_3 solution (0.1 mL). This was stirred at 70 °C for 14 hours, then concentrated to dryness under reduced pressure. A small amount of 1:1 dichloromethane:methanol was used to solubilize, then was precipitated in diethyl ether, which provided a red solid after filtration. **3** was purified further by preparative HPLC (30-80% MeCN in water + 0.1% TFA) to provide a purple solid (2 mg, 7%).

Analytical HPLC retention time 5.96 min; MS (ESI+) calculated for $C_{47}H_{46}N_3O_5S$ m/z $[M+H]^+$ 790.3; found 790.5. Estimated purity >99%.

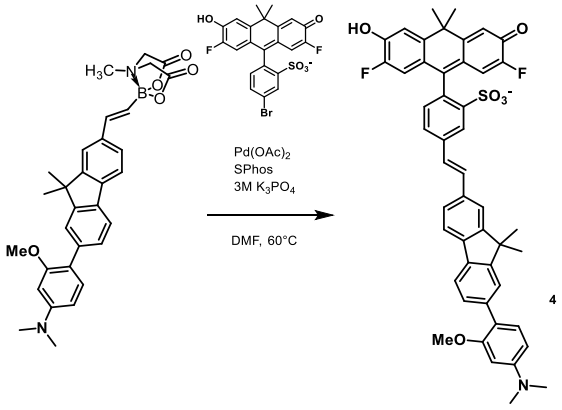

Synthesis of carbofluorescein-vinylfluorene indicator, 4

2,7-difluorosulfono carbofluorescein[4] (4 mg, 8 µmol), vinyl-MIDA boronate wire (Chapter 3, 6 mg, 12 µmol), palladium (II) acetate (0.1 mg, 0.4 µmol), and SPhos (0.3 mg, 0.7 µmol) were added to a flame dried Schlenk flask. The flask was evacuated and backfilled with N_2 (3X) before addition of anhydrous DMF (0.5 mL) and bubbled 3M K_3PO_4 solution (0.05 mL). The reaction was stirred at 60 °C for 14 hours, then concentrated to dryness under reduced pressure. This was taken up in a small amount of methanol, then triturated with diethyl ether to obtain **4** as a violet solid (5 mg, 83%), which was used without further purification.

Analytical HPLC retention time 5.81 minutes; MS (ESI+) calculated for $C_{48}H_{42}F_2NO_6S$ m/z $[M+H]^+$ 798.3; found 798.1. Estimated purity, 76%.

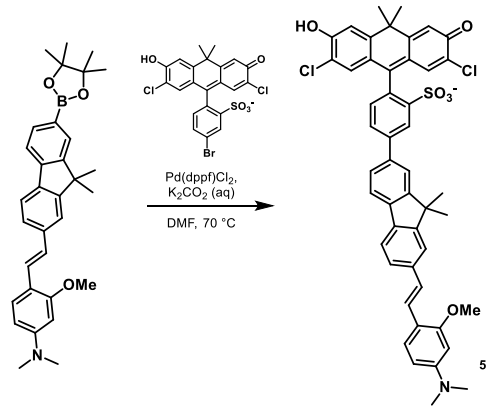

Synthesis of carbofluorescein-vinylfluorene indicator, 5

2,7-dichlorosulfono carbofluorescein[4] (10 mg, 0.02 mmol), vinyl-fluorene wire[5] (11 mg, 0.02 mmol), and Pd(dppf)Cl_2 (0.7 mg, 1 µmol) were combined in a flame dried Schlenk flask. This was evacuated and backfilled with N_2 (3X) before addition of anhydrous DMF (1 mL) and bubbled 5M K_2CO_3 solution (0.1 mL). This was stirred at 70 °C for 16 hours before concentrating to dryness under reduced pressure. After taking up in a small amount of methanol, **5** was recovered as a violet solid after trituration with diethyl ether (14 mg). Further purification by preparative HPLC (10-100% MeCN + 0.05% TFA) resulted in decomposition of the product.

Analytical HPLC retention time of the crude, 6.47; MS (ESI+) calculated for $C_{48}H_{42}Cl_2NO_6S$ m/z [M+H] 830.2; found 830.0. Estimated composition of crude: 67%.

A2.3 Schemes and figures

Scheme A1. *Fluorene-based indicators with red-shifted fluorophores*

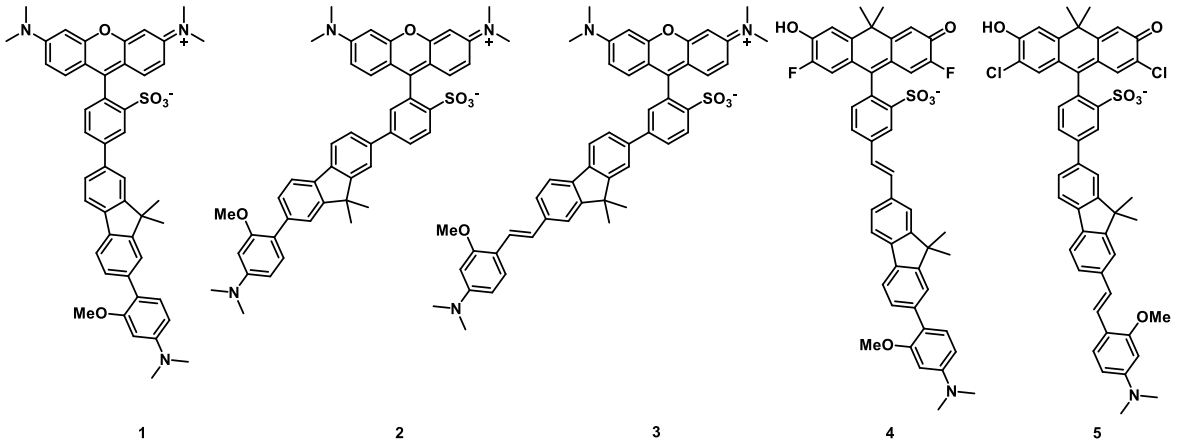

Scheme A2-2. *Synthesis of tetramethyl rhodamine fluorene indicators*

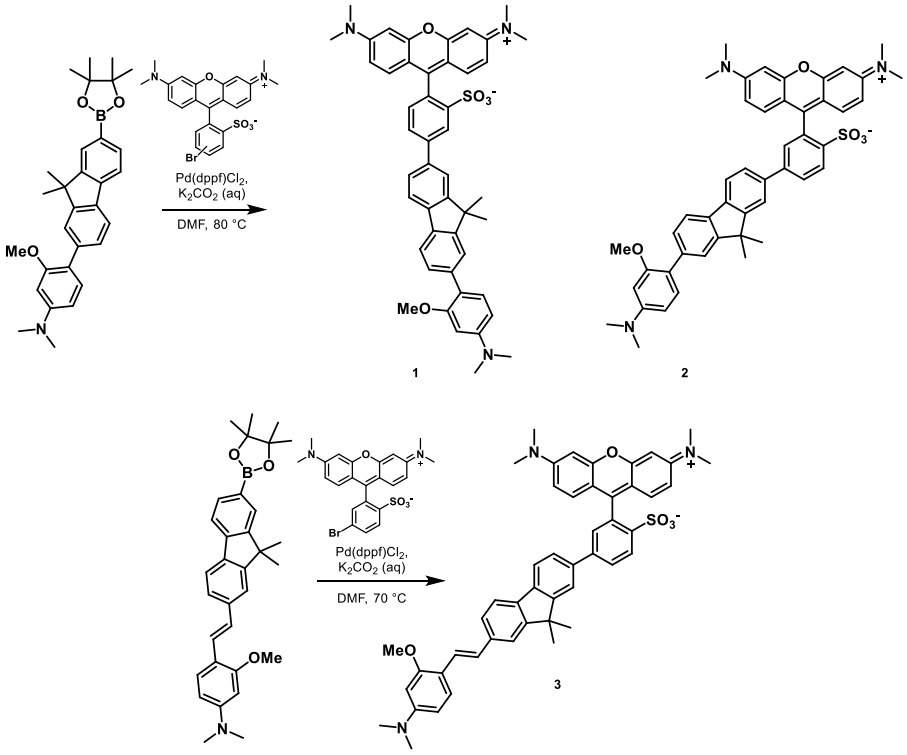

Scheme A2-3. *Synthesis of carborhodamine fluorene indicators*

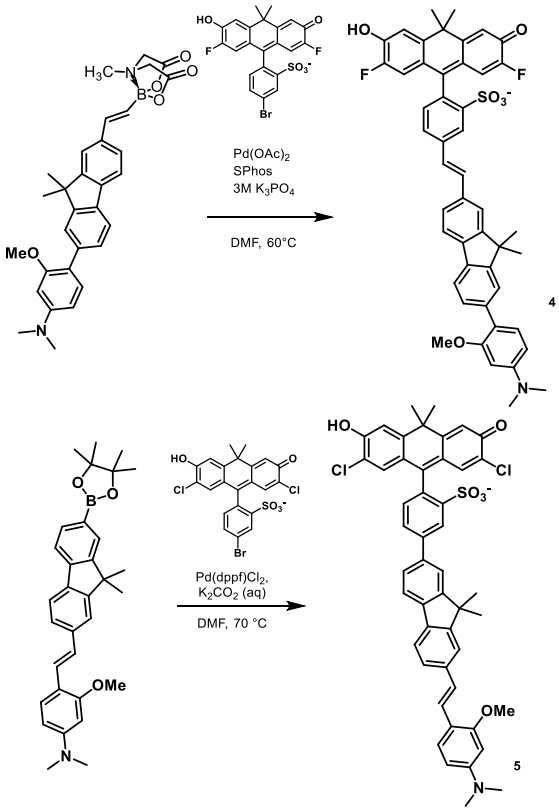

Figure A2-1. *Staining in HEK293T cells*

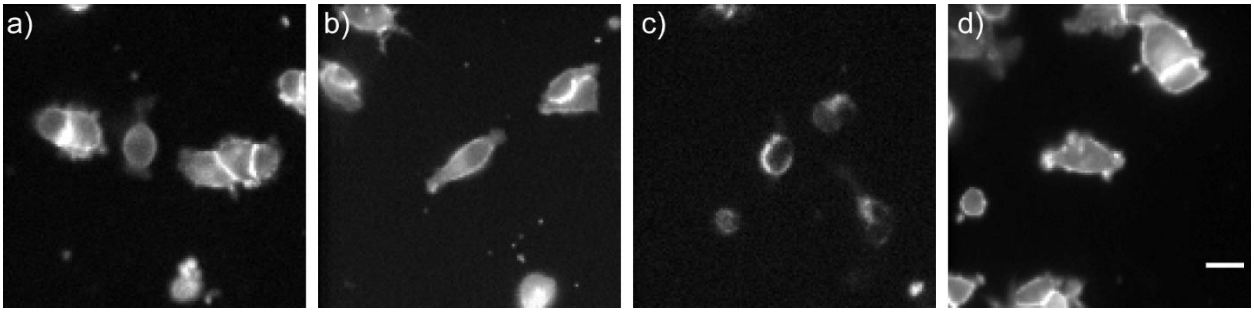

Figure A2-1. Staining in HEK293T cells. Fluorescence micrographs of compounds **1** (a), **2** (b), **3** (c), and **4** (d). Clear membrane staining is observed for **1, 2,** and **4**, however **3** has internalized. Scale bar is 20 µm.

Figure A2-2. *Voltage sensitivity in patch-clamped HEK293T cells*

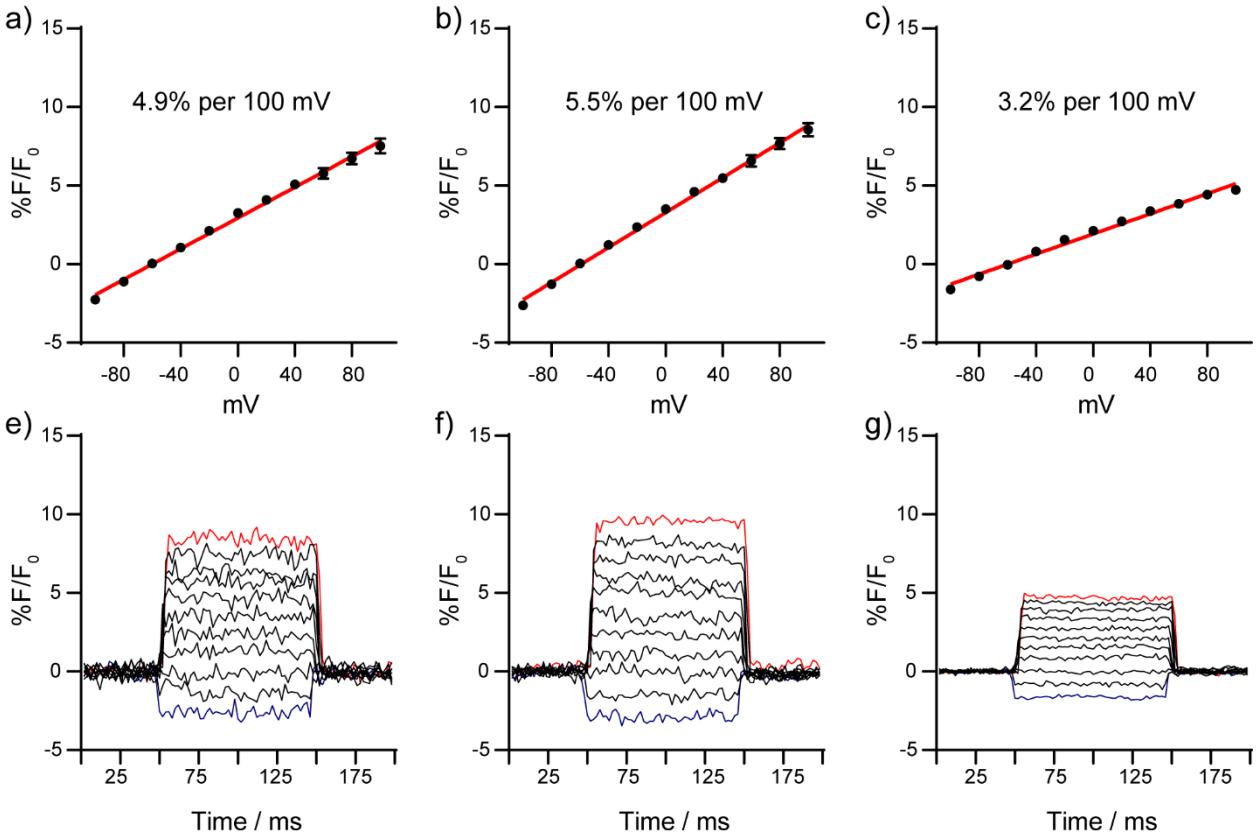

Figure A2-2. Voltage sensitivity in patch-clamped HEK293T cells. (a-c) Plots show the $\%F/F_o$ change for voltage steps made in whole-cell voltage clamp using compounds **1** (a), **2** (b), and **4** (c). Compound **3** was not sensitive to voltage changes at the plasma membrane (not shown). (e-g) Concatenated fluorescence changes showing response to changes in membrane potential during acquisition.

A2.4 References

(1) Weissleder, R. A Clearer Vision for in Vivo Imaging. *Nat. Biotechnol.* **2001**, *19*.

(2) Deal, P. E.; Kulkarni, R. U.; Al-Abdullatif, S. H.; Miller, E. W. Isomerically Pure Tetramethylrhodamine Voltage Reporters. *J. Am. Chem. Soc.* **2016**, *138* (29), 9085–9088.

(3) Huang, Y.-L.; Walker, A. S.; Miller, E. W. A Photostable Silicon Rhodamine Platform for Optical Voltage Sensing. *J. Am. Chem. Soc.* **2015**, *137*, 10767–10776.

(4) Ortiz, G.; Liu, P.; Naing, S. H. H.; Muller, V. R.; Miller, E. W. Synthesis of Sulfonated Carbofluoresceins for Voltage Imaging. *J. Am. Chem. Soc.* **2019**, *141* (16), 6631–6638.

(5) Boggess, S. C.; Gandhi, S. S.; Siemons, B. A.; Huebsch, N.; Healy, K. E.; Miller, E. W. New Molecular Scaffolds for Fluorescent Voltage Indicators. *ACS Chem. Biol.* **2019**, *14* (3), 390–396.

(6) Kulkarni, R. U.; Vandenberghe, M.; Thunemann, M.; James, F.; Andreassen, O. A.; Djurovic, S.; Devor, A.; Miller, E. W. In Vivo Two-Photon Voltage Imaging with Sulfonated Rhodamine Dyes. **2018**, *56* (39), 5171-5177.

Appendix 3:

Synthesis of Ratio-based Voltage Indicators

A3.1 Synopsis

The development of voltage sensitive dyes (VSDs) and genetically encodable voltage indicators (GEVIs) has proven to be an asset for studying electrophysiology in excitable cells. While these tools overcome many challenges associated with traditional electrophysiology methods,[1] they still have deficiencies that prevent their use in certain systems. Electrophysiology has the ability to report absolute membrane potential values with high temporal resolution, while current optical methods are limited to relative changes. While a recent method utilized voltage indicators to make absolute measurements of resting membrane potential in excitable cells using fluorescence lifetime,[2] this was limited to non-excitable cells. One method to overcome these challenges from a probe design lens is to develop an indicator with a ratio-based response to voltage changes. In this appendix, I outline the initial design and synthetic steps of a single-component, ratio-based voltage indicator based on the VoltageFluor scaffold that incorporates a second fluorophore for two-color ratio-based imaging (**Scheme A3-1**).

In theory, this design would work on the basis of FRET, with coumarin donating to the fluorescein dye head (**Scheme A3-1**). The ratio of fluorescein emission and coumarin emission at different membrane potential steps should change, as PeT will quench the fluorescein and be sensitive to membrane potential changes. The coumarin, which is not coupled to the molecular wire, should not be directly affected by PeT, and thus coumarin emission should remain unchanged.

I first built a coumarin-fluorescein conjugate linked by a piperazine-cysteic acid linker in order to ensure FRET would occur between the two fluorophores (**Scheme A3-2**). Condensation of 4-dimethylamino-2-hydroxybenzalhyde with diethylmalonate provided the coumarin, **1**. The linker was built from the carboxy group of 2,7-dichlorofluorscein, first by peptide coupling with Boc-piperazine and removal of the Boc group with TFA to yield **2**. Boc-cysteic acid was then coupled, and the Boc group removed again by TFA to yield **3**. In future voltage indicators, the sulfonate of the cysteic acid moiety will help with both water solubility and membrane localization of the indicator. **1** and **3** joined via a final peptide coupling with HATU to provide reference compound **4**. Purification proved difficult, as removal of excess coumarin **1** was not possible through trituration and normal-phase chromatography caused streaking of the product band. Spectroscopy studies in PBS (+0.1% SDS, pH = 7.2) reveal that compound **4** has the expected absorption max of the fluorescein (λ_{max} = 512 nm) while also having a second maximum band (425 nm) that can be attributed to the coumarin (**Figure A3-1**). Excitation at 420 nm provided strong emission of fluorescein (520 nm) and a weaker coumarin emission (463 nm). These initial results suggest FRET between the coumarin and fluorescein with the current linker is possible. It should also be highlighted that future work should include optimization of linker length and the coumarin fluorophore to increase the amount of secondary emission signal.

Synthesis of the voltage indicator proved challenging, as late stage Suzuki reactions to add the molecular wire caused hydrolysis of the coumarin amide bond to the cysteic acid linker (**Scheme A3-3**). The fluorene molecular wire was chosen for the full indicator, as the blue shifted wire absorption (relative to phenylene-vinylene wires) provides a clean window for the coumarin absorption band (**Figure A3-1**). Optimization of Suzuki reaction conditions may help solve this hydrolysis problem.

Other routes to circumvent this problem were attempted (**Scheme A3-4**). Cross-coupling of the fluorene molecular wire to fluorescein before adding the cysteic acid linker provided **8**. Coupling cysteic acid to coumarin first (**Scheme A3-2**) provided **9**, which was then directly coupled to **8** in a subsequent peptide coupling. However, no product was formed. In another route, Boc-cysteic acid was coupled to **5** and was subjected to Suzuki coupling with the fluorene molecular wire before Boc deprotection. TFA deprotection after cross coupling provided indicator **10**. Using HATU to incorporate the coumarin produced the product by HPLC, however separation from the coumarin starting material could not be achieved. Future work should focus on using equimolar coumarin and **10** with conditions that provide close to 100% conversion.

Due to concerns about dye internalization, I loaded a crude sample of **10** (material before attempted coupling with coumarin) onto HEK293T cells to check for membrane localization. Thankfully, **10** localized properly to the cell membrane with little internalization (**Figure A3-2**). Patch-clamp studies also showed that **10** retained voltage sensitivity, having a 9.4% F/F_o response per 100 mV change in membrane potential.

A3.2 Experimental section

A3.2.1 General methods for chemical synthesis and characterization

Palladium acetate was purchased from Strem Chemicals. Deuterated solvents were purchased from Cambridge Isotope Laboratories. All other reagents, including anhydrous solvents, were purchased from Sigma-Aldrich and used without further purification. References to previously synthesized compounds are provided along with characterization data. High performance liquid chromatography (HPLC) and low resolution ESI Mass Spectrometry were performed on an Agilent Infinity 1200 analytical instrument coupled to an Advion CMS-L ESI mass spectrometer. The column used for the analytical HPLC was Phenomenex Luna 5 μm C18(2) (4.6 mm I.D. × 125 mm) with a flow rate of 1.0 mL/min. The mobile phases were MQ-H2O with 0.05% trifluoroacetic acid (eluent A) and HPLC grade acetonitrile with 0.05% trifluoroacetic acid (eluent B). Signals were monitored at 254, 350 and 480 nm over 10 min with a gradient of 10-100% eluent B unless otherwise noted. Semi-preparative high-performance liquid chromatography (HPLC) was performed on the same system with a semi-preparative Phenomenex Luna C18(2) column. Preparative HPLC was performed using a Waters Acquity Autopurificaiton system equipped with a Waters XBridge BEH 5 μm C18 column (19 mm I.D. x 250 mm) with a flow rate of 30.0 mL/min, made available by the Catalysis Facility of Lawrence Berkeley National Laboratory (Berkeley, CA). The mobile phases were MQ-H2O with 0.05% trifluoroacetic acid (eluent A) and HPLC grade acetonitrile with 0.05% trifluoroacetic acid (eluent B). Signals were monitored at 254 and 350 nm over 20 min with a gradient of 10-100% eluent B, unless otherwise noted.

A3.2.2 Imaging, cell culture, and electrophysiology

For HEK293T cells, epifluorescence imaging was performed on an AxioExaminer Z-1 (Zeiss) equipped with a Spectra-X Light engine LED light (Lumencor), controlled with Slidebook (v6, Intelligent Imaging Innovations). Images were acquired with either a W-Plan-Apo 20x/1.0 water objective (20x; Zeiss. Images were focused onto an eVolve 128 EMCCD camera (EMCCD; Photometrix). Functional imaging of the fluorene VoltageFluors was performed at a sampling rate

of 0.5 kHz, all dyes were loaded at approximately 0.5 µM. Excitation was supplied a 475 nm LED with an intensity of 20.9 mW/mm^2.

Human embryonic kidney (HEK) 293T cells were acquired from the UC Berkeley Cell Culture Facility. Cells were passaged and plated onto 12 mm glass coverslips coated with Poly-D-Lysine (PDL; 1 mg/mL; Sigma-Aldrich) to a confluency of ~15% and 50% for electrophysiology and imaging, respectively. HEK293T cells were plated and maintained in Dulbecco's modified eagle medium (DMEM) supplemented with 4.5 g/L D-glucose, 10% fetal bovine serum (FBS), and 1% Glutamax.

For electrophysiological experiments in HEK293T cells and rat hippocampal neurons, pipettes were pulled from borosilicate glass (Sutter Instruments, BF150-86-10), with a resistance of 5–6 MΩ, and were filled with an internal solution; 125 mM potassium gluconate, 1 mM EGTA, 10 mM HEPES, 5 mM NaCl, 10 mM KCl, 2 mM ATP disodium salt, 0.3 mM GTP trisodium salt (pH 7.25, 285 mOsm). Recordings were obtained with an Axopatch 200B amplifier (Molecular Devices) at room temperature. The signals were digitized with a Digidata 1440A, sampled at 50 kHz and recorded with pCLAMP 10 software (Molecular Devices) on a PC. Fast capacitance was compensated in the on-cell configuration. For all electrophysiology experiments, recordings were only pursued if series resistance in voltage clamp was less than 30 MΩ. For whole-cell, voltage clamp recordings in HEK293T cells, cells were held at -60 mV and hyper- and de- polarizing steps applied from -100 to +100 mV in 20 mV increments.

A3.2.3 Synthetic methods

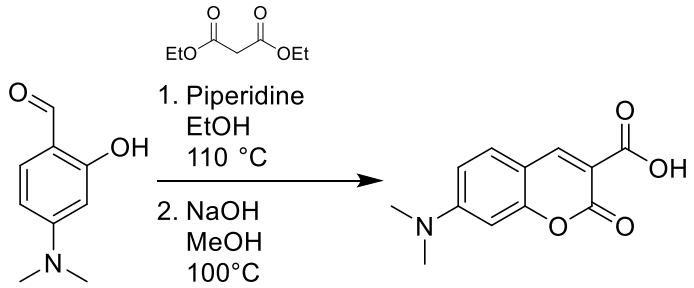

Synthesis of 3-carboxy-7-dimethylaminocoumarin, 1

4-(dimethylamino)-2-hydroxybenzaldehyde (0.5 g, 3 mmol) was suspended in ethanol (7.5 mL), then diethylmalonate (0.69 mL, 4.5 mmol) and piperidine (0.03 mL, 0.3 mmol) was added. This was refluxed at 110 °C for 16 hours, then cooled on ice to precipitate a yellow solid, which was collected by filtration (0.57 g, 72%).

A small portion of this solid (0.11 g, 0.43 mmol) was suspended in methanol (10mL) and 1 M NaOH. This was refluxed at 100 °C for two hours. The reaction was poured over ice, then yellow precipitate **1** was collected by filtration (46 mg, 46%).

Analytical HPLC retention time 4.92; MS (ESI+) calculated for $C_{12}H_{12}NO_4$ m/z $[M+H]^+$ 234.1; found 234.0. Estimated purity, 80%.

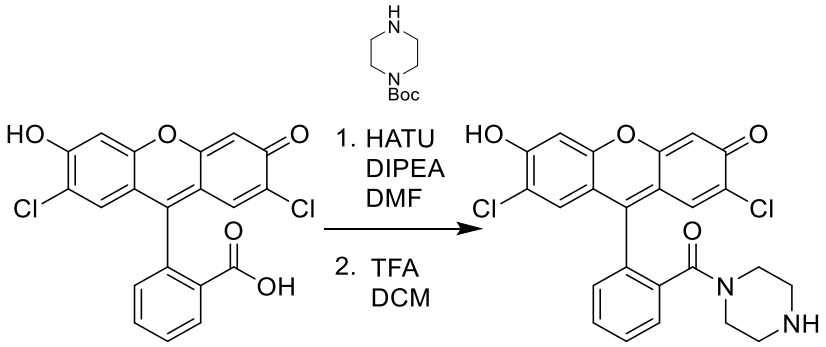

2, 57%

Synthesis of 2

2'-carboxy-2,7-dichlorofluorescein (0.9 g, 0.75 mmol), 1-Boc-piperazine (0.17 g, 0.9 mmol), and HATU (0.34 g, 0.9 mmol) were combined in DMF (1 mL), then diisopropylethylamine (0.6 mL, 3.8 mmol) was added. This was stirred for 12 hours, then extracted into 2:1 dichloromethane:isopropanol. This was washed with 1M HCl and brine (3X). Flash column chromatography (10% methanol in dichloromethane) provided Boc-protected fluorescein (0.36 g).

This material was suspended in a 1:1 dichloromethane:trifluoroacetic acid mixture (2 mL) and stirred for 1 hour. This was concentrated under reduced pressure, and TFA was azeotroped by addition of toluene, which was then concentrated again. This was repeated three times to provided **2** as a red solid (0.14 g, 57%)

Analytical HPLC retention time 3.24 min; MS (ESI+) calculated for $C_{24}H_{19}Cl_2N_2O_4$ m/z [M+H] 469.1; found 469.3. Estimated purity, 92%

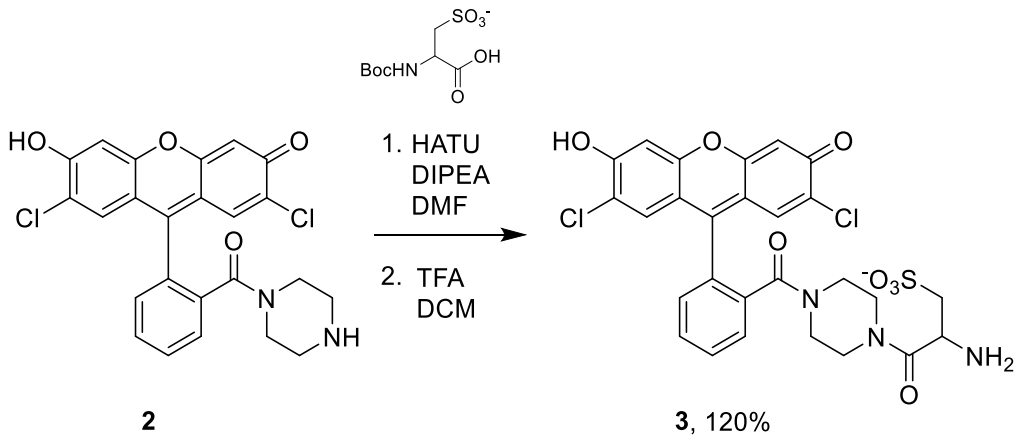

2 **3**, 120%

Synthesis of 3

Compound **2** (42 mg, 0.09 mmol), Boc-cysteic acid (29 mg, 0.11 mmol), and HATU (41 mg, 0.11 mmol) were combined in DMF (1 mL), then diisopropylethylamine (0.1 mL) was added. This was stirred for 12 hours, then concentrated to dryness under reduced pressure. This was then extracted

into 2:1 dichloromethane:isopropanol, then washed with combined brine and 1M HCl. This was dried with $MgSO_4$ and concentrated to dryness to provide a red solid (75 mg). This was suspended in 1:1 dichloromethane:isopropanol (2 mL) and stirred for 30 minutes. This was concentrated under reduced pressure, using toluene to help azeotrope TFA. This provided a red product (74 mg, 120%). This is likely still wet or contains unconsumed HATU. Further purification was avoided due to poor movement on standard silica and low quantity for HPLC. Further studies should utilize HPLC when scaled up.

Analytical HPLC retention time 3.79 min; MS (ESI+) calculated for $C_{27}H_{24}Cl_2N_3O_8S$ m/z $[M+H]^+$ 620.1; found 620.0. Estimated purity >99%.

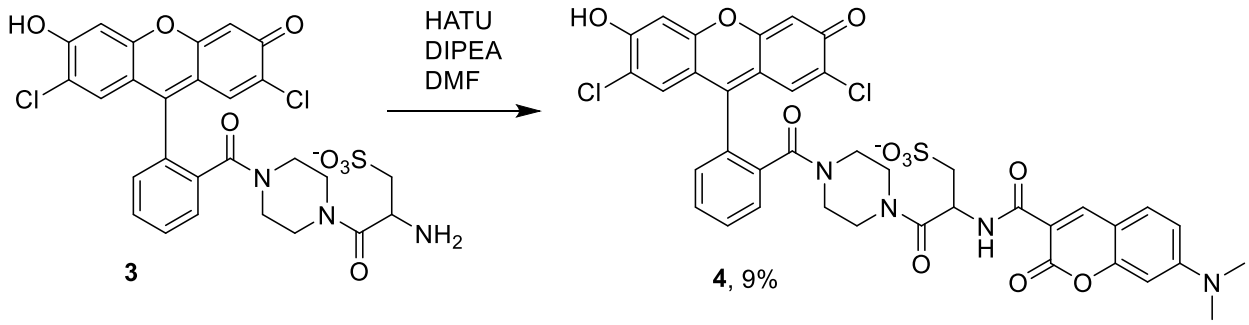

Synthesis of 4

3 (40 mg, 0.06 mmol), **1** (18 mg, 0.08 mmol), and HATU were combined in DMF (1 mL) then diisopropylethylamine (0.1 mL) was added. This was stirred for 12 hours before concentrating to dryness under reduced pressure. This was taken up in a small amount of 1:1 dichloromethane:methanol, then triturated with diethyl ether. The precipitate was collected by filtration, which provided **4** as a red solid. This was purified further by preparative TLC (30% methanol in dichloromethane). **4** was recovered as a red film (5 mg, 9%).

Analytical HPLC retention time 4.66 min; MS (ESI+) calculated for $C_{44}H_{41}Cl_2N_4O_{13}S$ m/z $[M+H]^+$ 835.1; found 835.3.

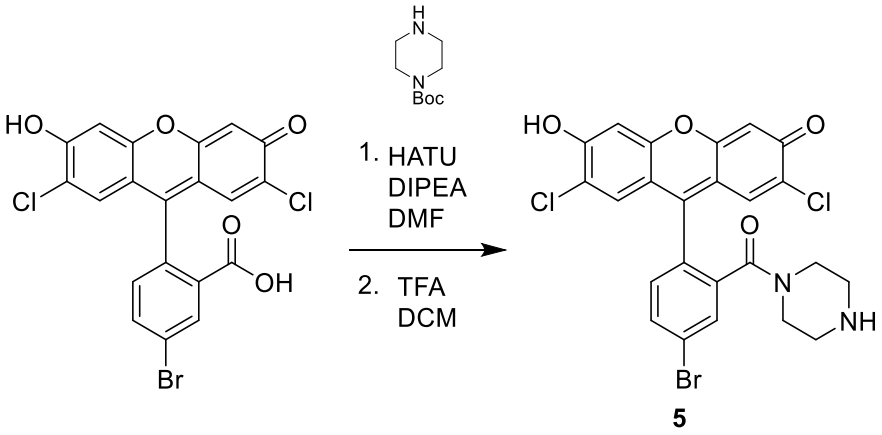

5

Synthesis of 5

5'-bromo-2,7-dichlorofluorescein (0.38 g, 0.78 mmol), N-Boc piperazine (0.22 g, 1.2 mmol), and HATU (0.45 g, 1.2 mmol) were combined in DMF (1 mL), to which diisopropylethylamine (0.7 mL) was added. This was stirred for 14 hours, then concentrated to dryness under reduced pressure. This was extracted into dichloromethane, then washed with 0.1 M HCl and brine. This was purified by flash column chromatography (2-5% methanol in dichloromethane + 1% formic acid) to yield a red solid (0.36 g). This was then suspended in 1:1 dichloromethane:trifluoroacetic acid (2 mL) and stirred for 30 minutes. This was concentrated to dryness under reduced pressure, using toluene to azeotrope TFA. 415 mg of a red solid was isolated, which was higher than the expected mass. Product is likely still wet or could use further purification. This was used in subsequent reactions as-is.

Analytical HPLC retention time 4.22 min; MS (ESI+) calculated for $C_{24}H_{18}BrCl_2N_2O_4$ m/z $[M+H]^+$ 547.0; found 546.9. Estimated purity >94%.

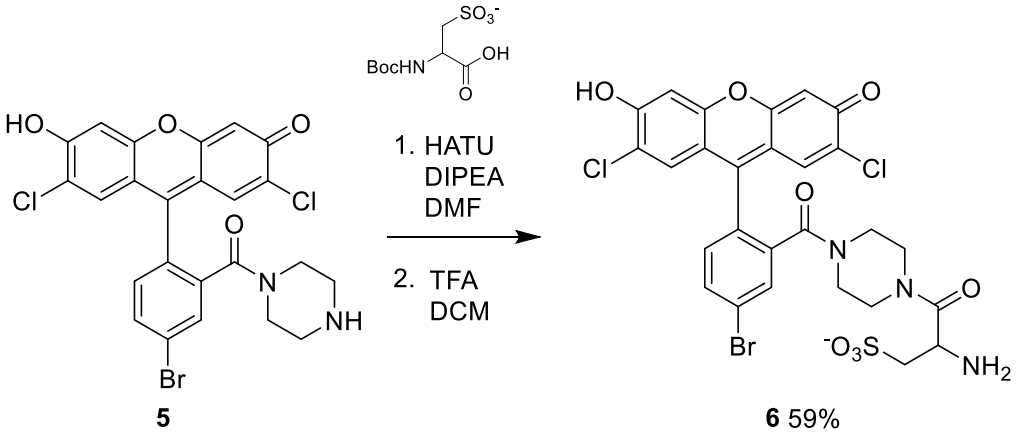

5 **6** 59%

Synthesis of 6

5 (0.15 g, 0.3 mmol), Boc-cysteic acid (89 mg, 0.33 mmol), and HATU (0.13 g, 0.33 mmol) were combined in DMF (2 mL), then DIPEA (0.2 mL) was added. This was stirred for 14 hours, then

the crude was precipitated in diethyl ether to provide an orange solid (0.24 g). This was then suspended in 1:1 DCM:isopropanol and stirred for 1 hour. This was concentrated under reduced pressure, then taken up in 1:1 DCM:MeOH. This was triturated with diethyl ether, and **6** was collected as a dark red solid (0.1 g, 59%)

Analytical HPLC retention time 4.27 min; MS (ESI+) calculated for $C_{27}H_{23}BrCl_2N_3O_8S$ m/z $[M+H]^+$ 698.0; found 697.9. Estimated purity 70%.

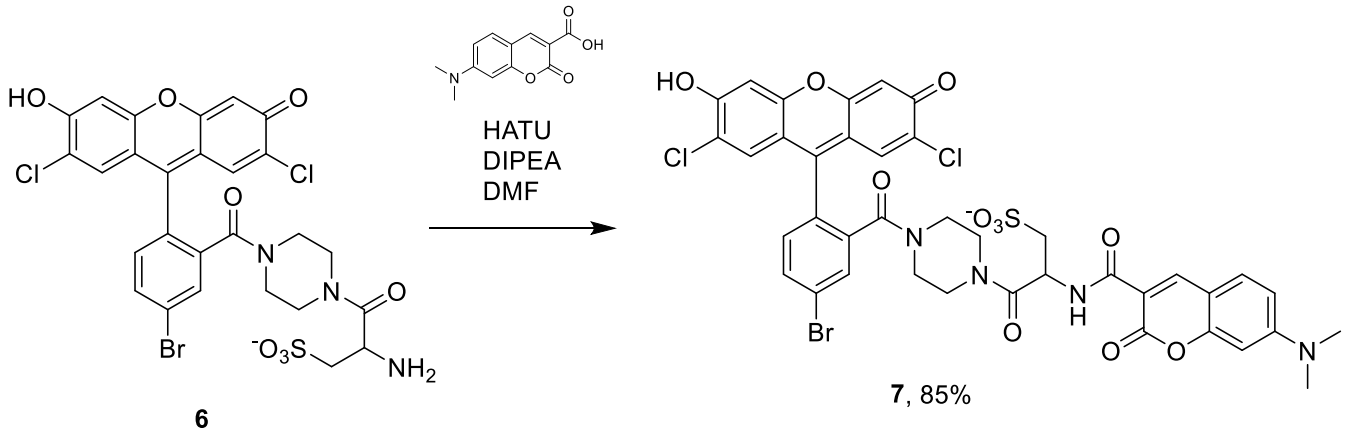

6

7, 85%

Synthesis of 7

6 (90 mg, 0.13 mmol), **1** (30 mg, 0.13 mmol), and HATU (49 mg, 0.13 mmol) were combined in DMF (1 mL), then DIPEA (0.1 mL) was added. This was stirred for 14 hours, then the crude was precipitated in diethyl ether to provide an orange solid (0.24 g). This was then suspended in 1:1 DCM:isopropanol and stirred for 1 hour. This was concentrated under reduced pressure, then taken up in 1:1 DCM:MeOH. This was triturated with diethyl ether, and **7** was collected as a dark red solid (0.1 g, 85%)

Analytical HPLC retention time 5.31 min; MS (ESI+) calculated for $C_{39}H_{32}BrCl_2N_4O_{11}S$ m/z $[M+H]^+$ 913.0; found 913.8. Estimated purity 70%.

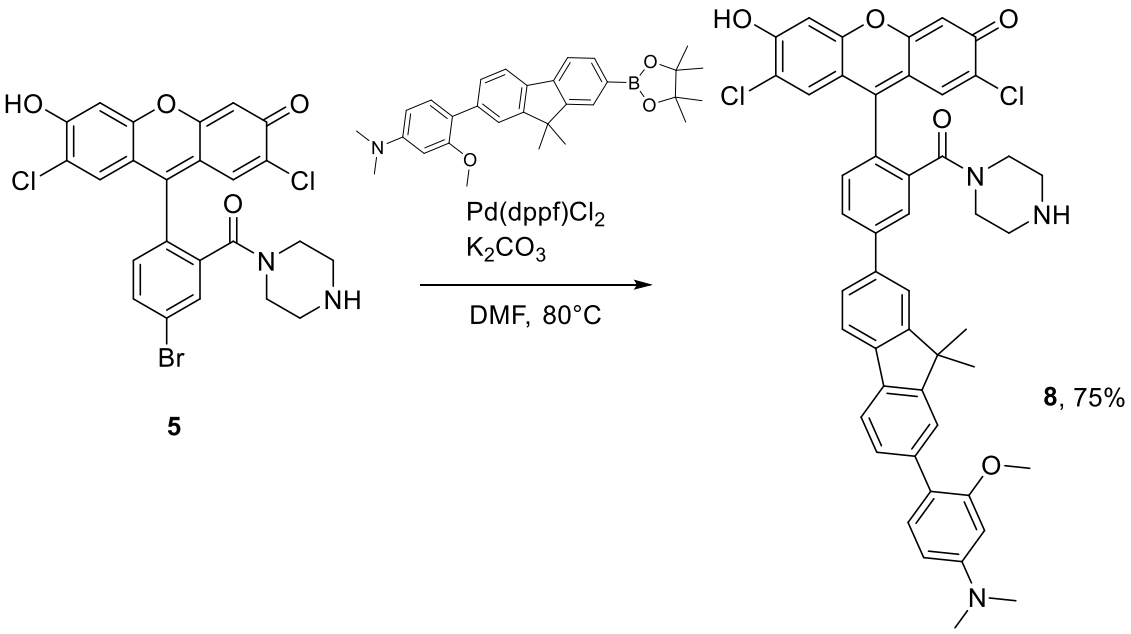

Synthesis of 8

Fluorene wire[3] (5 mg, 0.01 mmol), **5** (5.3 mg, 0.01 mmol), and $Pd(dppf)Cl_2$ (0.4 mg, 0.5 µmol) were combined in a flame dried Schlenk flask. This was evacuated and backfilled with N_2 (3X) before addition of anhydrous DMF (0.3 mL) and bubbled 5M K_2CO_3 solution (0.01 mL). This was stirred at 80 °C for 16 hours. This was concentrated to dryness, then taken up in 1:1 DCM:MeOH and triturated with diethyl ether. **8** was collected by filtration as a red solid (6 mg, 75%)

Analytical HPLC retention time 5.16 min; MS (ESI+) calculated for $C_{48}H_{43}Cl_2N_3O_5$ m/z $[M+H]^+$ 811.3; found 810.1. Estimated purity 95%.

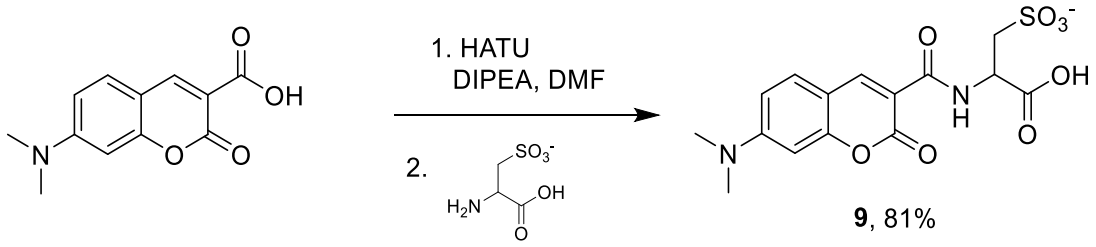

Synthesis of coumarin, 9

1 (15 mg, 0.06 mmol) and HATU (24 mg, 0.06 mmol) were combined in DMF (1 mL) and DIPEA (0.06 mL). This was stirred for 1 hour before addition of cysteic acid (11 mg, 0.06 mmol). This was stirred for another 16 hours, then concentrated to dryness. Taken up in 1:1 DCM:MeOH, then trituration with diethyl ether provided **9** as a yellow solid after filtration (20 mg, 81%)

Analytical HPLC retention time 3.32 min; MS (ESI+) calculated for $C_{15}H_{17}N_2O_8S$ m/z [M+H] 385.1; found 385.1. Estimated purity, 88%.

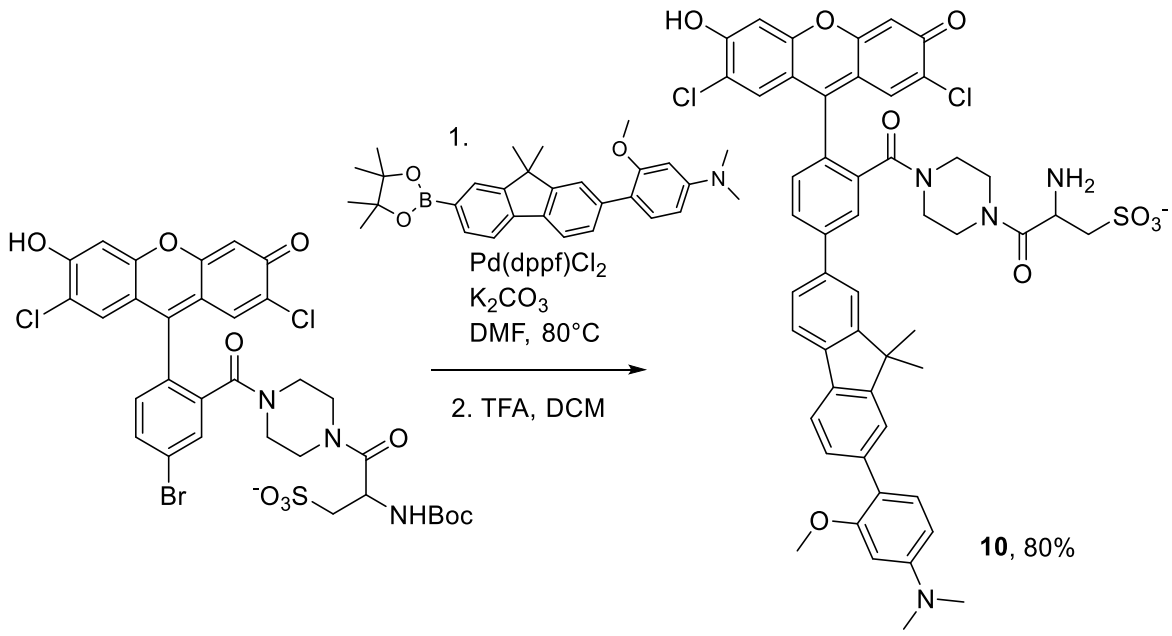

Synthesis of 10

Boc-protected intermediate from preparation of **6** was taken. 30 mg (0.038 mmol) was combined with fluorene wire[3] (21 mg, 0.05 mmol)), and $Pd(dppf)Cl_2$ (1.3 mg, 1.8 µmol) were combined in a flame dried Schlenk flask. This was evacuated and backfilled with N_2 (3X) before addition of anhydrous DMF (0.5 mL) and bubbled 5M K_2CO_3 solution (0.02 mL). This was stirred at 80 °C for 16 hours. This was concentrated to dryness, then taken up in 1:1 DCM:MeOH and triturated with diethyl ether. **10** was collected by filtration as a red solid (70 mg, overmass; HPLC retention time 5.57 min). This was then suspended in 1:1 DCM:TFA (2 mL) and stirred for 30 minutes. This was concentrated to dryness and azeotroped with toluene, recovering a sticky red solid (22 mg, 80%)

Analytical HPLC retention time 5.12 min; MS (ESI+) calculated for $C_{48}H_{43}Cl_2N_3O_5$ m/z $[M+H]^+$ 961.2; found 960.9. This was not pure enough for further reaction (~47%).

A3.3 Schemes and figures

Scheme A3-1. *Design of a ratio-based voltage indicator*

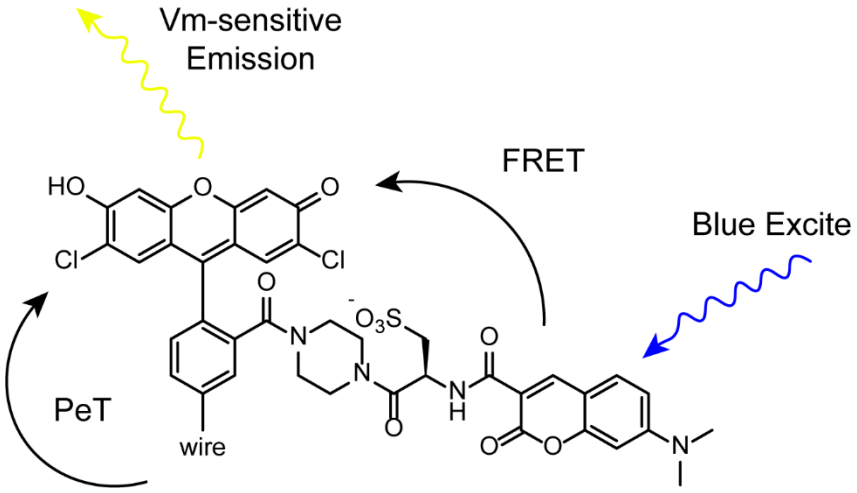

Scheme A3-2. *Synthesis of reference coumarin-fluorescein conjugate*

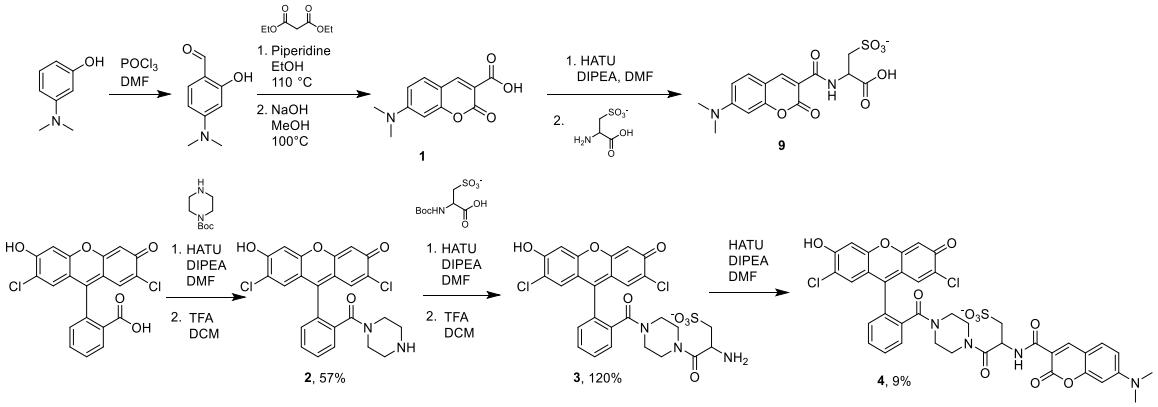

***Scheme A3-3**. Initial route to coumarin-fluorescein voltage indicator*

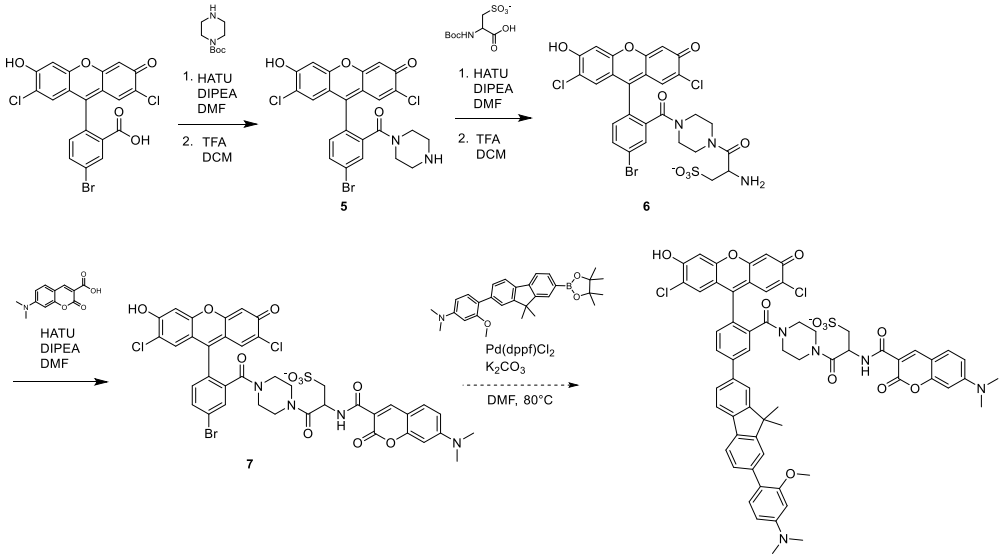

Scheme A3-4. *Alternative routes to reach coumarin-fluorescein voltage indicator.*

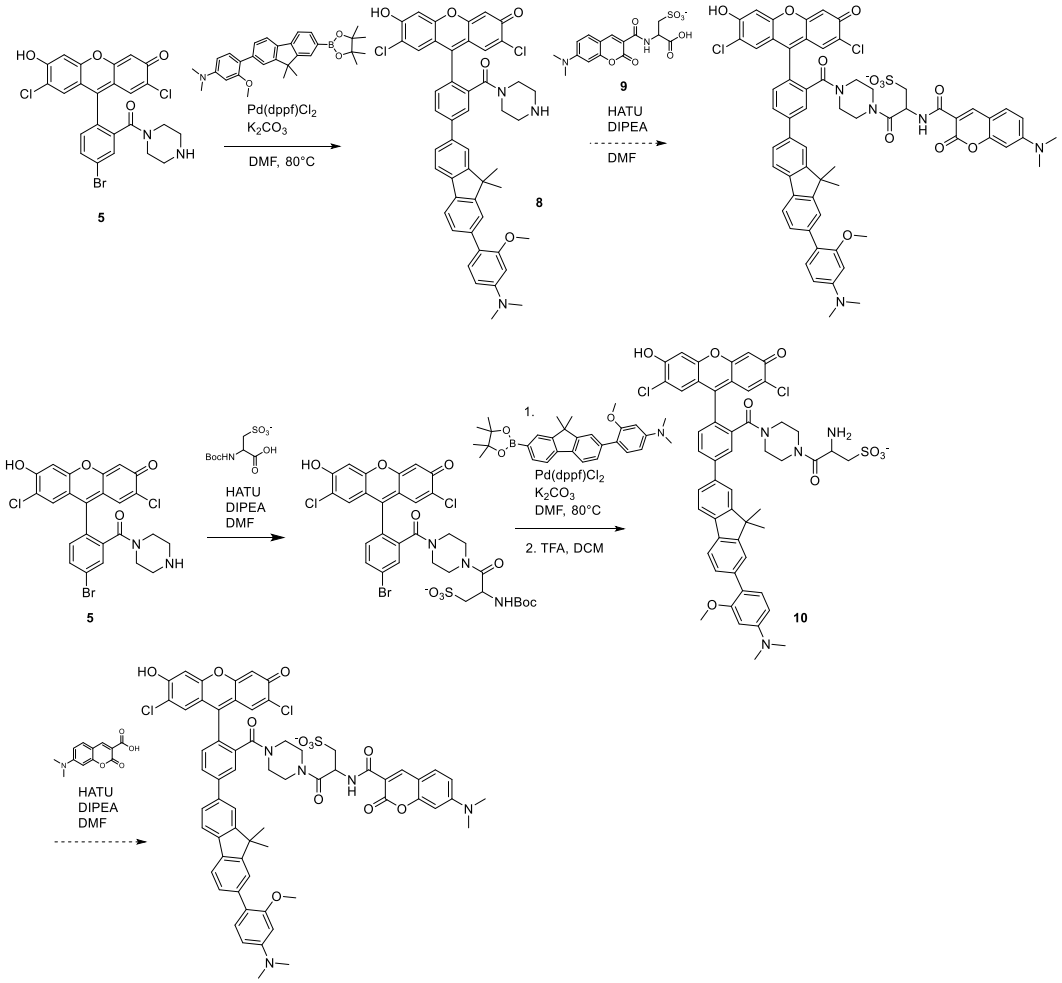

Figure A3-1. *Normalized absorption and emission of **4** compared to fVF 2*

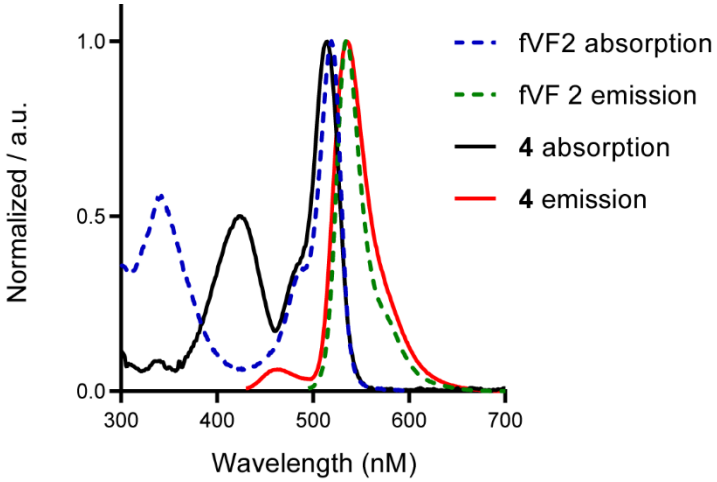

Figure A3-1. Normalized absorption and emission (PBS +0.1% SDS, pH = 7.2) of **4** compared to fVF 2. The coumarin absorption peak (425 nm) of **4** sits between the fluorene molecular wire and fluorescein peaks. **4** has the expected fluorescein absorption (λ_{max} = 512 nm) and emission (520 nm). A weaker coumarin emission (463 nm) is observed when excitation is applied at 420 nm.

Figure A3-1. *Characterization of compound* ***10*** *in HEK293T cells*

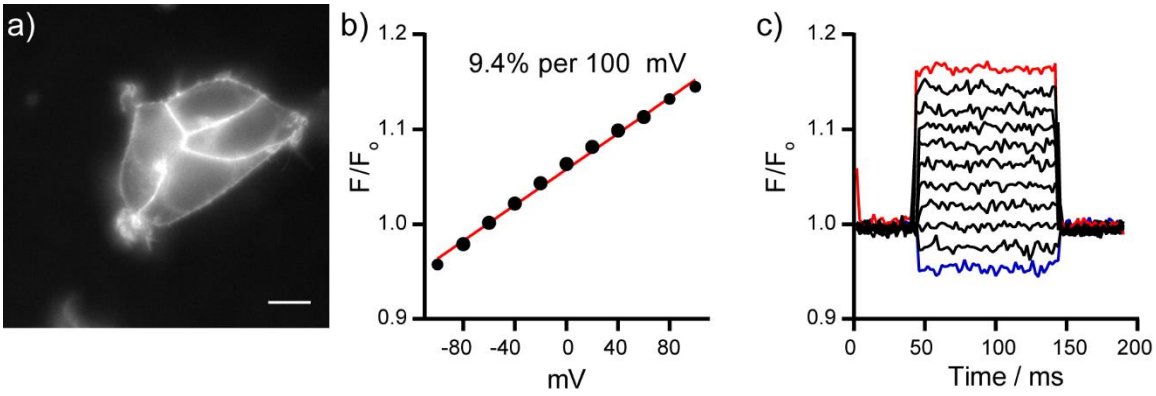

Figure A3-1. Characterization of compound **10** in HEK293T cells. (a) Epifluorescence micrograph of crude **10** in HEK293T cells, showing proper membrane localization. Scale bar is 10 μm. (b-c) Results from patch clamp experiments show **10** is sensitive to membrane potential changes (9.4% per 100 mV).

A3.4 References

(1) Knöpfel, T.; Song, C. Optical Voltage Imaging in Neurons: Moving from Technology Development to Practical Tool. *Nat. Rev. Neurosci.* **2019**, *20* (12), 719–727.

(2) Lazzari-Dean, J. R.; Gest, A. M. M.; Miller, E. W. Optical Estimation of Absolute Membrane Potential Using Fluorescence Lifetime Imaging. *Elife* **2019**, *8*.

(3) Boggess, S. C.; Gandhi, S. S.; Siemons, B. A.; Huebsch, N.; Healy, K. E.; Miller, E. W. New Molecular Scaffolds for Fluorescent Voltage Indicators. *ACS Chem. Biol.* **2019**, *14* (3), 390–396.